UNIVERSITE DE BOURGOGNE FRANCHE-COMTE

Ecole doctorale ES – Environnement Santé

UMR PAM (Procédés Alimentaires et Microbiologiques)

Equipe PAPC (Procédés Alimentaires et Physico-Chimie)

THESE DE DOCTORAT

Spécialité : Sciences de l'Alimentation

Thi Diem Uyen HUYNH

Soutenue publiquement : le 12 Octobre 2016

Structuration de matrices à base de pectine : formulation, caractérisation, fonctionnalités et libération contrôlée lors de l'encapsulation

Membres du jury :

Dr. Florence EDWARDS-LEVY (Université de Reims)	**Rapporteuse**
Pr. Christian SANCHEZ (Université de Montpellier)	**Rapporteur**
Dr. Sandrine BOURGEOIS (Université de Lyon)	**Examinatrice**
Pr. Frédéric DEBEAUFORT (UBFC)	**Examinateur**
Dr. Ali ASSIFAOUI	**Co-encadrant de thèse**
Pr. Odile CHAMBIN	**Directeur de thèse**

Remerciements

Ce travail a été réalisé dans le cadre d'une thèse à l'université de Bourgogne Franche-Comté avec l'aide financière du Ministère de l'Éducation et de la formation du Vietnam (MEF).

Je remercie vivement Madame le Docteur **Florence EDWARDS-LEVY** (Maître de Conférences HDR) et Monsieur le Professeur **Christian SANCHEZ** pour avoir accepté de rapporter ce travail. Qu'ils trouvent ici l'expression de ma sincère reconnaissance et de mes salutations respectueuses.

Je tiens tout particulièrement à exprimer ma gratitude à Madame le Docteur **Sandrine BOURGEOIS** et Monsieur le Professeur **Frédéric DEBEAUFORT** d'avoir bien voulu participer à mon jury de thèse et d'avoir accepté d'évaluer mes travaux.

Je tiens également à exprimer ma profonde gratitude à Madame la Professeur **Odile CHAMBIN** et Monsieur le Docteur **Ali ASSIFAOUI** de m'avoir accueillie au Laboratoire de Pharmacie Galénique – Dijon, laboratoire attaché à l'UMR PAM (Procédés Alimentaires et Microbiologiques), Equipe PAPC. Ils m'ont suivie tout au long de cette thèse. Je n'oublierai jamais leurs aides efficaces tant scientifique qu'expérimentale. Nos échanges réguliers, leurs connaissances et compétences ainsi que leur disponibilité m'ont permis de guider ce travail et de découvrir un nouveau domaine qui ne m'était pas familier. Ils m'ont témoignée leur soutien et leur aide surtout lors de la correction du français durant ces trois années et en particulier au cours de ces derniers mois.

J'exprime ma reconnaissance à Monsieur le Professeur **TRAN Van Nam,** Président de l'Université de Da-Nang, qui a signé les décisions pour me permettre de venir en France pour réaliser ce travail et à Monsieur le Professeur **NGUYEN Dinh Lam** pour m'aider à chercher un établissement d'accueil.

J'exprime toute ma reconnaissance à Mr. le Docteur **Taco NICOLAI** et Mr. le Docteur **Thomas KARBOWIAK** (Maître de Conférences HDR) d'avoir participé à mon comité de suivi de thèse.

Je remercie sincèrement Monsieur le Docteur **Adrien LERBRET**. Je lui suis très reconnaissante pour ses conseils et ses encouragements lors de la réalisation de ce travail et son aide pour la modélisation.

Je voudrais également exprimer ma reconnaissance à Madame le Docteur **Camille LOUPIAC** et à Madame **Bernadette ROLLIN** pour leurs conseils et leurs aides dans mes travaux.

J'exprime également mes sincères remerciements à tous les membres de l'équipe PAPC «Procédés Alimentaires et Physico-Chimie» - AgroSup – Dijon. Qu'ils soient assurés que j'ai trouvé au milieu d'eux une ambiance amicale et chaleureuse dont je garderai un excellent souvenir. Un grand merci à mes amis vietnamiens et mes amis français qui m'ont aidé beaucoup dans la vie quotidienne et m'ont donné des moments amicaux et agréables pendant tout le temps où j'ai été séparée de ma famille.

J’adresse enfin mes plus profonds sentiments à mes parents, à mon mari, et à toute ma famille qui, grâce à leur patience et leur encouragement m’ont permis d’affronter l’éloignement avec sérénité et de rester enthousiaste durant ces années de travail.

Je dédie ce travail à mon fils (**DAO Hoang Nguyen**) pour qu’il comprenne pourquoi j’ai été longtemps absente de la maison.

Avant-propos

Ce manuscrit est divisé en cinq chapitres possédant chacun leur numérotation de tableaux et de figures propre. Les références bibliographiques sont disposées en fin du manuscrit.

Bonne lecture !

Table of Contents

List of abbreviations and acronyms

ALMP	Amidated Low Methoxyl Pectin
DA	Degree of Amidation
DE	Degree of Esterification
EE	Encapsulation Efficiency
EY	Encapsulation Yield
FTIR	Fourier Transform InfraRed
Gal	Galacturonate
GalA	Galacturonic Acid
ICP-AES	Inductively Coupled Plasma Atomic Emission Spectroscopy
ITC	Isothermal Titration Calorimetry
LMP	Low Methoxyl Pectin
M^{2+}	Divalent cations
MD	Molecular Dynamics
MWCO	Molecular Weight Cut-Off
PGA	Polygalacturonic Acid
PMF	Potentials of Mean Force
polyGal	Polygalacturonate
SANS	Small Angle Neutron Scattering
SSIP	Solvent Separated Ion Pair
UV/VIS	Ultraviolet-Visible
WU	Water Uptake

INTRODUCTION GENERALE

Aujourd'hui les polyosides, et notamment les pectines, sont très utilisés comme matrices de vectorisation de molécules d'intérêt (arômes, antioxydants, antimicrobiens) (Liu *et al.*, 2003) grâce à leurs propriétés gélifiantes et filmogènes. Ce sont des polymères naturels, non toxiques, biodégradables et biocompatibles répandus en industrie agro-alimentaire et pharmaceutique. Les pectines sont constituées d'association d'acides galacturoniques (GalA) plus ou moins estérifiés et/ou amidés. Lorsque ces pectines sont faiblement méthylées (LMP), elles gélifient en présence d'un cation de réticulation comme les ions calcium Ca^{2+}. Ces pectines LM peuveut être utilisées notamment pour une libération colonique, d'où l'intérêt de contrôler l'encapsulation et la libération de la molécule d'intérêt. Pour se faire, il serait intéressant de pouvoir moduler la structure du réseau polyosidique formé en présence de cations de réticulation. Ceci peut être réalisé soit en modifiant le type de pectines soit en modifiant la nature du cation de réticulation.

Pour s'affranchir de la complexité de la structure naturelle de la pectine, il est intéressant de remplacer cette dernière par l'acide polygalacturonique (PGA) - principal constituant de la pectine car c'est une molécule linéaire et non ramifiée. L'étude en solution de ces deux polyosides (PGA et LMP) en fonction de la force ionique (teneur en NaCl) permettra de comprendre les différences de conformation de ces deux polymères (viscosité intrinsèque, flexibilité des chaînes, …) et l'impact de cette conformation sur leur capacité à fixer les cations divalents (Ca^{2+}). Il a été montré que le mécanisme d'association entre l'alginate et les ions calcium suit le modèle de la boîte à œufs (Grant *et al.*, 1973). Pour rappel, les deux constituants majoritaires de l'alginate (acide guluronique) et de la pectine (acide galacturonique, GalA) sont des énantiomères. Ce qui laisse penser que le mode d'association entre LMP et les ions calcium pourrait aussi être de type « boîte à œuf ». Il est donc important de vérifier si ce mode d'association est valable pour les ions calcium mais aussi pour d'autres cations divalents. De plus, des études ont proposé des mécanismes d'association entre la pectine et les ions calcium en régime dilué (Fang *et al.*, 2008; Ventura *et al.*, 2013). Ces mécanismes sont basés sur la formation d'abord de monocomplexes (galacturonate - Ca^{2+}) suivi de la formation de dimères (Gal-Ca-Gal) et enfin de multimères (association de plusieurs dimères). Une étape intermédiaire mais importante dans ces mécanismes est la formation de plusieurs réticulations ponctuelles (Borgogna *et al.*, 2013; Ventura *et al.*, 2013). Ces mécanismes dépendent certainement de la nature du cation divalent. Dans cette optique, il est intéressant d'étudier les interactions entre le PGA et plusieurs cations divalents afin de

proposer un mécanisme d'association plus généralisé tenant compte de la nature du cation de réticulation. Le mécanisme d'association ainsi que la structure du réseau polyosidique obtenu dépendent également de la concentration initiale du polyoside (Ventura *et al.*, 2013). Il sera donc intéressant d'étudier ces structures à une concentration en polysaccharide supérieure à la concentration de recouvrement des chaînes du polymère (c*). Ainsi l'étude cinétique (diffusion des cations de réticulation dans le gel et migration du front de gel) et structurale (propriétés viscoélastiques) des gels pourra apporter des informations complémentaires sur le mécanisme d'association à des concentrations proches de celles utilisées lors de la formation des matrices d'encapsulation. La compréhension de cet état permettra de mieux appréhender l'état final du réseau et de pouvoir le moduler pour obtenir des structures spécifiques avec des fonctionnalités bien définies et une libération ciblée de la substance active.

Le présent manuscrit est structuré en cinq chapitres, dont quatre sont exclusivement réservés aux résultats expérimentaux. Nous avons choisi de présenter les résultats expérimentaux sous forme d'articles soumis ou acceptés. Pour chaque chapitre, nous avons essayé d'adopter le même plan : une introduction expliquant le contexte et les enjeux de l'étude, suivi de l'article soumis/accepté et enfin une conclusion mettant en évidence les points importants à retenir.

Le premier chapitre est une revue bibliographique assez large qui présente le contexte lors de l'utilisation de la pectine dans des matrices pharmaceutiques ou alimentaires. Il décrit l'impact des propriétés intrinsèques de la pectine (structure, degrés d'estérification, distribution des résidus d'acide galacturonique, teneur en sucres neutres, masse moléculaire) et des facteurs extrinsèques (pH, force ionique, nature et teneur en cations divalents, concentration de la pectine) sur la conformation des chaînes de pectine en solution mais aussi sur l'aptitude de ces polyosides à fixer les cations divalents. Ensuite, nous présenterons les différents mécanismes d'association entre la pectine LM et des cations divalents en régime dilué ($c < c^*$) et en concentration élevée de pectine ($c \approx c^*$).

Dans le deuxième chapitre, nous nous sommes intéressés, de façon comparative, à l'étude de la conformation en solution de la pectine LMP et de l'acide polygalacturonique (PGA) ainsi qu'à leur capacité à fixer les ions calcium en fonction de la teneur en NaCl.

Dans le troisième chapitre, nous avons étudié, en régime semi-dilué ($c < c^*$), les associations entre ces deux polyélectrolytes et des cations divalents appartenant à la famille

des alcalinoterreux (Ca^{2+}, Ba^{2+}, Mg^{2+}) et un métal de transition (Zn^{2+}). Notre objectif est de décrire le mode d'association entre les acides carboxyliques du polymère et le cation divalent, de proposer un mécanisme d'association et d'obtenir des informations sur la structure finale du réseau polyosidique.

Dans le quatrième chapitre, nous avons étudié la cinétique de gélification et les propriétés rhéologiques des gels du PGA en fonction de la nature et de la concentration des cations divalents (Ca^{2+}, Zn^{2+}, Ba^{2+}, Mg^{2+}). Ces études ont été réalisées en régime concentré. L'objectif est d'évaluer l'impact de la concentration en cations divalents dans la migration du front de gel et sur la structure finale de ce dernier.

Nous nous sommes focalisés dans le dernier chapitre à l'étude des matrices d'encapsulation formulées à partir de trois types de polyosides (PGA, LMP, ALMP - pectine faiblement méthylée et amidée) pour encapsuler la rutine. Ainsi, nous avons étudié la cinétique de libération de cette molécule dans un milieu intestinal simulé en fonction de la nature du polyoside. Les résultats ont été ensuite discutés sur la base du réseau polyosidique développé en relation avec les propriétés rhéologiques des solutions polyosidiques.

Enfin, une conclusion reprendra l'ensemble des points que nous avons demontré au cours de ce travail de thèse et proposera des perspectives.

CHAPTER 1

BIBLIOGRAPHIC STUDY

1.1. Context of the study

In pharmaceutical industry, pectin can be used to formulate dosage forms for colonic delivery. Indeed, these dosage forms based on pectin are more resistant to the low pH in the stomach and could rapidly be degraded by microorganisms in the colon (Chotiko and Sathivel, 2016). These pharmaceutical dosage forms can be obtained by using a pectin solution containing an active pharmaceutical ingredient (API) in contact with a cross-linking cation (such as calcium ions). Thus these dosage forms can be produced using two methods (Fig. 1 - 1). In the first method, the gelation occurred instantaneously (Fig. 1-1a), producing the formation of pectinate beads. In the second method, the gelation occurred by a slow diffusion of the cations through a membrane (Fig. 1-1b), creating a pectinate film. After curing 5 min in divalent cation solution, these dosage forms were then collected and dried in an oven at 37 °C during 40 h and stored at 4 °C before using for their evaluation.

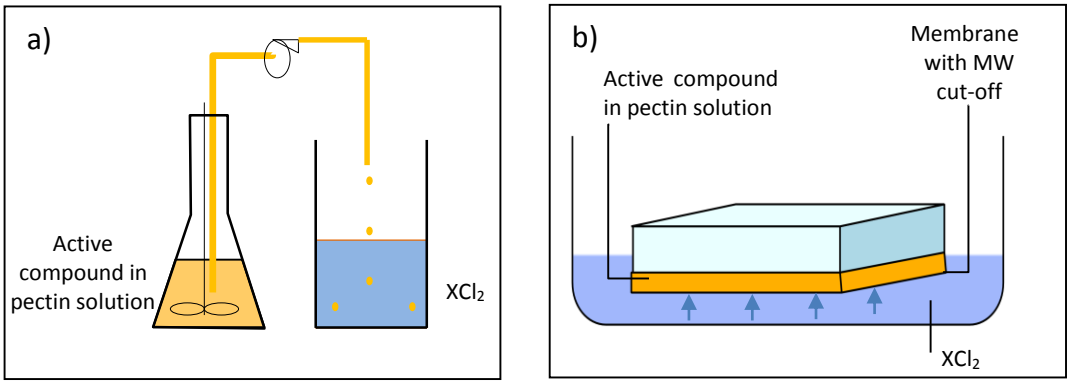

Fig. 1-1. Schematic illustration for encapsulation of active compound by ionic gelation: bead forms (a) and film forms (b)

Thus calcium pectinate dosage forms are widely used to encapsulate many drugs into microparticles such as theophylline (Dhalleine *et al.*, 2011), indomethacin and sulphamethoxazole (Munjeri *et al.*, 1997). These matrices could also be used for bioactive compounds in functional foods such as curcumin (Nguyen *et al.*, 2014), rutin (Luo *et al.*, 2015). During the gelation of the pectin, it was demonstrated that many parameters such as the nature and the content of the divalent cation, the nature and the concentration of the pectin can provide different structures of these dosage forms with various physicochemical and pharmaceutical properties.

Using LMP with the degree of esterification (DE) of 28% and at a concentration of 20 g L^{-1}, Jung *et al.* (Jung *et al.*, 2013) have shown that the encapsulation efficiency (EE) for indomethacin obtained about 38.9%, 45.3% and 54.8% when the Ca^{2+} concentrations were

100, 200 and 300 mM, respectively. The difference in the EE was explained by the structure of pectin beads in terms of the number of cross-links within the polymer matrix. In addition, they have noted that Ca^{2+} concentration was also an important factor to control the drug release rate. The EE increased and the release rate decreased significantly when the Ca^{2+} concentration increased from 100 mM to 300 mM (Jung *et al.*, 2013).

Additionally, drying condition and gelation time influence the size of beads, the EE and the release characteristics of drug from calcium pectinate beads (Sriamornsak and Nunthanid, 1999). According to Ahrabi *et al.*, the final structure of Ca-pectinate beads had an important effect on the drug release (Ahrabi *et al.*, 2000). The controlled drug release mechanism was mainly based on diffusion and erosion mechanisms. In fact, water should penetrate into the polymer network, which induces an increase of the swelling of the polymer and then the drug can diffuse out from the matrices. Thus, the swelling ability of hydrogel influences the drug release rates. Carbinatto *et al.* have studied the dissolution of pectin-amylose tablets (Carbinatto *et al.*, 2014). They have observed a low swelling rate which was attributed to the high cross-linking degree such that the mesh size of the polymer network limits the water entrance in the polymer structure and decreases the drug release rate. The swelling behavior may also depend on the pH and the ionic strength of the dissolution media. Sriamornsak and Kennedy showed that calcium-pectinate film swelled less in water and acidic media but extensively swelled in 100 mM NaCl (Sriamornsak and Kennedy, 2008). The high swelling of the film in 100 mM NaCl was due to the calcium-sodium ion exchange, creating a loose and porous structure, which allowed a high water uptake into the film. Assifaoui *et al.* (Assifaoui *et al.*, 2011) have shown that the composition of the dissolution media had an impact on the drug release profile (Fig. 1-2). The release profiles of rutin for both calcium (noted, CPGR) and zinc beads (noted, ZPGR) were lower in Gomori buffer than in the two others buffers studied, and no significant difference in CPGR and ZPGR dissolution profiles was observed. In Mc Ilvaine's buffer, the release profiles were different from CPGR and ZPGR; however, with these both beads 60% of rutin release was achieved after 3h of dissolution test. In Sorensen's buffer, rutin release was slower for ZPGR than for CPGR. Cations diffused from the bead surface and then interacted with the phosphate ions present in the dissolution medium to make a precipitate. In addition, this study showed that the nature of divalent cation (Ca^{2+}, Zn^{2+}) had an effect on the structure of pectin beads and thus on pharmaceutical and physicochemical properties (encapsulation efficiency, swelling properties, *in vitro* drug release). According to

the literature, we can note that the pharmaceutical and physicochemical properties of dosage forms depend on many parameters (the nature and the content of both the pectin and the cross-linking agents). The difference in the drug release profiles can be due to the difference in the structure of the network formed during the gelation process.

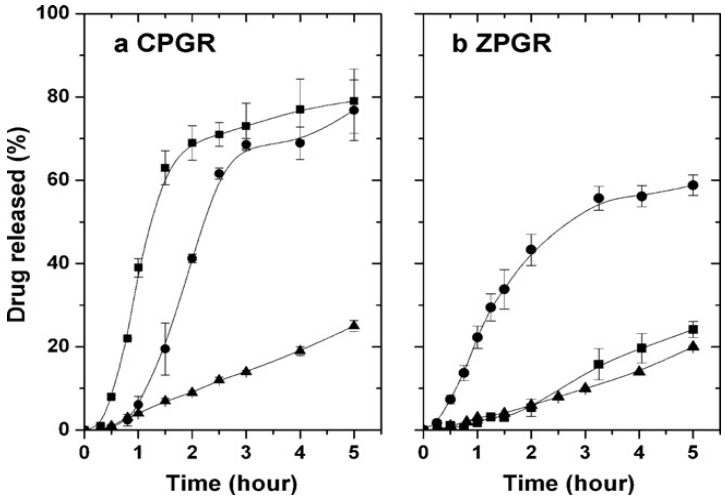

Fig. 1-2. Release profiles of rutin from calcium and zinc pectinate beads at fixed pH = 7.3 in three different buffers: square: Sorensen's, circle: Mc Ilvaine's and triangle: Gomori-buffer

The swelling of matrix also decreases with decreasing the DE and/or the DA due to an increase in the galacturonic acid (GalA) content in the pectin, thus decreasing macroporosity, reducing drug release ability and prolonging microsphere degradation time. Hence, it is favorable to create macroporosity in microspheres formed by amidated low methoxyl pectin (ALMP) and calcium ions (Girod *et al.*, 2010). In addition, the presence of amide groups in ALMP leads to a decrease of free carboxyl groups to cross-link with calcium ions. The gel structures are partially stable through the formation of hydrogen bonds between the amidated regions, forming less rigid gels (Alonso-Mougán *et al.*, 2002). Kim *et al.* (Kim *et al.*, 2016) have shown that the release of hydrophobic aroma compounds (alcohols, ketones, aldehydes, and esters) from freeze-dried gels of ALMP-Ca was higher than LMP-Ca. This can be explained by the ALMP required less calcium to form the gel and favored of the encapsulation of aroma compounds within pectin due to hydrogen bonding.

The aim of this thesis is to encapsulate active compound in pectin network using various divalent cations as cross-linking agents. We will focus on the study of the structure of the pectin (Section 1.2) and the conformation of this biopolymer in the solution (Section 1.3). Then, we will present the different mechanisms proposed by several authors for binding calcium to pectin in diluted regime (Section 1.4). When the concentration of the biopolymer

is high, the interaction between pectin and divalent cations induced the formation of a gel. Thus, we will discuss the rheological properties and the process of gelation of these systems (cation-pectin) (Section 1.5).

1.2. Overview on pectins

1.2.1. Sources of pectins

Pectins are a class of complex polysaccharides found in plant cell walls, where they play an important role as hydrating agents and cementing materials for the cellulosic network (Mualikrishna and Tharanathan, 1994). Pectins are extracted from cell walls of citrus and apple, less often also from grapefruit and sugar beet. Commercial pectins can be classified into high methoxyl pectin (HMP) with DE > 50% and low methoxyl pectin (LMP) with DE < 50% (Kim *et al.*, 1978). Moreover, amidated low methoxyl pectin (ALMP) is obtained from high methoxyl pectin when ammonia is used in the alkaline de-esterification process. ALMP is characterized by the DE and the DA. The number of sources used for the commercial production of pectins is limited because the ability of pectins to form gel depends on the molecular weight and the DE; the pectin from different sources does not have the same gelling ability due to variations in these parameters.

1.2.2. Structure of pectins

Pectin is extracted from cell walls by different methods, including hot acid, mild alkaline treatment, and chelating compounds. It has a complex structure, containing four galacturonic acid-rich polysaccharides: homogalacturonan, rhamnogalacturonan I, substituted galacturonan rhamnogalacturonan II (RG-II) and xylogalacturonan (XGA) (Fig. 1-3).

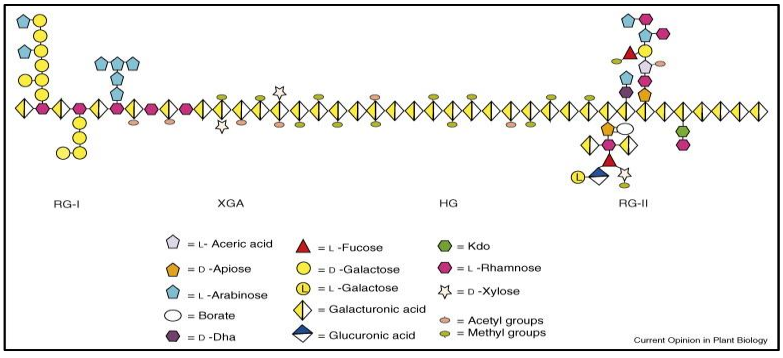

Fig. 1-3. Schematic structure of pectin showing homogalacturonan (HG), xylogalacturonan (XGA), rhamnogalacturonan I (RG-I) and rhamnogalacturonan II (RG-II) linked to each other (Scheller et al., 2007)

Consequently, pectin is an anionic polysaccharide that has linear regions formed by D - galacturonic acid (GalA) monomers, linked by α-(1,4) glycosidic bonds, and branched regions formed chiefly by various types of neutral monosaccharides (mainly rhamnose, xylose, mannose, glucose, galactose, and arabinose) linked together. The GalA units have carboxyl groups, which may be present as free carboxyl groups or methyl-esterified groups depending on the origin, isolation, and processing of pectin (Caffall and Mohnen, 2009; Mohnen, 2008; Ridley *et al.*, 2001; Thakur *et al.*, 1997; Yapo, 2011).

1.3. Conformation of pectin chains in solution

1.3.1. Solubility

Solubility of pectin in water is related to their degree of polymerization, number and distribution of methoxyl groups (Thakur *et al.*, 1997). Generally, solubility increases with decreasing molecular weight and increasing the esterified carboxyl groups. Thus, Tho *et al.* (Tho *et al.*, 2003) showed that pectinic acid with degree of esterification (DE) < 10% has a low water-solubility. Moreover, the pH, the temperature, the nature of the neutral sugar present have a marked effect on solubility (Rolin, 1993; Simpson *et al.*, 1984). It can be noted that the presence of D-glucose and other compounds (other monosaccharides, soluble dietary fiber) increase hydration and dispersibility characteristics of LMP. Dry powdered pectin in water has a tendency to hydrate very rapidly, which induces the formation of clumps. The solubilization of such clumps remains very slow (Thakur *et al.*, 1997). An increase of stirring and/or of temperature can overcome this problem. In addition, the presence of charged groups increases pectin solubility due to the electrostatic repulsions between carboxylate anions preventing aggregation of the polymer chains (BeMiller, 1986).

1.3.2. Physicochemical properties of pectin chains

1.3.2.1. Effect of the concentration of polyelectrolyte

The conformation and the flexibility of pectin take an important part in the structure-function relationship and their applications in food and pharmaceutical industries. Investigations on the viscosity of citrus pectin solutions in 0.1 M of NaCl were performed over a large range of concentrations extending from dilute to concentrated regimes (Axelos *et al.*, 1989). Fig. 1-4 shows the zero-shear specific viscosity (η_{sp}) as function of the coil overlap

parameter (the volume filling of a solution by a polymer) (C[η]). They observed a classical behavior with the transitions from dilute to semi-dilute solution at a specific concentration noted c*, and from semi-dilute to concentrated solution at an another critical concentration c** >> c*. The c* and c** are called overlap concentration and limit concentration, respectively. The c* was found at a value of 0.7 (corresponding to 5 g L^{-1} of pectin concentration) and the c** was obtained at an approximate value of 1 (corresponding to 10 g L^{-1} of pectin concentration). The gradients (slopes) for the dilute regime and concentrated regime were 1.2 and 3.3 for all studied pectin samples by Axelos *et al.* (Axelos *et al.*, 1989). Also, the overlap concentration c* obtained for the LMP (DE ~ 37%) at pH = 5 was equal to 4 g L^{-1} (Ström *et al.*, 2014).

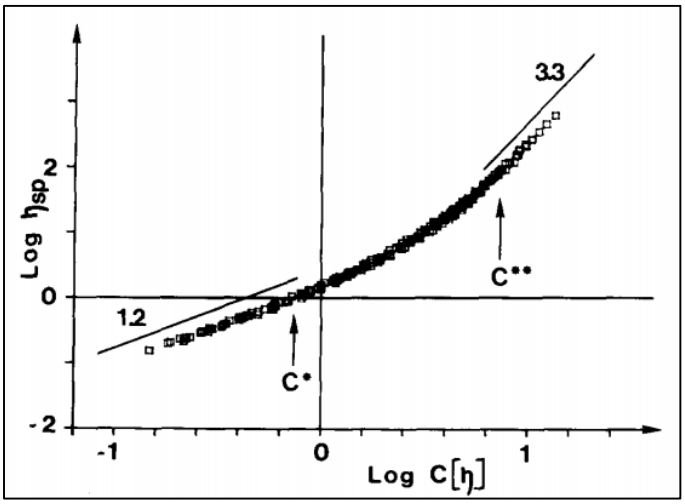

Fig. 1-4. η_{sp} versus c[η] curve in a log-log plot for all the citrus pectin samples with DM range between 30 and 72%. c is the overlap concentration between dilute and semi-dilute regimes; c** is the boundary concentration between semi-dilute and concentrated regions (Axelos et al., 1989)*

1.3.2.2. Effect of monovalent cations

Many authors have studied the interaction between polyelectrolytes (pectin, chitosan, xanthan, gellan, alginate) and various monovalent cations (Na^+, K^+, Li^+, NH_4^+) in order to evaluate the capacity of gelation (Graham, 1991; Karakasyan *et al.*, 2010; Wehr *et al.*, 2004) or to understand organization and flexibility of polymer chains (Baños *et al.*, 2014; Cros *et al.*, 1999). Indeed, several studies have shown that the conformation of positively charged polymers (chitosan (Morariu *et al.*, 2012)) or negatively charged polymers (xanthan (Carrington *et al.*, 1996), pectin (Jonassen *et al.*, 2013)) depends on the nature and the concentration of monovalent cations.

The flexibility parameter (B) was used to evaluate the flexibility of polymer chains, and it is related to the stiffness parameter (S) by the equation: $B = S/([\eta]^{\nu})$, where the exponent (ν) depends on the nature of the polymer and the intrinsic viscosity [η] at an ionic strength of 0.1 M could be correlated to the unperturbed dimensions of the molecules (Smidsrød and Haug, 1971). Chanliaud *et al.* (Chanliaud *et al.*, 1997) have found that the stiffness parameter of heteroxylans depends on the nature of the monovalent cation. Indeed, the values of the stiffness parameter were equal to 8.37, 5.57 and 4.25 for the polyelectrolyte in KCl, NaCl and LiCl solutions, respectively. Moreover, Yoo *et al.* (Yoo *et al.*, 2009) have suggested that the gel strength of LMP may be enhanced by using larger monovalent cations ($K^+ > Na^+ > Li^+$) and by lowering the DE value. The conformation of carrageenan (anionic polymer) at varying NaCl concentrations (0 - 0.1 M) was studied by the atomic force microscopy (Schefer *et al.*, 2015). They have shown that the flexibility of the polymer chains was greater at low NaCl concentration, whereas they have observed the formation of an intramolecular single helix at high NaCl concentration. Ström *et al.* (Ström *et al.*, 2014) have shown that the addition of monovalent ions (Na^+) changes the aggregation of stiffened pectin chains (at pH = 3) and induces a gel without divalent cations. The stiffened pectin chains may be due to the intra- and intermolecular hydrogen bonds, which are formed between protonated and unprotonated carboxyl groups (Walkinshaw and Arnott, 1981). With increasing Na^+ concentration, a decrease in hydrogen bonds and repulsive electrostatic interactions between the pectin chains caused the aggregation.

The linear flexibility of polymer chains is represented in terms of the persistence length (Lp). It is defined as the average projection length along the initial direction of the polymer chain (Morris *et al.*, 2008) (Fig. 1-5a). The number of monomers per persistence length depends on the solvent and the concentration of polymer. Indeed, Axelos *et al.* (Axelos *et al.*, 1987) have studied the citrus pectin (DE = 38%) in solution (0.4 – 24 g L^{-1} pectin; 100 mM NaCl, pH = 7) by viscosimetric measurements, small angle neutron scattering (SANS) and photon correlation spectroscopy. They have described this pectin as a semi-flexible molecule with a persistence length (Lp) of 4.5 nm, corresponding to 10 Gal monomers. Catoire *et al.* (Catoire *et al.*, 1997) have investigated the Lp of sodium pectate (25 g L^{-1}) in 2.5 mM NaCl solution by nuclear magnetic resonance study and found a Lp of 13 nm, corresponding to 29 Gal monomers. The difference in the persistence length may be due to the different concentrations of polymer and NaCl. A recent study (Schmidt *et al.*, 2009) have shown by

SANS measurements a classical behavior of polyelectrolyte chains in solution: a transition between a $q^{-1.7}$ behavior at low q (self-avoiding chain behavior) and a q^{-1} behavior at larger q (rod-like behavior) (Fig. 1-5b). They have also extracted a persistence length of 8 nm, which is different from what was obtained from earlier investigations. They have attributed this to the origin of the pectin and the experimental conditions (the concentration of the polyelectrolyte, the ionic strength, and the pH).

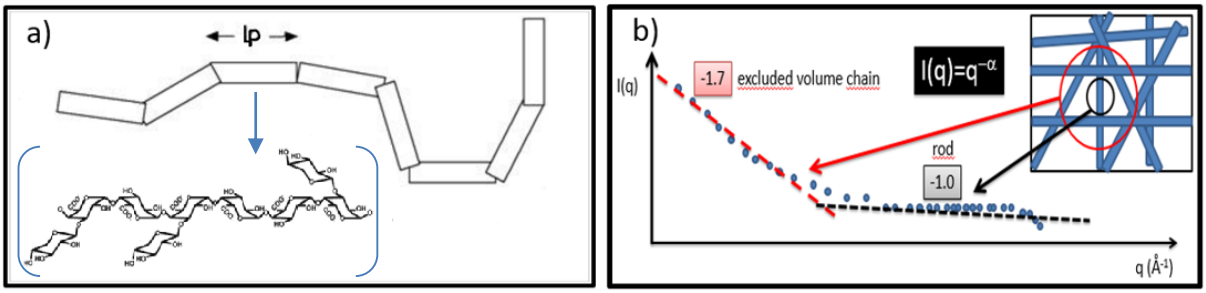

Fig. 1-5. Schematic representation of the persistence length (Lp) of a self-avoiding chain (a); representation of structural parameters found from SANS data for LMP (b)

Morris *et al.* (Morris *et al.*, 2008) have studied the conformation/flexibility of pectins with different DE (17 – 70%) in 0.1 M NaCl solution. They found an extended coil conformation with the persistence lengths all within the range Lp = 10 – 13 nm (for a fixed mass per unit length). The flexibility parameter B was determined by the intrinsic viscosity with the ionic strength and values between 0.072 and 0.017 indicating that pectins can be considered as a stiff molecules (Axelos and Thibault, 1991). Axelos and co-worker have also suggested that an increase in flexibility is noticeable with the increase of the DE and the amount of amide groups of the pectic acids (Axelos and Thibault, 1991).

Furthermore, Cros *et al.* (Cros *et al.*, 1999) have investigated the behavior of pectins with different degrees of methylation (DM = 28 – 73%) in 0.1 M NaCl solution by SANS, viscosimetric, and molecular modeling studies. They have found that the persistence lengths obtained from intrinsic viscosity measurements, ranged from 5.9 to 12.6 nm and did not depend on the DE, whereas those obtained by SANS were between 4.5 and 7.5 nm. These values correspond to 10 - 17 monomer units. In addition, the conformation of isolated pectin chains was studied by low angle laser light scattering, viscosity and size exclusion chromatography experiments in 0.2 M NaCl, giving values of 6.7 nm and 0.6 nm for the persistence length and the hydrodynamic diameter, respectively (Hourdet and Muller, 1991).

The intrinsic viscosity [η] is related to the specific volume of macromolecular species in the dilute solution (isolated macromolecules or aggregates) and the Huggins constant

(k_H – a polymer-solvent interaction parameter) can indicate the nature of the interactions between solvent molecules and the macromolecular species in the solution (Durand, 2007). It is also shown that the intrinsic viscosity of a polymer solution depends on the nature of the solvent, the temperature, and the concentration. Usually, for pectins, the intrinsic viscosity decreases when the ionic strength increases and when the degree esterification (DE) decreases (Fishman *et al.*, 2001; Morris *et al.*, 2008). Some studies have used the exponent (α) from the Mark-Houwink-Sakurada equation ($[\eta] = KM_w^{\alpha}$) to evaluate the conformation of LMP in solution. The value of α ranged from 0.5 to 0.8 may correspond to random coil in good solvent while α value ranged from 0.8 to 2 may correspond to rigid or rod-like (stiff chain) (Harding *et al.*, 1991). The value of $\alpha \approx 0.82$ indicated that the shape of pectin in water (DM = 6.7%) is a rod-like (Masuelli, 2011). Also, Hua *et al.* (Hua *et al.*, 2015) have indicated a stiff rod-like conformation of LMP in dilute solution. On the other hand, they have also suggested that the strong charge-charge repulsion of carboxyl groups in LMP at pH = 4.5 caused an increase of the rigidity and length of LMP. Moreover, the intermolecular electrostatic repulsions and steric hindrance are inversely proportional to intermolecular distance and have a negative effect on the expansion of LMP chains. Upon dilution, LMP chains are allowed to further extend and hydrate with neighboring water molecules, leading to a stiff rod-like conformation covered with hydration layers.

Fishman *et al.* (Fishman *et al.*, 2001) have investigated the turbidity of pectins with different DE (1.7 – 91%) in salt solutions (K^+, Na^+, Li^+). They have shown that the turbidity increases with increasing DE in most solvents because the percentage of GalA increases as DE decreases and this is more likely to cause precipitation by monovalent ions. Moreover, the turbidity depends on the nature of monovalent ions. Indeed, it appears that Li^+ gives the lowest turbidity comparing to others because Na^+ or K^+ may cause precipitation or gelation with LMP. Pectins in pure water have the higher turbidity than in solutions containing monovalent ions. This is probably due to the tendency of pectins to aggregate in water, which is reflected by the larger size and higher viscosity (Fishman *et al.*, 1989).

1.4. Binding of divalent cations to LMP in diluted regime (c < c*)

1.4.1. Mode of association between calcium and polyuronate chains

Understanding the conformation of LMP in solution allows to modulate the interaction between this polyelectrolyte and divalent cations. The interaction of Ca^{2+} with LMP has been

studied extensively. Indeed, the strength of this interaction is influenced by both intrinsic factors (molecular weight, distribution of methyl esters, side chains, DE) and extrinsic factors (pH, ionic strength, Ca^{2+} concentration, and temperature) (Capel *et al.*, 2005; Cardoso *et al.*, 2003; Fraeye *et al.*, 2009; Kjøniksen *et al.*, 2004; Lootens *et al.*, 2003; Ström *et al.*, 2007). Among these, pH is an important factor affecting the gelation of LMP. The electrostatic attractions are strongest when the pectin is almost fully negatively charged at pH > 4.5 (pH above the pKa of carboxyl groups). Hence gels can be easily formed in the presence of Ca^{2+} at high pHs (Capel *et al.*, 2006).

Calcium ions enter into cavities provided by the pairing of the polygalacturonate sequences which are described in terms of the so-called “egg-box” model (Fig. 1-6A) (Grant *et al.*, 1973). At a molecular scale, this model considers that a calcium ion is coordinated to 10 oxygen atoms from two guluronate chains. These include four hydroxyl oxygens (O1 - O4), one other oxygen (O5) and one carboxyl oxygen (O6) for each chain (Fig 1 - 7). However, this model was questioned by Braccini and Perez, who argued that the coordination of calcium in calcium-carbohydrate complexes is usually between 7 and 9 (Braccini and Pérez, 2001). Indeed, among all these oxygens, only four (O6 and O2/O3 from two opposite carboxyl and hydroxyl groups) strongly interact with calcium (distance < 3 Å) in a monodentate coordination. Because of the structural analogy between polyguluronate (alginate) and polygalacturonate (pectin) chains, the alginate system can be transposed to the pectate system. Thus, Braccini and Perez (Braccini and Pérez, 2001) have observed by MD simulations that the most favorable antiparallel associations of guluronate and galacturonate chains can be considered as “shifted egg-boxes”. This shift is small in the case of guluronate units (1.1 Å) and more pronounced in the case of galacturonate units (1.7 Å). This difference in the structure in galacturonate associations has three important consequences: (1) it leads to an efficient association with numerous van der Waals contacts (the chains fit into each other); (2) it reduces the original large cavity and provides two symmetrical sub-cavities of appropriate size for binding a calcium ion (Fig. 1-6B); (3) it creates an efficient periodic intermolecular hydrogen bonding network. Plazinski (Plazinski, 2011) has also suggested, by molecular dynamic simulations, a shifted egg-box model for calcium-polyguluronate chains. Such a coordination pattern was interpreted as the result of competition between water molecules and carboxylic groups of polyguluronate for calcium ions.

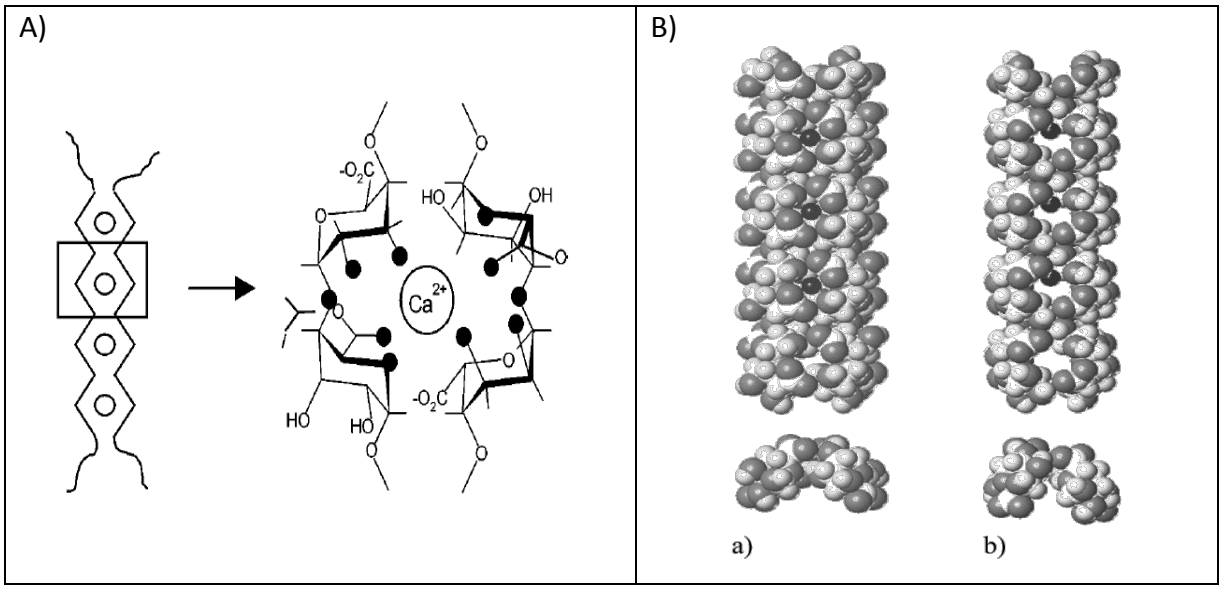

Fig. 1-6. (A) Egg-box structure of the cross-link between a calcium and guluronate monomers of two different alginate chains. (B) Comparison of the egg-box models for (a) guluronate and (b) galacturonate chains, respectively; dark circles represent the calcium ions (Braccini and Pérez, 2001)

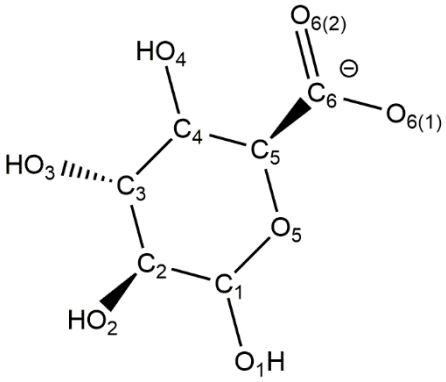

Fig. 1-7. Schematic structure of galacturonic acid

1.4.2. Mechanism of binding calcium to polyuronate

Considerable attention has been paid to the study of the binding mechanisms of pectin chains to explain the affinity of some anionic polysaccharides (alginate and pectin) towards divalent cations such as Ca^{2+} (Braccini and Pérez, 2001; Cescutti and Rizzo, 2001; Donati *et al.*, 2009; Fang *et al.*, 2008; Fang *et al.*, 2007; Grant *et al.*, 1973; Thom *et al.*, 1982). The association between LMP chains is due to three types of interactions: (i) hydrophobic association between methyl ester groups, (ii) hydrogen bonds between galacturonic acid and/or hydroxyl groups, and (iii) ionic interactions between galacturonate unit (Gal) groups mediated by Ca^{2+}-bridges (Kjøniksen *et al.*, 2004). Previous studies on calcium-pectin binding have shown that a minimal number of consecutive Gal groups, estimated to lie between 8 and 15, is required to form a

stable cross-link structure between two chains in the presence of calcium (dimerization) (Liners and Van Cutsem, 1991; Luzio and Cameron, 2008; Powell *et al.*, 1982). Chain association occurs by dimerization, which corresponds to long chain segments where cations are sandwiched within the dimer on specific sites along each of the inner surfaces (egg-box structure). The changes in the conformation and in the structure are due to the binding of these cations with carboxylate groups displacing some of the pre-condensed monovalent cations (Kohn, 1975).

Using isothermal titration calorimetry (ITC), De and Robinson found a two-step binding process between Ca^{2+} and alginate at various NaCl concentrations (0 - 100 mM) (De and Robinson, 2003). The first binding step was found to be entropically driven, whereas the second one exhibited a weaker affinity and was both entropically and enthalpically driven (De and Robinson, 2003). Indeed, they have shown with 10 mM of NaCl, the primary binding affinity between calcium and alginate was 77 x 10^4 M^{-1} and was entropically driven (ΔH_1 = 1.5 kJ.mol^{-1}) whereas the second binding affinity was weaker (K_2 = 1.3 x 10^4 M^{-1}) and both enthalpy and entropically and enthalpically driven (ΔH_2 = -16.1 kJ.mol^{-1}) . Fang *et al.* (Fang *et al.*, 2007) have also observed the shame shape of ITC thermogram for the binding of calcium to alginate (Annex 1) and they found thermodynamic parameters for the second process (K_2 = 1.1 x 10^4 M^{-1} and ΔH_2 = -15.0 kJ.mol^{-1}). From ITC data, Fang *et al.* have also proposed that the binding of Ca^{2+} to alginate occurs in multiple steps including monocomplexation at a low molar ratio, R = $[M^{2+}]/[Gal]$, followed by dimerization (0.25 < R < 0.55) and, then, by the lateral association of dimers (multimerization) (R > 0.55) (Fig. 1-8A) (Fang *et al.*, 2007).

It must be pointed out that owing to the rather low affinity constant for the COO^--M^{2+} interaction in various monoacids, monocomplexation refers to a state where the exchange between bound and unbound cations continuously occurs. For low methoxyl pectin (branched polymer), these authors (Fang *et al.*, 2008) suggested that only two steps occurred: mono-complexation (R < 0.25) followed by a progressive dimerization step (R > 0.25). The absence of significant lateral association with low methoxy pectin (LMP) was interpreted in terms of structural features of pectin: the random distribution of ester and/or amide groups along the pectin chain introduces much more defects into the formation of dimers and even hinders the subsequent lateral association of dimers (Fang *et al.*, 2008). According to above results, there were two thermal processes for LMP in the presence of calcium. The first process was entropically driven and may be ascribed not only to the formation of monocomplexes

between divalent cations and carboxylate groups (Fang *et al.*, 2007), but also to the formation of point-like cross-links (Ventura *et al.*, 2013). The second process was exothermic and may correspond to the formation of an ordered structure (dimers or multimers). Borgogna *et al.* (Borgogna *et al.*, 2013) suggested by means of viscosity, circular dichroism, light scattering, and fluorescence measurements on alginate that the point-like cross-links involve four guluronate residues arranged in a locally tilted conformation, which they referred to as "tilted egg-box" (Fig. 1-8B). It can be noted that cations from these point-like cross-links are probably loosely bound, which allows the subsequent dimer formation (strong cross-linking). When analyzing small-angle X-ray scattering (SAXS) data on LMP in the presence of calcium ions, Ventura *et al.* have underlined the importance of point-like cross-links in the gelation mechanism of LMP (Ventura *et al.*, 2013). Indeed, for low molar ratios, they suggested the coexistence of monocomplexes, dimers, and point-like cross-links. Their results imply that when the molar ratio increases, the number of rod-like junction zones (dimerization) decreases and the number of point-like crosslinks and monocomplexes increases (Fig. 1-8C). Furthermore, the binding mechanism is influenced by several factors such as the nature, the composition, and the concentration of the polymer, the pH, the ionic strength, the presence of anions, and, in particular, the nature of divalent cations.

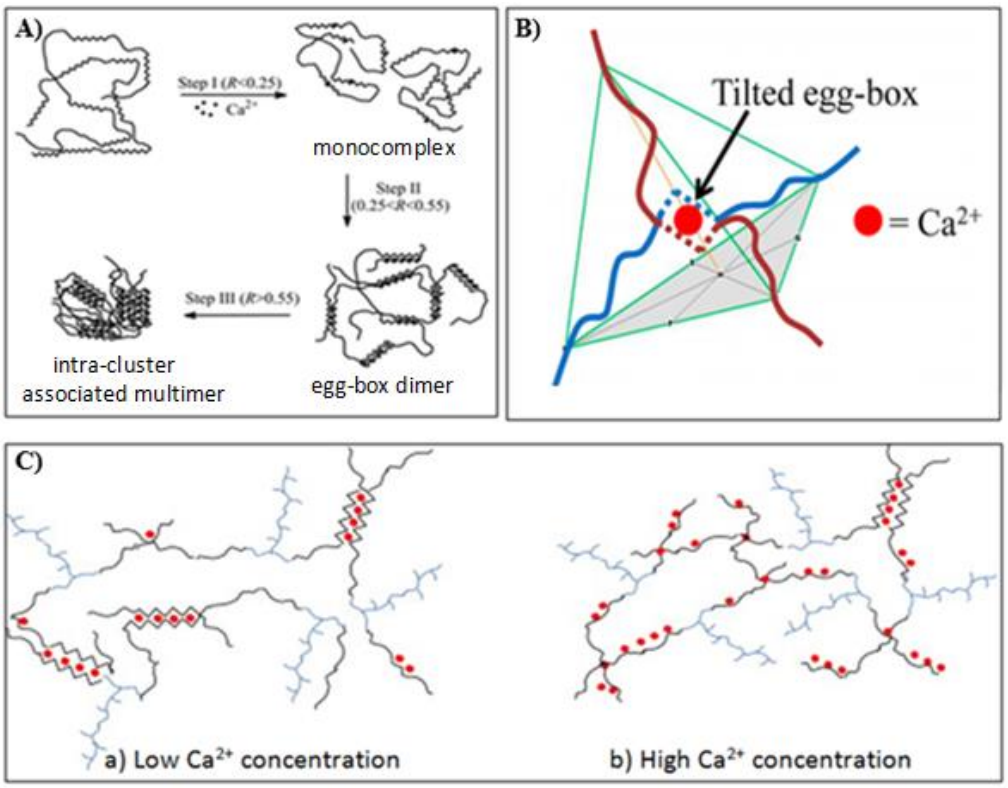

*Fig. 1-8. (A) Association mechanism of Ca-*alginate *(Fang et al., 2007); (B) "Tilted egg-box" - Orientations of alginate chains interact with the calcium are different (Borgogna et al.,*

2013); (C) Hypothetical structure of Ca-LMP at low Ca^{2+} concentration (a) and high Ca^{2+} concentration (b) (Ventura et al., 2013)

The affinity of alkaline earth metals for alginate and pectin was found to increase in the following order $Mg^{2+} << Ca^{2+} < Sr^{2+} < Ba^{2+}$ (Kohn, 1975). In addition, a comparative study of the interactions of Ca^{2+} and Mg^{2+} cations with polyGal using ultracentrifugation, conductometric titration, potentiometry and circular dichroism showed that Ca^{2+} cations were able to coordinate with two carboxylate groups and to induce inter-chain associations, whereas Mg^{2+} complexation with polyGal was electrostatic bound only (Malovíková *et al.*, 1994). Raman spectroscopy studies suggested different interaction modes between polyacrylate anionic polymers and divalent cations: the formation of covalent bonds in the case of Cu^{2+}, Zn^{2+} and Mn^{2+} and electrostatic interactions in the case of Mg^{2+} and Ba^{2+} (Koda *et al.*, 1983). Gelation with magnesium cations was also found to depend strongly on alginate's chemical composition, as the presence of long sequences of guluronate units favors faster gel formation (Donati *et al.*, 2009; Topuz *et al.*, 2012).

1.5. Binding of divalent cations to LMP in concentrated regime (gels)

The most important property of pectins is their ability to form gels in the presence of cations. LMP forms networks in the presence of most di- and trivalent ions, e.g., Ca^{2+} (Thibault and Rinaudo, 1985). Consequently, the carboxyl groups play an essential role in forming LMP gel with Ca^{2+}. It was also indicated that the zones of attachment between the chain molecules are necessary for gel formation (Owens *et al.*, 1954). Hence, the pectin concentration is adjusted at a high level in order to obtain a high GalA concentration. Moreover, the pH should be higher because dissociated carboxyl groups take part in the salt-like cross-linkages. The LMP gel can be easily formed in the presence of Ca^{2+} at pH > 4.5 due to fully charged carboxylate groups (Capel *et al.*, 2006). The size of the egg-box junction zones is limited by the presence of sequences containing methyl-esterified galacturonic acid residues (Ngouémazong *et al.*, 2012). The lifetime of a junction zone in LMP gel depends on the strength of the electrostatic bonds, which depends on the length of the uninterrupted GalA segments that can interact. The bonds are stable when there are at least seven uninterrupted carboxyl groups on each participating chain (Powell *et al.*, 1982).

In addition, the pectin concentration need to be adjusted at varying stoichiometric ratios, ($R = 2[Ca^{2+}]/[COO^{-}]$) through the expression in GalA concentration. The cation concentration for gel formation depends on the DE of each pectin and is adjusted so that the stoichiometric ratios was equal to 0.2 (Garnier *et al.*, 1993). The formation of gel networks is based on this ratio and increases with growth of ratio. Moreover, pectin concentration also affects the gel strength. An increase in gel strength as the pectin concentration increases is a result of more free carboxyl groups for calcium ion linkage through pectin chains, which are held together, forming a strong gel (El-Nawawi and Heikal, 1995; Fraeye *et al.*, 2010).

The gelling properties of LMP depend on intrinsic factors (the degree of esterification (DE) and its distribution, neutral sugar content, and average molecular weight) (O'Donoghue and Somerfield, 2008; Yapo, 2009) and extrinsic factors (the pH, the temperature, the ionic strength, the nature and the content of divalent cations, the concentration of pectin and the gelation time). The mechanical properties of gels are assessed by many parameters, such as the storage modulus (G') which corresponds to the rigidity of the gel (i.e. its elastic contribution) and the loss modulus (G") corresponding to the dissipated energy (i.e. its viscous contribution). Furthermore, the microstructure of gels could be observed by different techniques such as confocal laser scanning microscopy or atomic force microscopy. Indeed, Löfgren *et al.* (Löfgren *et al.*, 2002) have described LMP-Ca gel as a phase-separated structure by confocal laser scanning microscopy (micrometer scale). The images also gave information on the length scale of the structure. Alginate-Ca gel exhibited much thicker and elongated structures at Ca^{2+} concentration of 1.2 mM ($R > 0.60$) by the atomic force microscopy, compared to those observed at Ca^{2+} concentration of 0.2 mM due to the aggregation of egg-box dimers predominating at higher Ca concentration (1.2 mM) (Liao *et al.*, 2015).

1.5.1. Mechanism of gelation and kinetics

The gelling process of LMP depends strongly on the concentration of divalent cations. It has been shown for LMP gels (10 g L^{-1}) at pH 6 that increased Ca^{2+} concentration results in faster gel formation (Lootens *et al.*, 2003). Hence, the concentration of divalent cation influences rheological properties of LMP gels. When Ca^{2+} concentration increases, G' and G'' increase (Lootens *et al.*, 2003; Zhao *et al.*, 2015) but gels also become more brittle (Kastner *et al.*, 2012). Capel *et al.* (Capel *et al.*, 2006) have shown that the gel strength decreased with increasing Ca^{2+} concentration (1- 6 mM) due to the formation of heterogeneous thermal gels or precipitation. In addition, the gel strength could decrease because of the repulsive forces

between positive charges on the polymer chains when the divalent cations are in excess and formation of $M^{2+}(COO^{-})$ bonds, instead of the $M^{2+}(COO^{-})_2$, which characterize the cross-links (Silva *et al.*, 2003). The aggregation of dimer egg-box structures into multimer structures requires not only the large non-methylesterified GalA blocks (Ngouémazong *et al.*, 2012) but also large amount of divalent cations (Debongnie *et al.*, 1987).

The rheological properties were observed to be clearly dependent on both the nature of the divalent cations and the polyelectrolytes. Agulhon et co-workers have studied the structure of hydrogel prepared from divalent cations (Mn^{2+}, Co^{2+}, Cu^{2+}) and alginate by using small angle x-ray scattering (SAXS) (Agulhon *et al.*, 2012). According to the guluronate content, alginates were respectively designated as HG and LG for "High G-content" and "Low G-content"). The corresponding percentages of guluronate units in the alginate backbone were 63% and 33% respectively (Agulhon *et al.*, 2014). They have shown that Cu-HG, Cu-LG and Co- HG behaved as viscoelastic solids (G' > G'') and no flow zone (G'' > G') was detected even at very low values of the frequency ($\omega < 10^{-4}$ rad s^{-1}), indicating an infinite terminal relaxation time. Whereas, Mn-HG, Mn-LG and Co-LG presented both elastic and viscous character (G'' > G' and G' > G'') for entangled polymers characterized by a finite relaxation time.

The structures of these hydrogels revealed different nanostructures depending both on the nature of alginate and divalent cations. Cu^{2+} seemed to interact strongly with both mannuronic and guluronic residues and induced a comparable fibrillar morphology whatever the guluronic content. With Co^{2+}, the guluronic fraction impacted the hydrogel morphology: the hydrogel presented a fibrillar structure when HG was used, whereas a complex morphology was observed with LG alginate. Mn^{2+} hydrogels displayed the nonfibrillar morphology that could be due to the non-cooperative interchain associations for all alginate types used.

The diffusion of Ca^{2+} ions into a solution of negatively charged polyanion (the poly(2,2-disulfonyl-4,4-benzidine terephthalamide - PBDT) has been studied (Wu *et al.*, 2014). A drop (25 µL) of PBDT solution was dropped by a syringe onto a sliding glass, and the solution spread with diameter and thickness of about 1.5 cm and 150 µm, respectively. Subsequently, a drop (5 µL) of $CaCl_2$ solution was dropped on the central part of the PBDT solution (Fig. 1-9a). The bottom of $CaCl_2$ drop immediately became turbid once it contacted with the PBDT solution, indicating that some Ca^{2+} ions formed complex with PBDTs. The free Ca^{2+} ions diffused into the surrounding PBDT solution and formed a complex with PBDTs, the turbid area gradually

increased. The whole process was observed in situ under a polarizing optical microscope. Photo images were taken every 10 s for 10 min.

The boundary was defined as the gelation front, which was a thin ring with birefringence color opposite to that of the liquid crystalline gel (Fig. 1-9b). They showed that the formation of hydrogel with the orientation of PBDT was perpendicular to the diffusion direction of Ca^{2+} ions. As the Ca^{2+} concentration was high at the diffusion front, it was favorable for the negatively charged PBDT molecules to orient parallel to the diffusion front, which ensured more complexation. However, the gel matrix, which was previously formed, hindered to some extent the diffusion of Ca^{2+} ions. This effect was reflected when the flux of Ca^{2+} cannot gelate all the PBDTs at once.

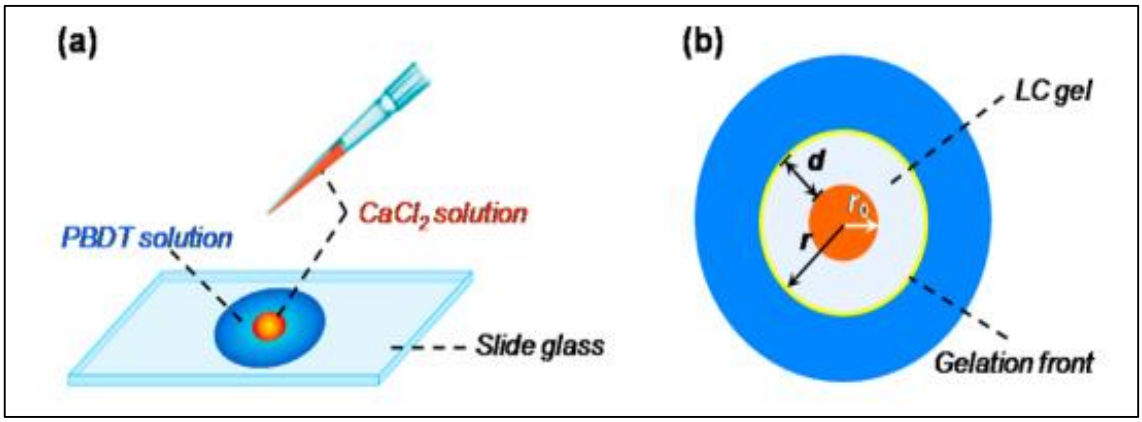

Fig. 1-9. (a) Schematic for the experimental diffusion of Ca^{2+} into PBDT solution. After one drop of $CaCl_2$ solution is dropped onto the central part of PBDT solution, the diffusion of Ca^{2+} induces the surrounding PBDT molecules orientation and gelation to form an anisotropic physical gel. (b) Top view of the diffusion system. r_0, r, and d denote the radius of $CaCl_2$ drop, radius of liquid crystalline (LC) gel, and the width of LC gel, respectively (Wu et al., 2014)

The LC gel width square (d^2) was plotted versus the diffusion time (t) in the following formula: $d^2 = 2Dt$, and the slope (D) of the linear lines gives the apparent diffusion coefficient of cations (Fig. 1-10). They have shown that the apparent D was affected by the nature and the concentration of cation, and the polymer concentration (C_p). Indeed, the apparent D increased when the Ca^{2+} concentration increased (Fig. 1-10a) and different slopes were observed for different metallic ions (Fig. 1-10b). In addition, increase in C_p decreased the apparent D of Ca^{2+} cations due to the consumption of more cations for complexation and the gel matrix hinders the diffusion of free cations. Moreover, comparing with the diffusion coefficient of Ca^{2+} in pure water (D_0), they have also found that when $C_{Ca}{}^{2+}$ = 100 mM, the D

was smaller than D_0 ($D/D_0 < 1$), whereas with C_{Ca}^{2+} = 500, 1000, and 2000 mM, the ratio of $D/D_0 > 1$.

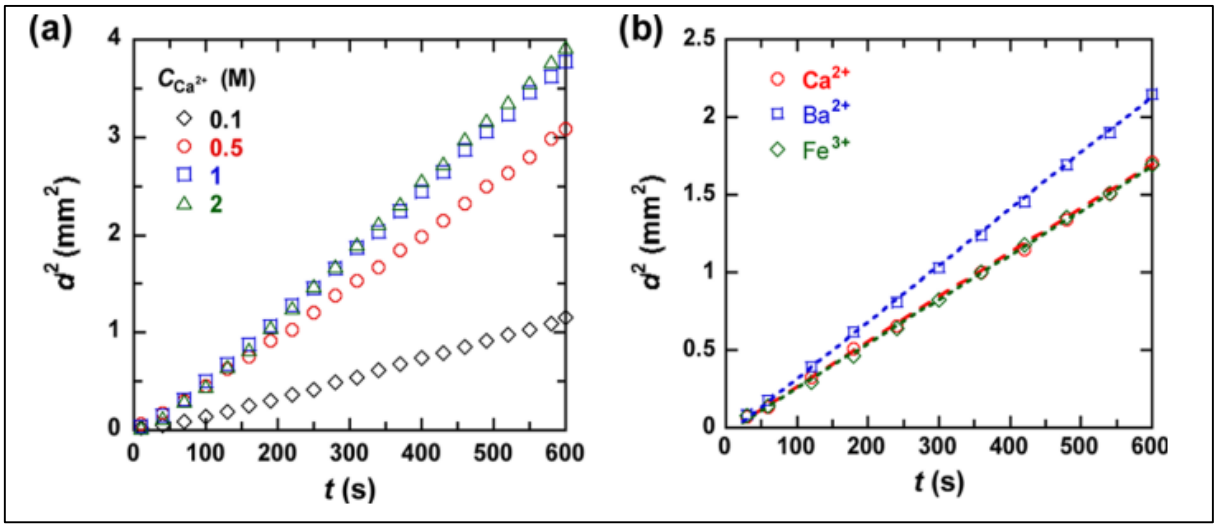

Fig. 1-10. Relationship of square of LC gel width (d^2) versus diffusion time (t): (a) systems with C_p = 10 g L^{-1} and different $C_{Ca^{2+}}$; (b) systems with C_p = 30 g L^{-1} and 500 mM of $CaCl_2$, $BaCl_2$, or $FeCl_3$

1.5.2. Effect of other factors on the gelation

- **Intrinsic factors**

The gelation of pectin in the presence of divalent cations such as calcium ions depends on the degree of esterification (DE) and the distribution of non-methyl-esterified galacturonic acid (GalA) residues. Indeed, when the DE of the pectin increases, the gel strength decreases as a result of low number of junction zones (Kim *et al.*, 1978; Kim *et al.*, 2008; Matthew *et al.*, 1990; Ngouémazong *et al.*, 2012). In this case, the network structures are governed by hydrogen bonding and hydrophobic interactions (Löfgren and Hermansson, 2007). Schmelter *et al.* (Schmelter *et al.*, 2002) have found that the elastic modulus G' of the de-methoxylated pectin gel was about 35 times higher than G' of a gel obtained with unmodified pectin in the presence of Ca^{2+} ions and pH = 4.5. Fraeye *et al.* (Fraeye *et al.*, 2010) have shown that more blockwise distribution of GalA allowed the formation of strong junction zones and stiff gels with Ca^{2+} ions. However, when the distribution of GalA was random and not long enough, the formation of junction zones by divalent cations was low. Consequently, the ability to form junction zones by divalent cations does not only depend on the amount of non-esterified galacturonic acid residues present but also on their distribution all along the polymer chain.

It is noted that pectins are characterized by an alternation of smooth (homogalacturonans) and hairy regions, rich in rhamnose and side-chains. The presence of rhamnose residue and neutral sugar side chains influences the rheological characteristics of Ca^{2+}-pectin gels. The insertion of a rhamnose unit will lead to the termination of a binding portion between Ca^{2+} ions and carboxyl groups of galacturonic acids (Lin *et al.*, 2005; Rees and Wight, 1971) but hydrogen bonding may occur between rhamnose segments (Silva *et al.*, 2003). Neutral sugar side chains are reported to improve the rheological characteristics of Ca^{2+}-pectin gels due to an increase in polymer chain entanglements (Hwang and Kokini, 1992; Ngouémazong *et al.*, 2012), eventually creating a tighter conformation, which allowed for stronger hydrophobic interactions and hydrogen bonding (Sousa *et al.*, 2015). Indeed, the neutral sugars, specifically arabinoses, which contain hydroxyl groups have been reported to contribute to the gelling of citrus pectin at temperatures below 50 °C (Kastner *et al.*, 2012). Investigating the elastic moduli (G') of gels by small amplitude shear strain oscillatory testing (at 25 °C, 1 Hz and using a torsion bar of 20 g cm), Oosterveld *et al.* (Oosterveld *et al.*, 2000) have found that the G' value decreased for sugar beet pectin degraded by enzymes (less neutral sugar), comparing to untreated pectins.

On the other hand, rhamnose inserts into the galacturonan chain rises hairy regions, thereby avoiding micelle formation with ensuing undesirable phenomena such as turbidity, syneresis, and precipitation (Voragen *et al.*, 1995). Moreover, sugar beet pectins have poor gelling properties due to a low molecular weight and a large proportion of hairy regions containing arabinose side chains (Hwang *et al.*, 1993). Hence, an enhancement of gelation properties was observed with sugar beet pectin when the amount of arabinose was decreased (Matthew *et al.*, 1990). Although the presence of branched domains in the pectin prevent the formation of junction zones with divalent cations because of steric hindrance (Yapo and Koffi, 2013).

Due to their chain configurations and their origin, pectin is known to have a wide range of molecular weight varying from 50 to 200 kDa (Fishman *et al.*, 1991). The gel strength of pectin is enhanced as the molecular weight increases (Brejnholt, 2010; Liang *et al.*, 2012). The high molecular weight promotes the interactions between LMP chains and increases the length of junction zones created by the association of pectin chains, giving pectin gels stronger (Chen *et al.*, 2014). Indeed, it has previously been suggested that the gel was formed much

slower when adding enzymes to degrade the "hairy" regions, due to the lower molecular weight of sugar beet pectin (Oosterveld *et al.*, 2000).

- **Extrinsic factors**

The pH change has an effect on the strength of Ca^{2+}-pectin gel. For LMP, lowering the pH below 3 leads to a weakening of the gel formed by Ca^{2+}, while for amidated pectin the gel is reinforced (Lootens *et al.*, 2003). Indeed, at pH values lower than 2.0, the electrostatic interactions become insignificant due to almost full protonation of charged groups, and as a result LMP chain becomes insensitive to Ca^{2+} (Capel *et al.*, 2006). Indeed, Löfgren *et al.* (Löfgren *et al.*, 2006) have tested the storage moduli (G') of LMP-Ca gel by a rheometer at 25 °C. They have shown that the highest G' was found at pH = 5 and pH = 7, followed by a lower value at pH = 4. G' was lowest at pH = 3 due to the weakened LMP-Ca^{2+} interaction when the undissociated form of the carboxyl groups dominated for LMP (DE = 30%) at the pectin concentration of 0.8% (w/w). The electrostatic attractions are strongest when the LMP is almost fully charged at pH > 4.5. Hence it was easy to understand that the change in the amount of the dissociated carboxyl groups can remarkably affect the coordination between Ca^{2+} and LMP (Wang *et al.*, 2014). Gels can be easily formed in the presence of Ca^{2+} at high pHs (Capel *et al.*, 2006).

The gelation rate and ageing process decline with increasing temperature due to an increase in entropy, which decreases the probability of contact between pectin chains (Cardoso *et al.*, 2003; Rao *et al.*, 1993). Thus, when temperature is decreased, the cross-linking process is favored and the gel network is stabilized because of low polymer chain mobility (Cardoso *et al.*, 2003; Sousa *et al.*, 2015). Also, a controlled temperature of LMP-cations system influences the gel structure. Cardoso *et al.* (Cardoso *et al.*, 2003) have measured the storage (G') of LMP-Ca gels at a fixed frequency of 1 Hz, with a low strain amplitude of 0.01. They showed that the G' increased with decreasing temperature from 70 °C to 5 °C.

The affinity of LMP towards divalent cations (such as Ca^{2+}) decreases when the ionic strength of the system increases (Garnier *et al.*, 1994). This can be explained by overshadowing the effect of the divalent cations by screening the charge of the polymer and decreasing the cross-links between the polysaccharide chains. In this case, monovalent cations will compete with divalent cations (Draget *et al.*, 1998; Silva *et al.*, 2003). At low monovalent salt concentration (NaCl, KCl, LiCl) the added divalent cations could promote a non-specific shielding of the long-range electrostatic repulsions between the highly negatively charged

polysaccharide chains, thus facilitating divalent cation interchain cross-links and increasing gel strength (Silva *et al.*, 2003).

It has been concluded that a smaller amount of Ca^{2+} ions is needed for gelation in the presence of NaCl (100 mM) than in salt-free pectin solutions (Axelos, 1990; Garnier *et al.*, 1993). Gels are formed more rapidly in salt-free solutions, but the shear moduli are lower than for gels containing salt (Axelos and Thibault, 1991).

On the other hand, the gelling process can be formed without divalent cation and dependent on the nature of monovalent salts. The gel strength may be enhanced by using larger monovalent cations ($K^+ > Na^+ > Li^+$) and by lowering the DE (Yoo *et al.*, 2009). It was also found that monovalent cations (Na^+ and K^+) induce gelation of LMP and the time required for gel formation depends on the monovalent cation concentration (Wehr *et al.*, 2004). Wang *et al.* (Wang *et al.*, 2014) have shown that the gelation of LMP could be formed under higher salt concentrations (≥ 100 mM NaCl) at pH = 3 without Ca^{2+}. Gel strength produced by Na^+ salts was obviously lower than that of Ca^{2+}-gel until the concentration of Na_2SO_4 was increased to 500 mM. The gel strength increased with a high amount of sodium salts due to water molecules that fully bound to LMP formed great amount of hydrogen bonds. According to Silva *et al.* (Silva *et al.*, 2003), at high concentration, monovalent salt could increase gel strength by increasing the shielding of electrostatic repulsion, promoting the participation of the monovalent cation in cross-link through polyanion/water/M^+/water/M^+/polyanion interaction.

Gelation time was defined as the time of abrupt increase in the shear modulus G' from the baseline, this was indicated by the detection of a modulus of 1 Pa (Matia-Merino *et al.*, 2004). Thus, G' as a function of time (dG'/dt) was used to determine exactly the point at which gelling started to occur for pectin gels (Kastner *et al.*, 2012). For LMP, Ca^{2+} ions interact with carboxyl groups and inter-connect galacturonan chains. Hence, the degree of blockiness influences the gelation time; the short gelation time is obtained for the pectin with high degree of blockiness (Löfgren *et al.*, 2005). Moreover, the gelation time decreases with an increase in the molecule weight (Yapo and Koffi, 2013; Zaidel *et al.*, 2012) and pectin content (Soltania and Madadlou, 2016). Whereas, the gel time is considerably increased by a small increase in the gel formation temperature (Durand and Bertrand, 1990).

In conclusion, it is important to know that these factors are influenced by each other and affected the textural properties of LMP gels (May, 1990; Thakur *et al.*, 1997). Indeed,

when the LMP concentration increases above about 3 g L^{-1}, the gel elasticity increases in proportion, without modifying the gelation temperature. However, lower LMP concentrations lead to a decrease of the gel strength and the gelation temperature due to intra-chain bonding (Capel *et al.*, 2006). Moreover, the hydrogel stiffness depends on many parameters including DE, macromolecular structure of the pectin backbone, the polymer and the calcium concentrations (Stephens *et al.*, 2006).

CHAPTER 2

EFFECT OF NaCl CONCENTRATION ON THE CONFORMATION AND ON THE STRUCTURE OF POLYGALACTURONATE AND PECTIN IN SOLUTION. ABILITY TO BIND CALCIUM IONS

Introduction

Les polyosides chargés négativement (pectines, alginates, carraghénanes) peuvent adopter un comportement différent en solution (conformation, mobilité des chaînes, …) en fonction de la force ionique (concentration en NaCl). L'organisation des chaînes de ces biopolymères peut avoir un impact sur leurs propriétés fonctionnelles telles que leur aptitude à fixer des cations divalents pour former des gels.

Dans ce chapitre présenté sous forme d'un article, nous nous sommes intéressés à l'étude de la conformation d'une pectine faiblement méthylée (notée LMP) en solution à différentes concentrations en NaCl (0, 1, 10 et 100 mM) à pH = 5,5. Il est à noter que la pectine est composée d'une association d'acides galacturoniques (GalA) plus ou moins estérifiés (Fig. 1-3, Chapitre 1). En comparaison, nous avons également étudié la conformation de l'acide polygalacturonique (noté PGA) en fonction de ces 4 concentrations en NaCl. L'étude du PGA permet de s'affranchir de la présence des groupements ester et de leur distribution aléatoire dans la pectine.

Dans un premier temps, nous avons suivi le degré de dissociation de l'acide galacturonique ($COOH \rightarrow COO^-$) en fonction du pH pour ces deux polyosides en solution à différentes concentrations en NaCl. Ensuite, nous avons suivi l'évolution de la viscosité intrinsèque en fonction de la concentration en NaCl. La viscosité intrinsèque a été corrélée aux rayons hydrodynamiques (R_H) obtenus par des mesures de diffusion dynamique de la lumière. Le traitement des données de la viscosité intrinsèque nous a permis d'obtenir des informations sur la flexibilité des chaînes de ces deux polyosides. Enfin, cette partie a été complétée par des mesures de diffusion des neutrons aux petits angles pour des solutions de LMP et de PGA. L'analyse des résultats nous a permis de déterminer la longueur de persistance (Lp) et de mettre en évidence l'état d'agrégation de ces deux polyosides.

Dans la deuxième partie, nous avons suivi l'évolution des ions calcium fixés par la pectine et par le PGA en fonction de la quantité des ions calcium ajoutée. Ceci a été réalisé en fonction de la concentration en NaCl. Les isothermes de fixation obtenus ont été modélisés afin d'obtenir les paramètres de fixation des ions calcium sur les deux biopolymères (constante d'affinité, nombre de site de fixation).

The aim of this work is to study the effect of the concentration of NaCl on the conformation and the structure of both polygalacturonate (polyGal) and low methoxyl pectin (LMP) and their ability to bind calcium ions.

Viscometric method is one of the most used and relevant methods to explore the behavior of polymer chains in solution. The experimental data give access to intrinsic viscosity from which the useful information can be evaluated: polymer-polymer interaction, polymer-solvent interaction, chain stiffness and hydrodynamic parameter of macromolecular chains in solution. Furthermore, dynamic light scattering (DLS) measurements can be used to determine the size of objects in solution. Small angle neutron scattering (SANS) measurements allow us to determine the persistence length (*L*p), which characterizes the stiffness of polyelectrolyte chains.

2.1. Materials and methods

2.1.1. Materials

Poly-D-galacturonic acid (95% of purity, Mw ~ 50 kDa) was purchased from Sigma (St Louis, MO). Low methoxylated pectin (Unipectin OF 300 C) was a gift from Cargill France with a DE ≈ 27 - 33%. Sodium chloride and calcium chloride were purchased from VWR, BDH Prolabo. All other reagents were analytical grade.

2.1.2. Fourier transform infrared spectroscopy (FTIR)

To study the functional groups (COO^-, COOH, $COOCH_3$) present in PGA and LMP powders, a Fourier- transform infrared spectroscopy (FTIR) analysis was carried out directly on bulk products. The spectra of the samples were recorded with a Bruker IFS 28 equipped with a DTGS detector and working in a spectral range of 4000 - 600 cm^{-1}, with a resolution of 2 cm^{-1}. A total of 32 scans were collected to obtain a high signal-to-noise ratio.

2.1.3. pH titrations

An adequate amount of PGA or LMP was introduced in a NaCl solution (0, 1, 10 and 100 mM) to obtain 0.5 g L^{-1} of the polyelectrolyte. The titration of the mixture was performed by the addition of successive amount of NaOH (0.1 M). The pH was then measured by using a MeterLab PHM240 at 25 °C. All the measurements were done at least in triplicate.

The relationship between the apparent dissociation constant (K_a) and the degree of dissociation (α) of the carboxylic groups of a polyacid is described by Eq. 2-1 (Zhang *et al.*, 1997):

$$pH = pK_a + \log\left(\frac{\alpha}{1-\alpha}\right) \Leftrightarrow \alpha = (1+10^{(pK_a-pH)})^{-1} \qquad \textit{Eq. 2-1}$$

where α is the fraction of dissociated acid groups (degree of ionization or degree of dissociation): α = [COO^-]/([COOH] + [COO^-]) and α = 0.5 corresponds to the pKa.

2.1.4. Determination of calcium free and bind to PGA and LMP

An exact amount of the polyelectrolyte (PGA or LMP) was gradually dissolved in a NaCl solution at three concentrations (1, 10 and 100 mM) in order to get a concentration of the polyelectrolyte equal to 1 g L^{-1}. The pH of these solutions was maintained to pH = 5.5 by adding NaOH (0.1 M). Taking into account the purification of the PGA (95 %), the degree of esterification of LMP (~ 30%) and the degree of dissociation of both PGA (0.97) and LMP (0.94) at the considered pH (5.5), the amount of galacturonate (Gal) in the PGA and the LMP solutions are 5.23 mM and 3.74 mM, respectively. A fixed volume (20 µL) of $CaCl_2$ (10 mM) was added to the solution of PGA or LMP (25 mL) under stirring. After a certain time of 2 min, the concentration of the free calcium [*F*] was measured using a calcium ion-selective electrode (ISE25Ca) coupled with a reference electrode. All the measurements were done at least in triplicate.

In order to obtain the parameters of the binding of calcium to PGA and LMP properties (affinity of binding, number of binding sites), data were plotted according to the Hill equation (Eq. 2-2) (Bordbar *et al.*, 1996):

$$\nu = \frac{[B]}{[Gal]} = \frac{g\ (K_{b,app}[F])^n}{1 + (K_{b,app}[F])^n} \qquad \textit{Eq. 2-2}$$

Where ν is the concentration of calcium bound [*B*] divided by the concentration of the Gal unit in the polyelectrolyte [Gal]; [*F*] is the free concentration of calcium determined by Ca - ISE; *g* is the number of binding sites; and *n* is the Hill coefficient, *n* = 1 for non-cooperative systems, *n* > 1 for cooperative systems, and *n* < 1 for anticooperative systems. $K_{b,app}$ is the apparent binding affinity constant.

2.1.5. Intrinsic viscosity measurements

The viscosity of polymer solutions (PGA, LMP) at various concentrations in the four concentrations of NaCl (0, 1, 10, 100 mM) was measured using a capillary viscometer

(SI analytics, Germany). The viscosimeter was immersed in a thermostatic water bath at 25 °C. After loading the sample into the viscosimeter, the solution was allowed to equilibrate at the bath temperature before starting the experiment. All experiments were done at least in triplicate.

The ratio of the viscosity of a polymer solution (η) to the pure solvent (η_0) is called relative viscosity (η_r):

$$\eta_r = \frac{\eta}{\eta_0} \qquad \textit{Eq. 2-3}$$

The specific viscosity (η_{sp}) is related to the increase in viscosity due to polymer molecules:

$$\eta_{sp} = \frac{\eta - \eta_0}{\eta_0} = \eta_r - 1 \qquad \textit{Eq. 2-4}$$

The intrinsic viscosity $[\eta]_H$ was determined by using the Huggins equation:

$$\frac{\eta_{sp}}{c} = [\eta]_H + k_H[\eta]_H^2 c \qquad \textit{Eq. 2-5}$$

Where c is the polymer concentration, η_{sp}/c is the reduced viscosity, k_H represents the Huggins constant which offers information about the polymer interactions and the solvent quality (Chamberlain and Rao, 2000; Higiro *et al.*, 2007).

2.1.6. Dynamic light scattering measurements (DLS)

DLS measurements allow to obtain information about the size of the objects in the solution, that is derived on the basis from Brownian motion. DLS measurements were performed on a laser light scattering instrument (Nicomp 380, Santa Barbara, California, USA). The measurements were carried out at 25 °C and 90° scattering angle. Solutions of PGA and LMP were prepared at a concentration of 1g L^{-1} in different NaCl concentrations (1, 10, 100 mM) and pH = 5.5. Each mixture was stirred for 15 min and filtered through a 0.45 µm filter (VWR® Syringe Filters, Cellulose Acetate) in order to remove dust.

Assuming that the scattering of the incoming light exhibits Gaussian statistics, the experimentally measured intensity autocorrelation function $g^2(q, t)$, which is related to the electric field correlation function $g^1(q, t)$ according to the Siegert relation:

$$g^2(q,t) = 1 + \beta|g^1(q,t)|^2 \qquad \textit{Eq. 2-6}$$

where β is treated as an empirical factor. In general, $g^1(q, t)$ may be expressed by a continuous distribution of decays:

$$g^1(q,t) = \int_0^\infty A(\Gamma)exp(-t/\Gamma)d\Gamma, \quad \Gamma = \frac{1}{Dq^2} \qquad \textit{Eq. 2-7}$$

where *A(Γ)* is the distribution of decay times, *D* is the diffusion coefficients, and *q* is the scattering vector and is calculated from equation:

$$q = \frac{4\pi n}{\lambda}\sin(\theta/2) \qquad \textit{Eq. 2-8}$$

with λ is the wavelength of the incident beam in a vacuum, θ is the scattering angle and n is the refractive index in the liquid.

The diffusion coefficients (*D*) was related to the hydrodynamic radius (R_H) by Stokes-Einstein equation:

$$D = \frac{k_B T}{6\pi\eta R_H} \qquad \textit{Eq. 2-9}$$

where k_BT is the Boltzmann energy, η is the solvent viscosity. A fit of the correlation function to an exponential decay combined with Stokes-Einstein relation gives:

$$\Gamma = \frac{6\pi\eta R_H}{k_B T q^2} \qquad \textit{Eq. 2-10}$$

from which the hydrodynamic radius (R_H) can be obtained if the absolute temperature (*T*) and solvent viscosity (η) are known. Moreover, the decay time is proportional to the hydrodynamic radius.

2.1.7. Small angle neutron scattering measurements

Small angle neutron scattering (SANS) measurements were performed on the PACE spectrometer (Laboratoire Léon Brillouin, CEA-Saclay, Gif-sur-Yvette, France). Three configurations were used with two different neutron wavelengths and two sample-detector distances (λ = 13 Å, D = 4.7 m; λ = 5 Å, D = 4.7 m; λ = 5 Å, D = 0.9 m) that cover the 0.0032 - 0.5 $Å^{-1}$ wave vector range. We applied standard corrections for sample volume, neutron beam transmission, empty cell signal, and detector efficiency to the raw signal to obtain scattering in absolute units, and then removed the signal from the buffer (Schmidt *et al.*, 2009). All experiments were done in NaCl solutions. D_2O was used as a solvent to improve contrast and lower the incoherent background.

2.2. Results and discussion

2.2.1. Investigating the functional groups of LMP and PGA

FTIR spectra give information on the main functional groups present in the pectin and PGA, and also allow to determine the ratio (CH_3COO^-/COO^-).

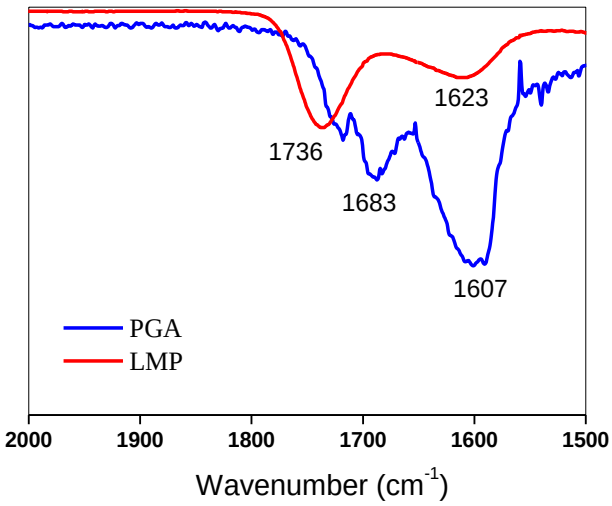

Fig. 2-1. FTIR spectra for PGA and LMP powders

FTIR spectra of PGA and LMP powders were measured in the region from 2000 to 700 cm^{-1}. In the below 1500 cm^{-1} region, the bands did not change significantly between the two polymers PGA and LMP (data not shown).

In the 1800 - 1500 cm^{-1} region, the evolution of the two functional groups could be followed: the carboxylate groups (COO^-): 1607 cm^{-1} and the carbonyl groups (C=O: COOH): 1683 cm^{-1} were present in the PGA; whereas, the carboxylate groups (COO^-): 1623 cm^{-1} and the carbonyl groups (C=O: COOH, $COOCH_3$): 1736 cm^{-1} were shown in the LMP (Assifaoui *et al.*, 2010; Synytsya *et al.*, 2003) (see Annex 2 for more details). In order to estimate the ratio of $COOCH_3/COO^-$, we calculated the area of both peaks. The percentages of the functional groups (COO^-, COOH) of the PGA sample were 75% and 25%. For LMP, the comparison between the two peaks (1736 cm^{-1}, 1623 cm^{-1}) allowed to estimate the DE. Our results in Fig. 2-1 showed a DE close to 39%. The DE value giving by the supplier is about 30%.

2.2.2. Effect of NaCl concentration on the degree of dissociation (α) of PGA and LMP

The dependence of the degree of dissociation (α) on the pH for PGA and LMP solutions at various NaCl concentrations (0, 1, 10 and 100 mM) is shown in Fig. 2-2. The increase of NaCl

concentration induced an increase of the degree of dissociation (α). Indeed, sodium ions screened the charges and thereby facilitating the dissociation of carboxylic acid (Hoogendam *et al.*, 1998). It can be observed that at a fixed pH (5.5), and in absence of NaCl, the degree of dissociation was below 0.9 for both LMP and PGA solutions. While at this pH for the three NaCl concentrations studied, the degree of dissociation seemed to be slightly stable and was about 0.94 and 0.97 for LMP and PGA, respectively.

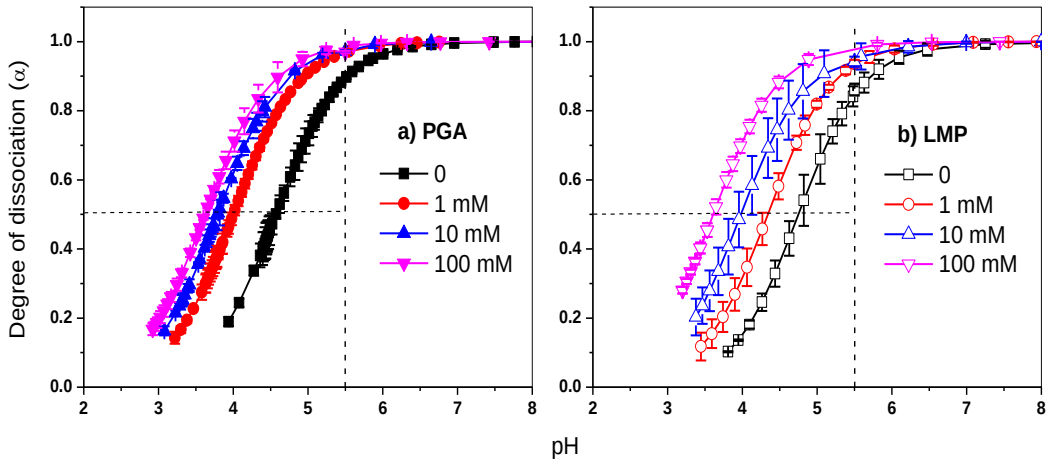

Fig. 2-2. pH dependence of degree of dissociation (α) of polymer in aqueous solution: PGA (a) and LMP (b) at different concentrations of NaCl

Fig. 2-3 presents the variation of the pKa (α = 0.5) of both PGA and LMP solutions as a function of the concentration of NaCl. It can be noted that the pKa decreased when the concentration of NaCl increased for both PGA and LMP. The decrease of the pKa may be due to the exchange between sodium and hydrogen ions which increased the amount of free hydrogen ions in the solution and thus decreased the pH. The effect of the concentration of salt on the behavior of the degree of dissociation was more pronounced in the case of LMP than for PGA. Indeed, at α = 0.5, the slope was more abrupt for LMP solution that for PGA solution (Fig. 2-3). LMP chains seemed to be more sensitive to changes in salt concentration. This could be due to the difference of structural features between PGA and LMP. The LMP contains ester groups (~ 30%) and presents a branched structure with high molecular weight. The presence of methyl groups decreases the hydrophilic character of LMP and causes the hydrophobic interactions between methoxy groups ($-OCH_3$) (Alonso-Mougán *et al.*, 2002).

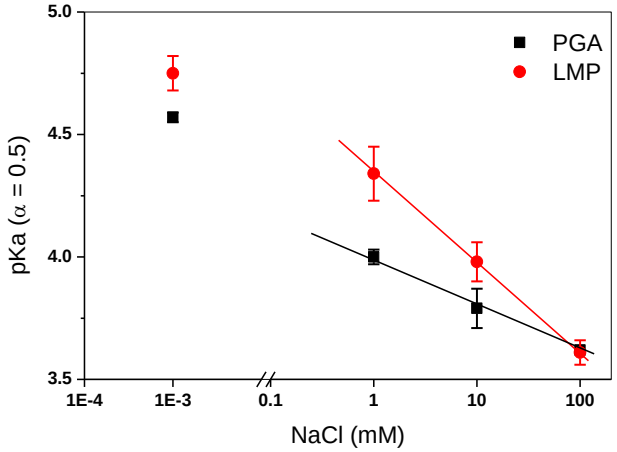

Fig. 2-3. Evolution of the pKa (α = 0.5) of PGA and LMP solutions (0.5 g L^{-1}) with the concentration of NaCl. Lines are to guide eyes

2.2.3. Effect of NaCl concentration on the conformation and the organization of LMP and PGA chains

2.2.3.1. Intrinsic viscosity and conformation

The reduced viscosity (η_{sp}/c) of both PGA and LMP was measured as function of the concentration of the polyelectrolytes in pure water and in the three NaCl concentrations (1, 10 and 100 mM) (Fig. 2-4).

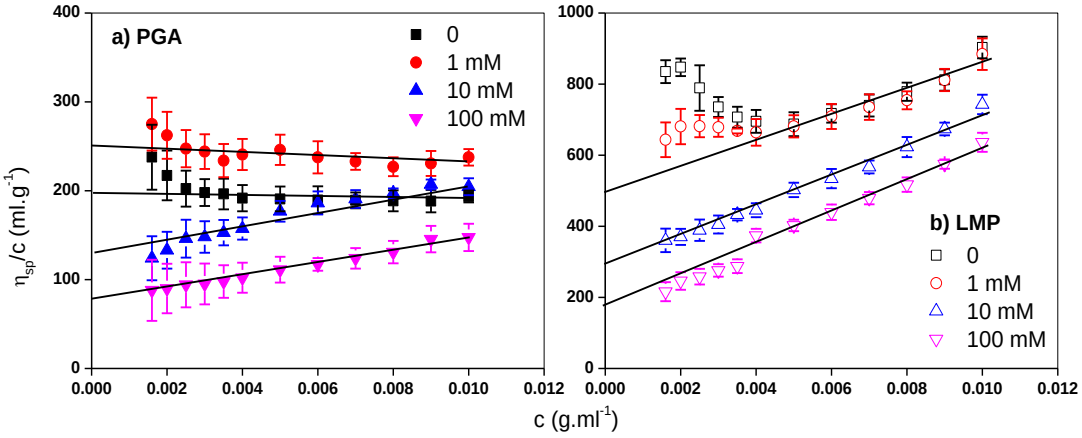

Fig. 2-4. Dependence of the reduced viscosity as a function of the polymer concentration for PGA (a) and LMP (b) solutions in pure water and in different NaCl concentrations

For both PGA and LMP, at low NaCl concentrations (≤ 1 mM), the reduced viscosity decreased with the increase in the polymer concentration until 4 g L^{-1} and then the reduced viscosity increased according to Huggins equation (Eq. 2-5). The decrease of the reduced viscosity at low concentration of the polymer was typical to the behavior of polyelectrolytes in dilute salt solution and was previously observed for other polyelectrolytes such as xanthan

(Brunchi *et al.*, 2014), hsian-tsao leaf gum (Lai and Chiang, 2002), HMP (high methoxyl pectin) and LMP (Yoo *et al.*, 2006), LMP and alginate (Lima *et al.*, 2009). This typical behavior was due to intra- and intermolecular repulsive electrostatic interactions (Ghimici *et al.*, 2009). However, a higher content of the polyelectrolyte units in the copolymer at constant degree of polymerization caused an increase of reduced viscosity, which means an increase of the coil dimension in solution (Ghimici *et al.*, 2009). It was also suggested that an intermolecular ordering or self-aggregation through hydrogen bonding and entanglement effects became increasingly significant at low concentration of monovalent cations (< 0.4 mM) (Vega *et al.*, 2015).

At higher NaCl concentrations (> 1 mM), the increase of the reduced viscosity was proportional to the concentration of the polyelectrolytes (Fig. 2-4). This may be explained by an increase in the amount of polymer chains resulted in large association.

Table 2-1. Effect of NaCl concentration on the intrinsic viscosity and the Huggins constant of PGA and LMP from Huggins equation

	Intrinsic viscosity (ml g^{-1})		k_H	
Concentration of NaCl, mM	LMP	PGA	LMP	PGA
0	530 ± 35	193 ± 17	0.11 ± 0.02	n.d.
1	524 ± 38	261 ± 28	0.11 ± 0.02	n.d.
10	277 ± 30	132 ± 8	0.58 ± 0.14	0.51 ± 0.14
100	187 ± 22	90 ± 16	1.26 ± 0.34	0.90 ± 0.51

Table 2-1 showed that the intrinsic viscosity for LMP was higher than for PGA indicating a high molecular weight of LMP comparing to PGA. In addition, as the NaCl concentration increased, the intrinsic viscosity decreased for both PGA and LMP. This may be due to the screen of the negative charges of the polyelectrolyte, which reduced the electrostatic repulsions between polyelectrolyte chains and thus induced a partial aggregation of the chains. Vega *et al.* (Vega *et al.*, 2015) have shown that the intrinsic viscosity of xanthan (branched anionic polyelectrolyte) decreased with increasing the concentration (0.1 - 10 mM) of monovalent cations (K^+, Na^+, Li^+) due to a conformational transition from a random coil to a single or double helix. Also, Carrington *et al.* (Carrington *et al.*, 1996) have shown a progressive collapse of xanthan with increasing ionic strength, which is reflected in reduced

shear and extensional viscosities. Morariu *et al.* (Morariu *et al.*, 2012) have also suggested that a decrease of the intrinsic viscosity for chitosan could be due to the increase of the polymer coil density, indicating the enhancement of the polymer-polymer intermolecular interactions when increasing the ionic strength.

It was difficult to obtain the Huggins constant (k_H) for PGA solutions at low NaCl concentrations (0 and 1 mM) (Table 2-1). In these solutions, the PGA chains were highly extended due to strong intramolecular repulsions. Consequently, the PGA chains did not favor the formation of the aggregates stabilized by hydrogen bonding (Gilsenan *et al.*, 2000). When the NaCl concentration increased, the k_H of PGA increased indicating an increase in the polymer-polymer interactions and a decrease in the polymer-solvent interactions (Simon *et al.*, 2003). For LMP, Huggins constants were low and about 0.1 in both pure water and 1 mM NaCl solution. For high concentration of NaCl, the k_H are equal to 0.5 and 1.2 in NaCl solution at 10 mM and 100 mM, respectively. Kontogiorgos *et al.* (Kontogiorgos *et al.*, 2012) have found k_H values for pectins in range between 0.43 and 0.58, indicating high chain flexibility in 100 mM NaCl and at pH = 7. According to Lapasin and Pricl, the high Huggins constant observed for LMP in NaCl (100 mM) can be an indication of the aggregation (Lapasin and Pricl, 1995). Li *et al.* (Li *et al.*, 2013) have found the same k_H (greater than 1) for LMP in acidic pH.

Pals and Hermans (Pals and Hermans, 1952) have proposed to evaluate the conformation of polyelectrolytes by means of stiffness parameter (noted *S*). This value can be determined by the slope of the linear dependence between the intrinsic viscosity and reciprocal of the square root of the ionic strength (Eq. 2-11):

$$[\eta] = [\eta]^* + SI^{-1/2} \qquad \textit{Eq. 2-11}$$

where $[\eta]^*$ represents the intrinsic viscosity at infinite ionic strength and *I* is the ionic strength of the solution, which is expressed as Eq. 2-12:

$$I = \frac{1}{2}\sum c_i z_i^2 \qquad \textit{Eq. 2-12}$$

where c_i is the concentration of ion *i* and z_i is its valence. For computation of ionic strength, we take into account the Na^+ and Cl^- ions from the NaCl solution.

The values of stiffness were equal to 6.6 for PGA and 11.8 for LMP (Fig. 2-5). It was shown that the stiffness of apple pectin (DM = 28%) was about 16.2 at pH = 7 in 100 mM NaCl (Garnier *et al.*, 1993). This value is slightly higher than the *S* parameter obtained in our study. This may be due to the high pH used in the work of Garnier and co-worker. Indeed, an increase of the pH caused an increase in the stiffness. Moreover, Morris *et al.* showed that the chain

stiffness increased with decreasing the DE of pectin (Morris *et al.*, 2000). In our study, the high stiffness (low flexibility) of the LMP in comparison to the PGA may be due to the presence of neutral sugars in the backbone of LMP (branched structure) as well as the presence of ester groups. Indeed, neutral sugars and ester groups may form strong hydrophobic interactions and hydrogen bonding between polymers chains, which may increase the rigidity of the polymer (Löfgren and Hermansson, 2007; Sousa et al., 2015).

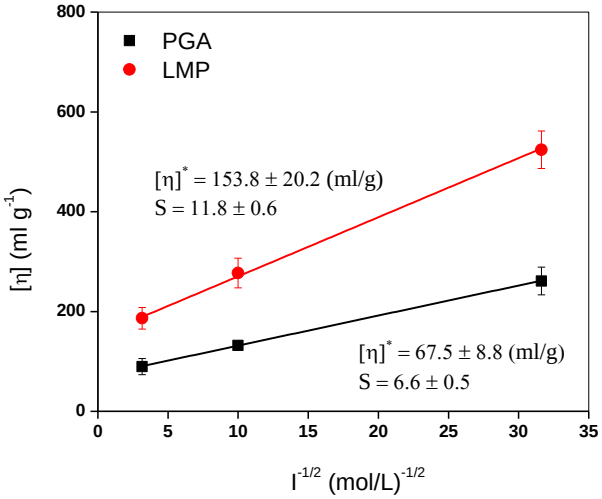

Fig. 2-5. Dependence of the intrinsic viscosity [η] as a function of the ionic strength ($I^{-1/2}$) for PGA and LMP solutions

Smidsrød and Haug (Smidsrød and Haug, 1971) have introduced the flexibility parameter, *B*, which can be determined according to the following Eq. 2-13:

$$B = \frac{S}{([\eta]_{0.1})^{\nu}} \qquad \textit{Eq. 2-13}$$

where $[\eta]_{0.1}$ is intrinsic viscosity at 0.1 mol/L ionic strength, ν is an exponent, depending on polyelectrolyte and a value of 1.27 for pectins was determined experimentally (McConaughy *et al.*, 2008).

In our study, the values of *B* obtained were 0.022 ± 0.005 for PGA and 0.016 ± 0.002 for LMP. This was in agreement with the *B* values obtained for pectins (0.034 - 0.044) with various DEs (0 - 27.3%) (Smidsrød and Haug, 1971) and for polyGal (0.032 – 0.043) extracted from the Aloe vera plant (DM = 2.0 – 5.8%) (McConaughy *et al.*, 2008). It was shown that dextran sulfate, amylose xanthate and polyvinyl alcohol sulfate had high *B* value (approx. 0.23) which meant very flexible polymer chain, whereas carboxymethylcellulose was known as a semi-flexible polymer being characterized by *B* value of 0.044 - 0.065 (Smidsrød and Haug, 1971). Thus, the values of *B* obtained for PGA and LMP may be indicated that these polymer

chains were semi-flexible. The flexibility parameter, *B* has been related to the intrinsic persistence length (*L*p) according to the empirical equation (Eq. 2-14) (Smidsrød and Christensen, 1991):

$$Lp \approx 0.18B^{-1.11} \qquad \text{Eq. 2-14}$$

Using the equation (Eq. 2-14), the *L*p was around 12.6 ± 3.2 nm and 18.5 ± 3.0 nm for PGA and LMP, respectively. These values are in same range as those obtained for LMP by other authors by calculating from the intrinsic viscosity: *L*p ~ 9.9 - 16.6 nm with DM = 4 - 45% (Axelos and Thibault, 1991), *L*p ~ 5.9 – 8.2 nm with DM = 2.0 - 5.8 (McConaughy *et al.*, 2008), and *L*p ~ 14 nm with DM = 36% (Abodinar *et al.*, 2014).

2.2.3.2. Determination of the size distribution by DLS

The autocorrelation functions $g^2(q, t)$ of PGA and LMP at three NaCl concentrations (1, 10 and 100 mM) are presented in Fig. 2-6a.

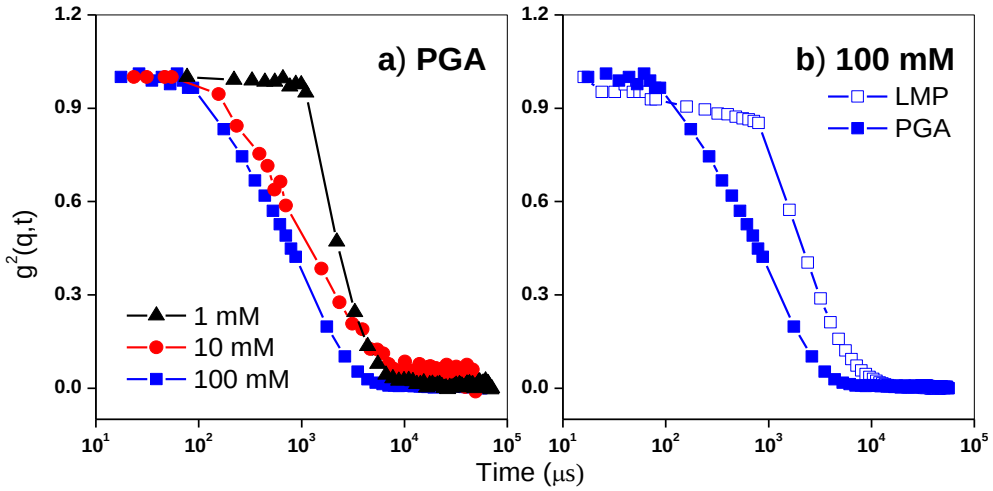

Fig. 2-6. Intensity autocorrelation function of PGA in different NaCl concentrations solutions (a); PGA and LMP in 100 mM NaCl concentration solutions (b); polymer concentration (1 g L^{-1}) at a scattering angle of 90° and 25 °C

The fit of the autocorrelation function allowed us to determine the decay time and therefore to obtain the hydrodynamic radius (R_H) (Eq. 2-7 and Eq. 2-10). Many studies showed a good fit between the decay time and R_H (Bulone *et al.*, 2002; Li *et al.*, 2013; Lima *et al.*, 2009). The hydrodynamic radius (R_H) for PGA and LMP solutions in the presence of NaCl at 25 °C are presented in Table 2-2.

Table 2-2. Hydrodynamic radius (R_H) for PGA and LMP solutions in the presence of different NaCl concentrations at 25 °C

NaCl concentration	$R_{H, DLS}$ (nm)	
	PGA	LMP
1 mM	325	-
10 mM	188	-
100 mM	114	357

As observed, the values of R_H for PGA decreased with increasing NaCl concentration. These findings were consistent with the results of intrinsic viscosity in Table 2-1. For ease of observation, the intrinsic viscosity [η] and the hydrodynamic radius (R_H) are represented by Fig. 2-7. These two parameters decreased with the increase in NaCl concentration. The decrease of these parameters may suggest enhanced polymer chain associations (Kjøniksen *et al.*, 2004) and the presence of more compact polymer entities in the solution (Jonassen *et al.*, 2012).

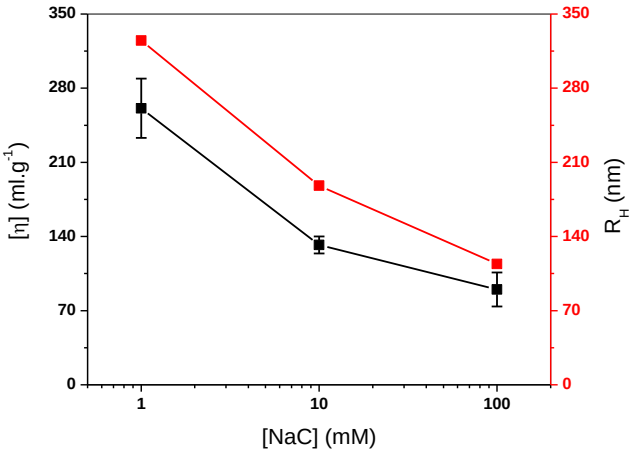

Fig. 2-7. The correlation between the intrinsic viscosity [η] and the hydrodynamic radius (R_H) of the PGA as function of the NaCl concentration

This tendency was not observed in the case of LMP (R_H = 107 nm at 1 mM NaCl and R_H = 38 nm at 10 mM NaCl), due certainly to the filtration step (pore size diameter = 450 nm) of the pectin solution. All chains must be held on the filter which may indicate that the size of pectin was higher than 450 nm at two NaCl concentrations (1 and 10 mM). The R_H values were expected to increase as the concentration of NaCl decreased. Lima *et al.* have investigated the effect of salt on the decay time by comparing the autocorrelation functions in the presence and the absence of NaCl. They have shown that the decay time was slower in pure water than

in 100 mM NaCl for LMP and alginate (Lima *et al.*, 2009). It can be noted that long decay time corresponds to high R_H. The findings presented for PGA are also in agreement with studies carried out by Schweins *et al.* (Schweins *et al.*, 2003) for polyacrylate. An increase of the NaCl concentration resulted in a decrease of the hydrodynamic radius (R_H). The same tendency was observed for chitosan in pure water, in comparison to saline solvents (50 and 150 mM) (Jonassen *et al.*, 2012). They have suggested that smaller and more compact particles could be formed in saline water compared to pure water (Jonassen *et al.*, 2012). In our study, an increase in the NaCl concentration can decrease intramolecular repulsive interactions so that the PGA chain is likely to have a compact three-fold structure (from 325 nm to 114 nm), which allows the formation of aggregates stabilized by hydrogen bonding (Li *et al.*, 2013).

Fig. 2-6b shows that the decay time of LMP was slower in 100 mM NaCl solution than that of PGA. Thus, the R_H value of LMP increased three-fold comparing to PGA in 100 mM NaCl (Table 2-2). This can be suggested that LMP created a more complex structure due to a highly branched structure.

2.2.3.3. Investigation of the structure by SANS

SANS measurements of PGA solution at different NaCl concentrations allow us to describe the local conformation of network of PGA. The SANS scattering intensity for PGA is presented in Fig. 2-8.

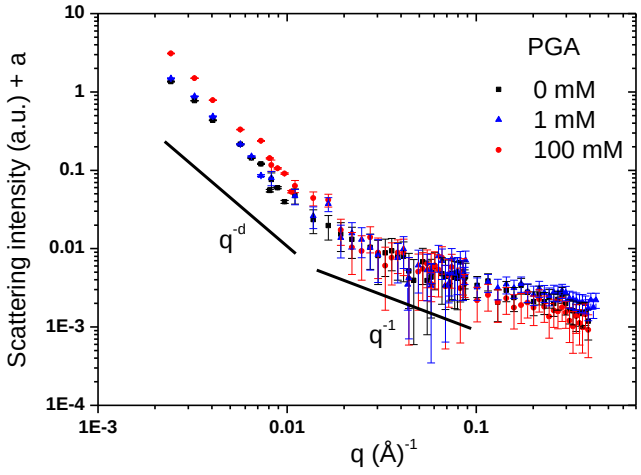

Fig. 2-8. SANS spectra of PGA solution (13.5 mM of GalA) in the absence and in the presence of NaCl (pH = 5.5, T = 25 °C)

The transition between a q^{-d}-like decay at low q, with $2 \leq d \leq 3$ (due to the presence of aggregated regions of PGA) and a q^{-1} decay at larger q, indicated rod-like behavior. The

aggregation was also observed for PGA by the viscosity intrinsic (Table 2-1). Indeed, a decrease of the intrinsic viscosity as the NaCl concentration increased, suggesting a partial aggregation of the PGA chains. The transition occurred at q* (between q^{-d} and q^{-1}), which corresponded to the q-limit of the regime for which the scattering exclusively arose from the chain stiffness (Muller *et al.*, 2011). The values of q* for PGA in 0, 1 and 100 mM NaCl solutions were 0.019, 0.019 and 0.023 $Å^{-1}$, respectively. The persistence length $Lp = 6/(\pi \times q^*)$ characterizes the stiffness and had a value of 10.1 nm for PGA in 0 and 1 mM NaCl, and 8.3 nm for PGA in 100 mM NaCl, which was compatible with the result of *L*p determined by empirical equation (Eq. 2-14) for PGA (Table 2-3). In addition, the values of *L*p were determined by calculating from the intrinsic viscosity and measuring by SANS (Table 2-3), indicating a difference between empirical and experimental data.

Table 2-3. Persistence length (Lp) for PGA and LMP solutions in the presence of different NaCl concentrations at 25 °C

NaCl concentration	$Lp_{, emp}$ (nm)		$Lp_{, SANS}$ (nm)
	PGA	LMP	PGA
0 mM	n.d.	n.d.	10.1
1 mM	n.d.	n.d.	10.1
100 mM	12.6 ± 3.2	18.5 ± 3.0	8.3

(n.d.: non-determined)

By adding NaCl in aqueous solutions, the polyGal chains undergo some changes, which induced a decrease in the persistence length and intrinsic viscosity. The structure formed by polyGal chains in water and in 1 mM NaCl solution was similar and easily to form aggregates via hydrogen bonding (Manunza *et al.*, 1997). McConaughy *et al.* (McConaughy *et al.*, 2008) have found that the persistence length of PGA (extracted from the Aloe vera plant) decreased, when salt was added, from 14 nm in 50 mM NaCl, at 11 nm in 100 mM NaCl, and 8.8 nm in 200 mM NaCl. Moreover, they have also shown that intermolecular interactions were stronger in 100 mM NaCl than in pure water by viscosity measurement, indicating a change in the critical entanglement concentration. The persistence length, calculated from MD simulations of PGA chains, was about 11 nm for protonated chains and about 30 nm for unprotonated chains (Noto *et al.*, 2005). The charged dimer showed specific and strong intramolecular hydrogen bond interactions that were enhanced by the presence of water molecules.

By using SANS measurement, we have also determined the *L*p for LMP (2.5 g L^{-1}) in sodium acetate buffer (80 mM, pH = 5.3) and the value was 7.6 nm. Data will be presented in

Chapter 3. The value of *L*p was lower for LMP than for PGA, indicating the higher flexibility for LMP chains. This may be explained by the difference of the nature and concentration of the solvent.

2.2.4. Effect of NaCl concentration on the ability of PGA and LMP to bind calcium ions

The interaction between calcium ions and both PGA and LMP (1 g L^{-1}) has been studied at the three NaCl concentrations. It must be pointed out that in the experimental conditions of this study (concentration of the polyelectrolytes and concentration ranges of both NaCl [1 - 100 mM] and calcium added [0 – 5.6 mM]), the turbidity remained constant and low which indicated that there is no gel (data not shown). This suggests that the size of the Ca-PGA or Ca-LMP complexes formed was small because they did not scatter light strongly.

Binding isotherms of calcium to PGA and to LMP are presented (Fig. 2-9) and fitted according to Hill equation (Eq. 2-2). Results showed that the binding isotherm of Ca-LMP seems to be more sensitive to the concentration of NaCl than the binding isotherm of Ca-PGA due to a steadily increasing slope for LMP. This high sensitivity was also observed for degree of dissociation (Fig. 2-3) and for the intrinsic viscosity (Table 2-1). Moreover, when the concentration of NaCl was higher than 10 mM, the amount of calcium required to bind the polyelectrolyte decreased. The negative charge of the polymer was increasingly screened, allowing pectin chains to approach each other, which in turn led to a decrease in the rate of the ionic bridging function (Axelos, 1990).

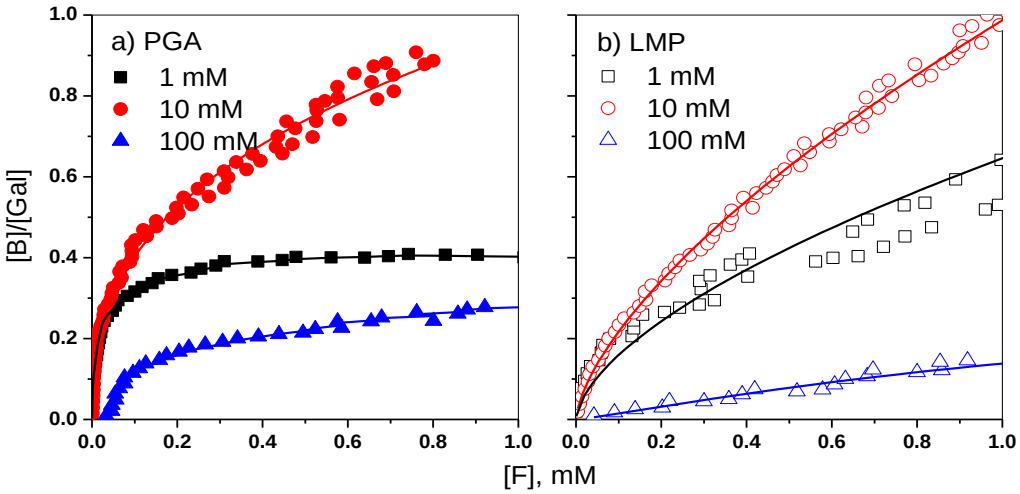

Fig. 2-9. Bound calcium normalized by the amount of Gal unit as a function of the free concentration of calcium ([F]) for PGA (a) and LMP (b) at three NaCl concentrations (pH = 5.5, T = 25 °C). Lines present the fit with Hill equation (Eq. 2-2)

The fitted data were presented in Table 2-4. The Hill coefficient (n), which is an indication of the cooperativity of binding was lower than 1 for two concentrations of NaCl (1 and 10 mM) and was higher than 1 for the concentration of NaCl equal to 100 mM. When $n < 1$ the binding is anti-cooperative, while when $n > 1$ the binding is cooperative. Using the Hill equation, Garnier *et al.* (Garnier *et al.*, 1994) have also found two types of interactions between LMP and calcium ions occurred according to the solvent conditions: an anti-cooperative binding in pure water and a cooperative binding in the presence of 100 mM NaCl. These findings were consistent with our results. In these two cases, there are multiples classes of binding sites with various binding constants (Bordbar *et al.*, 1996). It must be noted that the association binding constant ($K_{b,app}$) obtained by fitting data from Hill equation is not the true K_b since in a cooperative process there will be multiple true K_b (Invitrogen, 2006). Our results have shown that the $K_{b,app}$ decreased as the NaCl concentration increased for PGA (Table 2-4). This may be due to the inhibition of the electrostatic interactions between PGA and calcium ions when increasing the concentration of NaCl. In the case of LMP, the $K_{b,app}$ was low and remained constant with increasing the NaCl concentration. The diminution of $K_{b,app}$ was more pronounced in the case of the PGA than the LMP. This could be explained by the fact that LMP chains had lower mobility than the PGA chains due to the branched structure of pectin, which may hinder network formation of LMP in the presence of divalent cations. In addition, the amount of Gal in the LMP (3.74 mM) was lower than in the PGA (5.23 mM). Also, the random distribution of Gal residues along the pectin chain induced much more defects into the development of the network with calcium ions.

Table 2-4. The number of binding sites (g), Hill coefficient (n) and apparent binding affinity constant ($K_{b,app}$) of calcium ions for PGA and LMP at three NaCl concentrations using Hill model

		g	Hill coefficient (*n*)	$K_{b,app}$ (mM^{-1})
1mM	PGA	0.46 ± 0.02	0.67 ± 0.00	42.6 ± 7.3
	LMP	1.15 ± 0.14	0.55 ± 0.08	0.77 ± 0.4
10 mM	PGA	0.45 ± 0.04	0.85 ± 0.03	12.9 ± 1.4
	LMP	1.12 ± 0.17	0.79 ± 0.04	0.23 ± 0.3
100mM	PGA	0.32 ± 0.00	1.12 ± 0.14	5.2 ± 0.6
	LMP	0.94 ± 0.91	1.11 ± 0.04	0.5 ± 0.3

Fang *et al.* (Fang *et al.*, 2008) suggested a mechanism of binding calcium to LMP which correspond to i) the formation of monocomplexes between divalent cations and carboxylate groups followed by ii) the formation of dimers. In recent studies, an intermediate step was suggested corresponding to point-like crosslinks (Ventura *et al.*, 2013) or 'tilted egg-box' according to Borgogna *et al.* (Borgogna *et al.*, 2013). In the case of PGA which is similar to alginate, a third step (formation of multimers) must be considered (Fang *et al.*, 2007). The fitted data (Table 2-4) showed that the binding affinity constant of Ca-PGA decreased when the concentration of NaCl increased. This is in accordance with binding data of calcium ions to alginate obtained by isothermal titration calorimetry (ITC) (De and Robinson, 2003). They have found that the binding constant of calcium to alginate decreased as follows 1330, 771 and 309 mM^{-1} for 0, 10 and 100 mM, respectively. The ionic interaction between the alginate and calcium ions was electrostatic and was competitively inhibited by sodium ions. Moreover, the addition of NaCl may also reduce the water activity inducing thus an aggregation of polymer chains. This is in agreement with the results of intrinsic viscosity.

2.2.5. Discussion and conclusion

Two anionic polysaccharides (PGA and LMP) have been investigated to understand the effect of the sodium ions concentrations on the conformation of the polymer chains and their abilities to bind calcium ions. In the absence of sodium ions, it was shown that the degree of dissociation (α) of carboxylic acid (at pH = 5.5) was lower than 0.9 indicating that the dissociation is more difficult. We have demonstrated that the addition of sodium ions facilitated this dissociation. It can be noted that the LMP are more sensitive to the concentration of the NaCl in comparison with the PGA. This high sensitivity observed in LMP with the concentration of NaCl has an impact on the intrinsic viscosity and on the stiffness of the polymer chains. The Huggins constants were 0.51 for PGA and 0.58 for LMP, indicating flexible polymers in 10 mM NaCl solutions. The viscosity studies at 100 mM NaCl allowed to calculate the flexibility parameter (B) of 0.022 for PGA and 0.016 for LMP, indicating a semi-flexible polymer backbone for both polymers at this NaCl concentration. The intrinsic viscosity decreased at high NaCl concentration due to decreasing intra- and intermolecular repulsive electrostatic interactions. Also, DLS measurements showed that hydrodynamic radius (R_H) of PGA decreased with increasing NaCl concentration, suggesting a more compact structure. The R_H value of LMP in 100 mM NaCl solution increased three-fold in comparison to PGA in 100 mM NaCl. There is a good correlation between the intrinsic viscosity and the R_H

determined by DLS for PGA (Fig. 2-7). It can be noted that because of the high size of the LMP, the R_H can not be measured correctly by the DLS. Finally, the persistence length (*L*p) of PGA has been determined by SANS, indicating a conformational change in 100 mM NaCl solution with decreasing of *L*p (8.3 nm). The higher persistence length (10.1 nm) in 1 mM and 10 mM NaCl solutions, suggesting that PGA chain is highly extended and more rigid in solution (Morris *et al.*, 2010). Narayanan *et al.* have suggested that increasing the ionic strength (100 mM NaCl) of the solution decreased the electrostatic repulsive interaction between pectin molecules, which allow the gelation process to be formed more easily and so require less $CaCl_2$ than in pure water (Narayanan *et al.*, 2002). In addition, our results have shown that the Ca^{2+} affinity with PGA decreased in the following order of NaCl concentration: 1 mM > 10 mM > 100 mM due to the higher flexibility and the conformation of polymer chains.

Principaux résultats et conclusions

Nous avons étudié la conformation de la pectine (LMP) et de l'acide polygalacturonique (PGA) en solution à pH = 5,5 à différentes concentrations en NaCl (0, 1, 10 et 100 mM). A ce pH et en absence des ions sodium, le degré de dissociation est faible (α = 0,9). En présence des ions sodium, le degré de dissociation (α) est égal à 0,97 montrant ainsi que les deux polymères se trouvent majoritairement à l'état ionisé. Les courbes de neutralisation montrent que la dissociation des groupements carboxyliques (COOH) est peu sensible à la concentration en NaCl dans le cas du PGA contrairement à la pectine LMP.

A une concentration en NaCl donnée, les valeurs de la viscosité intrinsèque obtenues pour la pectine sont supérieures à celles obtenues pour le PGA en solution. La même tendance a été observée par des mesures du rayon hydrodynamique. Plus la concentration en NaCl augmente, plus la viscosité intrinsèque diminue indiquant une réduction des tailles en solution (Fig. 2-7). De plus, il a été montré que la longueur de persistance diminue quand la concentration en NaCl augmente. Ces changements peuvent être expliqués par la réduction de l'agrégation des chaînes de polyosides en augmentant la concentration du NaCl. Selon l'équation du Huggins, il a été montré que les chaînes de pectines deviennent plus rigides quand la concentration en NaCl passe de 10 mM (K_H (LMP) = 0,58 ; K_H (PGA) = 0,51) à 100 mM (K_H (LMP) = 1,26 ; K_H (PGA) = 0,90). Le traitement mathématique des courbes de viscosité intrinsèque en fonction de la concentration en NaCl a permis de calculer un paramètre qui traduit la rigidité (*stiffness*) des chaînes (S). Ainsi la rigidité des chaînes de la pectine est supérieure à celle des chaînes du PGA en présence de 100 mM de NaCl. L'étude de la capacité à fixer les ions calcium par la pectine et par le PGA dépend fortement de la concentration de NaCl. En effet, nous avons remarqué que la constante d'affinité diminue quand la concentration en NaCl augmente. Cette diminution est beaucoup plus prononcée dans le cas du PGA (Tableau 2-4). Ceci peut être expliqué par l'inhibition par les ions sodium des interactions électrostatiques entre LMP / PGA et les ions calcium. De plus, nous avons noté que la constante d'affinité du Ca-PGA est plus élevée que celle du Ca-LMP ; ceci peut être expliqué par la faible rigidité des chaînes (S) observée pour le PGA (S = 6,6) par rapport à la pectine (S = 11,8) (Fig. 2-5). En effet la faible rigidité des chaînes du PGA (flexibilité élevée) facilite la formation de réticulation (Gal-Ca-Gal). Enfin, nous avons montré que pour des faibles concentrations en NaCl (1 et 10 mM), la fixation des ions calcium est anti-coopérative (coefficient de Hill inférieur à 1).

CHAPTER 3

INTERACTION BETWEEN DIVALENT CATIONS (Ca^{2+}, Zn^{2+}, Ba^{2+}, Mg^{2+}) AND POLYELECTROLYTES (LMP AND PGA) IN DILUTE REGIME: STUDY OF THE STRUCTURE OF THE NETWORK AND THE MECHANISM OF GELATION

Introduction

Ce chapitre est composé de deux parties présentant chacune une publication parue dans des journaux internationaux (Assifaoui *et al.*, 2015) et (Huynh *et al.*, 2016).

Dans la première partie (Assifaoui *et al.*, 2015), nous avons étudié les interactions entre une pectine faiblement méthylée (LMP) et deux cations divalents (Ca^{2+} et Zn^{2+}) en solution dans un tampon acétate de sodium (80 mM, pH = 5,3). Dans une étude précédente (Dhalleine *et al.*, 2011), il a été montré que les microparticules préparées avec les ions zinc comme agent de réticulation (Zn-LMP) présentent un profil de libération de la substance active différent (retardé) des microparticules préparées avec les ions calcium (Ca-LMP). Ainsi, nous avons souhaité comprendre l'effet de la nature du cation divalent sur la structure du réseau formé en comparant les ions Ca^{2+} et les ions Zn^{2+}. Cette étude a été réalisée en régime dilué : la concentration en pectine est égale à 1 g L^{-1} ; ce qui correspond à une concentration en unité galacturonique (Gal) égale à 2,9 mM ($c < c^*$). Les structures (Ca-LMP et Zn-LMP) formées à différents ratios molaires (R = [Cation]/[Gal]) ont été étudiées à différentes échelles d'observations : macroscopique (mesures de la viscosité et de turbidité) et microscopique (diffusion des neutrons aux petits angles). Nous avons également déterminé les paramètres thermodynamiques de l'association entre le cation et la pectine (constante d'affinité, enthalpie d'association, stœchiométrie) à l'aide de la titration calorimétrique isotherme (ITC). Ces paramètres thermodynamiques permettront d'identifier les différentes étapes de l'association cation - biopolymère. Enfin, des simulations moléculaires dynamiques ont été réalisées sur des unités Gal et ces deux cations afin de comprendre le mode d'association Gal - cation et de prédire le mode d'association entre le cation et le polyGal.

Dans la deuxième partie (Huynh *et al.*, 2016), nous nous sommes intéressés à l'étude des interactions polygalacturonate (polyGal) et 4 cations divalents (Mg^{2+}, Ca^{2+}, Ba^{2+} et Zn^{2+}) afin de proposer un mécanisme d'association et d'expliquer les différences de structure observées. Nous avons choisi d'utiliser le polyGal afin de s'affranchir de la complexité de la pectine (présence de zones ramifiées et des groupes esters distribués aléatoirement dans la Fig. 1-3). De plus, les ions calcium et zinc appartiennent respectivement à la famille des alcalinoterreux (np^6) et aux métaux de transition (nd^8). Afin de comparer des cations de la même famille, nous avons choisi d'étudier les ions Mg^{2+} et Ba^{2+}. Dans cette étude, nous avons remplacé le tampon acétate utilisé lors de la première partie par une solution saline

(NaCl, 10 mM). En effet, les ions acétates pourraient interférer lors de l'association polymère - cations divalents. La concentration en polyGal est égale à 0,5 g L^{-1} ($c < c^*$) ce qui correspond à une concentration en unité galacturonate (Gal) égale à 2,7 mM. La concentration en NaCl (10 mM) a été fixée suite aux résultats obtenus dans le Chapitre 2 (concentration qui permet de fixer la force ionique, tout au long des autres expériences). La viscosité et la turbidité ont été mesurées à différents ratios molaires (*R*) pour les mélanges (Ca-polyGal, Zn-polyGal, Ba-polyGal et Mg-polyGal). Des mesures de titration calorimétrique (ITC) sur ces 4 systèmes ont été entreprises. Enfin des simulations moléculaires dynamiques ont été également réalisées.

PART 1

Structural behavior differences in low methoxy pectin solutions in the presence of divalent cations (Ca^{2+} and Zn^{2+}): a process driven by the binding mechanism of the cation with the galacturonate unit

Soft Matter

PAPER

View Article Online
View Journal | View Issue

Cite this: *Soft Matter*, 2015, **11**, 551

Structural behaviour differences in low methoxy pectin solutions in the presence of divalent cations (Ca^{2+} and Zn^{2+}): a process driven by the binding mechanism of the cation with the galacturonate unit†

Ali Assifaoui,*[ad] Adrien Lerbret,*[a] Huynh T. D. Uyen,[a] Fabrice Neiers,[b] Odile Chambin,[ad] Camille Loupiac[ac] and Fabrice Cousin[c]

In this paper, we compare the interactions between low methoxy pectin (LMP) and either Ca^{2+} or Zn^{2+} in semi-dilute solutions. Intrinsic viscosity and turbidity measurements reveal that pectin–calcium solutions are more viscous, but yet less turbid, than pectin–zinc ones. To get a molecular understanding of the origin of this rather unexpected behavior, we further performed isothermal titration calorimetry, small angle neutron scattering experiments, as well as molecular dynamics simulations. Our results suggest that calcium cations induce the formation of a more homogeneous network of pectin than zinc cations do. The molecular dynamics simulations indicate that this difference could originate from the way the two cations bind to the galacturonate unit (Gal), the main component of LMP: zinc interacts with both carboxylate and hydroxyl groups of Gal, in a similar way to that described in the so-called egg-box model, whereas calcium only interacts with carboxylate groups. This different binding behavior seems to arise from the stronger interaction of water molecules with zinc than with calcium. Accordingly, galacturonate chains are more loosely associated with each other in the presence of Ca^{2+} than with Zn^{2+}. This may improve their ability to form a gel, not only by dimerization, but also by the formation of point-like cross-links. Overall, our results show that zinc binds less easily to pectin than calcium does.

Received 19th August 2014
Accepted 7th November 2014

DOI: 10.1039/c4sm01839g

www.rsc.org/softmatter

Introduction

Pectin is an anionic polysaccharide present in the cell wall of various plants, which has been widely used in food and pharmaceutical industries as a gelling, stabilizing and/or encapsulating agent. It is well known that gelation occurs when pectin is in contact with divalent cations.[1–4] This gelling property has made pectin a suitable delivery system to escort active compounds from the mouth to the colon.[5] It may be used to create various dosage forms with specific drug release profiles. Pectin is composed of long sequences of partially methyl-esterified (1–4)-linked α-D-galacturonic residues (known as 'smooth regions' or homogalacturonan), interrupted by defects of other neutral sugars such as D-xylose, D-glucose, L-rhamnose, L-arabinose and D-galactose (known as the non-gelling 'hairy' region).[6] Depending on the number of methyl ester groups (referred to as the degree of esterification, DE) pectin is classified as high methoxy pectin (HMP) (DE > 50%) or low methoxy pectin (LMP) (DE < 50%). The affinity of LMP towards divalent cations increases when decreasing DE or ionic strength, and when increasing the polymer concentration. Moreover, the distribution of the galacturonate residues (deprotonated form of galacturonic acid, see Fig. S1 in the ESI†) has a strong effect on the polymer's ability to bind various divalent cations.

Considerable attention has been paid to the study of the binding mechanisms of pectin chains to explain the pectin's affinity towards divalent cations such as Ca^{2+}. The association between LMP chains is due to three types of interactions: (i) hydrophobic association between methoxyl ester groups, (ii) hydrogen bonds between galacturonic acid and/or hydroxyl groups, and (iii) ionic interactions between galacturonate unit (Gal) groups mediated by Ca^{2+}-bridges.[7] Previous studies on calcium–pectin binding have shown that a minimal number of consecutive Gal groups, estimated to lie between 8 and 15, is required to form a stable cross-link structure between two

[a]*UMR PAM, AgroSup Dijon - Université de Bourgogne, Dijon, France. E-mail: ali.assifaoui@u-bourgogne.fr; adrien.lerbret@u-bourgogne.fr*

[b]*CSGA, INRA-CNRS-Université de Bourgogne, Bd Sully, Dijon, France*

[c]*Laboratoire Léon Brillouin, CEA-Saclay, Gif-sur-Yvette, France*

[d]*Department of Pharmaceutical Technology, School of Pharmacy, Université de Bourgogne, Bd Jeanne d'Arc, Dijon, France*

† Electronic supplementary information (ESI) available: Details of all the MD simulations performed; schematic structure of the Gal unit; potentials of mean force for the interaction of cations with Gal and associated representative configurations; figure and movies on the binding of Gal chains in the presence of Ca^{2+} and Zn^{2+}. See DOI: 10.1039/c4sm01839g

chains in the presence of calcium (*dimerization*).[8–10] Chain association occurs by dimerization, which corresponds to long chain segments where the cations are sandwiched within the dimer on specific sites along each of the inner surfaces. This is commonly referred to as the egg-box model, originally proposed for the calcium–alginate complex by Grant *et al.*[11] Because pectin and alginate share a strongly similar structure (polygalacturonate and polyguluronate are nearly mirror images in structure) and binding behavior toward calcium, the egg-box model has been transposed to describe calcium–pectin binding, but its validity has not been established. At molecular scale, this model considers that calcium is coordinated to 10 oxygen atoms from two guluronate chains.[11] These include two hydroxyl oxygens (O2 and O3), two ether oxygens (O1/O4 and O5) and one carboxyl oxygen (O6) (see Fig. S1 in the ESI† for atom names) for each chain. But, this model was questioned by Braccini and Pérez, who argued that the coordination of calcium in calcium–carbohydrate complexes is usually between 7 and 9.[12] Indeed, among all these oxygens, only four (O6 and O2/O3 from two opposite carboxyl and hydroxyl groups) strongly interact with calcium (distance < 3 Å) in a monodentate coordination.

Fang *et al.*[13] showed by isothermal titration calorimetry that the binding of LMP to calcium is described by a two-step process: in step I (molar ratio R (Ca^{2+}/Gal) ≤ 0.25), the binding heat decreased, which was attributed to *monocomplexation* (binding of calcium with one Gal chain). In step II ($R > 0.25$), the binding heat increased, thereby indicating the formation of egg-box dimers (dimerization) through the pairing of monocomplexes.[13] They also suggested that the dimerization of pectin chains takes place progressively upon addition of calcium.

Pectin can be used as a drug delivery device to a specific site for targeted release. As LM pectins gel in the presence of divalent cations, they can be used to prepare pectinate gel beads containing a drug to be delivered. The drug release profile and encapsulation efficiency of pectin-based dosage forms (dry beads) strongly depend on the nature of the divalent cations used. For example, Assifaoui *et al.* showed that the drug release in pectin-based dosage forms prepared with calcium is faster than in those prepared with zinc.[14,15] This difference was explained by the higher swelling of the dosage forms when calcium was used instead of zinc. Further Fourier-transform infrared analysis showed that the bands of functional groups present in pectin are not affected when the content of zinc is increased, conversely to what happens in the presence of Ca^{2+}, indicating that zinc interacts with pectin to a lesser extent than calcium does.[16] It is likely that the properties of these beads are reminiscent from the structure of the gels formed in aqueous solution before being dried. Therefore, in the present paper, we investigate the differences between the binding processes of two divalent cations (Ca^{2+} and Zn^{2+}) to low methoxy pectin in semi-dilute solution at the molecular scale and describe how such a difference affects the properties of the solutions. The interactions of the divalent cations with LMP were studied by isothermal titration calorimetry (ITC) and by molecular dynamics (MD) simulations. Furthermore, the structures formed by the LMP in presence of cations at different length scales were investigated by coupling small angle neutron scattering (SANS), turbidity and viscosity measurements. Thanks to the combination of results from these different techniques, we finally propose a mechanism for the binding of calcium and zinc with LMP.

Materials and methods

Materials

The pectin used (Unipectin OF 300 C) is a low methoxylated citrus pectin from Cargill France with 81% of galacturonic acid content, and a degree of esterification (DE) of 30%. The intrinsic viscosity, $[\eta]$, at 30 °C in acetate buffer (pH = 5.3) is equal to 0.23 L g^{-1}. Note that the pH studied is 2 pH-unit above the pK_a of pectin's carboxylic groups to deprotonate them and obtain only galacturonate (Gal). Before use, we purified pectin using the alcohol-precipitation procedure.[17] Acetic acid, sodium acetate, calcium chloride dihydrate, zinc chloride and sodium perchlorate were of analytical grade (Sigma-Aldrich) and were used as received.

Methods

Sample preparation. We dispersed the pectin powder in an acetate buffer (pH = 5.3) composed of acetic acid (20 mM) and sodium acetate (80 mM). The final concentration of pectin was 1 g L^{-1}. Taking into account the Gal content (81%) and the DE (30%) of the pectin, the concentration of the Gal unit was equal to 0.56 g L^{-1}. This corresponds to a 2.90 mM concentration of Gal, since the molecular weight of the Gal unit is 194 g mol^{-1}. Calcium and zinc mother stock solutions were also prepared in the same acetate buffer and their concentrations were equal to 24 mM. For all experiments, different amounts of divalent cations were added to the pectin solution to obtain various molar ratios, R, (R = cation/Gal).

Turbidity measurements. We measured the turbidity of pectin solutions (2.90 mM of Gal) at different calcium and zinc concentrations in acetate buffer (pH = 5.3) using an ultraviolet-visible (UV) spectrophotometer (Biochrom Libra, France) at a wavelength of 500 nm and at room temperature. Samples were analyzed in a quartz cuvette with a cell path length of 1 cm. We introduced 2 mL of the pectin solution into the cell and then we added various amounts of calcium or zinc solution (24 mM) to obtain various cation/Gal ratios. The mixture was then stirred and the transmittance was recorded. All the measurements were done at least in triplicate. We determined turbidity, τ (cm^{-1}), from the following equation (eqn (1)):

$$\tau = \left(-\frac{1}{L}\right)\ln\left(\frac{I_t}{I_0}\right) \quad (1)$$

where L is the optical path length (=1 cm), and I_t and I_0 are the transmitted and incident light intensities, respectively.

Isothermal titration calorimetry. We used an isothermal titration calorimeter (VP-ITC microcalorimeter from GE Healthcare) to measure the enthalpies for the binding of Ca^{2+} or Zn^{2+} to pectin at 25 °C. Before each experiment, all solutions were degassed for 15 minutes. A volume of 5 μL of 24 mM of

divalent cation solution ($CaCl_2$ or $ZnCl_2$) was injected sequentially into a 1.46 mL titration cell initially containing either acetate buffer or the pectin solution (2.90 mM of Gal). Each injection lasted 20 s, and an interval of 1000 s was considered between successive injections. A rotating 250 μL Hamilton micro syringe ensuring constant stirring of the whole mixed dispersion at a speed of 250 rpm was employed for the homogenization during injection. The heat after each injection is derived by calculating the area under each peak. The total heat content, Q, of the solution contained in V_0 is given by eqn (2):

$$Q = [\mathrm{M}]_t \times V_0 \times N \times \Delta H \times \theta \quad (2)$$

where $[\mathrm{M}]_t$ is the total amount of the pectin in the cell, N is the number of binding sites per Gal unit, ΔH is the binding enthalpy and θ is the fraction of sites occupied by the ligand [L] (which here refers to Ca or Zn concentration). The binding isotherm obtained by integrating injection peaks could be fitted by a model of independent binding sites (eqn (3)) using a nonlinear least-squares minimization method implemented in the analysis software provided with the calorimeter (Microcal Origin software (v.7.0552)).

$$Q = V_0 \Delta H \times \left[[\mathrm{L}] + \frac{1 + [\mathrm{M}]_t N K_b - \sqrt{\left(1 + [\mathrm{M}]_t N K_b - [\mathrm{L}] K_b\right)^2 + 4 K_b [\mathrm{L}]}}{2\ K_b} \right] \quad (3)$$

Iterative curve fitting yielded thermodynamic parameters including the binding constant K_b, binding enthalpy ΔH, and stoichiometry N. A full thermodynamic profile is then obtained using the relationships shown in the following equation (eqn (4)).

$$\Delta G = \Delta H - T\Delta S = -RT \ln(K_b) \quad (4)$$

where ΔG, ΔH and ΔS are the Gibbs free energy, enthalpy and entropy of binding, respectively. T is the absolute temperature and $R = 8.314$ J mol^{-1} K^{-1} is the ideal gas law constant. All the measurements were done at least in triplicate.

Viscosity measurements. We performed viscosity measurements using a capillary viscosimeter (SI analytics, Germany) and measured the flow time. The viscosimeter was immersed in a thermostatic water bath at 30 °C. After loading the sample into the viscosimeter, the solution was allowed to equilibrate at the bath temperature before starting the experiment. All experiments were done at least in triplicate.

Small angle neutron scattering. We performed small angle neutron scattering (SANS) measurements on the PACE spectrometer (Laboratoire Léon Brillouin, CEA-Saclay, Gif-sur-Yvette, France). Three configurations were used with two different neutron wavelengths and two sample detector distances ($\lambda = 13$ Å and $D = 4.7$ m; $\lambda = 5$ Å and $D = 4.7$ m; $\lambda = 5$ Å and $D = 0.9$ m) that cover the 0.0032–0.5 Å^{-1} wave vector range. We applied standard corrections for sample volume, neutron beam transmission, empty cell signal, and detector efficiency to the raw signal to obtain scattering in absolute units, and then removed the signal from the buffer.[18] All experiments were done in acetate deutered buffer.

Molecular dynamics simulations. To better understand the way the two divalent cations interact with the Gal units of LMP, we performed molecular dynamics (MD) simulations using the CHARMM program.[19] We first investigated the structure of a pair of octameric Gal chains bridged by four divalent cations (see Fig. 4). The chains were built following an analogous procedure to that described by Braccini and Pérez[12,20] and put in a cubic simulation box of water molecules. Given that the structure of these complexes remained stable over the simulation time scale (20 ns), we then investigated the ability of Ca^{2+} and Zn^{2+} to induce the association of Gal chains. For this purpose, we performed 100 ns long simulations in which (i) the two Gal chains were initially dissociated from each other, and (ii) calcium or zinc cations were initially free (see Fig. S3 in the ESI†). We also run independent simulations of the two divalent cations alone in water to determine their average hydration number in the bulk. Finally, we performed additional umbrella sampling simulations to investigate more specifically the interaction strength of the divalent cations with either the carboxylate group of Gal or with water. All simulations were performed at a temperature of 300 K and chloride or sodium ions were added to the simulation boxes to ensure charge neutrality. Further details on all of these simulations are provided in the ESI.†

Results

Turbidity and viscosity measurements

The turbidity and intrinsic viscosity measurements of pectin solutions as a function of the molar ratio R (= cation/Gal) are presented in Fig. 1. At low molar ratios, turbidities remain constant – at a relatively low value (<0.05 cm^{-1}) – and similar for

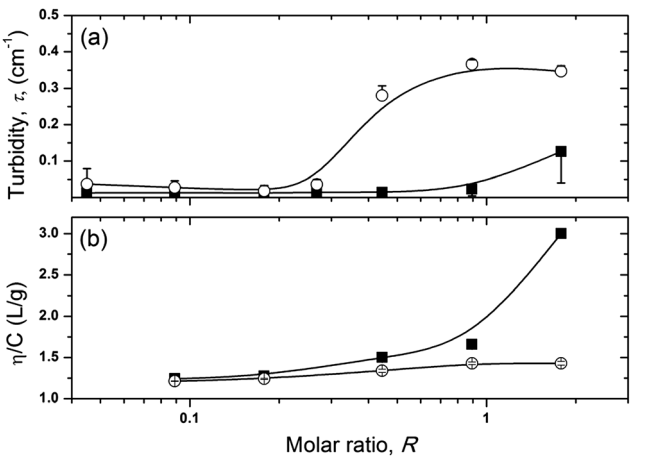

Fig. 1 (a) Evolution of turbidity at 500 nm and (b) intrinsic viscosity normalized by the concentration (η/C) ($T = 30$ °C) as a function of the molar ratio, R, (divalent cation/Gal) for calcium cations (black squares) and zinc cations (empty circles).

both cations (Fig. 1a). At $R = 0.27$, an abrupt increase of turbidity appears for pectin–Zn^{2+} solutions, while only a modest increase of turbidity is noted for pectin–Ca^{2+} solutions, at a much higher molar ratio ($R > 1.00$).

We then measured the intrinsic viscosity of pectin–cation mixtures at different molar ratios (Fig. 1b). At low molar ratios, intrinsic viscosity remains constant with a relatively low value ($\sim$1.25 L g^{-1}) and similar for both cations. Upon addition of calcium, we observe a slight increase of the intrinsic viscosity which accelerates at $R \sim 0.9$. Fang *et al.*[13] have found similar changes in relative viscosities of LMP solution (0.5 g L^{-1}) upon titration with calcium, but at $R \sim 0.25$. The difference of the inflexion ratio may be due to the type of the studied pectin (molecular weight, ramification, DE,…) and to its concentration (1 g L^{-1} in our study). Besides, the intrinsic viscosity does not change significantly whatever the amount of zinc added in the studied ratio range. The very low increase of viscosity and steep increase of turbidity of the zinc solution are counter-intuitive and suggest that the gel formed is very heterogeneous. Indeed, the strong rise of turbidity probably reveals the formation of large-scale density fluctuations that strongly scatter light. Yet, the slight increase of viscosity implies that such heterogeneous zones interconnect weakly with each other. The opposite trends observed for the gel formed by LMP upon addition of calcium suggest comparatively a more homogeneous structure of the gel at the mesoscopic scale.

Thermodynamic behavior of the cation–pectin complex

The interactions between pectin and various divalent cations may induce a release (exothermic) or an uptake (endothermic) of heat. Thermodynamic measurement obtained by ITC provides quantification of the change in energy when going from the free to the bound state. The binding enthalpy (ΔH) is presented for LMP solution as a function of the nature of divalent cations at various molar ratios (Fig. 2). Both endothermic (at low molar ratios $\leq$0.3) and exothermic (at high molar ratios >0.3) phenomena are observed, thereby suggesting that the binding mechanism is characterized by at least two processes. The first process is endothermic and may be ascribed to the formation of both monocomplexes between divalent cations and carboxylate groups[13] and of *point-like cross-links* (formation of one Gal–cation–Gal bridge between two Gal chains).[21] The second process is exothermic and corresponds to the formation of an ordered structure that can be attributed to the formation of dimers (or multimers). The existence of these two thermal transitions is in agreement with the findings obtained by several authors.[13,22] For instance, Fang *et al.* have observed a reduction of binding heat in the first step followed by an increase of binding heat in the second step.[13]

For the first injections of divalent cations slight differences appear between the titration curves of calcium and zinc (Fig. 2). These differences then vanish for higher molar ratios. The thermodynamic parameters determined by fitting the positive part of the curves with a model of independent binding sites using eqn (3) and (4) are summarized in Table 1. The initial portions of the calorimetric titration curves show that the enthalpy of the zinc–LMP complex ($\Delta H = 18.1 \pm 5.6$ kJ mol^{-1}) is higher than the enthalpy of the calcium–LMP complex ($\Delta H = 12.1 \pm 0.3$ kJ mol^{-1}), but the binding sites for both calcium and zinc complexes present similar free energy ($\Delta G \sim -24.6$ kJ mol^{-1}). It may imply an enthalpy–entropy compensation for both calcium and zinc pectin complexes. The binding of cations to Gal groups is entropy driven, since the dehydration of both cations and carboxylate groups leads to a significant entropy gain (release of tightly bound water molecules), which overbalances the unfavorable enthalpy change.[23] We also observe that the site number, N, is higher for calcium than for zinc cations. We can suppose that only a few Gal groups are associated to zinc cations (one cation for $\sim$5 and $\sim$14 units of Gal for calcium and zinc, respectively). Furthermore, the binding enthalpy changes from positive to negative at around $R = 0.25$ and $R = 0.35$ for calcium and zinc, respectively, indicating that at these ratios, the binding process becomes exothermic ($\Delta H < 0$) and corresponds to the second step (dimerization), in line with previous studies.[13,24]

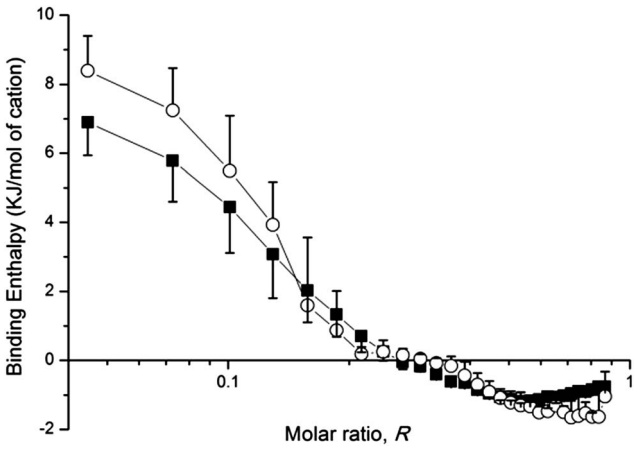

Fig. 2 Binding enthalpy, ΔH, *versus* molar ratio, R, obtained from ITC analysis for calcium cations (black squares) and zinc cations (empty circles).

Molecular description of the cation–pectin complex

SANS measurements of pectin with and without divalent cations (Ca^{2+} and Zn^{2+}) allow us to describe the local conformation of pectin in solutions and gels, and to determine the persistence length of the polymer. The SANS scattering intensity for pectin (2.90 mM of Gal) in the presence of calcium and zinc cations was investigated at two molar ratios corresponding to the positive ($R = 0.09$) and the negative ($R = 0.44$) binding enthalpies observed by ITC (Fig. 3).

A transition between a q^{-d}-like decay at low q, with $3 \leq d \leq 4$ (due to the branched structure of pectin and/or to the presence of aggregated regions) and a q^{-1} decay at larger q (rod-like behavior) is found. This transition occurs at q^* ($\sim$0.02 $Å^{-1}$), which corresponds to the q-limit of the regime for which the scattering exclusively arises from the chain stiffness.[18,25] The persistence length $L_p = 6/(\pi \times q^*)$ characterizes this stiffness and lies in the range of 50–70 Å, depending on the

Table 1 Thermodynamic parameters of the first step of divalent cation–LMP interactions at pH 5.3 and at 25 °C determined with the model of independent binding sites from the Microcal origin software. N is the number of binding sites per Gal unit, K_b is the binding constant, ΔH is the binding enthalpy, ΔS is the entropy and ΔG is the free energy

	N	10^{-3} K_b (M^{-1})	ΔH (kJ mol^{-1})	$T\Delta S$ (kJ mol^{-1})	ΔG (kJ mol^{-1})
Ca	0.19 ± 0.03	20.5 ± 0.3	12.1 ± 0.3	36.6 ± 0.4	−24.6 ± 0.1
Zn	0.07 ± 0.04	21.5 ± 7.6	18.1 ± 5.6	42.6 ± 4.6	−24.5 ± 0.9

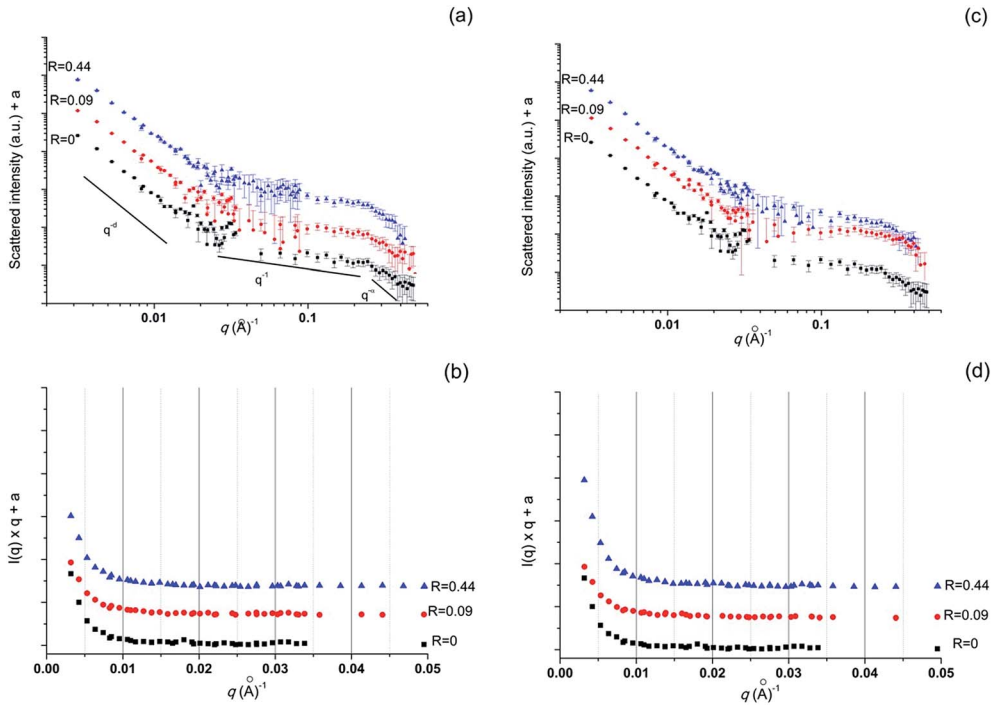

Fig. 3 SANS spectra of pectin solution (2.90 mM of Gal) in the presence of calcium (a) and zinc (c) cations. Graphs (b) and (d) correspond to $I(q) \times q$ *versus* q for calcium and zinc, respectively. All experiments were done in acetate buffer and at fixed temperature (pH = 5.3, T = 25 °C, respectively).

concentration of pectin. Previous studies have found a q^* value around 0.04 $Å^{-1}$, which gives a persistence length of the order of 80 Å for pectin (10 g L^{-1}) in 25 mM buffer, corresponding to 16–17 sugar units.[18] We observed a second break of slope around q = 0.2 $Å^{-1}$ that could represent the thickness of monomers (or cross-section). Unfortunately, the large uncertainty arising from the solvent subtraction in this regime does not allow a proper evaluation of such cross-section dimensions. After the introduction of calcium, no significant changes are observed. The intersection between the two regimes q^{-d} and q^{-1} is similar, indicating that the L_p remains constant for the two studied molar ratios. To better evaluate differences in the structure of the pectin in the presence of divalent cations, the scattering intensity is fitted by a squared-Lorentz function according to the Debye–Bueche model (DB) (eqn (5)). Note that this model is applied for $q < q^*$.

$$I(q) = \frac{I_0}{\left(1 + q^2\Xi^2\right)^2} \quad (5)$$

where I_0 is the zero-q scattering intensity and Ξ is the characteristic length of gel inhomogeneities or two-phase separated structures. It was demonstrated that the scattered intensity is proportional to the product of 3 quantities: (i) squared fluctuation in scattering length density ($\Delta\rho^2$) between the phases, (ii) a volume fraction (ϕ), and (iii) Ξ^3 according to the equation eqn (6):[26]

$$I_0 = 8\pi\phi\Delta\rho^2\Xi^3 \quad (6)$$

The DB model includes a correlation length Ξ that is interpreted as a distance between the network nodes. The Ξ values obtained from the fitted data are around 374 ± 24 Å for pectin alone, and decrease (~300 Å) when calcium or zinc is added, indicating a collapse of the structure (Table 2). When calcium cations are further added to pectin, no significant changes in the local conformation are observed (Ξ, I_0 and $\phi\Delta\rho^2$ increase moderately when R increases from 0.09 to 0.44). When zinc cations are added, we observe an increase of both Ξ and I_0 for R = 0.44, which induces an increase of $\phi\Delta\rho^2$. If we assume that the volume fraction ϕ in the pectin chain is constant in all

Table 2 Ratio R dependence of the characteristic length, Ξ, and I_0 determined by fitting the SANS spectra against eqn (5) ($q < 0.02$ Å^{-1}). $\phi\Delta\rho^2$ is then obtained from eqn (6)

Molar ratio, R	Ξ (Ca) (Å)	Ξ (Zn) (Å)	I_0 (Ca) (cm^{-1})	I_0 (Zn) (cm^{-1})	$\phi\Delta\rho^2$ (Ca)	$\phi\Delta\rho^2$ (Zn)
0	374 ± 24	374 ± 24	14.5 ± 2.8	14.5 ± 2.8	11.0×10^{-9}	11.0×10^{-9}
0.09	301 ± 14	290 ± 15	6.7 ± 0.9	6.2 ± 0.9	9.8×10^{-9}	10.0×10^{-9}
0.44	306 ± 14	329 ± 18	9.5 ± 1.3	16.7 ± 2.7	13.0×10^{-9}	19.0×10^{-9}

mixtures, it can easily be shown that the squared fluctuation in density ($\Delta\rho^2$) is almost 2 times higher for $R = 0.44$ than for the other molar ratio. Since all phases contain at the same time pectin and buffer, this squared fluctuation in density arises from variation of local concentration of pectin. The increase of $\Delta\rho^2$ in the case of high amounts of zinc may be explained by the formation of pectin-rich and pectin-poor domains within the gel. The absence of such local important fluctuations of concentrations in the case of calcium shows that the system is clearly more homogeneous than with zinc.

Molecular dynamics simulations

We then performed MD simulations to try to understand at the atomistic scale how the two divalent cations interact with the Gal units of LMP. Fig. 4 shows the time-averaged structure of the complex formed by two Gal octamers in the antiparallel arrangement in the presence of either Ca^{2+} or Zn^{2+}. Significant differences are found in the way the cations interact with the Gal chains: whereas Ca^{2+} interacts only with carboxylate groups of Gal, Zn^{2+} interacts also with neighboring hydroxyls. The structure formed in the presence of calcium deviates from that previously determined by Braccini and Pérez,[12] and even more from that of the egg-box model, first hypothesized by Grant *et al.*[11] It must be pointed out that in ref. 12 galacturonate or guluronate chains were assumed to be rigid and the water solvent was not considered explicitly. As such, these calculations did not consider any conformational changes that may occur upon chain association and neglected the competition between water and carboxylate groups for binding to divalent cations, which influences their coordination (see results from Fig. 5). Recent molecular dynamics simulations of guluronate chains in explicit water[27,28] actually showed that guluronate chains are twisted. Interestingly, the interaction of Ca^{2+} with carboxylate groups of Gal chains is bidentate, similar to that observed for Ca^{2+} bridging together two guluronate chains,[28] whereas that of Zn^{2+} is monodentate. It must be pointed out that in the egg-box model, four oxygens from two opposite carboxyl and hydroxyl groups strongly interact with calcium in a monodentate coordination. Therefore, our results clearly indicate that only zinc associates in an egg-box-like configuration (Fig. 4c).

To understand why Ca^{2+} and Zn^{2+} differ in their interactions with Gal chains, we determined the potentials of mean force (PMF) for the interaction of these cations with either water or with a Gal monomer by means of umbrella sampling simulations (see the Molecular dynamics simulation section in the ESI†). A PMF describes the change in the free energy of the

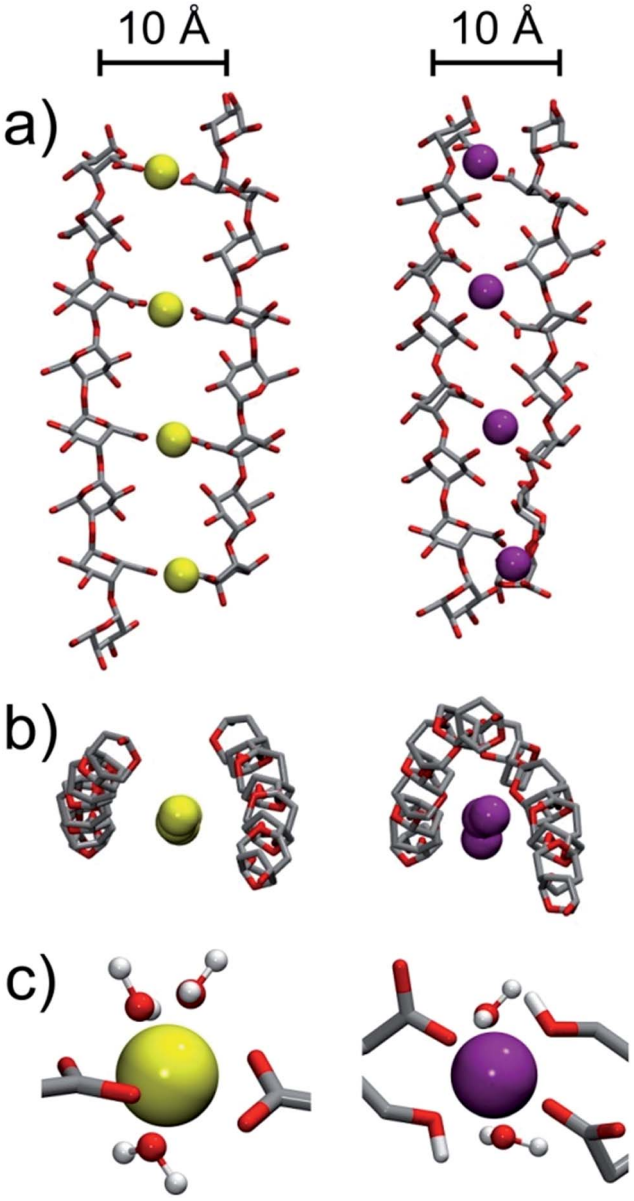

Fig. 4 Time-averaged structures formed by two Gal chains in the antiparallel arrangement in the presence of either calcium (left panels) or zinc (right panels) cations: (a) side view and (b) top view. (c) Examples of configurations of calcium and zinc interacting with Gal chains. For clarity, the atoms shown correspond to heavy atoms in (a), to heavy ring atoms in (b), and to the closest atoms from the divalent cations in (c). Furthermore, water molecules in the first hydration shell of the two divalent cations are also represented in (c).

system as a function of a reaction coordinate. It is thus very useful to determine free energy barriers and minima between two interacting species (either cation and water or cation and Gal in our study). The PMFs for the interaction between cations and water (Fig. 5a) exhibit two minima that correspond to water molecules located in the first and second hydration shells of the cations, respectively. These minima are found at shorter distances for Zn^{2+} (2.1 and 4.3 Å) than for Ca^{2+} (2.3 and 4.6 Å), consistent with the smaller size, higher charge density and stronger affinity for water of Zn^{2+} with respect to Ca^{2+}. The energy barrier to exchange a water molecule from the 1st to the 2nd solvation shell is much larger for Zn^{2+} (34 kJ mol^{-1}) than for Ca^{2+} (about 15 kJ mol^{-1}), which suggests that the kinetics for desolvating Zn^{2+} is much slower than that for Ca^{2+}. The PMFs for the interaction of the divalent cations with a Gal monomer exhibit three main features (Fig. 5b): (i) two deep minima close to each other, at distances ranging from 2.5 to 3.3 Å, (ii) an energy barrier at distances close to 3.7 and 4.0 Å, and (iii) a relatively shallow and broad minimum at distances between 4.5 and 5.5 Å. The two deep minima correspond to configurations where the cations are in contact with either one (monodentate coordination) or two oxygens from the carboxylate group of Gal (bidentate coordination). Interestingly, the global minimum of the PMF for Ca^{2+} (at r = 2.5 Å) corresponds to a bidentate coordination with the carboxylate group (minimum (1) in the inset of Fig. 5b), whereas that for Zn^{2+} (at r = 3.2 Å) corresponds to a monodentate one (minimum (2) in the inset of Fig. 5b). This result appears consistent with the MD study of Iskrenova-Tchoukova *et al.*,[29] who found that the interactions of Mg^{2+} and Ca^{2+} with a carboxylate group are preferentially monodentate and bidentate, respectively. These authors ascribed the monodentate coordination of Mg^{2+} to its strong interaction with water, which makes unlikely the loss of an additional first-shell water molecule for binding to the other carboxylate oxygen. This reason probably holds true when comparing Zn^{2+} and Ca^{2+}, since Zn^{2+} interacts much more strongly with water than Ca^{2+} does, given its smaller radius. Besides, the free energy barriers at distances close to 3.5 Å separate the contact ion pair (CIP) configurations from the solvent separated ion pair (SSIP) ones, where the carboxylate group and the divalent cations share with each other their hydration shells (see Fig. S2 in the ESI†). The corresponding energy barrier is remarkably larger for zinc than for calcium (about 16 kJ mol^{-1} *vs.* 8 kJ mol^{-1}), in line with the larger free energy barrier to exchange water between the 1st and the 2nd hydration shells of zinc (Fig. 5a). Accordingly, the PMFs in Fig. 5b suggest that binding to the carboxylate groups of Gal chains takes longer for zinc than for calcium. Moreover, the free energy difference between the global minimum (the most stable CIP) and the free state for cation–carboxylate association is significantly more favorable for zinc than for calcium (about 53 kJ mol^{-1} *vs.* 41 kJ mol^{-1}). Both the strong cation–Gal interaction observed for Zn^{2+} and its monodentate coordination – which induces an egg-box-like configuration – explain why the Gal chains stay closer to each other than in the presence of Ca^{2+} (Fig. 4).

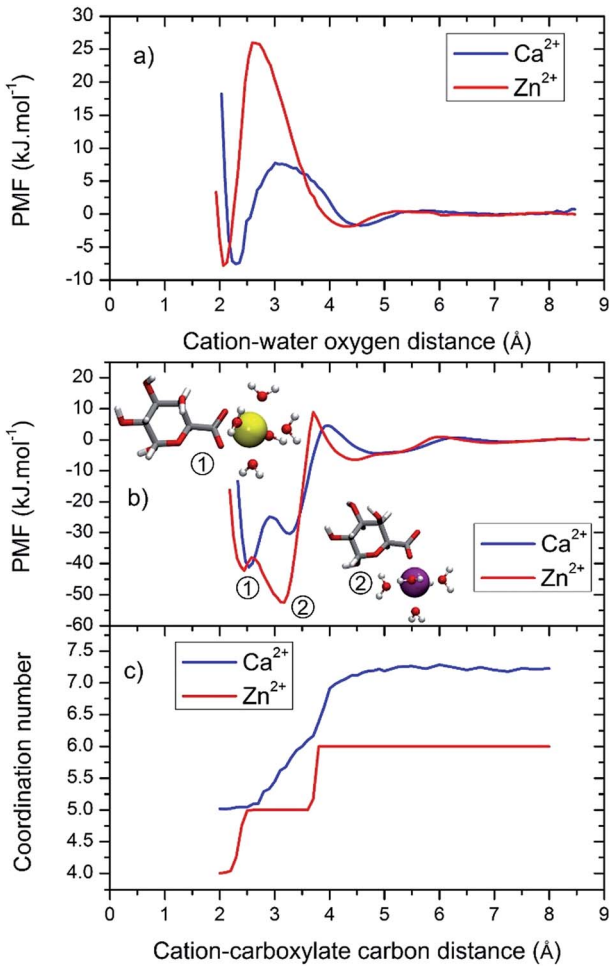

Fig. 5 Potentials of mean force (PMFs) for the interaction between the divalent cations and either (a) water or (b) Gal. The global minima (1) and (2) – inset pictures in (b) – correspond to configurations where Ca^{2+} and Zn^{2+} are in contact with the carboxylate group of Gal in the bidentate or the monodentate coordination, respectively. The average numbers of water molecules in the first hydration shell of Ca^{2+} and Zn^{2+} as a function of their distances from the carboxylate group of Gal are shown in (c).

We then calculated the averaged numbers of water molecules found in the first shell of the divalent cations as a function of their distances from the carboxylate group of Gal (Fig. 5c). At distances r > 6 Å, these numbers are close to 7.2 and 6.0 for Ca^{2+} and Zn^{2+}, respectively, in line with those that we determined from complementary MD simulations of the cations in the bulk (7.22 ± 0.44 and 6.00 ± 0.01). They also lie in the range of coordination numbers reported in the literature from numerous experimental and computational studies (6.2–9 for Ca^{2+} and ≈6 for Zn^{2+}, see, *e.g.* ref. 30 and 31 and references therein). The behaviors of the coordination numbers of Ca^{2+} and Zn^{2+} are strikingly different when these cations approach closer and closer from the carboxylate group of Gal. The coordination number of Ca^{2+} steeply decreases upon binding to the carboxylate group of Gal, so that Ca^{2+} loses on average about 1.5 and 2.1 water molecules in the monodentate and bidentate coordinations, respectively. In contrast, the coordination number of Zn^{2+} decreases to ~5 when Zn^{2+} binds to Gal in the monodentate and bidentate coordinations. Such different

behaviors probably originate from the differences found in the free energy barriers that water molecules from the 1st hydration shell of the cations need to cross to exchange with 2nd shell water molecules (Fig. 5a). This water exchange process is obviously much more unlikely for water hydrating Zn^{2+} than for those hydrating Ca^{2+}, as reflected by the much lower standard deviation for the coordination number of Zn^{2+} in comparison with that of Ca^{2+} found for these cations in the bulk (0.01 *vs.* 0.44).

We then investigated the ability of Ca^{2+} and Zn^{2+} to induce the association of Gal chains. For this purpose, we performed simulations in which (i) the two Gal chains were initially dissociated from each others, and (ii) calcium or zinc cations were initially not bound to the Gal chains (see Fig. S3 in the ESI†). We determined the number of contacts formed between the cations and carboxylate groups to describe the binding process (Fig. 6). A cation–Gal contact was considered to exist if the distance between the cation and the C6 atom of Gal residues (see Fig. S1 in the ESI† for atom names) was lower than 3.65 Å. This distance criterion was established from the C6–cation pair radial distribution functions (data not shown) and corresponds to distances shorter than the distances of the desolvation free energy barriers in Fig. 5b. The simulations show that the binding of Ca^{2+} cations to Gal (monocomplexation) occurs in the 1–5 ns time range, whereas that of Zn^{2+} lies in the 4–42 ns range. The much longer times found for Zn^{2+} are fully consistent with the larger free energy barrier in the PMF for the interaction of Zn^{2+} with the Gal monomer (Fig. 5b).

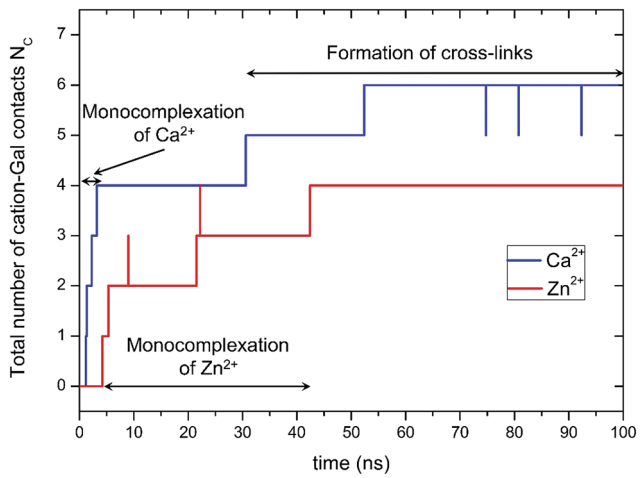

Fig. 6 Time evolution of the total number of contacts formed between the divalent cations and the carboxylate groups of the Gal chains, N_c. A contact was considered to be formed if the distance between the cations and the C6 atom of Gal units was lower than 3.65 Å. Any cation–Gal complexation increases N_c by 1. Accordingly, a Gal–cation–Gal bridge accounts for two contacts. In the initial configuration (t = 0 ns), the two Gal chains are dissociated and none of the divalent cations is in contact with them (N_c = 0). In the final configuration (t = 100 ns), the monocomplexation of both Ca^{2+} and Zn^{2+} is completed (that is, each cation is in contact with Gal), but only Ca^{2+} has induced the association of the two Gal chains (formation of cross-links). Fig. S3, Movies S1 and S2† on these simulations are provided in the ESI.†

Furthermore, within the time scale of these simulations (t = 100 ns), no association of the two Gal chains is observed in the presence of Zn^{2+} (N_c = 4 corresponds to the monocomplexation of each cation with the Gal chains), whereas Ca^{2+} cations induce the formation of two bridges between the two Gal chains at simulation times of about 30 and 50 ns (N_c = 6 indicates that the 4 cations are complexed with Gal and that two Gal–cation–Gal cross-links are formed). Fig. 6 also reveals that the monocomplexation process occurs before the formation of cross-links and thus before dimerization. In addition, these simulations clearly suggest that the formation of point-like cross-links between Gal chains enables the formation of a stable three-dimensional network.

Discussion

In the absence of divalent cations, the low-q-dependence of SANS spectra is much larger than that expected for a chain with a self-avoiding behavior ($I(q) \propto q^{-1.7}$), thereby indicating that LMP chains show signs of self-association (Fig. 3). This may stem from (i) inter- and/or intramolecular hydrogen bonds between hydroxyl and/or carboxylate groups of pectin, or from (ii) hydrophobic association between methyl groups of methyl-esterified α-D-galacturonic or rhamnose residues for instance. The association between chains is probably rather loose and highly fluctuating, since (i) the hairy regions of pectin prevent an efficient packing between adjacent chains for straightforward steric reasons, and (ii) the interaction between the carboxylate groups of neighbouring Gal residues is not favorable owing to their electrostatic repulsion. To better illustrate this, schematic representations of the structure formed by LMP in either the absence or in the presence of the zinc and calcium cations that can be deduced from our results are shown in Fig. 7.

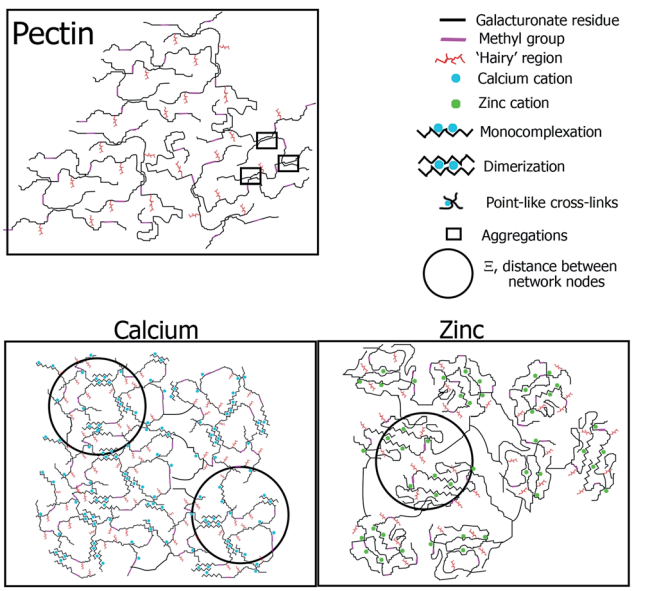

Fig. 7 Suggested scheme for the network of calcium and zinc pectin complexes at R = 0 (pectin alone) and R = 0.44.

At low molar ratios ($R < 0.25$), the binding enthalpy determined in ITC experiments is endothermic indicating that the binding between divalent cations and LMP is entropically driven. For the first cation injections, the binding enthalpy is higher for zinc ($\Delta H = 18.1$ kJ mol^{-1}) than for calcium ($\Delta H = 12.1$ kJ mol^{-1}). Thus, the binding of zinc to carboxylate groups of Gal is more difficult than the binding of calcium. This is in agreement with the larger free energy desolvation barrier of zinc compared to calcium found in our MD simulations (Fig. 5a), which show that water molecules hydrating zinc are less exchangeable than those hydrating calcium. Moreover, we observed an abrupt decrease of the gel's Ξ from 374 Å to respectively 301 Å for calcium and 290 Å for zinc when the ratio R increases from 0 to 0.09, showing a reduction of the distance between the network nodes. Since the decrease of the correlation length Ξ cannot arise from the formation of monocomplexes, it necessarily stems from (i) the formation of point-like cross-links between neighbouring chains, in agreement with Ventura *et al.*,[21] (ii) and/or from the formation of dimers and multimers (Fig. 7). In other words, the SANS data show that both monocomplexes and point-like cross-links already coexist at low molar ratios. This is consistent with the rather strong binding of divalent cations to Gal found in the MD simulations, which makes likely the formation of Gal–cation–Gal bridges already at low molar ratios. Our findings suggest that the partial monocomplexation of pectin is sufficient to form a network connected by stable point-like cross-links.

At intermediate and high molar ratios ($R > 0.25$), pectin chains become closer to each other, forming an ordered structure which corresponds to the exothermic process observed in ITC. This process was assigned to the dimerization step (association between two chains bridged by cations) observed by several authors.[13,21,22,32] According to SANS findings, Ξ lengths are similar for both $R = 0.09$ and $R = 0.44$ ($\Xi \sim 300$ Å) when calcium was added. The local structure (Table 2) and the macroscopic behavior (Fig. 1b) of the LMP–Ca did not change significantly, meaning that the dimerization may occur at the same time as the formation of monocomplexes and junction zones. This is in line with Fang *et al.*, who concluded that in contrast to alginate, the dimerization of LMP with calcium emerges immediately upon addition of calcium even if the stoichiometry ($R = 0.25$) is not satisfied.[13] They have shown that this dimerization consists mainly in the formation of point-like cross-links, which can be explained by the blockwise and random distribution of ester groups present in pectin that prevent the formation of long sequences of pectin–calcium–pectin bridges.

When zinc cations are added, a small increase of the Ξ length ($\sim$329 Å) accompanied by a twofold increase of the squared fluctuation in density ($\Delta\rho^2$) are observed for $R = 0.44$, showing the formation of large concentration fluctuations within the gel. The typical sizes of these density fluctuations are large enough to scatter light, explaining the increase of the turbidity observed for LMP–Zn (Fig. 1a) at such R. This indicates that aggregation and local shrinkage may occur. Indeed, it is important to remember that the forces that cause aggregation, *e.g.* local charge neutralization of carboxylate groups by adding cations, will often also be accompanied by shrinkage of the same aggregates.[33] Jonassen *et al.* have recently studied by dynamic light scattering and turbidity measurements the interaction between LMP and zinc cations.[34] They supposed that the addition of zinc cations induces the formation of a semi-cross-linked polymer network. The formation of such aggregates in the presence of zinc makes the distribution of pectin in the solution very heterogeneous and reduces its ability to form a percolating network. It has thus a minor influence on the macroscopic viscosity, as observed in Fig. 1b. As a consequence, the average overlap between chains (interactions between distinct aggregates) decreases. In contrast to zinc, the turbidity of calcium–LMP solutions increases slowly when the calcium cation is added indicating the progressive formation of aggregates. The low increase of turbidity may be also due to the presence of both aggregates (large objects with refractive index distinct from that of the medium) and to the formation of a continuous network (larger and less compact objects that have a refractive index closer to that of the medium), as confirmed by SANS measurements (Table 2). The formation of this continuous network can explain the steady increase of intrinsic viscosity observed at $R > 0.9$ (Fig. 1b). MD simulation of two Gal chains in the presence of divalent cations (Fig. S3, Movies S1 and S2 in the ESI†) confirms these observations. Indeed, at a given simulation time ($t = 100$ ns), both calcium and zinc were bound to the Gal chains (Fig. S3b in the ESI†). However, calcium induces the association of the two Gal chains, which can be considered as a precursor of a percolating network, while the two Gal chains remain dissociated in the presence of zinc. This may be explained by the mode of interaction between calcium and Gal (Fig. 4a): the bidentate coordination makes the association of Gal chains looser and also improves their ability to associate with each other, not only by dimerization, but also by the formation of point-like cross-links. Conversely, the mode of interaction between zinc and Gal, which looks closer to the egg-box model (monodentate coordination and tighter association of Gal chains, Fig. 4a), reduces the number of topological ways in which chains may associate with each other. For instance, chains should probably be more aligned with each other in the presence of zinc than in the presence of calcium for association to occur.

Conclusion

In this study, we investigated the interactions between low methoxy pectin and either Ca^{2+} or Zn^{2+} in semi-dilute solutions at different scales in association with MD simulation. Our results show that the addition of divalent cations changes the structure and the organization of LMP chains in several ways. The strong binding of cations to the carboxylate groups of Gal residues (monocomplexation) favors the formation of cross-links and/or the dimerization (or multimerization) of adjacent chains *via* bridges between neighbouring carboxylate groups. These associations of adjacent chains reduce the average distance between the nodes of the network formed (as indicated by the characteristic length Ξ determined from SANS measurements). In addition, our results suggest that the

network of pectin chains formed in the presence of Ca^{2+} is more homogeneous than the one formed in the presence of Zn^{2+}. The difference in this structure can be attributed to the way the cations interact with Gal. Indeed, MD simulations evidenced that the dehydration of zinc is more difficult than that of calcium. They also showed that zinc interacts with both carboxylate and hydroxyl groups of Gal, in a similar way to that described in the egg-box model, whereas calcium only interacts with carboxylate groups. These two different modes of interaction induce very different mobilities of chains; thus, calcium pectin seems to be more flexible than zinc pectin. This may explain why dosage forms prepared with calcium pectinate are more sensitive to water uptake than those made up with zinc, as observed previously,[14,16] and thus, why drug release is much faster in the case of calcium pectinate forms.

Conflict of interest

The authors declare no competing financial interest.

Acknowledgements

The ITC results were obtained with equipment from the technical platform RMB (Rhéologie et structure des Matériaux Biologiques) (AgroSup Dijon-Université de Bourgogne). The use of computational facilities at the Computing Center of the University of Bourgogne, DSI-CCUB, is gratefully acknowledged.

References

1 P. Cescutti and R. Rizzo, *J. Agric. Food Chem.*, 2001, **49**, 3262–3267.
2 V. M. Dronnet, M. A. V. Axelos, C. M. G. C. Renard and J.-F. Thibault, *Carbohydr. Polym.*, 1998, **35**, 29–37.
3 D. Thom, G. T. Grant, E. R. Morris and D. A. Rees, *Carbohydr. Res.*, 1982, **100**, 29–42.
4 M. Torre, A. R. Rodriguez and F. Saura-Calixto, *Food Chem.*, 1995, **54**, 23–31.
5 L. Liu, M. L. Fishman, J. Kost and K. B. Hicks, *Biomaterials*, 2003, **24**, 3333–3343.
6 A. G. J. Voragen, W. Pilnik, J.-F. Thibault, M. A. V. Axelos and C. M. G. C. Renard, *Food Polysaccharides and Their Applications*, Taylor & Francis, New York, 1995, 354–397.
7 A.-L. Kjøniksen, M. Hiorth and B. Nyström, *Eur. Polym. J.*, 2004, **40**, 2427–2435.
8 F. Liners and P. Van Cutsem, *Micron Microsc. Acta*, 1991, **22**, 265–266.
9 G. A. Luzio and R. G. Cameron, *Carbohydr. Polym.*, 2008, **71**, 300–309.
10 D. A. Powell, E. R. Morris, M. J. Gidley and D. A. Rees, *J. Mol. Biol.*, 1982, **155**, 517–531.
11 G. T. Grant, E. R. Morris, D. A. Rees, P. J. C. Smith and D. Thom, *FEBS Lett.*, 1973, **32**, 195–198.
12 I. Braccini and S. Pérez, *Biomacromolecules*, 2001, **2**, 1089–1096.
13 Y. Fang, S. Al-Assaf, G. O. Phillips, K. Nishinari, T. Funami and P. A. Williams, *Carbohydr. Polym.*, 2008, **72**, 334–341.
14 A. Assifaoui, O. Chambin and P. Cayot, *Carbohydr. Polym.*, 2011, **85**, 388–393.
15 C. Dhalleine, A. Assifaoui, B. Moulari, Y. Pellequer, P. Cayot, A. Lamprecht and O. Chambin, *Int. J. Pharm.*, 2011, **414**, 28–34.
16 A. Assifaoui, C. Loupiac, O. Chambin and P. Cayot, *Carbohydr. Res.*, 2010, **345**, 929–933.
17 B. M. Yapo, *Food Res. Int.*, 2009, **42**, 1197–1202.
18 I. Schmidt, F. Cousin, C. Huchon, F. Boué and M. A. V. Axelos, *Biomacromolecules*, 2009, **10**, 1346–1357.
19 B. R. Brooks, C. L. Brooks, A. D. Mackerell, L. Nilsson, R. J. Petrella, B. Roux, Y. Won, G. Archontis, C. Bartels, S. Boresch, A. Caflisch, L. Caves, Q. Cui, A. R. Dinner, M. Feig, S. Fischer, J. Gao, M. Hodoscek, W. Im, K. Kuczera, T. Lazaridis, J. Ma, V. Ovchinnikov, E. Paci, R. W. Pastor, C. B. Post, J. Z. Pu, M. Schaefer, B. Tidor, R. M. Venable, H. L. Woodcock, X. Wu, W. Yang, D. M. York and M. Karplus, *J. Comput. Chem.*, 2009, **30**, 1545–1614.
20 I. Braccini, R. P. Grasso and S. Pérez, *Carbohydr. Res.*, 1999, **317**, 119–130.
21 I. Ventura, J. Jammal and H. Bianco-Peled, *Carbohydr. Polym.*, 2013, **97**, 650–658.
22 C. K. Siew, P. A. Williams and N. W. G. Young, *Biomacromolecules*, 2005, **6**, 963–969.
23 L. Ge, M. Vernon, S. Simon, Y. Maham, J. Sjöblom and Z. Xu, *Colloids Surf., A*, 2012, **396**, 238–245.
24 Y. Fang, S. Al-Assaf, G. O. Phillips, K. Nishinari, T. Funami, P. A. Williams and L. Li, *J. Phys. Chem. B*, 2007, **111**, 2456–2462.
25 F. Muller, S. Manet, B. Jean, G. Chambat, F. Boué, L. Heux and F. Cousin, *Biomacromolecules*, 2011, **12**, 3330–3336.
26 P. Debye and A. M. Bueche, *J. Appl. Phys.*, 1949, **20**, 518–525.
27 W. Plazinski, *J. Comput. Chem.*, 2011, **32**, 2988–2995.
28 A. Wolnik, L. Albertin, L. Charlier and K. Mazeau, *Biopolymers*, 2013, **99**, 562–571.
29 E. Iskrenova-Tchoukova, A. G. Kalinichev and R. J. Kirkpatrick, *Langmuir*, 2010, **26**, 15909–15919.
30 J.-P. Piquemal, L. Perera, G. A. Cisneros, P. Ren, L. G. Pedersen and T. A. Darden, *J. Chem. Phys.*, 2006, **125**, 054511.
31 J. C. Wu, J.-P. Piquemal, R. Chaudret, P. Reinhardt and P. Ren, *J. Chem. Theory Comput.*, 2010, **6**, 2059–2070.
32 I. Donati, S. Holtan, Y. A. Morch, M. Borgogna, M. Dentini and G. Skjak-Brak, *Biomacromolecules*, 2005, **6**, 1031–1040.
33 L. T. T. Trinh, H. M. L. Lambermont-Thijs, U. S. Schubert, R. Hoogenboom and A.-L. Kjøniksen, *Macromolecules*, 2012, **45**, 4337–4345.
34 H. Jonassen, A. Treves, A.-L. Kjøniksen, G. Smistad and M. Hiorth, *Biomacromolecules*, 2013, **14**, 3523–3531.

PART 2

Binding of divalent cations to polygalacturonate: a mechanism driven by the hydration water

THE JOURNAL OF PHYSICAL CHEMISTRY B

Article

pubs.acs.org/JPCB

Binding of Divalent Cations to Polygalacturonate: A Mechanism Driven by the Hydration Water

Uyen T. D. Huynh,[†,§] Adrien Lerbret,[*,†] Fabrice Neiers,[‡] Odile Chambin,[†] and Ali Assifaoui[*,†]

[†]UMR PAM, Equipe PAPC, and [‡]CSGA INRA-CNRS, Université Bourgogne Franche-Comté, 21000 Dijon, France

[§]Danang College of Technology, University of Danang, Danang, Viet Nam

Supporting Information

ABSTRACT: We have investigated the interactions between polygalacturonate (polyGal) and four divalent cations (M^{2+} = Ba^{2+}, Ca^{2+}, Mg^{2+}, Zn^{2+}) that differ in size and affinity for water. Our results evidence that M^{2+}−polyGal interactions are intimately linked to the affinity of M^{2+} for water. Mg^{2+} interacts so strongly with water that it remains weakly bound to polyGal (polycondensation) by sharing water molecules from its first coordination shell with the carboxylate groups of polyGal. In contrast, the other cations form transient ionic pairs with polyGal by releasing preferentially one water molecule (for Zn^{2+}) or two (for Ca^{2+} and Ba^{2+}), which corresponds to monodentate and bidentate binding modes with carboxylates, respectively. The mechanism for the binding of these three divalent cations to polyGal can be described by two steps: (i) monocomplexation and formation of point-like cross-links between polyGal chains (at low M^{2+}/Gal molar ratios, R) and (ii) dimerization (at higher R). The threshold molar ratio, R^*, between these two steps depends on the nature of divalent cations and is lower for calcium ions ($R^* < 0.1$) than for zinc and barium ions ($R^* > 0.3$). This difference may be explained by the intermediate affinity of Ca^{2+} for water with respect to those of Zn^{2+} and Ba^{2+}, which may induce the formation of cross-links of intermediate flexibility. By comparison, the lower and higher flexibilities of the cross-links formed by Zn^{2+} and Ba^{2+}, respectively, may shift the formation of dimers to higher molar ratios (R^*).

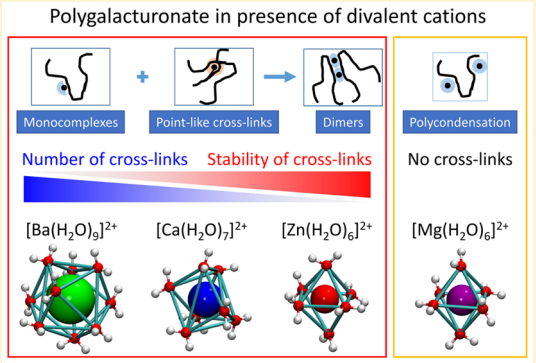

INTRODUCTION

The interaction between multivalent cations and anionic polysaccharides such as pectin and alginate is of major interest for a wide range of applications in the food, pharmaceutical, and pollutant treating industries.[1−4] The binding between multivalent cations (e.g., Ca^{2+}, Zn^{2+}, Cu^{2+}, Co^{2+}, Ni^{2+}, and Fe^{3+}) and these polysaccharides usually leads to the formation of hydrogels with properties that depend on the nature (size, valence electron shell, and coordination number) and the amount of the cations.[5−9] Among these polysaccharides, pectin, which is found mainly in the primary cell walls of most plants, can bind multivalent cations and forms gels that can be used to entrap drugs or to immobilize cells and enzymes. Pectin is composed of a long sequence of partially methyl-esterified (1−4)-linked α-D-galacturonate residues. The regular polygalacturonate (polyGal) backbone is interrupted by 1−2-linked L-rhamnose residues that constitute sites of attachment for other sugar chains.[10,11] The ability of pectin to bind multivalent cations stems from the presence of carboxylate groups in polyGal and depends strongly on both the degree of methylation and the number of consecutive non-methylated carboxylate groups.

Many papers have tried to elucidate how the structure and the conformation of these anionic polysaccharides (alginate and pectin) evolve in the presence of multivalent cations.[6,12−17] The changes in the conformation and in the structure are due to the bindings of these cations with carboxylate groups, which displace some of the precondensed monovalent cations.[18] The affinity of alkaline earth metals for alginate and pectin was found to increase in the following order: $Mg^{2+} \ll Ca^{2+} < Sr^{2+} < Ba^{2+}$.[18] In addition, a comparative study of the interactions of Ca^{2+} and Mg^{2+} cations with polyGal by means of ultracentrifugation, conductimetry, potentiometry, and circular dichroism showed that Ca^{2+} cations were able to coordinate with two carboxylate groups and to induce interchain associations, whereas Mg^{2+} complexation with polyGal was electrostatic only.[19] Raman studies suggested different interaction modes between polyacrylate anionic polymers and divalent cations: the formation of covalent bonds in the case of Cu^{2+}, Zn^{2+}, and Mn^{2+} and electrostatic interactions in the case of Mg^{2+} and Ba^{2+}.[20] Gelation with magnesium cations was also found to depend strongly on alginate's chemical composition, as the presence of long sequences of guluronate units favors faster gel formation.[13,21]

The association between alginate and Ca^{2+} has been the most studied one,[15,22−24] and it was assumed to follow the "egg-box"

Received: November 10, 2015
Revised: January 12, 2016
Published: January 15, 2016

DOI: 10.1021/acs.jpcb.5b11010
J. Phys. Chem. B 2016, 120, 1021−1032

model proposed by Grant et al.[16] This model has subsequently been transposed to describe the calcium−pectin association, but its validity has not been corroborated. From molecular mechanics calculations, Braccini and Perez[12] have proposed a "shifted egg-box" model to describe the calcium pectinate structure. Our recent molecular dynamics simulations of galacturonate chains in explicit water showed that the "egg-box" model is more adapted for zinc cations than for calcium ones.[5] Indeed, we found that Zn^{2+} interacts with both carboxylate and hydroxyl groups of galacturonate units, in a similar way to that described in the "egg-box" model, whereas calcium cations only interact with carboxylate groups. By means of isothermal titration calorimetry (ITC) measurements, De and Robinson found a two-step binding process between Ca^{2+} and alginate at various NaCl concentrations (0−100 mM).[25] The first binding step was found to be entropically driven, whereas the second one exhibited a weaker affinity and was both entropically and enthalpically driven.[25] From ITC data, Fang et al. proposed that the binding of Ca^{2+} to alginate occurs in multiple steps including monocomplexation at a low molar ratio, $R = M^{2+}/Gal$, followed by dimerization ($0.25 < R < 0.55$) and, then, by the lateral association of dimers (multimerization) ($R > 0.55$).[15] It must be pointed out that owing to the rather low affinity constant for the COO^--M^{2+} interaction in various monoacids, monocomplexation refers to a state where the exchange between bound and unbound cations continuously occurs. For low methoxy pectin (branched polymer), these authors[14] suggested that only two steps occurred: monocomplexation ($R < 0.25$) followed by a progressive dimerization step ($R > 0.25$).[14] The absence of significant lateral association with low methoxy pectin (LMP) was interpreted in terms of structural features of pectin:[14] the random distribution of ester and/or amide groups along the pectin chain introduces much more defects into the formation of dimers and even hinders the subsequent lateral association of dimers. In line with the results of Fang et al.,[14] we also observed two thermal processes for LMP in the presence of calcium and zinc ions.[5] The first process was entropically driven and may be ascribed not only to the formation of monocomplexes between divalent cations and carboxylate groups,[15] but also to the formation of point-like cross-links.[5,26] The second process was exothermic and may correspond to the formation of an ordered structure (dimers or multimers). Borgogna et al.[27] suggested by means of viscosity, circular dichroism, light scattering, and fluorescence measurements on alginate that the point-like cross-links involve four guluronate residues arranged in a locally tilted conformation, which they referred to as "tilted egg-box". It can be noted that cations from these point-like cross-links are probably loosely bound, which allows the subsequent dimer formation (strong cross-linking). When analyzing small-angle X-ray scattering (SAXS) data on LMP in the presence of calcium ions, Ventura et al. have underlined the importance of point-like cross-links in the gelation mechanism of LMP.[26] Indeed, for low molar ratios, they suggested the coexistence of monocomplexes, dimers, and point-like cross-links. Their results imply that when the molar ratio increases, the number of rod-like junction zones (dimerization) decreases and the number of point-like cross-links and monocomplexes increases. In our recent study,[5] small-angle neutron scattering measurements (SANS) showed that increasing the molar ratio from 0.09 to 0.44 did not change significantly the mesh size of the network, suggesting that point-like cross-links are already formed at low molar ratios, thus stabilizing the network, in line with the study of Ventura et al.[26] The binding mechanism is definitely influenced by several factors such as the nature, the composition, and the concentration of the polymer, the pH, the ionic strength, the presence of anions, and, in particular, the nature of divalent cations. For instance, our SANS measurements evidenced that the network of pectin chains formed in the presence of calcium cations is more homogeneous than the one formed in the presence of zinc cations.[5]

The aim of this study is to investigate the binding process of four divalent cations (Mg^{2+}, Ca^{2+}, Ba^{2+}, and Zn^{2+}) to polygalacturonate (polyGal) in semidilute solution and to propose a mechanism for the binding of each divalent cation with polyGal. We first choose cations from the alkaline earth metal group with an increasing ionic radius (Mg^{2+}, Ca^{2+}, Ba^{2+}) and a similar electronic structure for the valence shell (np^6). According to the Hofmeister series, the kosmotropic effect increases in the following order: $Mg^{2+} > Ca^{2+} > Sr^{2+} > Ba^{2+}$.[28] Then we choose to study Zn^{2+} because it has a similar size to that of Mg^{2+}, but it exhibits a different electronic structure for the valence shell (3d). In addition, Zn^{2+} was used to design pectin drug delivery systems with specific properties.[29] Furthermore, we investigate the interaction of these cations with polyGal rather than with LMP. PolyGal is a well-defined anionic linear homopolymer that can form a gel only via the formation of polyGal−cation−polyGal bridges. In contrast, LMP exhibits a branched structure and contains hydrophobic units that may favor chain association. We have investigated the binding energy between these cations and polyGal by ITC at various molar ratios ($R = M^{2+}/Gal$). The characteristics of the polyGal network in the presence of the four divalent cations were studied by viscosity and turbidity measurements. Finally, we performed molecular dynamics (MD) simulations to further describe the Gal−cation interactions as well as the association of polyGal chains.

MATERIALS AND METHODS

Materials. Poly-D-galacturonic acid (95% purity, $M_w \sim 50$ kDa), calcium chloride dihydrate, and barium chloride were obtained from Sigma (St. Louis, MO). Anhydrous sodium chloride, zinc chloride, and magnesium chloride were purchased from VWR, BDH Prolabo.

Methods. *Sample Preparation.* The polygalacturonic acid powder was gradually dissolved in a 10 mM solution of NaCl, and the pH was adjusted to 5.5 using a NaOH solution (1 M). The pH studied is 2 pH units above the pK_a of carboxylic groups (about 3.5) so as to obtain mostly polygalacturonate (polyGal). The final solution (0.5 g L^{-1}) was filtered through a 0.45 μm filter (Minisart High Flow, Milian, USA). Taking into consideration the degree of purity of polyGal (95%) and the molecular weight of the galacturonate (Gal) unit (176 g mol^{-1}), the molar concentration of polyGal is equal to 2.70 mM of Gal. The stock solutions of calcium, zinc, barium, and magnesium cations were also prepared in the same solution of NaCl (10 mM), and their concentrations were equal to 13.5 mM.

Turbidity Measurements. The turbidity of polyGal solutions at different calcium, zinc, barium, and magnesium concentrations in 10 mM solution of NaCl (pH = 5.5) were measured using an ultraviolet−visible (UV) spectrophotometer (Biochrom Libra, France) at a wavelength of 435 nm and at room temperature. Samples were analyzed in a quartz cuvette with a cell path length of 1 cm. Various molar ratios ($R = M^{2+}/Gal$) were analyzed using 2 mL of the polyGal solution (2.7 mM) and an adequate volume of the divalent cation solution (13.5

DOI: 10.1021/acs.jpcb.5b11010
J. Phys. Chem. B 2016, 120, 1021−1032

mM). The mixture was then stirred, and the transmittance was recorded. All the measurements were done at least in triplicate. Turbidity, τ (cm^{-1}), can be determined from the equation

$$\tau = \left(-\frac{1}{L}\right)\ln\left(\frac{I_t}{I_0}\right) \quad (1)$$

where L is the optical path length (= 1 cm), and I_t and I_0 are the transmitted and incident light intensities, respectively.

Viscosity Measurements. The specific viscosity measurements were performed using a capillary viscosimeter (SI analytics, Germany). The viscosimeter was immersed in a thermostatic water bath at 30 °C. After loading the sample into the viscosimeter, the solutions with and without polyGal were allowed to equilibrate at the bath temperature before starting the experiment. The specific viscosity (η_{sp}) then corresponds to $(\eta_s - \eta_0)/\eta_0$, where η_s and η_0 refer to the viscosities of the solutions with and without polyGal, respectively. All experiments were done at least in triplicate. The specific viscosities were measured for the four divalent cations (Ca^{2+}, Zn^{2+}, Ba^{2+}, Mg^{2+}) at various molar ratios from 0 to 0.6.

Determination of the Amount of Divalent Cations Entrapped into the PolyGal Network. Solutions of the four divalent cations (Ca^{2+}, Zn^{2+}, Ba^{2+}, Mg^{2+}) were prepared at five molar ratios (R = 0, 0.1, 0.2, 0.3, 0.4) as described above. Each mixture was stirred for 15 min and filtered through a 0.2 μm filter (Syringe Filter, Fisherbrand, China). The filter was washed with 5 mL of distilled water. The quantification of divalent cations in the filtrate was performed by inductively coupled plasma atomic emission spectroscopy (ICP-AES) iCAP 7400. The content of divalent cations entrapped into the polyGal network corresponds to the difference between the content of divalent cations initially introduced and that present in the filtrate. It must be pointed out that the amount of unbound cations could be overestimated because particles of size lower than 0.2 μm can pass through the filter. All the measurements were done in duplicate.

Isothermal Titration Calorimetry. An isothermal titration calorimeter (VP-ITC microcalorimeter from GE Healthcare) was used to determine the enthalpies for the binding of divalent cations to polyGal at 25 °C. Before each experiment, all solutions were degassed for 15 min. A portion of the divalent cation solutions ($CaCl_2$, $ZnCl_2$, $BaCl_2$, $MgCl_2$) was injected sequentially into a 1.46 mL titration cell initially containing either a 10 mM NaCl solution or the polyGal solution (2.70 mM of Gal). In order to study the binding over a broad range of molar ratios, we performed various experiments by changing the concentration of divalent cations [L], the volume of divalent cations injected (V_{cat}), and the time interval between successive injections (Δt) (Table S1 in Supporting Information). For the first binding isotherm ($0 < R < 0.43$), the parameters [L], V_{cat}, and Δt were equal to 13.5 mM, 3 μL (for the first 15 injections) and 5 μL (for the 16 following ones), and 1000 s, respectively. To describe more accurately the low molar ratio range ($0 < R < 0.05$), a second binding isotherm was done where the concentration of divalent cations was diluted four times (3.4 mM), and V_t and Δt were set to 3 μL and 1000 s, respectively. A rotating 125 μL Hamilton microsyringe ensuring constant stirring of the whole mixed dispersion at a speed of 250 rpm was employed for the homogenization during injection. The heat after each injection was derived by calculating the area under each peak. The total heat content, Q, of the solution contained in V_0 is given by the equation

$$Q = [M]_t V_0 N \Delta H \theta \quad (2)$$

where $[M]_t$ is the total amount of polyGal in the cell, N is the number of binding sites per Gal unit, ΔH is the binding enthalpy, and θ is the fraction of sites occupied by ligand [L] (which here refers to Ca^{2+}, Zn^{2+}, Ba^{2+}, or Mg^{2+} concentration). The binding isotherm obtained by integrating injection peaks was fitted by a model of independent binding sites (eq 3) using a nonlinear least-squares minimization method implemented in the Chasm software.[30]

$$Q = V_0 \Delta H \times \left[[L] + \frac{1 + [M]_t N K_b - \sqrt{(1 + [M]_t N K_b - [L]K_b)^2 + 4K_b[L]}}{2K_b}\right] \quad (3)$$

Iterative curve fitting yielded thermodynamic parameters including the binding constant K_b, the binding enthalpy ΔH, and the stoichiometry N. A full thermodynamic profile was then obtained using the relationship

$$\Delta G = \Delta H - T\Delta S = -RT\ln(K_b) \quad (4)$$

where ΔG, ΔH, and ΔS are the Gibbs free energy, enthalpy, and entropy of binding, respectively. T is the absolute temperature, and R = 8.314 J mol^{-1} K^{-1} is the ideal gas law constant. All the measurements were done at least in triplicate.

Molecular Dynamics Simulations. We performed molecular dynamics (MD) simulations in a similar way as in ref 5 to understand how the four divalent cations interact with Gal. For this purpose, we first performed umbrella sampling simulations to determine the potentials of mean force (free energy profiles) for the interaction of the divalent cations either with water or with the carboxylate group of Gal. To describe the association of Gal chains in aqueous solution, we then performed standard 100 ns long MD simulations of two octameric Gal chains at a ratio R of 0.25 (4 divalent cations for a total of 16 Gal units) that allows the dimerization of Gal chains in the egg-box model.[12,16] The length of these Gal chains (8 monomers) corresponds approximately to the minimal length (9−20 monomers) necessary to form dimers of oligogalacturonates in the presence of calcium determined experimentally.[18,31,32] In the initial configuration of these simulations, the two Gal chains were neither in contact with each other nor with any divalent cations (see Figure 5a). We also run independent simulations of the divalent cations alone in water to determine their average hydration number, the structure of their hydration shell, and their total interaction energy with water in the bulk. All simulations were performed at a temperature of 300 K, and chloride or sodium ions were added to the simulation boxes to ensure charge neutrality. Further details on all of these simulations are provided in ref 5 and in the molecular dynamics simulation section in the Supporting Information. All simulations were performed using the CHARMM program,[33] version c35b1.

RESULTS

Characteristics of the Cation−PolyGal Network. The specific viscosity and the turbidity of polyGal solutions, as well as the amount of divalent cations bound to polyGal, are presented as a function of the molar ratio R for Ca^{2+}, Zn^{2+}, Ba^{2+}, and Mg^{2+} in Figure 1.

DOI: 10.1021/acs.jpcb.5b11010
J. Phys. Chem. B 2016, 120, 1021−1032

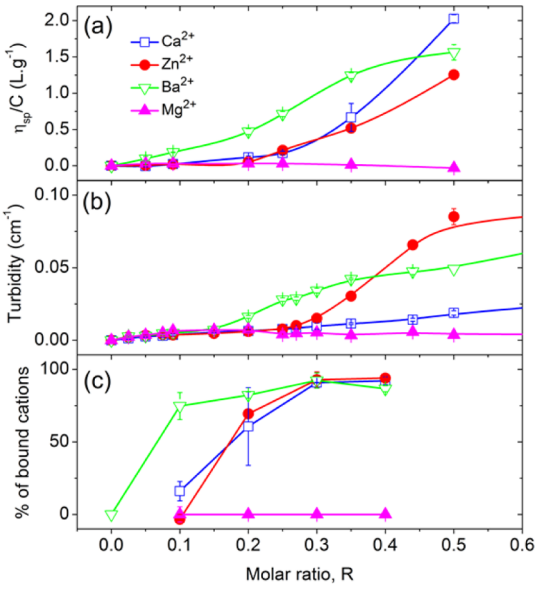

Figure 1. Evolution of the specific viscosity (η_{sp}/C) (a), of the turbidity at 435 nm (b), and of the amount of bound divalent cations (c) for a polyGal solution (2.7 mM of Gal, 10 mM NaCl, pH= 5.5, T = 25 °C) as a function of the molar ratio, R (M^{2+}/Gal), for calcium ions (empty blue squares), zinc ions (full red circles), barium ions (empty green down triangles), and magnesium ions (full magenta up triangles).

At low molar ratios ($R \leq 0.1$), the specific viscosity and turbidity remain constant and close to zero and then start to increase at higher molar ratios for Ca^{2+}, Zn^{2+}, and Ba^{2+}. The onsets for the increases in specific viscosity appear at a molar ratio R of 0.1 for Ba^{2+} and of about 0.25 for Ca^{2+} and Zn^{2+} (Figure 1a). The onsets for the increases of turbidity, which may reveal the formation of large-scale density fluctuations that strongly scatter light, are also shifted to high molar ratios in the following order: $Ba^{2+} < Zn^{2+} < Ca^{2+}$ (Figure 1b). Furthermore, the amount of divalent cations entrapped into the polyGal network increases and exceeds 75% of entrapped cations first for Ba^{2+} (at R = 0.1) and then for Ca^{2+} and Zn^{2+} (at R = 0.3) (Figure 1c). Interestingly, the turbidity, the specific viscosity, and the amount of divalent cations bound to polyGal (Figure 1) remain constant and close to zero upon the addition of Mg^{2+} over the molar ratio range studied here, thereby indicating that Mg^{2+} does not participate in the network formation, in line with the Manning's counterion condensation theory.[13,34] Note that the method used to estimate the amount of bound cations is not very accurate. Malovikova et al. have used a more accurate method (ultracentrifugation) to separate polyGal from the unbound calcium or magnesium and found that the amount of magnesium is the same before and after the centrifugation, in line with our results (Figure 1c).[19]

Thermodynamic Behavior of the Cation−PolyGal Complex. The binding isotherms [$0 < R < 0.43$] of divalent cations to polyGal are presented in Figure 2. Their shapes differ a lot from one divalent cation to the other. For Ca^{2+} addition (Figure 2a), two processes are observed: an abrupt decrease of binding enthalpy at low molar ratios ($R < 0.05$, step 1) followed by a large and progressive increase of binding enthalpy (step 2). Only three injections described the first process in the initial

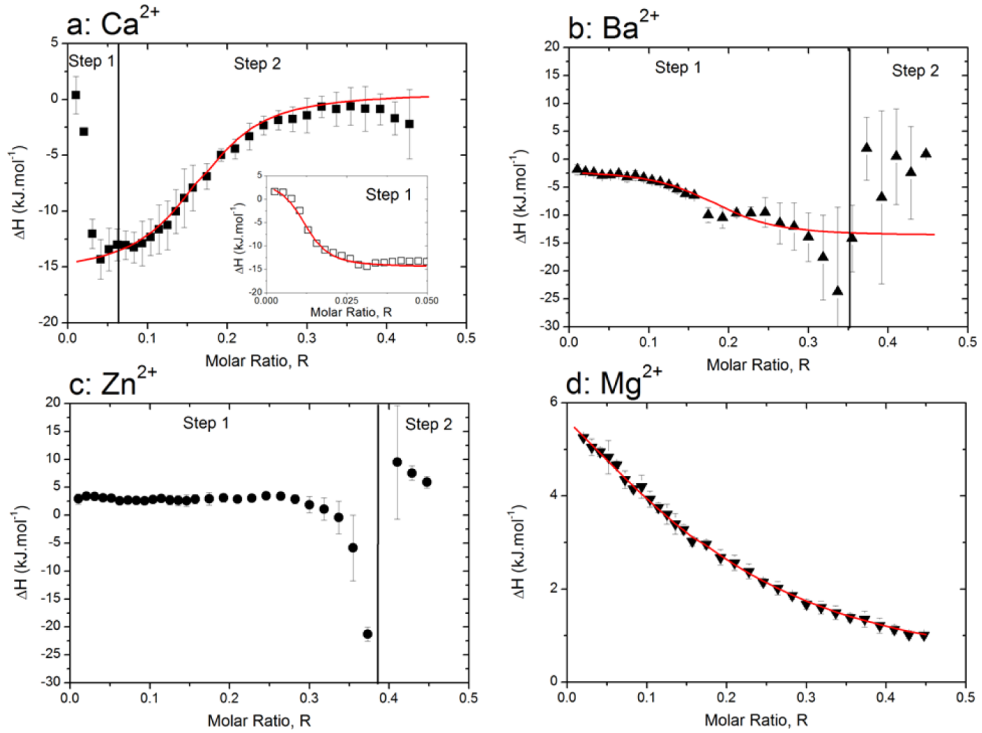

Figure 2. Binding enthalpy (ΔH) as a function of the molar ratio, R = M^{2+}/Gal, for Ca^{2+} (a), Ba^{2+} (b), Zn^{2+} (c), and Mg^{2+} (d). The inset in (a) corresponds to the additional low-ratio titration performed to better describe the first step of binding for calcium ions. Red lines correspond to the fits obtained with the model of independent binding sites using the Chasm software.[30] We could not fit the titration curve for Zn^{2+} as well as the second process in the binding of Ba^{2+} to polyGal, given that the steep changes in ΔH of the two processes occur over a very narrow molar ratio range. The experiments were done at pH = 5.5, in 10 mM of NaCl, and at a temperature of 25 °C. The data shown have been averaged over three independent titrations.

DOI: 10.1021/acs.jpcb.5b11010
J. Phys. Chem. B 2016, 120, 1021−1032

Table 1. Thermodynamic Parameters Derived from the Fit with the Model of Independent Binding Sites of the Binding Enthalpy (ΔH) as a Function of the Molar Ratio R of Added Divalent Cations into a PolyGal Solution (2.7 mM Gal, 10 mM NaCl, pH = 5.5, and T = 25 °C)[a]

		N	$10^{-4}K_b$ (M^{-1})	ΔH (kJ mol^{-1})	$T\Delta S$ (kJ mol^{-1})	ΔG (kJ mol^{-1})
Ca^{2+}	step 1	0.01 ± 0.00	28.0 ± 5.0	18.8 ± 2.1	49.9 ± 4.3	−31.0 ± 3.0
	step 2	0.17 ± 0.01	3.3 ± 1.2	−16.6 ± 2.7	9.1 ± 3.6	−25.7 ± 1.0
Ba^{2+}	step 1	0.18 ± 0.02	6.9 ± 2.7	28.5 ± 8.7	55.9 ± 8.1	−27.4 ± 0.9
	step 2			n.d.[b]		
Zn^{2+}	step 1			n.d.		
	step 2			n.d.		
Mg^{2+}	step 1	0.17 ± 0.01	0.26 ± 0.0	10.0 ± 0.3	29.5 ± 0.1	−19.5 ± 0.1

[a] N is the number of binding sites per galacturonate unit, K_b is the binding constant, ΔH is the binding enthalpy, ΔS is the entropy, and ΔG is the free energy. For each divalent cation, three independent titration curves were fitted separately with the CHASM software.[30] [b] n.d.: thermodynamic parameters were not determined because we were not able to fit reliably the corresponding data.

titration measurements that we performed, which did not allow an accurate determination of the associated enthalpy change. Therefore, we did a second titration of polyGal using a 4 times diluted solution of Ca^{2+} to increase the number of data points in this low molar ratio region [0−0.05] (inset of Figure 2a). The thermodynamic parameters obtained from the fitting procedure reveal that the first process has a higher affinity (K_1 = 28 × 10^4 M^{-1}) than the second one (K_2 = 3.3 × 10^4 M^{-1}) and is entropically driven, in contrast to the second one (Table 1). Previous studies have also described two distinct binding processes for binding calcium ions to alginate[15,25] or to low methoxy pectin.[5] The first step could be due to the dehydration of cations and may correspond to both monocomplexation and the formation of point-like cross-links. The second step, which is an indication of the cooperative formation of an ordered structure, may arise from the formation of dimers. The variation of binding enthalpy (decrease followed by an increase) may indicate a change in the nature of cross-links, from point-like cross-links to dimers. The distinction between these two types of cross-links has been evidenced by Borgogna et al. for the binding of calcium and magnesium to alginate by using viscosity, circular dichroism, light scattering, and fluorescence measurements.[27]

Moreover, in line with the thermodynamic parameters from ITC (Table 1), De and Robinson found that the first process for binding Ca^{2+} to alginate has also a higher affinity than the second one (with 10 mM of NaCl, K_1 = 77 × 10^4 M^{-1} and K_2 = 1.2 × 10^4 M^{-1}) and that it is entropically driven, whereas the second one is both entropically and enthalpically driven (ΔH_1 = 1.45 kJ mol^{-1} and ΔH_2 = −16.05 kJ mol^{-1}). Furthermore, their study revealed that the thermodynamic parameters for the first process (K_1 and ΔH_1) decrease when the concentration of NaCl increases from 0 to 100 mM.[25] In addition, Fang et al.[15] have observed the same shape of ITC thermogram for the binding of Ca^{2+} to alginate in acetate buffer (20 mM) and found thermodynamic parameters for the second process (K_2 = 1.1 × 10^4 M^{-1} and ΔH_2 = −15.0 kJ mol^{-1}) in line with our results (Table 1). In our previous study, we have also observed two phenomena for the binding of calcium ions to low methoxy pectin in acetate buffer (20 mM), but we could only fit the first process, which was entropically driven (K_1 ∼ 2 × 10^4 M^{-1} and ΔH_1 = 12.1 ± 0.3 kJ mol^{-1}), given the low enthalpy change of the second process.[5]

The titration of polyGal with Ba^{2+} shows a decrease in binding enthalpy (step 1) followed by an abrupt increase (Figure 2b). Such a binding behavior is roughly analogous to that of Ca^{2+}. However, the limit between the two processes occurs at much larger ratios for Ba^{2+} (R ∼ 0.35) than for Ca^{2+} (R ∼ 0.05). Furthermore, the decrease of ΔH seems to proceed in two successive steps for barium ions, but the too low amplitude and the too large error bars of data points led us to fit with only one process. Similarly, the increase in ΔH is not well-defined enough to allow a consistent fit of the associated process. As for calcium binding, the thermodynamic parameters for Ba^{2+} show that the first process is entropically driven but has an affinity constant about 4 times lower (Table 1).

For Zn^{2+} addition, the binding enthalpy remains almost constant up to a molar ratio of 0.3 (Figure 2c). Then, similarly to calcium and barium ions, we observe a decrease (step 1) followed by an increase of ΔH (step 2), but these two processes occur over a very small molar ratio range [0.3−0.45] with large error bars, which make their fit unreliable. These huge variations are probably related to the increase of turbidity observed at a similar molar ratio (Figure 1b). It is particularly interesting that the titration curves of polyGal with Zn^{2+} and with Ca^{2+} differ so much from each other, given that the thermodynamic parameters for the binding of Zn^{2+} and Ca^{2+} to low methoxy pectin (LMP) were rather similar in our previous study.[5] Such a difference in the binding of zinc ions to polyGal and to LMP could first be ascribed to the difference in the nature of the two biopolymers, namely, the lower amount of Gal units in LMP, the presence of branched zones, and the presence of ester groups and their random distribution. It could also stem from the presence of acetate counterions in the preparation of LMP solutions, which may compete with LMP for binding zinc cations.[5] The above reasons may also explain the much higher binding affinity (K_1 = 28 × 10^4 M^{-1}) observed for Ca-polyGal in comparison with that Ca-LMP (K_1 = 2.05 × 10^4 M^{-1}). This is in accordance with previous ITC studies, which suggest that thermodynamic parameters depend on the experimental conditions such as pH, temperature, ionic strength, and nature of counterions (acetate, phosphate).[13,15,25,35,36]

For Mg^{2+} addition, only one process is observed in the molar ratio range studied (Figure 2d). This process is entropy driven and has an affinity about 100 times lower than that of Ca^{2+} (Table 1). Donati et al. have found similar trends for the binding of Mg^{2+} to analogous anionic polysaccharides (mannuronan, guluronan, and the polyalternating copolymer), but with even lower affinity constant and binding enthalpy.[13] They described Mg^{2+} ions as "diffusely bound" counterions in line with Manning's counterion condensation theory.[34]

Molecular Simulation. The above results evidence that the four divalent cations considered in this study bind in different

DOI: 10.1021/acs.jpcb.5b11010
J. Phys. Chem. B 2016, 120, 1021−1032

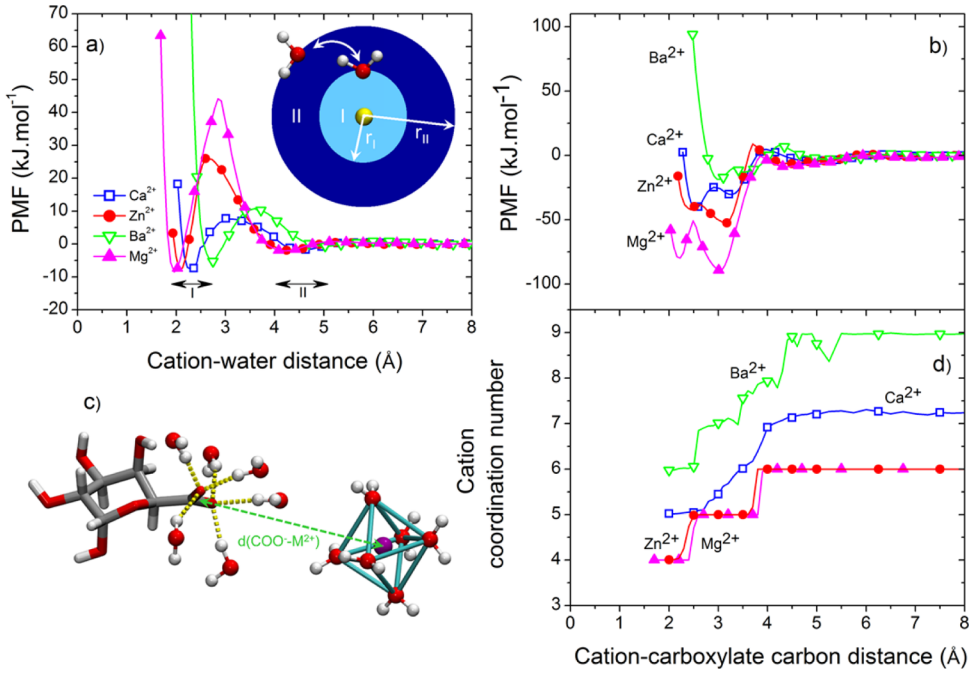

Figure 3. Potentials of mean force (PMFs) for the interaction between the divalent cations and either (a) water molecules or (b) Gal. A snapshot from the umbrella sampling simulation of Gal in the presence of Mg^{2+} is shown in (c). For clarity, only water molecules from the first hydration shell of Mg^{2+} or from those of the carboxylate oxygens are shown, and dashed yellow lines represent hydrogen bonds. The average coordination numbers of the cations as a function of the cation−carboxylate carbon distance are shown in (d). Symbols for Ca^{2+}, Zn^{2+}, Ba^{2+}, and Mg^{2+} are empty blue squares, full red circles, empty green down triangles, and full magenta up triangles, respectively. For clarity, about one of five data points was represented as symbols in (a), (b), and (d).

ways to polyGal and probably lead to distinct structures of the polyGal network. To understand how these cations interact with polyGal at the atomistic scale, we performed a series of MD simulations. We first computed the potentials of mean force (PMFs, that is, free energy profiles) for unbinding a water molecule from the first coordination shell of the divalent cations by means of umbrella sampling simulations. The two minima, I and II, that appear in these PMFs (Figure 3a) relate to water molecules from the first and the second hydration shells of the cations, respectively. The positions of these minima, r_I and r_{II}, agree reasonably well with experimental values[37] and increase in the following order: Mg^{2+} < Zn^{2+} < Ca^{2+} < Ba^{2+} (Table 2).

Table 2. Data for the Divalent Cation−Water Interactions: Coordination Number, CN, Cation−Water Interaction Energy, $E_{int}(M^{2+}-Water)$, Mean Cation−Water Oxygen Distances for Water Molecules in the First and Second Hydration Shells, r_I and r_{II}, and Free Energy Barrier, $\Delta G^{\#}$, for the Exchange of a Water Molecule from the First to the Second Coordination Shell of the Cations[a]

cation	CN	$E_{int}(M^{2+}-water)$ (kJ mol^{-1})	r_I (Å)	r_{II} (Å)	$\Delta G^{\#}$ (kJ mol^{-1})
Ca^{2+}	7.2 ± 0.4	−7039 ± 42	2.3	4.6	15
Ba^{2+}	8.9 ± 0.4	−6684 ± 34	2.7	5.0	16
Zn^{2+}	6.0 ± 0.01	−7146 ± 30	2.1	4.3	34
Mg^{2+}	6.0 ± 0.00	−7367 ± 32	2.0	4.2	53

[a]CN and $E_{int}(M^{2+}-water)$ were determined from standard MD simulations of one divalent cation in the bulk, that is, in the presence of 1000 water molecules, while r_I, r_{II}, and $\Delta G^{\#}$ were derived from the PMFs shown in Figure 3a.

The ranking for Mg^{2+}, Ca^{2+}, and Ba^{2+} corroborates the observation that the M^{2+}−water distance generally increases with the cation radius for alkaline earth metals. Moreover, the exchange of a water molecule from the first to the second coordination shell is characterized by a much larger activation free energy, $\Delta G^{\#}$, for Mg^{2+} and Zn^{2+} (about 53 and 34 kJ mol^{-1}, respectively) than for Ca^{2+} and Ba^{2+} (about 15 and 16 kJ mol^{-1}, respectively; see Table 2), which implies much lower exchange rate constants, k, for the former two cations. For example, Allnér et al.[38] determined values of 6.4 × 10^3 and 2.4 × 10^{10} s^{-1} for Mg^{2+} and Ca^{2+}, respectively, when using the same simulation parameters for cations and water as those employed here.

The PMFs for unbinding the divalent cations from the carboxylate group of a Gal monomer (Figure 3b) show two deep minima at short distances (between about 2.0 and 3.7 Å, depending on the considered cation, Table 3) that are separated from a rather shallow and broad minimum at larger distances (4.5−5.5 Å, Table 3) by a significant dehydration free energy barrier. The two deep minima represent contact ion pair (CIP) configurations,[39] in which the cations bind with either one or two oxygens from the carboxylate group of Gal (monodentate and bidentate coordinations, respectively). Ba^{2+} and Ca^{2+} bind preferentially to the carboxylate group of Gal in a bidentate coordination, while the monodentate coordination is favored for Mg^{2+} and Zn^{2+}. The result for Ca^{2+} agrees with those of Fu et al., who found that Ca^{2+} tends to interact in a bidentate coordination with a guluronate monomer (a stereoisomer of the Gal unit).[40] Bidentate and monodentate coordinations of Ca^{2+} and Mg^{2+} with the carboxylate groups of a natural organic matter molecular fragment were also reported by Iskrenova-Tchoukova et al.[39] As it will be shown below, the monodentate coordination of Zn^{2+} and Mg^{2+} with the

DOI: 10.1021/acs.jpcb.5b11010
J. Phys. Chem. B 2016, 120, 1021−1032

Table 3. Data for the Divalent Cation−Gal Interactions: Mean Cation−Carboxylate Carbon Distances, r_{mono}, r_{bi}, and r_{SSIP} for Cations in the Monodentate, Bidentate, and Solvent-Separated Ion Pair (SSIP) Configurations, Respectively, and Free Energy Barrier, $\Delta G^{\#}$, for the Dehydration of Gal (That Is, for the Exchange of a Water Molecule from the Monodentate to the SSIP Configuration)[a]

cation	r_{bi} (Å)	r_{mono} (Å)	r_{SSIP} (Å)	$\Delta G_{desolv}^{\#}$ (kJ mol^{-1})
Ca^{2+}	2.5	3.3	4.9	26
Ba^{2+}	3.0	3.5	5.2	21
Zn^{2+}	2.4	3.2	4.5	61
Mg^{2+}	2.2	3.0	4.4	89

[a]All these data were derived from the PMFs for the cation−Gal interactions shown in Figure 3b.

carboxylate group of Gal stems from their tighter interaction with water (Mg^{2+} < Zn^{2+} < Ca^{2+} < Ba^{2+}) (Table 2), which strongly disfavors the loss of any water molecule from their first hydration shell. In addition, striking differences emerge on the free energy barriers, $\Delta G_{desolv}^{\#}$, that separate the monodentate configurations from the solvent-separated ion pair (SSIP) ones, where water molecules form bridges between the divalent cations and the carboxylate group of Gal. They are considerably larger for magnesium and zinc ions than for calcium and barium ions (Figure 3b and Table 3), consistent with the larger free energy barriers for the exchange of water molecules between the first two hydration shells of magnesium and zinc ions (Figure 3a and Table 2).

The above results clearly suggest that the binding modes of the divalent cations with Gal are intimately related to their affinities with water. Therefore, we determined the mean numbers of water molecules found in their first coordination shell, CN (Figure 3d). At distances r > 6 Å, these coordination numbers are similar to those obtained from independent simulations of the divalent cations in the bulk (Table 2), and they fairly agree with those reported in the literature (usually 6 for Mg^{2+} and Zn^{2+}, from 6.2 to 9 for Ca^{2+}, and about 9.5−9.7 for Ba^{2+}; see e.g. refs 37, 41, and 42 and references therein). The six water molecules from the first hydration shell of Mg^{2+} and Zn^{2+} define an octahedron (Figure 4a), in line with previous experimental and numerical studies.[37,43] In contrast, the structure of the hydration shells of Ca^{2+} and Ba^{2+} is much more irregular (Figure 4a). Accordingly, the hydration numbers of Zn^{2+} and Mg^{2+} decrease abruptly when these cations approach closer and closer from the carboxylate group of Gal, whereas those of Ca^{2+} and Ba^{2+} decrease progressively (Figure 3d). Furthermore, our simulations reveal that the structures of the coordination shells of the cations tend to be preserved upon their binding to Gal, with the substitution of one or two oxygen atoms from water by those from the carboxylate group of Gal (Figure 4b). It is indeed unlikely that the two oxygens from the carboxylate group of Gal, which are separated by an average distance of 2.4 Å, can fit into the octahedral hydration shells of Mg^{2+} and Zn^{2+} (the average distance between the oxygens of two neighboring water molecules is about 2.8 Å), since this would distort the rather regular octahedral first coordination shell of these cations. It is also worth noticing that this octahedral organization mimics the local structure hypothesized in the egg-box model, in which the divalent cation interacts with Gal in a monodentate coordination (see for instance Figure 2 in ref 12).

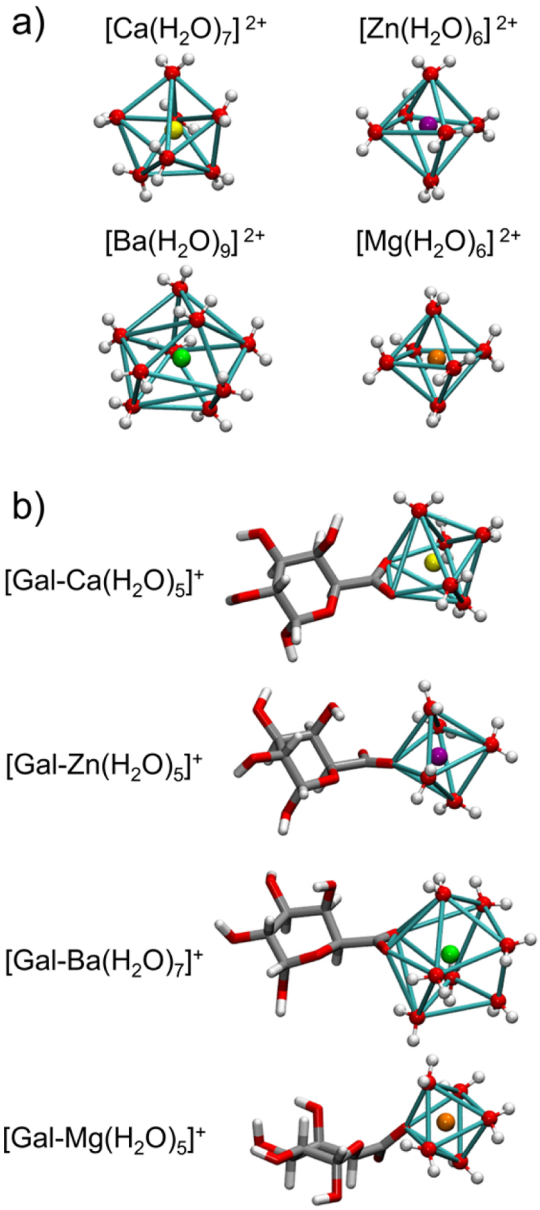

Figure 4. Examples of structures of the first coordination shells of the divalent cations in the bulk (a) and after their complexation with Gal (b). Configurations in (a) were obtained from standard MD simulations of the cations in the bulk, while those shown in (b) were extracted from umbrella sampling simulations and correspond to the global minima in the PMF for the Gal−cation interaction (Figure 3b). For clarity, the cations are represented by small spheres, and lines are drawn between the oxygen atoms found in their first coordination shell.

The above results provide valuable and detailed information on the monocomplexation of cations to Gal. To describe the full association process between Gal chains in aqueous solutions (monocomplexation, formation of cross-links, dimerization), we then run simulations of two octameric Gal chains in the presence of four cations (R = 0.25) (Figure 5). The time evolution of the total number of cations bound to the carboxylate groups of Gal (Figure 5b and Movies S1−S4) exhibit significant differences between the cations. First, no Mg^{2+} cation forms any stable contact with polyGal in the simulation, at variance with the other divalent cations. This is in line with the experimental results obtained from viscosity,

DOI: 10.1021/acs.jpcb.5b11010
J. Phys. Chem. B 2016, 120, 1021−1032

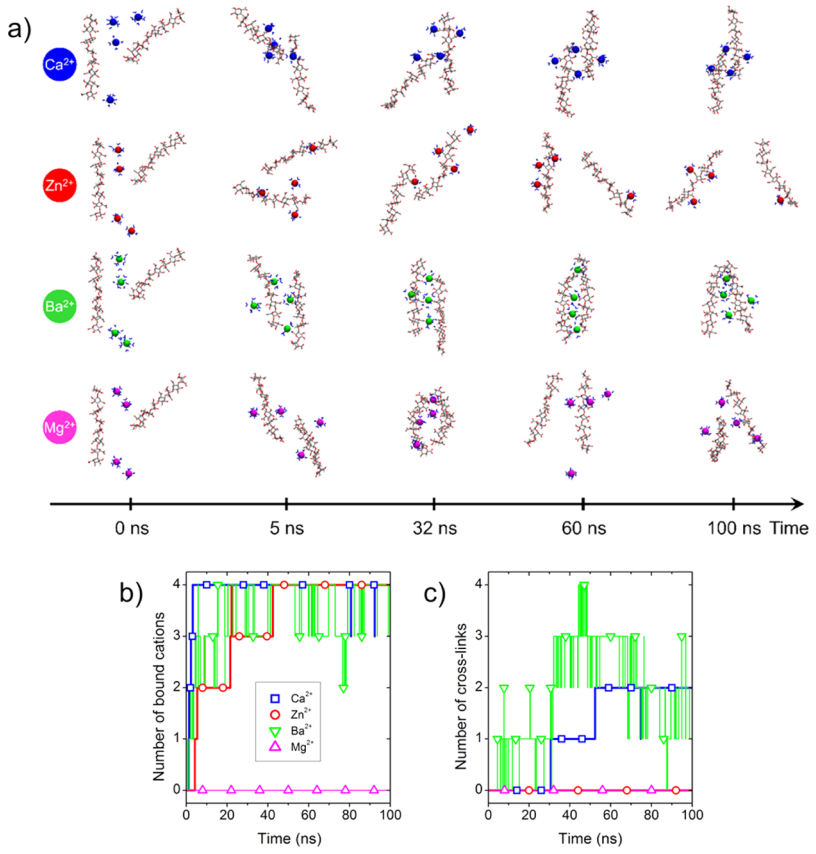

Figure 5. (a) Snapshots from simulations of two polyGal chains in the presence of the divalent cations (Ca^{2+}, Zn^{2+}, Ba^{2+}, Mg^{2+}) at different simulation times (0, 5, 32, 60, and 100 ns from left to right). In the initial configurations (t = 0 ns), the two Gal chains are dissociated, and none of the divalent cations are in contact with them. In the final configuration (t = 100 ns), the monocomplexation of Ca^{2+}, Zn^{2+}, and Ba^{2+} cations is completed (that is, each cation is bound to at least one polyGal chain), but no Mg^{2+} cation is bound. Moreover, only Ca^{2+} and Ba^{2+} cations have induced the association of the two polyGal chains via the formation of Gal−M^{2+}−Gal bridges. For clarity, only the water molecules from the first hydration shell of the divalent cations are shown, and sodium cations are not represented. The corresponding time evolutions of the numbers of cations bound to polyGal and of the numbers of cross-links formed between the polyGal chains are shown in (b) and (c), respectively. Movies on these simulations are provided in the Supporting Information.

turbidity, and the amount of Mg^{2+} bound to polyGal (Figure 1) and also from ITC measurements (Figure 2d and Table 1). The weak interaction between Mg^{2+} and polyGal can be ascribed to the stronger interaction of Mg^{2+} with its hydration water molecules, which makes very stiff the octahedral structure of its first hydration shell.

Besides, the full monocomplexation of Ca^{2+} and Zn^{2+} cations is completed within 10 and 42 ns, respectively, and once bound to polyGal, these cations do not dissociate afterward (Figure 5b). Then, two cross-links are formed between the Gal chains in the presence of Ca^{2+}, but none with Zn^{2+} in the time range investigated (100 ns, Figure 5c). This suggests that the dehydration free energy barrier in the Zn^{2+}−Gal PMF is probably too high for this process to occur within the time scale of our simulations. At variance with the other cations, the Ba^{2+} cations bound to polyGal may dissociate in less than 10 ns, and both the formation and the breakage of cross-links between polyGal chains are observed, consistent with the much less deeper minima found in the PMF for the cation−Gal interaction for this cation (Figure 3b).

DISCUSSION

In the present study, we investigated the association between various divalent cations (Mg^{2+}, Ca^{2+}, Ba^{2+}, and Zn^{2+}) and polygalacturonate (polyGal). The amount of bound cations, the viscosity and the turbidity (Figure 1) increased in a similar way upon the addition of divalent cations (Ca^{2+}, Ba^{2+}, and Zn^{2+}). These increases indicated that the formation of the polyGal network occurred and started at molar ratios R^* specific to each divalent cation. Similarly, the binding enthalpy first decreases and then increases upon the addition of divalent cations (Ca^{2+}, Ba^{2+}, and Zn^{2+}). The first step in the binding of divalent cations to polyGal probably corresponds to the formation of monocomplexes (Gal−M^{2+}, Figure 6).[15] However, given the low binding constants between the investigated divalent cations and monoacids, monocomplexation alone can probably not explain why about 75% of the added Ba^{2+} cations are trapped at a molar ratio of 0.1 (Figure 1c). We can suppose that the formation of point-like cross-links (Gal−M^{2+}−Gal) may occur, thereby explaining the results of Figure 1c. Therefore, we conclude that the monocomplexation and the formation of point-like cross-links probably occur simultaneously and may appear as a unique process in ITC data (Figure 6). The second step can be attributed to the rearrangement of polyGal chains, which may include the formation of dimers, and to the formation of supplementary point-like cross-links. These events may create a continuous 3D network, as suggested by the increase of viscosity (Figure 1a). Given the low concentration of polyGal (0.5 g L^{-1}), we assume that the formation of multimers—as suggested by Fang et al.[15] for alginate—is very

DOI: 10.1021/acs.jpcb.5b11010
J. Phys. Chem. B 2016, 120, 1021−1032

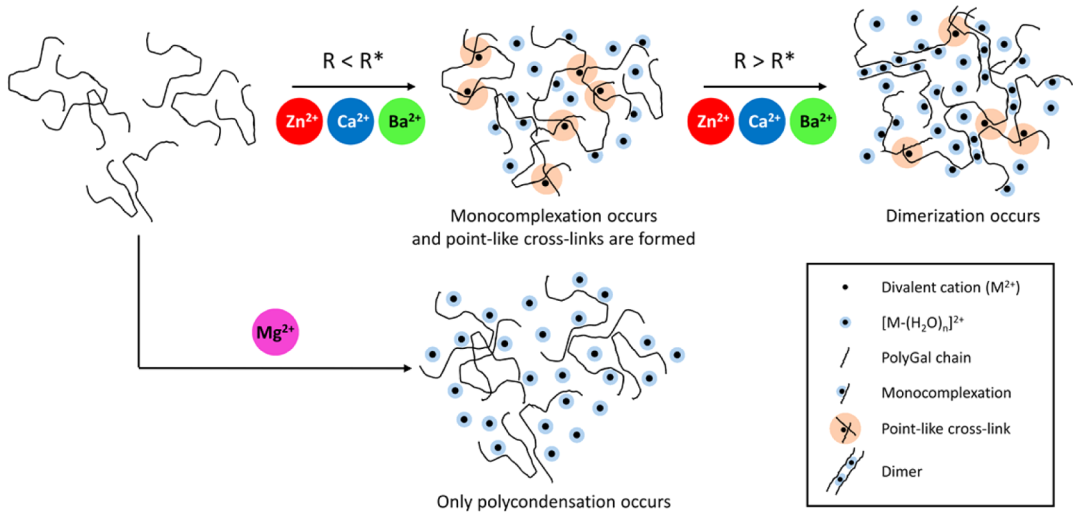

Figure 6. Schematic representation of the association steps between the divalent cations and polyGal chains as deduced from our results. In the absence of divalent cations ($R = 0$), polyGal chains may be assumed to be distributed randomly in the solution. For Ca^{2+}, Ba^{2+}, and Zn^{2+} additions, the monocomplexation and the formation of point-like cross-links occur upon increasing R. Above a threshold molar ratio R^*, the network of polyGal chains reorganizes and dimers as well as supplementary point-like cross-links are formed in the presence of Ca^{2+}, Ba^{2+}, and Zn^{2+}. R^* depends on the considered divalent cation (Ca^{2+}, Ba^{2+}, or Zn^{2+}), owing to differences in the stability (or lifetime) of the point-like cross-links that they form with polyGal chains, which are related to their affinity for water. R^* is lower for Ca^{2+} than for Ba^{2+} and Zn^{2+} because Ca^{2+} exhibits an affinity for water intermediate between those of Ba^{2+} and Zn^{2+}. For Mg^{2+} addition, only the polycondensation of Mg^{2+} cations around polyGal chains seems to occur upon increasing R, given the high affinity of Mg^{2+} cations for water, which makes their dehydration unlikely.

unlikely. Interestingly, the onset molar ratio for the increase of binding enthalpy appears at lower molar ratios than those observed in viscosity and turbidity measurements. A sufficiently high amount of point-like cross-links is probably needed to create inhomogeneities large enough to scatter light and possibly also to form a continuous tridimensional network that can be detected by turbidity and viscosity measurements (Figure 6). The results on the binding of Mg^{2+} to polyGal are strikingly different from those obtained for the three other divalent cations (Ca^{2+}, Ba^{2+}, and Zn^{2+}). The amount of bound cations, the viscosity, and the turbidity remain low and near to zero (Figure 1), which indicates that the polyGal network is not formed.[13,21] Moreover, the binding enthalpy shows only a decrease upon the addition of Mg^{2+}, which may be attributed to polycondensation (Figure 6).

Besides, the thermodynamic parameters obtained from ITC indicate that the first step of binding is entropy driven, in line with the results of De and Robinson.[25] The entropy contribution ($T\Delta S$), which can be attributed to the dehydration of both the cation and the biopolymer, is approximately 2 times higher for barium and calcium bindings ($T\Delta S \sim 50$ kJ mol^{-1}) than for Mg^{2+} binding ($T\Delta S \sim 30$ kJ mol^{-1}) (Table 1). The free energy profiles on the M^{2+}−Gal interaction indicate that Mg^{2+} exhibits the highest affinity for Gal among the studied cations (Figure 3b). In contrast, the free energy obtained from ITC for the first step is the lowest for Mg^{2+} (Table 2). We can conclude that in the case of Mg^{2+}−polyGal the monocomplexation does not happen because Mg^{2+} cannot release water molecules from its first hydration shell. Therefore, the reduction of binding enthalpy may be due to the sharing of water molecules from the first layer of hydration of Mg^{2+} with the oxygens from the carboxylate group of Gal units (solvent-separated ion pair, SSIP, configuration[39]). Thus, the mechanism of association between Mg^{2+} and polyGal consists only in polycondensation under the experimental conditions (polyGal and Mg^{2+} concentrations) investigated. Donati et al.[13] indicated that the gelation of Mg^{2+}−alginate solutions does not occur owing to weak interactions between the cations and the polymer. These results also appear in agreement with the predominantly outer-sphere complexes formed by Mg^{2+} with the phosphate and carboxylate groups of nucleic acids and proteins, since its affinity for water is higher than that of negatively charged groups.[44] Note, however, that alginate−Mg^{2+} gels can be produced under peculiar conditions (long gelation time, high concentration of polymers, and high molar ratio).[21]

Besides, even though the mechanism for the association between polyGal and divalent cations seems to be the same for Ca^{2+}, Ba^{2+}, and Zn^{2+} (Figure 6a), we can define the threshold molar ratio (R^*) between the two steps, which strongly depends on the nature of the divalent cation. Our MD simulations reveal that the dehydration free energy barrier of the divalent cations decreases as follows: $Zn^{2+} > Ca^{2+} > Ba^{2+}$ (Figure 3b), so that we expect the stability (or lifetime) of the point-like cross-links formed by M^{2+} to decrease in the same order. It is possible that the higher stability of the cross-links formed by zinc cations arises from the nature of the Gal−M^{2+} interaction. Indeed, Zn^{2+} might interact with Gal via a 3d electron−lone pair interaction, which does not exist for divalent alkaline earth metal ions[45] and which cannot be considered in classical MD simulations. The binding of Zn^{2+} with electronegative groups indeed exhibits a partially covalent character and does not simply stems from Coulombic interactions between charged groups.[45] Accordingly, a density functional theory (DFT) study of the complexation of a series of divalent cations with guluronate and mannuronate disaccharides showed that the complexation of transition metal cations with the disaccharides occurs through the formation of strong coordination-covalent bonds, whereas alkaline earth metal cations form ionic bonds with these uronates.[46]

The low variation in binding enthalpy upon addition of zinc cations ($R < 0.3$, Figure 2c) suggests that few and stable point-

DOI: 10.1021/acs.jpcb.5b11010
J. Phys. Chem. B 2016, 120, 1021−1032

like cross-links are formed and are not broken upon further addition of zinc cations. At higher molar ratios ($R > 0.3$), huge variations of binding enthalpy were observed upon addition of Zn^{2+} (Figure 2c). It is plausible that zinc cations then screen the strong electrostatic repulsions between neighboring polyGal chains, thereby favoring their associations and contributing to the increase in viscosity of the Zn^{2+}–polyGal solution (Figure 1a). The time necessary to reorganize the structure of the polyGal network between successive additions of Zn^{2+} increases dramatically and probably exceeds the time interval fixed between two successive injections in ITC measurements (ITC raw data indicate that equilibrium is not reached at such high molar ratios; see data provided in Figure S3).

The increases of viscosity, turbidity, and amount of bound cations (Figure 1) and the decrease of binding enthalpy (Figure 2b) suggest that point-like cross-links are formed as soon as barium cations are added to the polyGal solution. Their formation is probably favored by the low affinity of Ba^{2+} for water, which makes its dehydration easier. This is in line with the low apparent dynamic hydration number of barium ions (0.35) in comparison with those of calcium ions (2.10) and zinc ions (2.18).[44] For dimerization (second step) to occur, a sufficiently high number of point-like cross-links must be formed. In the case of barium ions, this is achieved at higher molar ratios because of the low stability of these cross-links. In contrast, the intermediate stability of the cross-links formed in the presence of Ca^{2+} allows the second step to occur at very low molar ratios ($R < 0.1$). We suppose that polyGal chains remain highly flexible in the presence of calcium cations, so that such cross-links can be broken to form more organized structures (dimers) at higher molar ratios, as the progressive increases in viscosity and turbidity suggest (Figure 1). This hypothesis is consistent with the MD simulations, which show that the cross-links formed by calcium ions are more stable than the ones formed by barium ions (Figure 5).

CONCLUSION

Divalent cations are well-known to induce the gelation of anionic polysaccharides with various physicochemical properties, which are directly linked to their specific interactions at molecular scale. The interaction between polyGal and four divalent cations (M^{2+}) was studied in order to understand how the intrinsic characteristics of M^{2+} (ionic radius, charge density, energy of interaction between M^{2+} and water molecules, coordination number, etc.) influence the mechanism of association and, thus, the final structure of the formed network. Three divalent alkaline earth cations with increasing hydration free energies ($Ba^{2+} < Ca^{2+} < Mg^{2+}$) were considered. Another divalent cation (Zn^{2+}) with a similar size as that of Mg^{2+} but with a different valence shell electronic configuration (3d instead of *n*p) was also considered. The interaction between these divalent cations and polyGal was studied in the semidiluted regime and at various molar ratios, *R*. The molecular dynamics (MD) simulations show that the association between divalent cations and galacturonate (Gal) is monodentate for Mg^{2+} and Zn^{2+} and bidentate for Ca^{2+} and Ba^{2+}, which induces the release of one and two water molecules from the hydration shell of the cations, respectively.

The combination of MD simulations, ITC, viscosity, and turbidity measurements allowed us to propose a mechanism for the binding of divalent cations (Ca^{2+}, Ba^{2+}, and Zn^{2+}) to polyGal (Figure 6): (1) the formation of monocomplexes and of point-like cross-links and (2) the formation of dimers. In Mg^{2+}–polyGal solutions, only polycondensation seems to occur (Figure 6), in accordance with previous studies.[13,34] Our results evidence that the affinity of the divalent cations for water molecules ($Ba^{2+} < Ca^{2+} < Zn^{2+} < Mg^{2+}$) drives their local interaction modes with galacturonate. These differences have consequences on the number and the stability (lifetime) of the cross-links formed between polyGal chains, which are a key step for the mechanism of association. The cross-links formed must probably be of adequate stability and numerous enough to allow the dimerization step to occur. Among the four divalent cations, Ca^{2+} best fulfills these requirements. It would be interesting to check whether these observations could be generalized to analogous polysaccharides with increasing complexity: polymannuronate, polyguluronate, alginate, and pectin.

ASSOCIATED CONTENT

Supporting Information

The Supporting Information is available free of charge on the ACS Publications website at DOI: 10.1021/acs.jpcb.5b11010.

Details of all the MD simulations performed; schematic structure of the Gal unit; ITC raw curves for the three types of titration performed (PDF)

Movie on the binding of polyGal chains in the presence of Ca^{2+} (MPG)

Movie on the binding of polyGal chains in the presence of Zn^{2+} (MPG)

Movie on the binding of polyGal chains in the presence of Ba^{2+} (MPG)

Movie on the binding of polyGal chains in the presence of Mg^{2+} (MPG)

AUTHOR INFORMATION

Corresponding Authors

*E-mail: adrien.lerbret@u-bourgogne.fr (A.L.).

*E-mail: ali.assifaoui@u-bourgogogne.fr (A.A.).

Notes

The authors declare no competing financial interest.

ACKNOWLEDGMENTS

The ITC results were obtained with equipment from the technical platform RMB (Rhéologie et structure des Matériaux Biologiques) (AgroSup Dijon-Université de Bourgogne Franche-Comté). We are grateful to Dr. Fabrice Cousin (Laboratoire Léon Brillouin, CEA – Saclay, France) for critical reading and comments on the manuscript. We are indebted to Dr. Vu H. Le (Massachusetts Institute of Technology) for modifying the CHASM software to allow the analysis of our ITC data. The use of computational facilities at the Computing Center of the University of Bourgogne, DSI-CCUB, is gratefully acknowledged.

REFERENCES

(1) Itoh, K.; Hirayama, T.; Takahashi, A.; Kubo, W.; Miyazaki, S.; Dairaku, M.; Togashi, M.; Mikami, R.; Attwood, D. In Situ Gelling Pectin Formulations for Oral Drug Delivery at High Gastric pH. *Int. J. Pharm.* **2007**, *335*, 90–96.

(2) Liu, L.; Fishman, M. L.; Kost, J.; Hicks, K. B. Pectin-Based Systems for Colon-Specific Drug Delivery Via Oral Route. *Biomaterials* **2003**, *24*, 3333–3343.

(3) Vandamme, T. F.; Lenourry, A.; Charrueau, C.; Chaumeil, J.-C. The Use of Polysaccharides to Target Drugs to the Colon. *Carbohydr. Polym.* **2002**, *48*, 219–231.

DOI: 10.1021/acs.jpcb.5b11010
J. Phys. Chem. B 2016, 120, 1021–1032

(4) Camci-Unal, G.; Pohl, N. L. B. Quantitative Determination of Heavy Metal Contaminant Complexation by the Carbohydrate Polymer Chitin. *J. Chem. Eng. Data* **2010**, *55*, 1117−1121.
(5) Assifaoui, A.; Lerbret, A.; Uyen, H. T. D.; Neiers, F.; Chambin, O.; Loupiac, C.; Cousin, F. Structural Behaviour Differences in Low Methoxy Pectin Solutions in the Presence of Divalent Cations (Ca^{2+} and Zn^{2+}): A Process Driven by the Binding Mechanism of the Cation with the Galacturonate Unit. *Soft Matter* **2015**, *11*, 551−560.
(6) Cescutti, P.; Rizzo, R. Divalent Cation Interactions with Oligogalacturonides. *J. Agric. Food Chem.* **2001**, *49*, 3262−3267.
(7) Chang, Y.; McLandsborough, L.; McClements, D. J. Interactions of a Cationic Antimicrobial (ε-Polylysine) with an Anionic Biopolymer (Pectin): An Isothermal Titration Calorimetry, Microelectrophoresis, and Turbidity Study. *J. Agric. Food Chem.* **2011**, *59*, 5579−5588.
(8) Dronnet, V. M.; Renard, C. M. G. C.; Axelos, M. A. V.; Thibault, J.-F. Binding of Divalent Metal Cations by Sugar-Beet Pulp. *Carbohydr. Polym.* **1997**, *34*, 73−82.
(9) Selvarengan, P.; Kubicki, J. D.; Guégan, J.-P.; Châtellier, X. Complexation of Carboxyl Groups in Bacterial Lipopolysaccharides: Interactions of H^+, Mg^{2+}, Ca^{2+}, Cd^{2+}, and UO_2^{2+} with Kdo and Galacturonate Molecules Via Quantum Mechanical Calculations and NMR Spectroscopy. *Chem. Geol.* **2010**, *273*, 55−75.
(10) Grasdalen, H.; Einar Bakøy, O.; Larsen, B. Determination of the Degree of Esterification and the Distribution of Methylated and Free Carboxyl Groups in Pectins by ^{1}H-N.M.R. Spectroscopy. *Carbohydr. Res.* **1988**, *184*, 183−191.
(11) Voragen, A. G. J.; Pilnik, W.; Thibault, J.-F.; Axelos, M. A. V.; Renard, C. M. G. C. *Pectins, In: Food Polysaccharides and Their Applications*; Stephen, A. M., Ed.; Dekker: New York, 1995; Vol. *10*, pp 287−339.
(12) Braccini, I.; Perez, S. Molecular Basis of Ca^{2+}-Induced Gelation in Alginates and Pectins: The Egg-Box Model Revisited. *Biomacromolecules* **2001**, *2*, 1089−1096.
(13) Donati, I.; Asaro, F.; Paoletti, S. Experimental Evidence of Counterion Affinity in Alginates: The Case of Nongelling Ion Mg^{2+}. *J. Phys. Chem. B* **2009**, *113*, 12877−12886.
(14) Fang, Y.; Al-Assaf, S.; Phillips, G. O.; Nishinari, K.; Funami, T.; Williams, P. A. Binding Behavior of Calcium to Polyuronates: Comparison of Pectin with Alginate. *Carbohydr. Polym.* **2008**, *72*, 334−341.
(15) Fang, Y.; Al-Assaf, S.; Phillips, G. O.; Nishinari, K.; Funami, T.; Williams, P. A.; Li, L. Multiple Steps and Critical Behaviors of the Binding of Calcium to Alginate. *J. Phys. Chem. B* **2007**, *111*, 2456−2462.
(16) Grant, G. T.; Morris, E. R.; Rees, D. A.; Smith, P. J. C.; Thom, D. Biological Interactions between Polysaccharides and Divalent Cations: The Egg-Box Model. *FEBS Lett.* **1973**, *32*, 195−198.
(17) Thom, D.; Grant, G. T.; Morris, E. R.; Rees, D. A. Characterisation of Cation Binding and Gelation of Polyuronates by Circular Dichroism. *Carbohydr. Res.* **1982**, *100*, 29−42.
(18) Kohn, R. Ion Binding on Polyuronates-Alginate and Pectin. *Pure Appl. Chem.* **1975**, *42*, 371−397.
(19) Malovíková, A.; Rinaudo, M.; Milas, M. Comparative Interactions of Magnesium and Calcium Counterions with Polygalacturonic Acid. *Biopolymers* **1994**, *34*, 1059−1064.
(20) Koda, S.; Nomura, H.; Nagasawa, M. Raman Spectroscopic Studies on the Interaction between Divalent Counterion and Polyion. *Biophys. Chem.* **1983**, *18*, 361−367.
(21) Topuz, F.; Henke, A.; Richtering, W.; Groll, J. Magnesium Ions and Alginate Do Form Hydrogels: A Rheological Study. *Soft Matter* **2012**, *8*, 4877−4881.
(22) Aslani, P.; Kennedy, R. A. Studies on Diffusion in Alginate Gels. I. Effect of Cross-Linking with Calcium or Zinc Ions on Diffusion of Acetaminophen. *J. Controlled Release* **1996**, *42*, 75−82.
(23) Donati, I.; Holtan, S.; Morch, Y. A.; Borgogna, M.; Dentini, M.; Skjak-Brak, G. New Hypothesis on the Role of Alternating Sequences in Calcium-Alginate Gels. *Biomacromolecules* **2005**, *6*, 1031−1040.
(24) Li, L.; Fang, Y.; Vreeker, R.; Appelqvist, I.; Mendes, E. Reexamining the Egg-Box Model in Calcium-Alginate Gels with X-Ray Diffraction. *Biomacromolecules* **2007**, *8*, 464−468.
(25) De, S.; Robinson, D. Polymer Relationships During Preparation of Chitosan−Alginate and Poly-L-Lysine−Alginate Nanospheres. *J. Controlled Release* **2003**, *89*, 101−112.
(26) Ventura, I.; Jammal, J.; Bianco-Peled, H. Insights into the Nanostructure of Low-Methoxyl Pectin−Calcium Gels. *Carbohydr. Polym.* **2013**, *97*, 650−658.
(27) Borgogna, M.; Skjåk-Bræk, G.; Paoletti, S.; Donati, I. On the Initial Binding of Alginate by Calcium Ions. The Tilted Egg-Box Hypothesis. *J. Phys. Chem. B* **2013**, *117*, 7277−7282.
(28) Cacace, M. G.; Landau, E. M.; Ramsden, J. J. The Hofmeister Series: Salt and Solvent Effects on Interfacial Phenomena. *Q. Rev. Biophys.* **1997**, *30*, 241−277.
(29) Assifaoui, A.; Chambin, O.; Cayot, P. Drug Release from Calcium and Zinc Pectinate Beads: Impact of Dissolution Medium Composition. *Carbohydr. Polym.* **2011**, *85*, 388−393.
(30) Le, V. H.; Buscaglia, R.; Chaires, J. B.; Lewis, E. A. Modeling Complex Equilibria in Isothermal Titration Calorimetry Experiments: Thermodynamic Parameters Estimation for a Three-Binding-Site Model. *Anal. Biochem.* **2013**, *434*, 233−241.
(31) Liners, F.; Thibault, J.-F.; Van Cutsem, P. Influence of the Degree of Polymerization of Oligogalacturonates and of Esterification Pattern of Pectin on Their Recognition by Monoclonal Antibodies. *Plant Physiol.* **1992**, *99*, 1099−1104.
(32) Powell, D. A.; Morris, E. R.; Gidley, M. J.; Rees, D. A. Conformations and Interactions of Pectins: II. Influence of Residue Sequence on Chain Association in Calcium Pectate Gels. *J. Mol. Biol.* **1982**, *155*, 517−531.
(33) Brooks, B. R.; Brooks, C. L.; Mackerell, A. D.; Nilsson, L.; Petrella, R. J.; Roux, B.; Won, Y.; Archontis, G.; Bartels, C.; Boresch, S.; et al. CHARMM: The Biomolecular Simulation Program. *J. Comput. Chem.* **2009**, *30*, 1545−1614.
(34) Manning, G. S. Limiting Laws and Counterion Condensation in Polyelectrolyte Solutions: IV. The Approach to the Limit and the Extraordinary Stability of the Charge Fraction. *Biophys. Chem.* **1977**, *7*, 95−102.
(35) Espinal-Ruiz, M.; Parada-Alfonso, F.; Restrepo-Sánchez, L.-P.; Narváez-Cuenca, C.-E.; McClements, D. J. Interaction of a Dietary Fiber (Pectin) with Gastrointestinal Components (Bile Salts, Calcium, and Lipase): A Calorimetry, Electrophoresis, and Turbidity Study. *J. Agric. Food Chem.* **2014**, *62*, 12620−12630.
(36) Sinn, C. G.; Dimova, R.; Antonietti, M. Isothermal Titration Calorimetry of the Polyelectrolyte/Water Interaction and Binding of Ca^{2+}: Effects Determining the Quality of Polymeric Scale Inhibitors. *Macromolecules* **2004**, *37*, 3444−3450.
(37) Ohtaki, H.; Radnai, T. Structure and Dynamics of Hydrated Ions. *Chem. Rev.* **1993**, *93*, 1157−1204.
(38) Allnér, O.; Nilsson, L.; Villa, A. Magnesium Ion−Water Coordination and Exchange in Biomolecular Simulations. *J. Chem. Theory Comput.* **2012**, *8*, 1493−1502.
(39) Iskrenova-Tchoukova, E.; Kalinichev, A. G.; Kirkpatrick, R. J. Metal Cation Complexation with Natural Organic Matter in Aqueous Solutions: Molecular Dynamics Simulations and Potentials of Mean Force. *Langmuir* **2010**, *26*, 15909−15919.
(40) Fu, H.; Liu, Y.; Adrià, F.; Shao, X.; Cai, W.; Chipot, C. From Material Science to Avant-Garde Cuisine. The Art of Shaping Liquids into Spheres. *J. Phys. Chem. B* **2014**, *118*, 11747−11756.
(41) Piquemal, J.-P.; Perera, L.; Cisneros, G. A.; Ren, P.; Pedersen, L. G.; Darden, T. A. Towards Accurate Solvation Dynamics of Divalent Cations in Water Using the Polarizable Amoeba Force Field: From Energetics to Structure. *J. Chem. Phys.* **2006**, *125*, 054511.
(42) Wu, J. C.; Piquemal, J.-P.; Chaudret, R.; Reinhardt, P.; Ren, P. Polarizable Molecular Dynamics Simulation of Zn(II) in Water Using the Amoeba Force Field. *J. Chem. Theory Comput.* **2010**, *6*, 2059−2070.
(43) Callahan, K. M.; Casillas-Ituarte, N. N.; Roeselová, M.; Allen, H. C.; Tobias, D. J. Solvation of Magnesium Dication: Molecular

DOI: 10.1021/acs.jpcb.5b11010
J. Phys. Chem. B 2016, 120, 1021−1032

Dynamics Simulation and Vibrational Spectroscopic Study of Magnesium Chloride in Aqueous Solutions. *J. Phys. Chem. A* **2010**, *114*, 5141−5148.
(44) Collins, K. D. Ion Hydration: Implications for Cellular Function, Polyelectrolytes, and Protein Crystallization. *Biophys. Chem.* **2006**, *119*, 271−281.
(45) Binder, H.; Zschörnig, O. The Effect of Metal Cations on the Phase Behavior and Hydration Characteristics of Phospholipid Membranes. *Chem. Phys. Lipids* **2002**, *115*, 39−61.
(46) Agulhon, P.; Markova, V.; Robitzer, M.; Quignard, F.; Mineva, T. Structure of Alginate Gels: Interaction of Diuronate Units with Divalent Cations from Density Functional Calculations. *Biomacromolecules* **2012**, *13*, 1899−1907.

DOI: 10.1021/acs.jpcb.5b11010
J. Phys. Chem. B 2016, 120, 1021−1032

Principaux résultats et conclusions

Nous avons étudié les interactions entre différents cations divalents (Ca^{2+}, Zn^{2+}, Ba^{2+}, Mg^{2+}) et deux biopolymères (PGA et LMP) en régime dilué. Plusieurs aspects (structural, thermodynamique et mécanistique) ont été pris en compte.

Dans un premier temps, nous nous sommes intéressés à la structuration du réseau formé par ces cations en association avec le PGA et la pectine (LMP). Nous avons ainsi montré que le réseau formé avec les ions calcium est visqueux et homogène ; alors que le réseau formé avec les ions zinc est hétérogène. L'étude des mélanges Ca-LMP et Zn-LMP par diffusion des neutrons aux petits angles a montré qu'à faible ratio molaire (R = [Cation]/[Gal] = 0,09), la taille caractéristique du réseau polymérique devient faible indiquant la formation de réticulations ponctuelles. Pour les forts ratios molaires (R = 0,44), les fluctuations de densité sont plus élevées dans le cas du mélange Zn-LMP indiquant une structure plus hétérogène en accord avec les résultats de turbidité (Fig. 7, Partie 1, Chapitre 3). Pour les ions magnésium, nous avons montré que la turbidité et la viscosité restent constantes et proches de celle du polyGal seul, indiquant que ce cation ne forme pas de gel macroscopique, ce qui est confirmé par d'autres auteurs (Donati, 2009; Manning, 1977). Dans le cas des ions baryum, nous avons observé une augmentation à la fois de la turbidité et de la viscosité avec l'ajout des ions Ba^{2+}. De plus, nous avons remarqué que 75% des ions ajoutés sont piégés dans le réseau du polyGal.

Dans un deuxième temps, nous nous sommes intéressés à l'étude de l'énergie d'interaction entre ces deux biopolymères et les 4 cations divalents. Ainsi, l'ITC a montré que l'enthalpie d'association (ΔH) entre les ions calcium ou zinc et la pectine (LMP) est positive (endothermique) pour des faibles ratios molaires (R). Lorsque ce ratio molaire augmente, nous avons remarqué que l'enthalpie d'association diminue puis devient négative pour le mélange Ca-LMP à R = 0,25 et pour le mélange Zn-LMP à R = 0,35. De même, nous avons observé ces deux processus pour les associations entre cations divalents (Ca^{2+}, Ba^{2+} et Zn^{2+}) et polyGal. Dans le cas de l'association Mg^{2+} et polyGal, un seul processus a été observé. Ce processus est entropique et présente une constante d'affinité 100 fois plus faible que l'association Ca- polyGal. Il a été décrit que, dans ce cas, l'association est due à une condensation des ions magnésium autour des chaînes du polyGal (Manning, 1977). Pour les trois autres cations (Ca^{2+}, Ba^{2+} et Zn^{2+}), nous avons suggéré la présence de deux processus : le premier est endothermique et pourrait être dû à la formation de monocomplexes (cation - Gal) et de zones

de réticulations ; le second processus est exothermique et pourrait être dû à une réorganisation des chaînes (formation des dimères). Le ratio molaire qui correspond au passage du premier au second processus, noté *R** dépend de la nature du cation : il est faible pour l'association Ca- polyGal (*R** = 0,01) et élevé pour les associations Ba-polyGal et Zn-polyGal (*R** = 0,3).

Afin de comprendre l'origine de ces processus et la différence de structure, nous avons réalisé des simulations moléculaires dynamiques sur différents systèmes comme le montre la figure ci-dessous (Fig. 3-1).

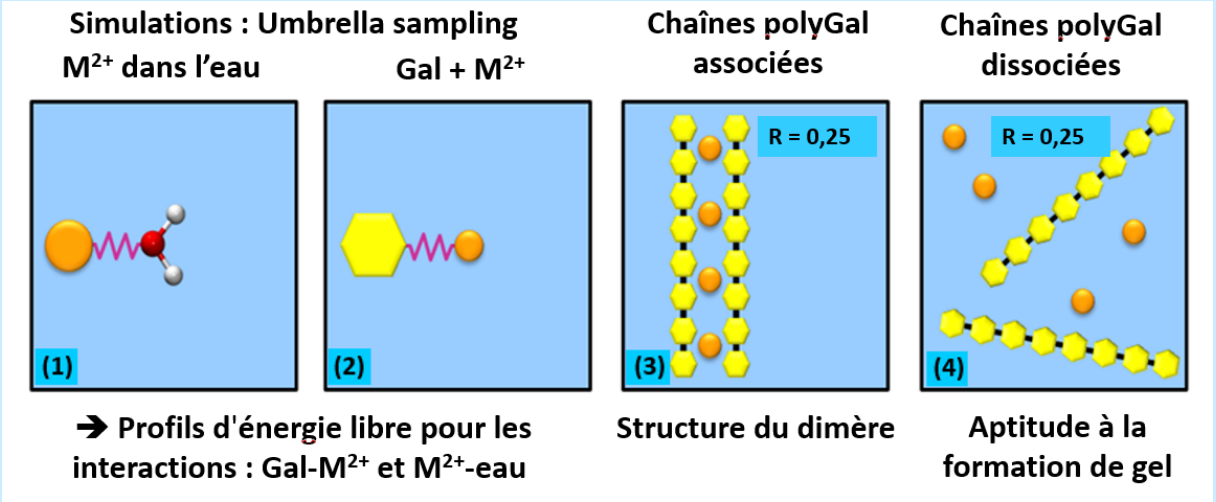

Fig. 3-1. Systèmes simulés de différentes étapes réalisées dans des expériences de simulations moléculaires dynamiques

Les interactions entre les molécules d'eau de la première sphère de coordination et le cation (simulation 1) augmentent selon l'ordre suivant : $Mg^{2+} > Zn^{2+} > Ca^{2+} > Ba^{2+}$. A partir de ce résultat, il est évident que les ions magnésium maintiennent leur sphère d'hydratation, ce qui expliquerait la difficulté de former des gels pour ce cation. Nous avons également étudié l'énergie d'association d'un cation avec une unité galacturonate (simulation 2). Cette simulation, nous a permis de conclure que le Zn^{2+} se fixe à un seul oxygène du groupement carboxylate (mode monodentate) ; alors que le Ca^{2+} et le Ba^{2+} se fixent sur les deux oxygènes du groupement carboxylate (mode bidentate). La structure obtenue (simulation 3) dans le cas de l'association de 4 cations Zn^{2+} avec 2 chaînes composées de 8 unités Gal (octamère) est similaire à une structure de type boîte à œuf (*egg-box model*). Ce modèle n'est pas applicable à la structure obtenue par l'association des cations Ca^{2+} et Ba^{2+} avec les 2 octamères. Enfin, nous avons étudié l'évolution de ces 2 octamères en présence de 4 cations divalents (simulation 4) afin d'avoir des informations sur les mécanismes d'association (Figure 5, Partie 2, Chapitre 3).

- Pour les ions calcium, nous avons remarqué la formation de monocomplexes dès les premiers temps de simulation (5 ns). Ensuite, des réticulations ponctuelles relativement stables ont été observées.
- Pour les ions zinc, nous avons observé uniquement la formation de moncomplexes (dans la durée de la simulation 100 ns). La formation des réticulations ponctuelles semble être difficile à se produire.
- Pour les ions baryum, nous avons observé la formation de moncomplexes et des réticulations ponctuelles dès les premiers temps de simulations (5 ns). Toutefois, ces réticulations ponctuelles sont instables. En effet, nous avons observé une dissociation des 2 octamères à des temps plus élevés.
- Pour les ions magnésium, nous avons noté que Mg^{2+} ne perd pas ses 6 molécules d'eau de la sphère d'hydratation. L'association se fait donc par un partage d'une molécule d'eau de la sphère avec les carboxylates du polyGal.

Pour conclure, la combinaison de ces techniques, nous a permis de proposer un mécanisme d'association qui est composé de deux étapes : i) formation de monocomplexes et de réticulations ponctuelles et ii) formation de dimères. Le passage de l'étape (i) à l'étape (ii) est caractérisé par un ratio molaire critique (*R**) qui dépend de la nature du cation divalent. Ce ratio critique dépend du nombre et de la stabilité des réticulations ponctuelles entre le polymère et le cation. *R** est élevé dans le cas des associations Ba-polyGal et Zn-polyGal. Pour le Ba-polyGal, le nombre de ces réticulations est important mais instable. Alors que dans le cas du Zn-polyGal, ces réticulations sont stables mais leur nombre est faible (Fig. 3-2). Dans le cas de l'association Ca-polyGal, le nombre et la stabilité de ces réticulations ponctuelles semblent être adéquats ce qui permet d'avoir un ratio molaire critique (*R**) plus faible.

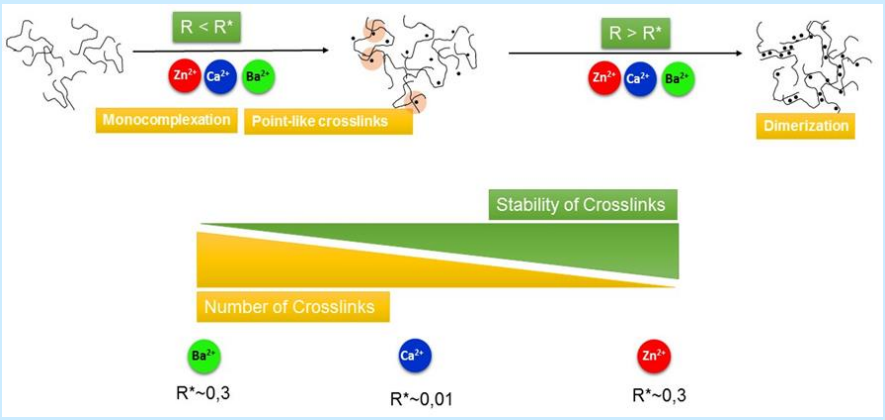

Fig. 3-2. Représentation schématique des étapes de l'association entre les cations divalents (Ca^{2+}, Zn^{2+}, Ba^{2+}) et les chaînes de polyGal

CHAPTER 4

GEL OF POLYGALACTURONATE AND DIVALENT CATIONS (Ca^{2+}, Zn^{2+}, Ba^{2+}, Mg^{2+})

Introduction

Dans ce chapitre, présenté sous forme d'un article, nous nous sommes intéressés à la fabrication et à la caractérisation physicochimique des gels de polygalacturonate (polyGal) en présence de différents cations divalents (Ca^{2+}, Zn^{2+}, Ba^{2+} et Mg^{2+}). La concentration en polyGal utilisée pour former les gels est égale à 10 g L^{-1}. Cette concentration est voisine la concentration de recouvrement (c*). La gélification se fait par diffusion progressive des cations à travers une membrane de dialyse vers la solution du polyGal.

Dans un premier temps, nous avons établi un diagramme d'état qui consiste à faire varier la concentration initiale du cation divalent [10 - 750 mM] et le temps de gélification [10 - 1440 min]. Ensuite, nous avons déterminé les propriétés viscoélastiques de ces gels. Nous nous sommes intéressés à la mesure du module élastique (G') et du module visqueux (G"). Comme la formation du gel est un processus dynamique, les changements du comportement rhéologique durant le développement du gel peuvent fournir les informations supplémentaires sur l'importance du rôle des différents facteurs (nature du cation divalent, concentration en cation, temps) au cours de la gélification.

Nous nous sommes également intéressés à la cinétique de gélification en suivant la turbidité du système au cours du temps à différentes distances de la membrane de diffusion. Ceci a été réalisé à l'aide d'un Turbiscan. A partir de ces résultats, nous avons pu déduire la constante de diffusion des cations en fonction de la nature et de la concentration initiale de ces cations divalents.

The ability of pectins to form gels in the presence of divalent cations is the first property of these biopolymers and plays a significant role in food and pharmaceutical industries. The rheological properties of gel are clearly dependent on the nature and the concentration of the divalent cations. Moreover, the diffusion of cations in the polyelectrolyte solution is necessary for the formation of hydrogel, but the study of the gelation kinetics is still limited.

In this chapter, PGA is used to avoid the branching structure of pectin. The gelation kinetics of PGA with different divalent cations (Ca^{2+}, Zn^{2+}, Ba^{2+}, Mg^{2+}) and the physical properties of gel will be investigated. Through which, we can better understand the affinity interaction between divalent cations and polygalacturonate (polyGal) in solution and also be relevant to new practical applications for PGA in dried state (film, bead or microparticle). First, the dynamic rheological test is used to evaluate the physical properties of polyGal gel. Then the migration of gel front formed by PGA solution and different divalent cations (Ca^{2+}, Zn^{2+}, Ba^{2+}, Mg^{2+}) is studied using the Turbiscan technique. Furthermore, this chapter aims to develop a suitable method of gel forming for the determination of the physical properties of PGA gel as a function of the gelling time, the nature and the concentration of cations.

4.1. Materials and methods

4.1.1. Materials

Poly-D-galacturonic acid (95% of purity, Mw ~ 50 kDa), calcium chloride dihydrate, and barium chloride were obtained from Sigma (St Louis, MO). Sodium chloride, zinc chloride, and magnesium chloride anhydrous were purchased from VWR, BDH Prolabo. All reagents were analytical grade.

4.1.2. Preparation of polyGal gels

Polygalacturonic acid solution was prepared by dissolving PGA (10 g L^{-1}) in a solution of NaCl (0.01 M). The pH was adjusted to pH = 5.5 with sodium hydroxide in order to transform the PGA into polygalacturonate (polyGal). Thus, 10 mL of the viscous polyGal solutions were placed in a plastic box with an inner diameter of 8.8 mm and covered by a hydrated dialysis membrane (SnakeSkin, 10K MW Cut-Off). This plastic box was then immersed in the different divalent cation solutions ($CaCl_2$, $ZnCl_2$, $BaCl_2$ and $MgCl_2$) as shown in the Fig. 4-1.

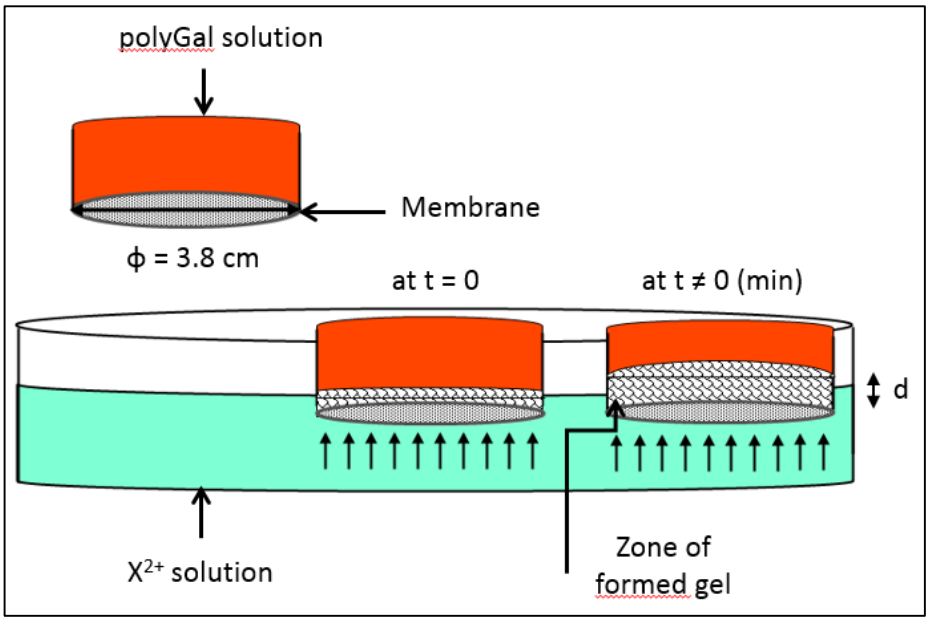

Fig. 4-1. Experimental setup for forming the gel of divalent cations (Ca^{2+}, Zn^{2+}, Ba^{2+} and Mg^{2+}) and polyGal solution (10 g L^{-1}). At t ≠ 0, the gelation occurs and the gel thickness (d) increases

Two main parameters were studied: the concentration of divalent cations (10, 50, 100, 250, 500 and 750 mM) and the residence times (15, 30, 70, 150, 1020 and 1440 min). All experiments were done at room temperature and were done in triplicate.It can be noted that in some case (especially for low divalent cation concentration and short time), gels were not formed. When the gel was formed, the amount of the dry matter ($m_{\text{dried gel}}$) in the gel was determined by drying the gel at 105 °C during 40 h. Taking into account the thickness (d) and the diameter of the gel (ϕ = 3.8 cm), we were able to determine the gel density (ρ_{gel}) according to the following Eq. 4-1.

$$\rho_{gel} = \frac{m_{dried\ gel}}{\pi \times (\phi/2)^2 \times d} \qquad \textit{Eq. 4-1}$$

4.1.3. Rheological experiments

For each gel, the viscoelastic properties were recorded using a stress-controlled dynamic rheometer (MCR 302 from Anton Paar) equipped with parallel plates geometry (diameter of 25 mm) at T = 25 °C. Thus, two viscoelastic properties (G' and G'') were measured: the G' (storage modulus) corresponds to the elastic properties and the G'' (loss modulus) describes the viscous properties. The normal force was adjusted to 0.5 N in order to maintain a good contact between the plate and the gel. We first performed frequency sweep experiments from 0.5 to 100 rad s^{-1} at a fixed shear stress (50 Pa). We have also performed shear stress sweep experiments from 10 to 100 Pa at a fixed angular frequency (10 rad s^{-1}). These experiments allowed us to define the linear viscoelastic region (LVR), where the viscoelastic properties are

independent of the angular frequency and the shear stress. Each experiment was triplicated in order to check the reproducibility and the coherence of registered data.

4.1.4. The determination of the front gel diffusion

During the formation of the gel, cations diffuse through the dialysis membrane and crosslink the polyGal chains (Fig. 4-1). This may induce an increase of the turbidity of the polyGal solution. The evolution of this turbidity as function of the distance of the dialysis membrane and as function of the time can be performed by using the Turbiscan Lab (Formulaction, France). This device works with a pulsed near-infrared light source (λ = 880 nm) and two synchronous detectors for transmission (at 180°) and backscattering (at 45°), which move up and down along a cylindrical glass tube containing the sample, with data collection every 40 µm (Bru *et al.*, 2004). The evolution of this turbidity may give an indication of the diffusion of the front gel. Into the Turbiscan test tubes (60 mm height, 27.5 mm external diameter), we have introduced 15 mL of the polyGal solutions (10 g L^{-1}). In a smaller tube (40 mm height, 150 mm external diameter), we introduced various divalent cation solutions ($CaCl_2$, $ZnCl_2$, $BaCl_2$ or $MgCl_2$) with different cation concentrations (50, 250 or 750 mM). The two tubes were separated by the dialysis membrane (10K MWCO). In this case, the diffusion of the cations occurred from the top to the bottom (Fig. 4-2). During the experiments, the temperature inside the Turbiscan tube was around of 25 °C. Light transmittance was recorded as a function of the time and each distance from the bottom to the top of the tube (0 - 35 mm). Optical transmittance decreased with time because of the turbidity increased due to gel formation. To analyze the results, we chose the point from which began to appear the first plateau (onset); it was marked by small red circles (Fig. 4-2) (see Annex 3 for more details).

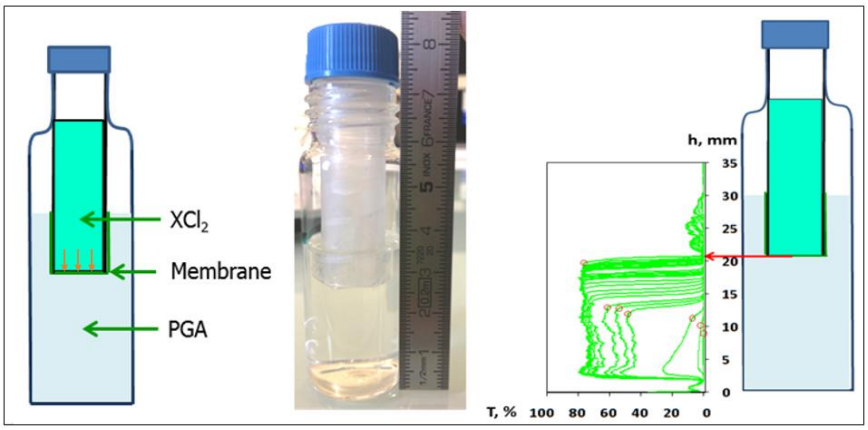

Fig. 4-2. Diagram of experiment and analysis of results based on the transmission data that was collected by Turbiscan from bottom to top of the Turbiscan tube and then plotted as a function of sample height (0 - 35 mm)

4.2. Results and discussion

4.2.1. Phase diagram

When Mg^{2+} was used as crosslinking agent, the polyGal gel was not formed at each concentration of $MgCl_2$ tested (up to 750 mM) and at a residence time of 24 hours. This was in accordance with previous studies (Donati *et al.*, 2009; Selvarengan *et al.*, 2010). In addition, we have shown in Part 2 - Chapter 3 that the turbidity and the viscosity of Mg-polyGal ($c < c^*$) remained constant and low, indicating that gel was not formed. For the three other cations (Ca^{2+}, Zn^{2+}, Ba^{2+}), the gel forming ability was dependent on time and cation concentration. We measured the thickness of the gels as function of the concentration of divalent cation and the time for Ca-polyGal, Zn-polyGal and Ba-polyGal (Fig. 4-3).

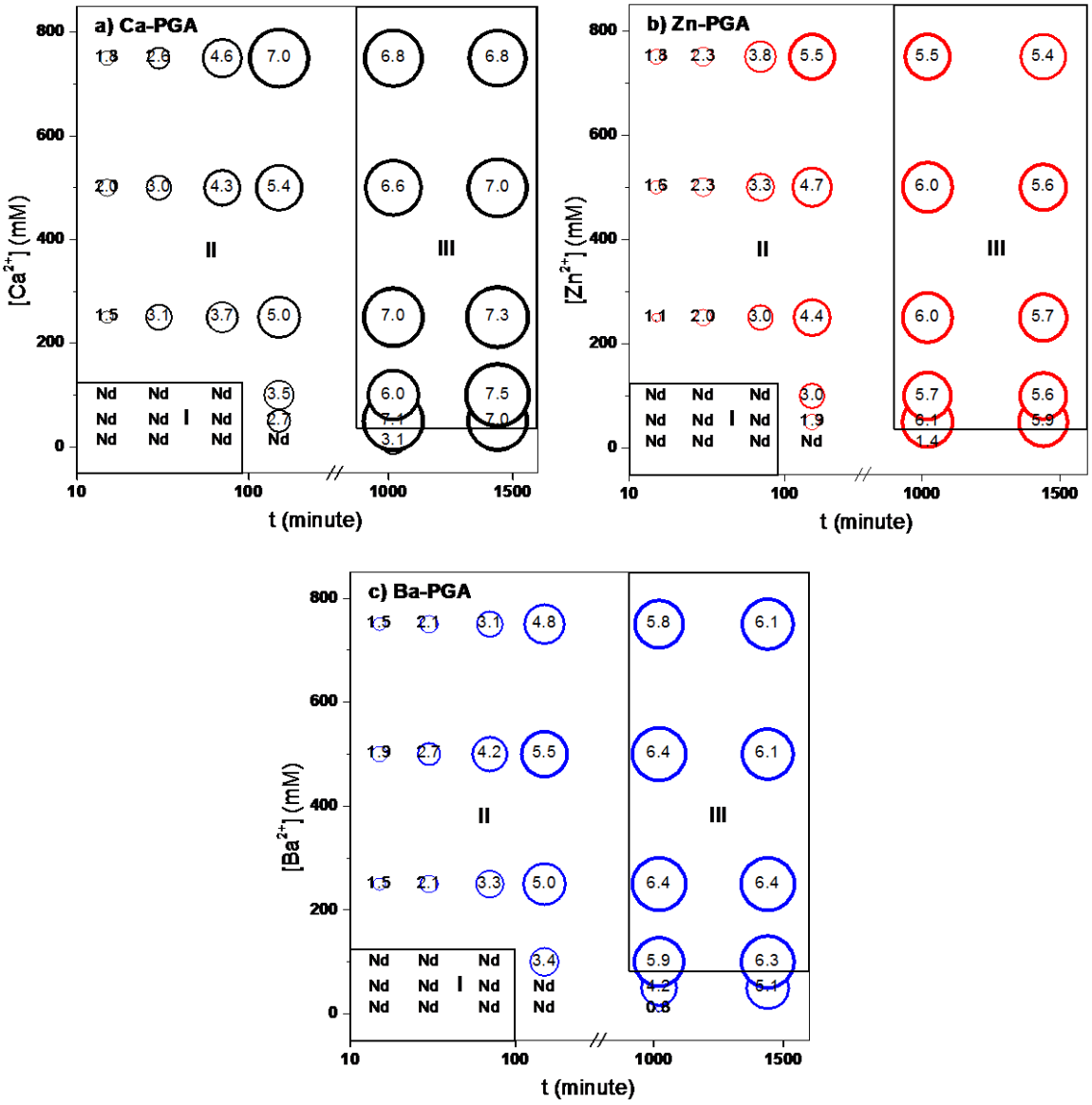

Fig. 4-3. Evolution of the gel thickness: Ca-polyGal (a), Zn-polyGal (b), Ba-polyGal (c) that has undergone a normal force of 0.5 N, according to the gelation time and the cation

concentration (which varies from 10 mM to 750 mM). The concentration of PGA was 10 g L^{-1} (5.4 mM galacturonic acid); (Nd: not determined); the diameter of circle was related to the gel thickness (when the thickness increased the size of the circle increased)

Whatever the nature of the cations (Ca^{2+}, Zn^{2+}, Ba^{2+}), we distinguished three zones:

- Zone I: the gel thickness was too thin to be measured correctly. In this zone, we can consider that the gel was brittle.
- Zone II: the gel thickness was both time and cation concentration dependent. In this zone, the gelation was not finished. Indeed, an increase of the thickness was observed with time and also with increasing the concentration of divalent cation.
- Zone III: the gelation was supposed to be achieved. Indeed, the gel thickness did not change significantly whatever the amount of the divalent cation and the residence time.

For low concentration of divalent cation (around 10 mM, which corresponded to molar ratio (R = $[M^{2+}]/[Gal]$ = 0.2), the gelation can only occur when the residence time is about 17 hours. It can be noted that gels could be obtained at low concentration of divalent cation. Yang *et al.* (Yang *et al.*, 2013) have prepared hydrogel using alginate (10 g L^{-1}) and low concentration of the calcium chloride (4 mM). McConaughy *et al.* (McConaughy *et al.*, 2008) have demonstrated that the *Aloe Vera* polysaccharide (galacturonate polymer) was able to form strong in-situ gels at low polymer (2 g L^{-1}) and Ca^{2+} concentrations (< 10 mM).

In the zone II, we can observe that the gel thickness was more sensitive to the variation of the residence time than the concentration of the divalent cation.

In the zone III, it can also be observed that the thickness of polyGal gels at high residence time decreased in the following order: Ca^{2+} > Ba^{2+} > Zn^{2+} whatever the cation concentration. This can be related to the difference in the 3D network of the polysaccharide in the presence of different cations. In our previous study (refer to Part 1, Chapter 3), we have shown that Ca-LMP was more homogeneous than Zn-LMP, and we have supposed that the Ca-LMP was more flexible (Part 1, Chapter 3). In the following, we focused on the preparation of polyGal gels (10 g L^{-1}) with three divalent cations (Ca^{2+}, Zn^{2+}, Ba^{2+}) at two cation concentrations (250 mM and 750 mM) and various gelation times (0 - 24 hours).

4.2.2. Rheological properties of gels

4.2.2.1. Investigation of the linear regime

It is important to determine the linear viscoelastic region (LVR) for all obtained gels in order to determine the experimental conditions (frequency and shear stress) in which the G' and G'' are stable. Thus, we have measured the viscoelastic properties of polyGal gels at two opposite conditions: (a) 100 mM/gelation time of 2.5 h and (b) 750 mM/gelation time of 17 h which allowed to obtain two gels with the lowest thickness (a) and with the highest thickness (b). These experiments were done for the three divalent cations (Ca^{2+}, Zn^{2+}, Ba^{2+}). Fig. 4-4 shows the evolution of G' and G" of two types of gels as a function of the shear stress. These experiments were performed at a specific angular frequency of ω = 10 rad s^{-1}. In each analysis, both moduli values (G' & G") were found to be almost constant for applied stress values starting at 50 Pa. In order to compare our results within the LVR region, we have chosen fixed angular frequency of 10 rad s^{-1} and shear stress of 50 Pa corresponding to 0.1% of deformation.

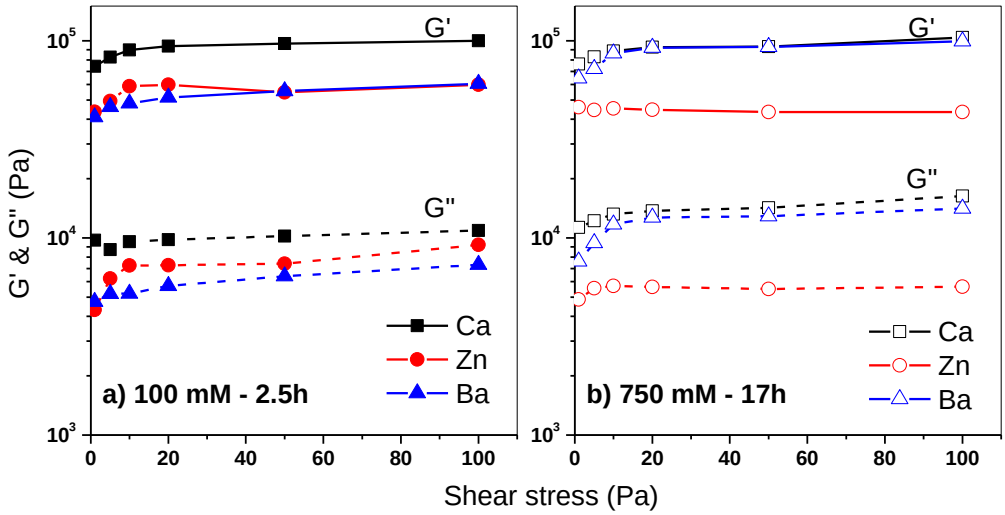

Fig. 4-4. Investigation of the linear region by shear stress experiments performed on Ca-polyGal, Zn-polyGal and Ba-polyGal gels: G' (straight line), G" (dashed line); ω = 10 rad s^{-1}

4.2.2.2. Variation of storage and loss moduli with the gelation time

For all studied samples (whatever the nature and the concentration of divalent cation and the gelation times), no crossover point between G' and G'' was detected throughout the frequency range studied (data not shown). The evolution of G' and G'' as function of gelation time was presented for the three types of gels (Ca-polyGal, Zn-polyGal and Ba-polyGal) at two cation concentrations of 250 and 750 mM (Fig. 4-5). It can be noted that the elastic

contribution was predominant (G' > G"), whatever the cation concentration and the gelation time. The storage moduli (G') ranged between 2 x 10^4 and 6 x 10^4 Pa for 250 mM of divalent cations and between 4 x 10^4 and 8 x 10^4 Pa for 750 mM of divalent cations. Agulhon *et al.* (Agulhon *et al.*, 2014) have studied alginate hydrogels prepared with high guluronate concentration (20 g L^{-1}) and three divalent cations (Mn^{2+}, Co^{2+}, Cu^{2+} at 100 mM). They found that the gels prepared with Cu^{2+} had the higher G' value (5.1 x 10^4 Pa), whereas, for Co^{2+} and Mn^{2+}, the G' was smaller (5400 and 2000 Pa) and was dependent on frequency. The polyGal gels obtained in our study could be compared to Cu-alginate gels obtained by Agulhon *et al.* (Agulhon *et al.*, 2014). Generally, we have observed a progressive increase of the storage and loss modulus as function of the gelation time followed by a plateau (stabilization of the G' and G''). The increase of G' with the time of gelation may indicate that the gelation continued to occur and thus the network structure continued to evolve. The time, at which the beginning of this plateau was observed, was noted t_p, and the corresponding storage modulus was noted G'_p. These two parameters (t_p and G'_p) depended on the nature and the concentration of the divalent cation. For low cation concentration (250 mM), the t_p was constant and equal to 150 min whatever the nature of the cation; while the G'_p increased as the following order: G'_p (Ca-polyGal) > G'_p (Ba-polyGal) ≈ G'_p (Zn-polyGal). This revealed that the network structure of Ca-polyGal gels was stronger than the network structures of other divalent cations studied (Zn^{2+} and Ba^{2+}).

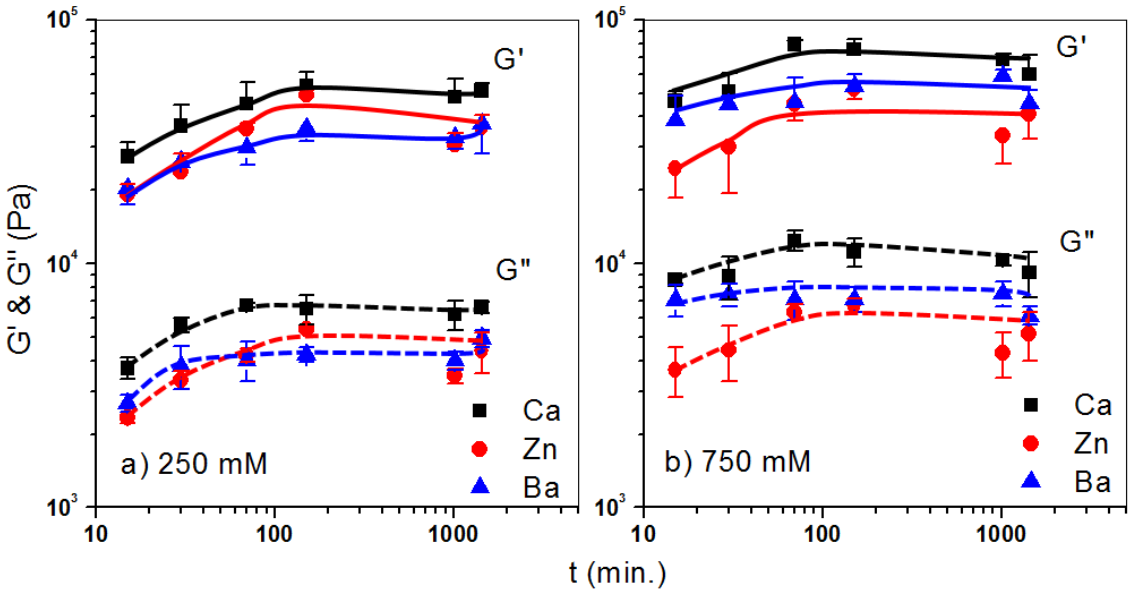

Fig. 4-5. Influence of the cation concentration on the viscoelastic properties: G' (straight line), G" (dashed line) of Ca^{2+}-polyGal, Zn^{2+}-polyGal and Ba^{2+}-polyGal gels over the gelling time: (a) 250 mM and (b) 750 mM (T = 25 °C; σ = 50 Pa; ω = 10 rad s^{-1}). Lines are to guide eyes

At high cation concentration (750 mM), the t_p of Ca-polyGal and Zn-polyGal were about 100 min (shorter than the time observed for the cation concentration of 250 mM). The storage modulus at the plateau (G'_p) of Ca-polyGal was higher than others. For Ba-polyGal, the G' did not change significantly with the gelation time indicating that the network structure of this gel is not affected with the time gelation. With the increase of divalent cation concentration, the G' and G'' increased, especially for Ca^{2+} and Ba^{2+} gels.

We have also measured the thickness of the gel and the amount of dry matter in the gel as function of the gelation time for the three types of gels at the divalent cation concentration of 250 mM (the gel thickness was the highest at this concentration Fig. 4-3). These measurements allowed us to determine the gel density according to Eq. 4-1 (Fig. 4-6).

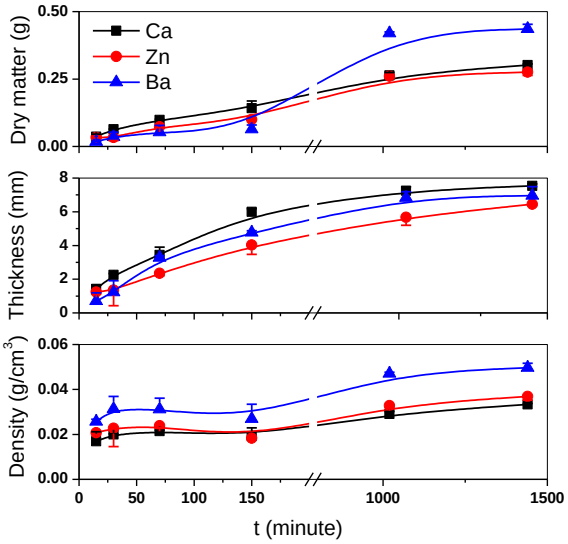

Fig. 4-6. Influence of the gelling time on the dry material, the gel thickness, and the density of Ca-polyGal, Zn-polyGal and Ba-polyGal gels at divalent cation concentration of 250 mM

As the gelation time increased, both the dry matter and the thickness increased and then were stabilized. The gel density calculation showed that the gel became denser with the gelation time. We suggested the presence of two successive steps in gel formation: i) the diffusion of divalent cations first increased the thickness of the gel without any changes in the gel density ($0 < t < 180$ min), ii) then the thickness of the gel was unchanged but with an increase of the gel density (Fig. 4-7).

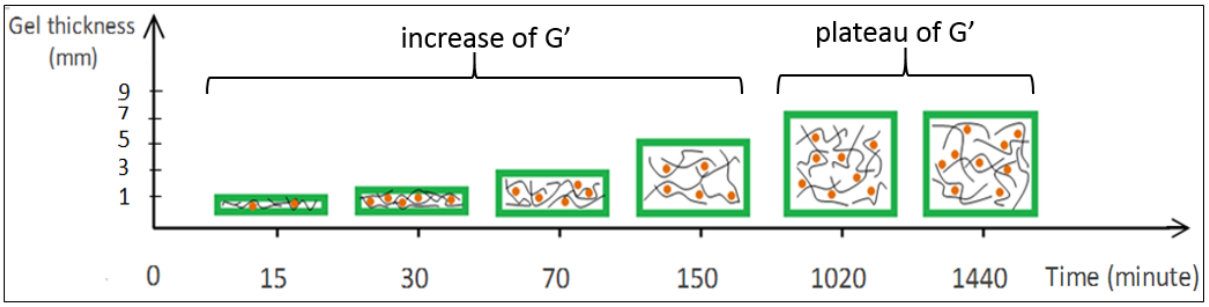

Fig. 4-7. Diagram illustrates the influence of the gelling time on the thickness and the density of gel

In the case of polyGal gels, the evolution of the gel density could confirm the mechanism of binding suggested for polyGal mixture in the diluted regime (Figure 6, Part 2, Chapter 3). The increase of molar ratio can be easily correlated to the increase of gelation time (as the gelation time increased, the molar ratio increased). The first step of the binding mechanism due to the formation of monocomplexes and point-like cross-links could be correlated to the increase of the thickness of the gel. The second step due to the formation of dimers could be due to the densification of the gel (Fig. 4-7). It can be noted that the gel density for Ba-polyGal was higher than for Ca-polyGal and Zn-polyGal. The gel density can be related to the affinity of cations for the polyGal chains. The binding affinity of Ba^{2+} cations for the polyGal was higher than for the other cations as shown in Chapter 3. Indeed, we have observed, in the diluted regime, that the viscosity and turbidity were high when Ba^{2+} cations were used instead of the other cations (Ca^{2+}, Zn^{2+}, and Mg^{2+}) (Figure 1, Part 2, Chapter 3). In addition, the amount of Ba^{2+} entrapped into the polyGal network was high. In the case of Ba- polyGal gels, the increase of the gel density could be explained by the high number of point-like cross-links observed in polyGal mixtures.

4.2.3. Measurement of gel front migration

As the gelation time increased, the divalent cations diffused through the dialysis membrane and interacted with galacturonate units. This may induce an increase of the turbidity. Using Turbiscan technique, we were able to follow the turbidity of the mixture with time and at various distances from the membrane to the bottom of the Turbiscan tube (Fig. 4- 2). In the Chapter 3, we have shown that the turbidity of Mg-polyGal mixtures (diluted regime, 0.5 g L^{-1}) was low and close to zero (Figure 1, Part 2, Chapter 3). In addition, Mg^{2+} cations are not able to form gel with polyGal. However, in the case of Mg-polyGal mixtures, we have observed an increase of the turbidity, which may be due to the high concentration of

the polymer (10 g L^{-1}). Thus, we have measured the evolution of the turbidity in the Mg- polyGal mixtures. The same experiments were done for Ca-polyGal, Zn-polyGal and Ba- polyGal gels (Annex 4). In these measurements, we have attributed the onset of the increase of the turbidity to the front of the gel. It can be noted that the front gel was moving downward in the vertical direction. Therefore, the thickness of the gel layer (d) increased with time. In this study as already described, the diffusion of the gel front was limited in time by diffusion of the divalent cation (Potter *et al.*, 1994; Skjåk-Bræk *et al.*, 1989). Because of the slow diffusion of divalent cations, a model of $d^2 = 2D_{gel}t$ was used to understand the limitations of this model (Einstein, 1926), where D_{gel} is the diffusion coefficient of the gel front which may be related to the divalent cation diffusion coefficient ($cm^2\ s^{-1}$); d is the gel thickness (cm) and t is the gelation time (s).

We observed a linear relationship between the square gel thickness (d^2) and the gelation time t, as shown in Fig. 4-8. The diffusion coefficients of the front gel (D_{gel}) were listed in Table 4-1. It is well known that the diffusion coefficients of the four divalent cations in pure water (D_0) at 25°C were 7.4 x 10^{-6}; 8.5 x 10^{-6}; 7.0 x 10^{-6}; and 7.1 x 10^{-6} $cm^2\ s^{-1}$ for Ca^{2+}, Zn^{2+}, Ba^{2+} and Mg^{2+}, respectively (Hazel and Sidell, 1986; Weast *et al.*, 1986).

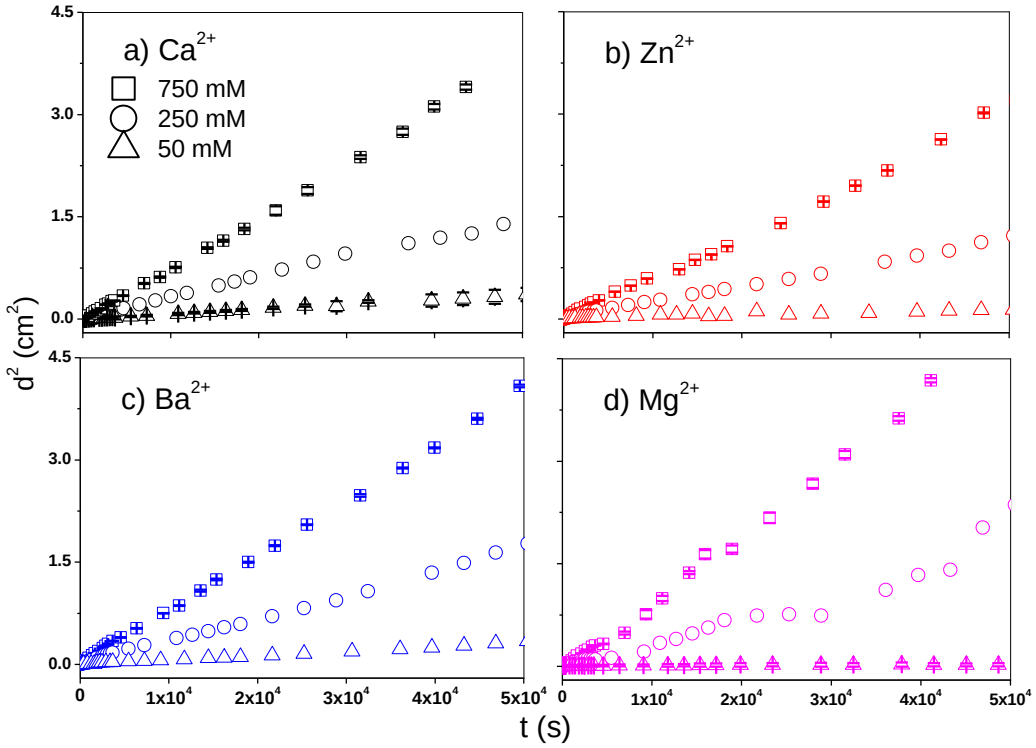

Fig. 4-8. Relationship of gel thickness (d^2) versus gelation time (t) of polyGal and different divalent cations: Ca^{2+}(a), Zn^{2+}(b), Ba^{2+} (c) and Mg^{2+} (d) at three cation concentrations (750, 250 and 50 mM)

Table 4-1. Diffusion coefficients of the front gel (D_{gel}) for various divalent cations and at three cation concentrations (50, 250 and 750 mM)

Type of gel	Divalent cation concentration, mM	Molar ratio	Diffusion coefficient (D_{gel}), 10^6 cm^2 s^{-1}	D_{gel}/D_0
Ca-polyGal	50	0.9	3.9 ± 0.6	0.5
Ca-polyGal	250	4.6	16.0	2.2
Ca-polyGal	750	13.9	39.0 ± 0.5	5.3
Zn-polyGal	50	0.9	2.7 ± 0.2	0.3
Zn-polyGal	250	4.6	11	1.3
Zn-polyGal	750	13.9	31 ± 0.0	3.6
Ba- polyGal	50	0.9	4.6 ± 0.1	0.7
Ba-polyGal	250	4.6	19.0	2.7
Ba-polyGal	750	13.9	40.0 ± 0.1	5.7
Mg-polyGal	50	0.9	0.2 ± 0.0	0.03
Mg-polyGal	250	4.6	23.0	3.24
Mg-polyGal	750	13.9	49.0 ± 0.5	6.90

The diffusion coefficients of the front gel (D_{gel}) increased as the concentration of the divalent cations increased. The same tendency was observed in previous studies (Kim, 1990; Potter *et al.*, 1994; Wu *et al.*, 2014). Kim has studied the effect of calcium chloride concentration on the effective diffusion coefficient of calcium ion within the calcium alginate layer during the gel formation process (Kim, 1990). The diffusion coefficient appeared to increase with increasing concentration of calcium chloride solution, probably due to macropore formation at higher concentration (> 125 mM). Potter *et al.* have suggested, using magnetic resonance imaging, that the diffusion of calcium ions through the gel network was dependent on the initial concentration of the calcium, the ionic strength of the alginate solution, and the size of pores in the gel which was formed (Potter *et al.*, 1994). Wu *et al.* have studied the diffusion of Ca^{2+} into aqueous solution of a rigid polyanion, poly-(2,2'-disulfonyl-4,4'-benzidine terephthalamide) at different polymer and calcium concentrations (Fig. 1-9, Chapter 1) (Wu *et al.*, 2014). For low concentration of calcium cations (100 mM), the coefficient diffusion, measured by using a polarizing optical microscope, was smaller than the diffusion coefficient D_0 of Ca^{2+} in pure water ($D/D_0 < 1$), whereas for high calcium concentrations (500, 1000, and 2000 mM) the coefficient diffusion was higher ($D/D_0 > 1$). Because of the high viscosity of polyelectrolyte solution, the gelation was essentially a cation-diffusion limited reaction (Wu *et al.*, 2014). The diffusion of divalent cation was affected by

the complexation between the carboxylate groups and the divalent cation which induced the gelation according two aspects as suggested by (Wu *et al.*, 2014):

i) the reaction front continuously consumes the free cations just diffused through previously formed gel matrix which hinders the diffusion of divalent cations over the reaction front. This becomes more important especially when the fresh flux of cations can not bind all carboxylate groups. This effect could be observed for low divalent cation concentration (50 mM).

ii) When the divalent cation concentration is high, the reaction front immobilizes divalent cations and decreases the amount of local free cations, forming a sharp concentration gradient of mobile cations at the diffusion front. Therefore, the complexation, which builds up a sharp concentration gradient at the diffusion front, should promote the diffusion process (250 and 750 mM).

The value of diffusion coefficient of the front gel changed as the function of the nature and the initial concentration of divalent cation used. At the concentration of 50 mM, the diffusion coefficient decreased following the order: $Ba^{2+} > Ca^{2+} > Zn^{2+} > Mg^{2+}$ (Table 4-1). We have previously shown that the mechanism for binding divalent cations (Ca^{2+}, Ba^{2+}, Zn^{2+} and Mg^{2+}) to polyGal, in diluted regime, depended on the affinity of the divalent cations for water molecules and followed by the order: $Ba^{2+} < Ca^{2+} < Zn^{2+} < Mg^{2+}$ (Part 2, Chapter 3). The greater the affinity for water, the more difficult for cations to interact with polyGal. Hence, this explained the diffusion of gel front of Ba^{2+} was higher than Ca^{2+} and Zn^{2+} whatever the divalent cation concentrations. The interaction of Mg^{2+} cations with polyGal was a weak process (non-gelling) and only electrostatic (Selvarengan *et al.*, 2010). Donati *et al.* (Donati *et al.*, 2009) have attributed these interactions to the polycondensation process. We have suggested that the Mg^{2+} cation interacted so strongly with water from its hydration shell which did not allow to form the monocomplexation (the first step of the mechanism of gelation). Thus the polycondensation may be due to the sharing water molecules from the first coordination shell of Mg^{2+} and the carboxylate groups of polyGal (Figure 6, Part 2, Chapter 3). It can be noted that for high concentration of Mg^{2+} (250 and 750 mM), we have observed a thin soft gel layers on the dialysis membrane. Previous work (Topuz *et al.*, 2012) showed that Mg^{2+} ions induced alginate gelation. The gelation in this system occurred at 5 - 10 times higher concentration of ions than reported for calcium based gels. In addition, the storage modulus (G') of the gel obtained with alginate (50 g L^{-1}) and Mg^{2+} (300 mM) after 24h of gelation was around 1000 Pa which was 60 times lower than Ca-polyGal (Fig. 4-5).

4.2.4. Conclusion

Aside from Mg^{2+}, all the three divalent cations (Ca^{2+}, Zn^{2+}, Ba^{2+}) can form a gel even at low cation concentration (10 mM) if the gelling time is long enough ($t_{gel} \geq 17h$). We have noted that an increase of the initial concentration of the divalent cation can decrease the gelling time. The rheological properties (elastic and viscous moduli) were observed to be dependent on the nature and the concentration of divalent cations and also on the gelling time. These viscoelastic properties increased with the gelling time to reach a plateau. It was observed that the Ca-polyGal is more rigid than the two other gels (Zn-polyGal and Ba-polyGal). The determination of the dry matter and the thickness of the gels allowed us to get information on the density of the gels. In general, we have observed that the gel density is stable and low for low gelling time ($t_{gel} \leq 150$ min). At the same gelling time, the G' of the gel increases. The diffusion of the cations may form many point-like cross-links which may increase the thickness of the gel. This increase could be balanced by the increase of the number of cross-linked chains. We then suggested that this step is due to the formation of monocomplexes and point like crosslinks which is in accordance with the step 1 proposed in Part 2 - Chapter 3. When $t_{gel} > 150$ min, the G' reached a plateau. At this time, we can suppose that all the polymer chains are cross-linked. According to the mechanism proposed in Chapter 3, we can attribute this second step to the formation of dimers. However, it is possible that this second step could not occur because of the high concentration of the polyGal (10 g L^{-1}) and the initial concentration of the divalent cations.

The diffusion coefficient of the front gel (D_{gel}) increased with increasing the initial concentration of divalent cations. Taking into account the diffusion of the cations (D_0) in the pure water, we have observed that the ratio (D_{gel}/D_0) was below 1 when the cation concentration is low (50 mM). This ratio was above 1 for high concentration of divalent cation (250 or 750 mM). Moreover, the diffusion rate of front gel decreased following the order $Ba^{2+} > Ca^{2+} > Zn^{2+}$ whatever the initial concentration of divalent cations. This may be explained by the low affinity of the divalent cations for water molecules and so the high affinity for cations to interact with polyGal was in the same order: $Ba^{2+} > Ca^{2+} > Zn^{2+}$ (Part 2, Chapter 3).

The study of the rheological properties and the gelation kinetics on PGA gels could help us to understand the behavior of these matrices in dried state (film, bead or microparticle) and to better control the release of active compounds encapsulated in these matrices.

Principaux résultats et conclusions

Nous avons préparé des gels de polygalacturonate (polyGal) par diffusion des cations divalents (Ca^{2+}, Zn^{2+}, Ba^{2+}, et Mg^{2+}) à travers une membrane de dialyse. Plusieurs paramètres ont été étudiés : la concentration initiale du cation divalent et le temps de gélification (t_{gel}). Nous nous sommes intéressés aux propriétés viscoélastiques des gels mais aussi à la cinétique de gélification.

Nous avons dans un premier temps réalisé un diagramme d'état qui a mis en évidence la présence de 3 zones : i) une zone où la gélification ne peut pas se produire (temps de gélification < 2 heures et concentration en cations divalents < 100 mM), ii) une zone où la gélification dépend fortement de la concentration initiale du cation et iii) une zone où la formation du gel est achevée (l'épaisseur du gel n'évolue plus). Cette dernière zone qui est peu sensible à la concentration initiale du cation apparaît à des temps de gélification élevé (t_{gel} > 17 heures). Il est à noter que les ions magnésium ne forment pas de gels dans les conditions étudiées (temps de gélification compris entre 10 min et 24 heures et concentration initiale en cations comprise entre 10 mM et 750 mM).

Ensuite, nous avons étudié l'évolution des propriétés viscoélastiques (G' et G'') des gels de polyGal en fonction du temps de gélification à deux concentrations initiales en cations (250 mM et 750 mM) pour les trois cations (Ca^{2+}, Ba^{2+} et Zn^{2+}). Nous avons remarqué que tous les gels présentent un caractère élastique (G' > G''). Lorsque le temps de gélification augmente, le module élastique (G') augmente puis se stabilise au bout de 2 heures quelle que soit la nature du cation divalent pour une concentration 250 mM. La valeur de G' de ce plateau notée G'_p suit l'ordre suivant : Ca-polyGal > Zn-polyGal ≈ Ba- polyGal. De plus, la densité reste faible et constante pour des temps de gélification faibles puis augmente pour des temps plus élevés. Il est à noter que la densité des gels de Ba- polyGal est plus élevée que celui des gels de Ca-polyGal. En se basant sur ces résultats, nous avons proposé un mécanisme qui est en accord avec celui proposé dans le Chapitre 3. En effet, nous observons deux étapes : i) la formation de monocomplexes et de réticulations ponctuelles qui peut être corrélée à une augmentation de l'épaisseur du gel sans changement notable de la densité. La deuxième étape (ii) est due à la formation de dimères qui peut expliquer la densification du gel (Fig. 4-7).

Enfin, nous avons suivi la diffusion du front du gel lors de la gélification du polyGal en fonction de la nature du cation divalent (Ca^{2+}, Zn^{2+}, Ba^{2+}, et Mg^{2+}) à trois concentrations

initiales du cation (50, 250 et 750 mM). A 50 mM, nous avons remarqué que le coefficient de diffusion du front de gel suit l'ordre suivant : $Ba^{2+} > Ca^{2+} > Zn^{2+} > Mg^{2+}$ (Table 4-1) ; ceci peut être relié à l'affinité entre le cation et les molécules d'eau de sa sphère de coordination. En effet, l'affinité du cation pour l'eau augmente selon l'ordre inverse : $Ba^{2+} < Ca^{2+} < Zn^{2+} < Mg^{2+}$ (Partie 2, Chapitre 3). Pour des concentrations initiales en cation élevées (250 et 750 mM), nous avons remarqué que la diffusion du cation est plus élevée que la diffusion du cation dans l'eau pure. Ainsi, nous pouvons en conclure que le mécanimse d'association est concentration dépendante.

CHAPTER 5

MICROPARTICLES BASED ON POLYURONATES: RELATIONSHIP BETWEEN GELATION AND RELEASE PROPERTIES

Introduction

Après avoir évalué la conformation et la structure du PGA et de la pectine LMP en solution, leur capacité à fixer différents cations divalents et avoir étudié la formation des gels, le Chapitre 5 présente l'utilisation des trois types de polyuronates (PGA, LMP et ALMP) pour la fabrication de microparticules contenant de la rutine.

La rutine est un flavonoïde bénéfique pour la santé mais elle est peu soluble dans l'eau, sensible au pH et à la lumière, ce qui rend son utilisation et sa biodisponibilité délicates. L'encapsulation de la rutine à partir de différents polysaccharides est une solution pour résoudre ces difficultés et protéger la molécule tout en contrôlant les propriétés de relargage.

Dans une première partie, nous avons fabriqué des microparticules par gélification ionique avec du calcium et trois polyuronates : l'acide polygalacturonique (PGA, pureté de 95%), une pectine faiblement méthylée (LMP, DE = 27 - 33%) et une pectine faiblement méthylée amidée (ALMP, DE = 22 - 28%, DA = 20 - 24%). Nous avons fixé la concentration en polyuronates en se référant à la teneur en acide galacturonique (GalA), ce qui a permis d'avoir la même viscosité des solutions. Ces microparticules ont toutes été fabriquées à partir de la même quantité de rutine. Puis nous avons caractérisé les microparticules obtenues en évaluant leur taille, leur forme, leur efficacité d'encapsulation, leur capacité d'absorption en eau, leur libération de calcium et la cinétique de libération de la rutine dans un milieu intestinal simulé (pH = 7,4).

Dans une seconde partie, nous avons préparé des gels avec ces trois mêmes polyuronates. Nous avons alors déterminé leur capacité à fixer les ions calcium (mesures d'affinité de liaison) ainsi que les propriétés viscoélastiques des gels formés à l'aide d'un rhéomètre dynamique.

La finalité de ce chapitre est d'examiner s'il peut être établi des relations entre les propriétés du gel et les propriétés des microparticules, notamment la libération de la rutine. L'objectif est de comprendre la différence de structure des matrices formées à base de polyuronates et de voir leur répercussion sur les propriétés macroscopiques de ces microparticules afin de pouvoir les maîtriser dans un procédé industriel lors d'applications soit agroalimentaires soit pharmaceutiques.

In this chapter, we have produced three types of microparticles containing an active substance with three polyuronates: low methoxyl pectin (called LMP), amidated low methoxyl pectin (called ALMP) and a homogeneous backbone of polygalacturonic acid (called PGA). The active substance used was rutin (quercetin-3-O-rutinoside) which is a flavonoïd compound not chemically stable when exposed to light but with important properties for human health due to antioxidant properties (Calabrò *et al.*, 2005). The obtained microparticles were characterized in terms of size, shape, yield, encapsulation efficiency, water uptake and *in vitro* release. Complementary studies on the polyuronate solutions and gels as the ability of the three polyuronates to bind calcium ions and the viscoelastic properties of the gels were performed in order to relate the macroscopic properties of the microparticles to the structure of the gels.

5.1. Materials and methods

5.1.1. Materials

Rutin hydrate (purity ≥ 94%), Tris (hydroxymethyl) aminomethane and Polygalacturonic acid (PGA) (purity ≈ 95%) were purchased from Sigma-Aldrich, Germany. Low methoxyl pectin (LMP) (Unipectin 300C, DE ≈ 27 - 33%) and Amidated low methoxyl pectin (ALMP) (Unipectin 305C, DE ≈ 22 - 28% and DA ≈ 20 - 24%) were obtained from Cargill (France). Sodium chloride and calcium chloride were purchased from VWR, BDH Prolabo. All reagents were analytical grade.

5.1.2. Rheological behavior of polyuronate solution

The rheological behavior of polyuronate solutions (ALMP, LMP and PGA) in 0.01 M NaCl solution at pH 5.5 were investigated using HAAKE Viscotester 550 (Thermo Scientific, France) with spindle and cup sensor at controlled temperature (T = 25.0 ± 0.5 °C). The salt (NaCl 0.01M) was used in order to screen electrostatic interactions (Lootens *et al.*, 2003). The pH used in this study is higher than the pKa of the three pectins (pKa_{ALMP} = 3.4 - 4.5 (Löfgren *et al.*, 2006), pKa_{LMP} = 4.0 and pKa_{PGA}= 3.8). The rheological behavior of each kind of polyuronate solution was performed as the function of the concentration of polyuronate (60, 50, 40, 30, 20 and 10 g L^{-1}). Data analysis was done with HAAKE RheoWin Job Manager Software. Different rheological models were tested to fit data. The best fit was obtained with a power law model. The Ostwald De Waele power law model (Mancini *et al.*, 1996) was chosen and indicated that

the flow of polyuronate solutions can be expressed by the pseudoplastic model, which is given by the Eq. 5-1:

$$\tau = K\gamma^n \qquad \textit{Eq. 5-1}$$

where: τ = shear stress; γ = shear rate; K = flow consistency index and n = flow behavior index ($n < 1$ in the case of pseudoplastic fluid).

5.1.3. Encapsulation of rutin in calcium pectinate microparticles and microparticle characterizations

5.1.3.1. Microparticles preparation

The encapsulation of rutin was prepared by the ionotropic gelation method described by Chambin *et al.* (Chambin *et al.*, 2006). Polyuronate solutions were prepared by dissolving PGA (20 g L^{-1}), LMP (30 g L^{-1}) and ALMP (40 g L^{-1}) in 0.01 M NaCl solution (pH = 5.5) using magnetic stirring at high speed (700 rpm) for 1h. If we take into consideration the DE and DA of PGA, LMP, and ALMP, we can calculate the amount of galacturonic acid (GalA) in these three polyuronates. Indeed, 20 g L^{-1} of PGA, 30 g L^{-1} of LMP and 40 g L^{-1} of ALMP correspond to 108, 119 and 120 mM of GalA, respectively. To these polyuronate solutions, we introduced an exact amount of rutin to obtain a concentration of 20 g L^{-1}. The mixtures were stirred then at room temperature for 2h. The suspension (polyuronate and rutin) was pumped and poured dropwise into a solution of 750 mM $CaCl_2$ (pH = 4.5 - 5) using an IPC Ismatec pump with a 2 mm needle in diameter (the volume rate of the pump is 3 ml/min). The cross-linking was instantaneous, producing pectinate beads. After a curing time of 5 min in $CaCl_2$ solution, beads were then collected and dried in an oven at 37 °C during for 40 h and stored at 4 °C before using. The obtained microparticles were noted: PGA-Ca, LMP-Ca, and ALMP-Ca. The size and the shape of these beads before drying were characterized by optical microscopy (stereomicroscope CETI). For microparticles (dried beads), the water content was determined using an infrared moisture analyzer at 150 °C until the stabilization of weight stabilization was achieved (OHAUS MB35, Switzerland).

5.1.3.2. Encapsulation efficiency and encapsulation yield (EE and EY)

For each type of microparticles, 50 mg were introduced in 10 mL of phosphate buffered solution (pH = 7.4), until their total degradation. 1 mL of dispersion was taken and adjusted to 20 ml with phosphate buffered solution (pH = 7.4). The absorbance was measured at 268 nm by a spectrophotometer. A standard curve of rutin was obtained to calculate the amount of

rutin (concentration range from 10 mg/L to 80 mg/L, R^2 > 0.99). All experiments were performed in triplicate.

The EE (encapsulation efficiency) and EY (encapsulation yield) of rutin in calcium pectinate microparticles were determined by the Eq. 5-2 and Eq. 5-3:

$$EE(\%) = \frac{Q_E}{Q_M} \times 100 \qquad \textit{Eq. 5-2}$$

$$EY(\%) = \frac{Q_E}{Q_T} \times 100 \qquad \textit{Eq. 5-3}$$

where Q_E was the amount of rutin encapsulated, Q_T was the total of rutin used; Q_M was the total amount of microparticles.

5.1.3.3. Water uptake study

100 ± 1 mg of each type of microparticles (PGA-Ca, LMP-Ca, and ALMP-Ca) were placed in a dissolution basket (Sotax 2830) and soaked in 250ml of tris buffer (pH = 7.4) at 37 °C with magnetic stirring at constant speed (250 rpm). Tris buffer was prepared with 25 mL of Tris ($C_4H_{11}NO_3$, 0.2 M) and 20.7 mL of HCl (0.2 M), diluted to 100 mL. The microparticles were periodically removed (every 15 min for 3 h) and drained with filter paper to remove excess water. Then the change in weight was measured until mass equilibrium had been achieved. The water uptake (*WU*) was calculated using the Eq. 5-4. All experiments were performed in triplicate.

$$WU(\%) = \frac{w_t - w_0}{w_0} \times 100 \qquad \textit{Eq. 5-4}$$

where w_t is the weight of the microparticles at a specific time, and w_0 is the initial weight of the dry microparticles. During the water uptake tests, a fraction of the media was collected, and the amount of calcium released from the microparticles was determined by the calcium ion-selective electrode using an automatic titration systems (TitroLine® 6000 - IS Analytics - France).

5.1.3.4. Dissolution studies in simulated intestinal fluid

100 ± 1 mg of each microparticle were weighed and introduced in 1L of simulated intestinal fluid (tris buffer, pH = 7.4). The experiment was performed at 37 °C with a paddle speed of 50 rpm in a dissolution apparatus SOTAX AT7 Smart (type II apparatus). Samples of 3 mL each were withdrawn at 15, 30, 45, 60 min and then every 30 min until 300 min. The amount of released rutin was assessed by absorbance measurement at 268 nm (Uvikon UV

spectrophotometer). Then the percentage of released rutin was determined and plotted over time. All experiments were performed in triplicate. The drug release profiles were fitted by Korsmeyer–Peppas model (Ritger and Peppas, 1987):

$$\frac{M_t}{M_\infty} = kt^n \qquad \textit{Eq. 5-5}$$

where M_t represents the fraction of drug released at time t and M_∞ is the total amount of drug in the system. M_t/M_∞ is the fraction of drug released at time t, k is the rate constant incorporating structural and geometric characteristics of the device and n is the release exponent, indicating the drug release mechanism.

5.1.4. Gel properties

5.1.4.1. Calcium binding affinity

In order to determine the amount of calcium bound by the three types of polyuronate solutions as function of added calcium, the concentrations of these biopolymers were reduced to avoid the gelation of the solution. Thus, the concentrations of the PGA, LMP and ALMP were 1.0 g L^{-1}, 1.5 g L^{-1} and 2.0 g L^{-1}, respectively. All these solutions were prepared in 0.01 M NaCl solution and at fixed pH = 5.5. The polyuronate solution (25 mL) was titrated by a solution of $CaCl_2$ (100 mM). After each calcium addition, the amount of the free calcium was assessed by the calcium ion-selective electrode (ISE25Ca) using an automatic titration system (TitroLine® 6000 - IS Analytics - France). The fixed calcium ($[Ca]_{fixed}$) is calculated from the difference between the total added calcium and the free calcium. The fixed calcium was then normalized by the galacturonate concentration [Gal] in each polyuronate to obtain the bound ($B = [Ca]_{fixed}/[Gal]$).

To characterize the binding mechanism and highlight links formation between polyuronate and calcium ions, experimental data from binding isotherms were plotted in terms of Scatchard plots (Dronnet *et al.*, 1996; Lips *et al.*, 1991), where the bound (B) divided by free calcium concentration ($B/[Ca]_{free}$) was expressed versus B. The $B/[Ca]_{free}$ was expressed in mM^{-1}.

5.1.4.2. Rheological experiments

- **Preparation of gels and rheological characterizations**

The polyuronate solutions used for gel fabrication were prepared in the same conditions used for microparticles preparation. Thus, the concentrations of PGA, LMP and

ALMP were 20 g L^{-1}, 30 g L^{-1} and 40 g L^{-1}, respectively. Then 10 mL of the polyuronate solutions were placed in plastic boxes covered by a dialysis membrane (SnakeSkin 10000 MW cut-off) in contact with $CaCl_2$ solution 750 mM at room temperature for 24 hours. Only calcium cations can diffuse through this membrane inducing the formation of polyuronate gels. The obtained gels were drained with filter paper to remove the excess of water and unbound calcium (free calcium). Viscoelastic properties of each kind of polyuronate gels were then determined using a stress-controlled dynamic rheometer (MCR 302 from Anton Paar®) equipped with parallel plates geometry (diameter of 25 mm) at T = 25 °C. At the beginning of the measurement, the thickness of each gel was measured. Then, a normal force close to 0.5 N was applied to ensure a good mechanical contact between the gel and the plate of the rheometer. The results of dynamic rheometer were expressed by three main parameters as a function of the shear angular frequency (ω) ranging from 0.5 to 100 rad s^{-1}: (a) the storage modulus (G'), corresponding to the elastic property of the gel; (b) the loss modulus (G''), corresponding to the viscous property of the gel), and (c) the loss tangent (tanδ = G”/G’), corresponding to molecular mobility transitions. For the three gels, we compared the rheological parameters (G’, G’’ and tanδ) at fixed stress and angular frequency equal to 50 Pa and 9 rad s^{-1}, respectively. In these conditions, the system remained in the linear viscoelastic regime. For each formulation, at least three gels were prepared to check the reproducibility and the coherence of measured data.

5.2. Results and discussion

5.2.1. Rheological behavior of polyuronate solution

All polyuronate solutions exhibited a shear thinning behavior in agreement with results of others references for high concentration (> 20 g L^{-1}) (Jantrawut *et al.*, 2013; Stoddart *et al.*, 1969). Fig. 5-1 showed the evolution of the consistency (K) as function of the concentration of the polyuronates for PGA, LMP, and ALMP. As expected, the consistency increases with the concentration of the polyuronate. It can be noted that the consistency index (K) values are similar for PGA (20 g L^{-1}) LMP (30 g L^{-1}) and ALMP (40 g L^{-1}). This may justify the choice of the three concentrations for the three polyuronates (PGA, LMP and ALMP). In addition, at these concentrations and taking into account the DE and the DA, the concentrations of galacturonic acid (GalA) in the three types of polyuronates are similar (PGA - 108 mM; LMP - 119 mM; ALMP - 120 mM).

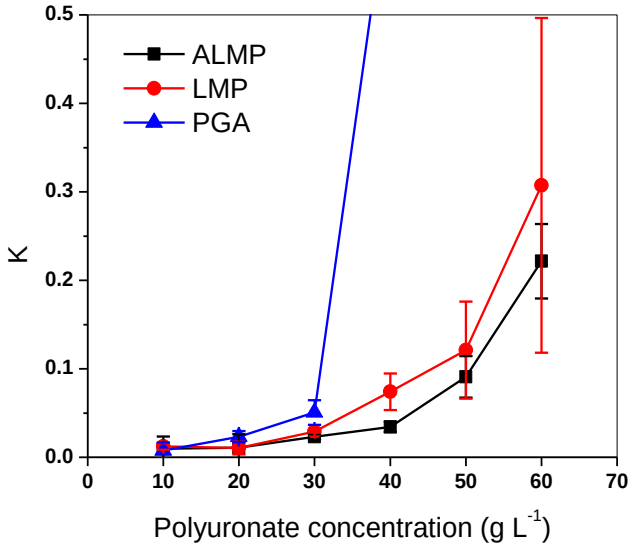

Fig. 5-1. Evolution of the consistency index (K) of polyuronate solutions as a function of the concentration for ALMP, LMP, and PGA

5.2.2. Microparticle properties

5.2.2.1. General properties

By ionotropic gelation, beads were formed instantaneously when polyuronate solution containing rutin was in contact with calcium ions. The beads were formed at pH = 5.5, where more than 94% are in the carboxylate groups formed. Inter- and intramolecular electrostatic repulsions occurred, and cross-links between the polyuronate chains were possible through Ca^{2+} bindings to the carboxyl groups. After drying, microparticles were obtained and their physicochemical properties (EE, EY, rutin lost, moisture content, size) are determined in Table 5-1.

Table 5-1. Encapsulation efficiency (EE) and encapsulation yield (EY) of polyuronate microparticles

	ALMP - Ca	LMP - Ca	PGA - Ca
Microparticle size (mm)	1.9 ± 0.3	2.5 ± 0.5	3.9 ± 0.7
Moisture content (% w/w)	10.7 ± 1.7	11.9 ±0.4	13.4 ± 0.3
Rutin lost (%)	15.5	3.3	2.2
EE (%)	20.8 ± 2.2	27.3 ± 2.7	21.2 ± 0.1
EY (%)	76.9 ± 8.3	99.8 ± 10.6	89.4 ± 0.5

Ionotropic gelation method gave high encapsulation yield (more than 75%) for rutin encapsulation with the best yield for LMP-Ca microparticles. During the encapsulation process, the amounts of rutin lost were more important for ALMP-Ca than for PGA-Ca and LMP-Ca microparticles. This could be related to the structure of the gel obtained with ALMP-Ca microparticles. This gel seems to be more flexible allowing a high diffusion of the rutin into the crosslinking solution during the curing time. After drying, the microparticle size of ALMP-Ca was significantly lower than for LMP-Ca and PGA-Ca microparticles. In addition, the ALMP-Ca microparticles present the lowest moisture content. It can be noted that the size and the moisture content are correlated (when the size decreased, the moisture content decreased also). This could be explained by a lower retention of calcium in ALMP-Ca system, leading to decreasing the number of intermolecular cross-links between the negatively charged carboxylate groups of the pectin chains and the positively charged calcium ions. Therefore, the structure ALMP-Ca is highly loose and induces the lower water retention in microparticles and smaller microparticles (Das *et al.*, 2010).

5.2.2.2. Water uptake study and calcium release from microparticles

- **Water uptake study**

Water uptake capacity was, in fact, the first stage for the rutin release from the microparticles. The kinetics of water uptake of polyuronate microparticles was studied in simulated intestinal fluid (Tris buffer, pH = 7.4) (Fig. 5-2). The results showed that water uptake capacity of ALMP-Ca microparticles was higher than for LMP-Ca and PGA-Ca indicating that the network structure (flexibility of the polymer chains) of these three dosage forms is polymer dependent. We can then suppose that the flexibility of the network increases according the following order: PGA-Ca < LMP-Ca << ALMP-Ca. In the case of ALMP-Ca microparticles, the highest water uptake capacity may be due to the ease of creating hydrogen bonding between amide groups with water molecules (Gross *et al.*, 1980). Moreover, the ionization of amino groups rose an osmotic pressure inside the matrix, which facilitated the water uptake. In fact, it can be supposed that the osmotic pressure caused a relaxation of the polymeric network, followed by water absorption. The matrix swelling took place until the osmotic pressure equilibrated the forces of cross-linking bonds that maintain the structure of the polymer network stable (Jug *et al.*, 2012). Sriamornsak and Kennedy (Sriamornsak and Kennedy, 2008) have investigated the swelling and the diffusion of theophylline through Ca^{2+}- pectin films, and they have shown a high capacity of water uptake of ALMP-Ca in

comparison with LMP-Ca, in agreement with our results. They have attributed this to a lower number of calcium cross-links.

The presence of methoxy groups in the polyuronate backbone increases the water uptake capacity (Thakur *et al.*, 1997), thus the capacity of water uptake of LMP-Ca microparticles was slightly higher than PGA-Ca microparticles. Also, Iijima *et al.* (Iijima *et al.*, 2002) have shown that the swelling ratio decreases with decreasing DE and/or DA.

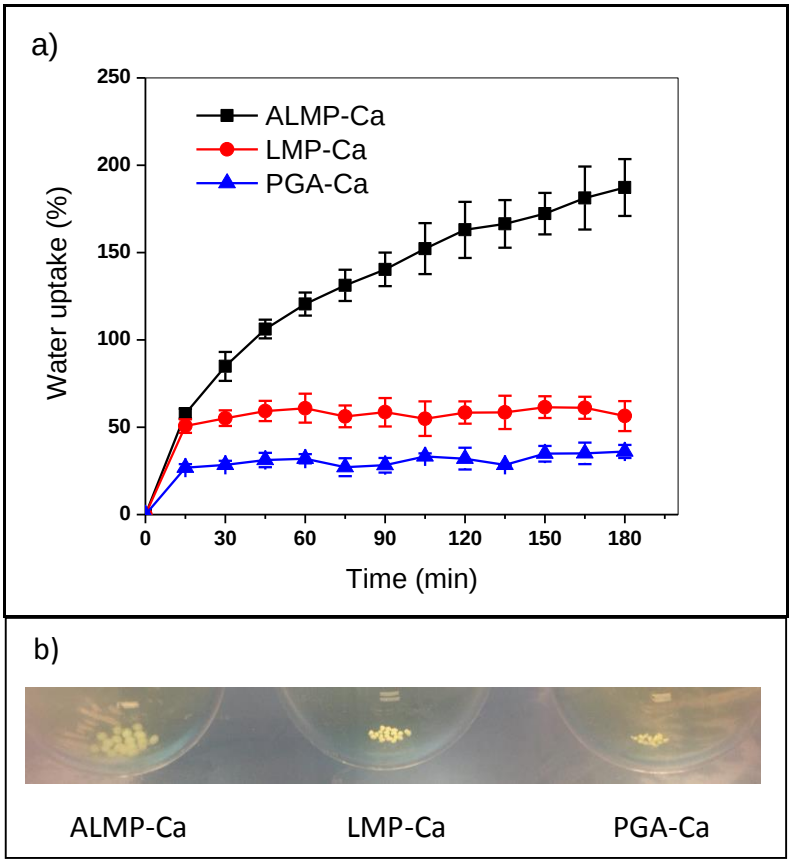

Fig. 5-2. (a) Kinetics of water uptake of polyuronate microparticles in simulated intestinal fluid (pH = 7.4) ; (b) Photos of the microparticles at the end of the experiment

The photos of the three types of microparticles at 180 min showed that the percentage of water uptake was correlated to the swelling of microparticles: an increase in size for ALMP-Ca microparticles, whereas no significant change in size for LMP-Ca and PGA-Ca microparticles.

During the water uptake measurements, calcium release from these three types of microparticles was also measured (Fig. 5-3). For the three types of microparticles, calcium release was faster for the first 10 min due to the release of the calcium non-bound (free) present on the surface of the microparticles. Then the release rate of calcium was slower. The

final concentration of calcium released was higher for ALMP-Ca than for LMP-Ca and PGA-Ca. It was noted that the microparticles after 180 min in the simulated intestinal fluid were not disaggregated indicating that there was still a significant amount of calcium in the microparticles to maintain the structure. The high amount of calcium released from ALMP-Ca microparticles can be explained by the partial loss of the structure when this matrix absorbed water by forming hydrogen bonds with water due to amide groups (Capel *et al.*, 2006). Indeed, Löfgren *et al.* have shown that the storage moduli of ALMP gels were considerably low at pH = 7, which might be a consequence of increased electrostatic repulsions between the pectin chains (Löfgren *et al.*, 2006). This may favor the release of Ca^{2+} ions.

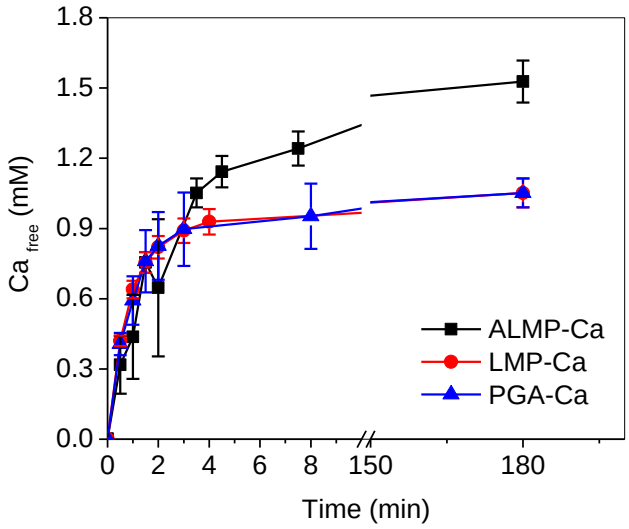

Fig. 5-3. Calcium release from the three types of polyuronate microparticles in simulated intestinal fluid (pH = 7.4)

5.2.2.3. Dissolution studies in simulated intestinal fluid

Rutin release of three kinds of microparticles (ALMP-Ca, LMP-Ca, and PGA-Ca) was assessed *in vitro* in a simulated intestinal fluid (Tris buffer, pH = 7.4). The dissolution profiles were presented in Fig. 5-4. The type of microparticle strongly affects rutin release profiles. Rutin was released from ALMP-Ca microparticles faster than from LMP-Ca and PGA-Ca microparticles. Close to 80% of rutin was released after 300 min for ALMP-Ca microparticles, whereas there were only 23% and 20% for LMP-Ca and PGA-Ca microparticles at the same time, respectively.

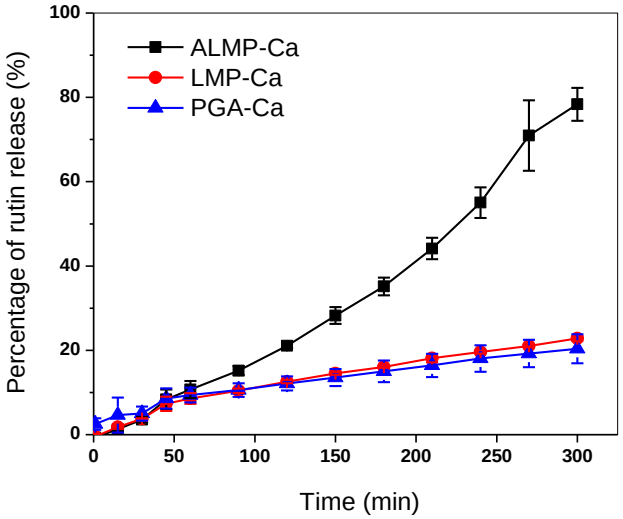

Fig. 5-4. Dissolution profiles of polyuronate microparticles in simulated intestinal fluid (pH = 7.4)

Rutin release from ALMP-Ca microparticles occurred by hydration, swelling and erosion of the ALMP matrix. This could be related to the water uptake capacity of ALMP microparticles, which was also the highest in comparison with other microparticles. With increasing the water uptake, the mobility of the polymer chains increased and so the subsequent rutin diffusion through the matrix into the dissolution medium. Several authors (Assifaoui *et al.*, 2011; Jantrawut *et al.*, 2013) have previously studied the rutin release in LMP-Ca microparticles using the same simulated intestinal fluid and found a similar release profile for LMP-Ca beads in this study. Furthermore, few studies compared the release with different kinds of pectin. Burapapadh *et al.* (Burapapadh *et al.*, 2012) have observed a slower itraconazole release for LMP nanoparticles in comparison to ALMP nanoparticles. This behavior might be explained by the strength of pectin matrix with a rupture of pectin matrix in ALMP-based nanoparticles, leading to immediate release of itraconazole. Recent studies showed that the release of hydrophobic aroma compounds (alcohols, ketones, aldehydes, and esters) from ALMP-Ca gels was found to be higher than from LMP-Ca gels (Kim *et al.*, 2016). These results are opposite to their previous results (Kim *et al.*, 2014), where they found a low release of hydrophilic aroma compounds (benzaldehyde, diacetyl) from ALMP-Ca gels. They suggested that amidation of pectin reduces the release of hydrophilic aroma compounds, possibly as a result of the greater degree of hydrogen bonds formed by the amide groups in pectin and molecules of hydrophilic aroma compound. This discrepancy could be explained by the difference in gel preparation, particularly to the concentration of sucrose and calcium

used, the properties of aroma compounds and type of pectin used. Furthermore, when the calcium concentration was high, the aroma release was found to be affected by the hydrogen bonding that occurs between the aroma compounds and amide groups. The release of rutin (hydrophobic flavonoid) from ALMP-Ca microparticles was higher than from LMP-Ca microparticles and PGA-Ca microparticles, in agreement with the result of Kim *et al.* (Kim *et al.*, 2016). Also, Tho *et al.* (Tho *et al.*, 2005) explained that cross-linking between ALMP and calcium could take place on the surface preventing the total dissolution of particles, but the interaction was weak between aroma and pectin in the inner part of particles so aroma can easily diffuse when particles were swelled.

To propose a mechanism of drug release, *in vitro* data were fitted by Korsmeyer–Peppas model (Eq. 5-5) (Ritger and Peppas, 1987). All the microparticles showed good linearity (R^2 = 0.966 - 0.991) and the fit parameters are presented in Table 5-2.

Table 5-2. Parameters obtained from the fit of rutin dissolution curves using the Korsmeyer– Peppas model

Types of microparticles	Parameters of Korsmeyer-Peppas equation		
	R^2	n	k
ALMP-Ca	0.991	1.305	0.044
LMP-Ca	0.966	0.787	0.279
PGA-Ca	0.973	0.510	1.085

For LMP-Ca and PGA-Ca microparticles, the release exponent (*n*) values were 0.787 and 0.510 respectively, indicating that release mechanism was anomalous ($0.43 < n < 0.85$) (Siepmann and Siepmann, 2008) suggesting that two phenomena were involved in the release: drug diffusion and swelling of the polymer. For ALMP-Ca microparticles, *n* value was above 1 indicating that rutin release followed the super case II transport mechanism controlled by swelling and relaxation of matrix. This could be attributed due to polymer dissolution and enlargement or relaxation of polymeric chain (Nayak *et al.*, 2014). The super case II transport mechanism was also found for curcumin release in ALMP-Ca beads (Nguyen *et al.*, 2014). To better understand the drug release mechanism and the part of diffusion and polymer swelling/ erosion in drug dissolution from the polyuronate microparticles, another approach can be used considering that the two phenomena controlling drug release are additive (Peppas and Sahlin, 1989). So Eq. 5-6 could be used.

$$\frac{M_t}{M_\infty} = k_1 t^m + k_2 t^{2m} \qquad \textit{Eq. 5-6}$$

In Eq. 5-6, the first term is the diffusion contribution, the second term corresponds to the polymer relaxational contribution. The coefficient *m* is the diffusion exponent, k_1 is the diffusion constant and k_2 is the relaxation (erosion) constant. The fitted parameters are presented in Table 5-3.

Table 5-3. Part of diffusion and swelling in release mechanism

Types of microparticles	Parameters of Peppas & Sahlin equation		
	k_1	k_2	m
ALMP-Ca	0.10	0.00	1.04
LMP-Ca	0.50	0.00	0.67
PGA-Ca	1.27	0.07	0.41

By comparison of Eqs. 5-5 and 5-6, it was concluded that *m* is different to *n* when the relaxational mechanism is significant (Peppas and Sahlin, 1989). Here, *n* and *m* could be considered as similar value; k_1 values were always higher than k_2 values so the rutin release mechanism was predominantly governed by rutin diffusion through polyuronate matrix and the matrix structure controls drug release. The higher was the water uptake, the higher was rutin release due to facilitated diffusion.

5.2.3. Gel properties

5.2.3.1. Calcium binding affinity

In semi-diluted regime, the binding calcium to the three types of polyuronates was presented in Fig. 5-5a (bound, B = $[Ca]_{fixed}/[Gal]$) as a function of total added calcium concentration) and described by the Scatchard plots ($(B/[Ca]_{free})$ was expressed versus B) in Fig. 5-5b. It can be noted that for these measurements, the concentrations of the three polyuronates was low in order to avoid the gelation. Indeed, the concentrations of PGA, LMP and ALMP are 1.0 g L^{-1}, 1.5 g L^{-1} and 2.0 g L^{-1}, respectively. At these concentrations, the amount of GalA for each polyuronate was similar (equal to 5.4 mM, 5.97 mM and 6.02 mM, respectively).

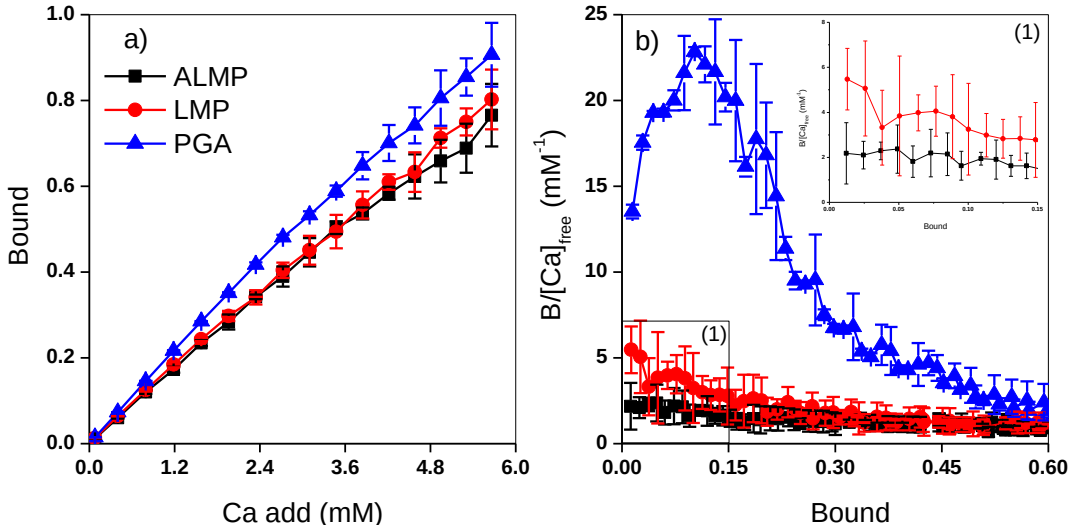

Fig. 5-5. (a) Influence of the polyuronates on the calcium binding at pH = 5.5 and at 25 °C; (b) Analysis of the calcium binding curves by the Scatchard plot with the inset in (b) corresponding to the zoom of ALMP and LMP for low bound values.

Fig. 5-5a revealed that the affinity of PGA chains for calcium ions was slightly higher than with ALMP and LMP. It is well known that four free galacturonate units (Gal) bind one Ca^{2+} ion (Grant *et al.*, 1973). Thus, the presence of functional groups such as methyl esters and amide groups and their random distribution could decrease the amount of Ca bound to LMP and ALMP. For PGA, known as homogalacturonan, the network of PGA-Ca was more homogenous than others and so the amount of calcium bound was higher. Moreover, Racape *et al.* (Racape *et al.*, 1989) indicated that ALMP needed less calcium than LMP for gel formation.

Scatchard plots were presented in Fig. 5-5b for three types of polyuronates. The convex shape of the data for PGA indicated a positive cooperative binding during the first phase of binding as it has been described previously (Smidsrød, 1974; Xin *et al.*, 2015). This convex region of the Scatchard plot also displayed two steps which correlated well with those reported by Huynh *et al.* (Huynh *et al.*, 2016) for the mechanism of the binding of PGA and Ca^{2+} ions: i) monocomplexation and formation of point-like cross-links between polyGal chains at R < 0.1 and ii) dimerization at higher R. Whereas, for LMP and ALMP, this phenomenon was not so clearly observed. However, these pectins had more than one group of binding sites because curved lines were obtained in the Scatchard plot rather than a straight line (Fig. 5-5b) (Rosenthal, 1967) and electrostatic bonding was combined with others bonds such as hydrogen bonds and Van der Walls bonds.

- *5.2.3.2. Rheological experiments rheological characterizations*

In the case of gels (high concentration of polyuronate), the storage modulus (G') and the loss modulus (G'') were determined at fixed stress and angular frequency (50 Pa and 9 rad s^{-1}) for three types of gels: ALMP-Ca, LMP-Ca, and PGA-Ca. The viscoelastic properties were presented in Fig. 5-6.

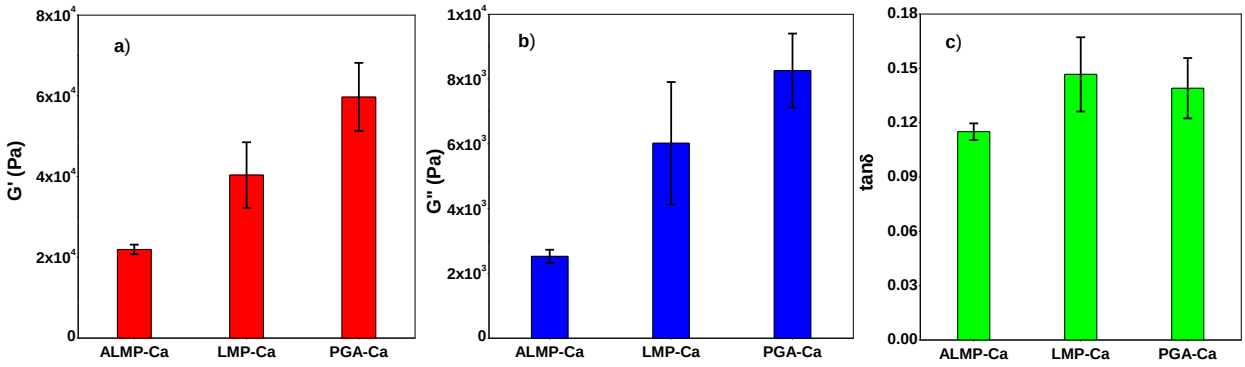

Fig. 5-6. Effect of type of polyuronate gels on (a) storage modulus (G'), (b) loss modulus (G'') and (c) tanδ of gels

After a certain time of gelation (24 h), the thickness of the gels obtained were equal to 6.8 ± 0.4, 7.1 ± 0.1, 6.3 ± 0.3, for PGA-Ca, LMP-Ca and ALMP-Ca, respectively. It can be noted that the thickness of ALMP-Ca gel was lower than the two others gels. For ALMP-Ca microparticles, the particle size was also lowest as well as the moisture content and this could be linked to the gel thickness (Table 5-1). Fig. 5-6 showed that the viscoelastic properties (G' and G'') increased in the following order: ALMP-Ca gel < LMP-Ca gel < PGA-Ca gel. For the tanδ, a slight decrease was observed for ALMP-Ca gel. The low G' and G'' observed for ALMP-Ca gel may indicate that the network of the gel is less rigid and more flexible. According to Braccini and Pérez, the gel strength of pectin was influenced by hydrogen bonds as well as Ca^{2+}-coordinated bridges (Braccini and Pérez, 2001). These junction zones also involved water molecules, which corresponded to non-freezable bound water (Ping *et al.*, 2001) and Ca-polyuronate gels were known as hygroscopic gels. However, the amount of water-binding strongly depended on of the type of polyuronate.

Although the concentration of galacturonic acid was similar for three types of polyuronates (PGA - 108 mM; LMP - 119 mM; ALMP - 120 mM), we can then suggest that the difference observed on the rheological properties are due to the distribution of galacturonate residues. Ngouémazong *et al.* (Ngouémazong *et al.*, 2012) have attributed the increase of G' not only to an increase in the number of junction zones per pectin chain but also to an increase

in the size of junction zones and the number of dimerised chains occurring in the gels. Table 5-1 showed that the PGA-Ca microparticles size was highest as well as their moisture content after drying, and this may be due the high gel thickness observed. Moreover, a strong gel or a high storage modulus (G') for PGA-Ca gel (Fig. 5-6a) depended on the large non-methoxylated-GalA blocks on the PGA chains, and formation of dimers with Ca^{2+} was favored (Fraeye *et al.*, 2009; Ngouémazong *et al.*, 2012). Whereas the junction zones were limited for ALMP-Ca gel by the discontinuous distribution of the carboxylate groups as a result of the presence of methoxy and amide groups, decreasing the storage modulus (G') and loss modulus (G") and the subsequent gel strength (Fig. 5-6a, b). For LMP-Ca gel, the behavior was intermediate due to the presence of only methoxy groups. A higher DE in LMP induced a low number of junction zones with Ca^{2+} and gel texture was loose, manifested by decreasing G'. Hence, the water absorption capacity was improved (Sriamornsak and Kennedy, 2008). Moreover, the lowest storage modulus for ALMP-Ca gel could be explained by the fact that ALMP formed less crosslinking (Gal-Ca-Gal), being responsible for the stiffness of the gel (Lootens *et al.*, 2003; Racape *et al.*, 1989). Furthermore, Löfgren *et al.* have shown that the storage modulus (G') of the ALMP-Ca gel had large variations when pH was changed: the highest storage modulus was obtained at pH = 3 due to the amide groups strengthened the gel network by hydrogen bonds (Löfgren *et al.*, 2006). Whereas, at pH = 5 and pH = 7, the storage modulus was considerably lower, which might be a consequence of increased electrostatic repulsions between the pectin chains, preventing hydrogen bonds from being formed (Capel *et al.*, 2006).

The storage modulus (G') and the loss modulus (G'') were about 2 or 3 times lower for ALMP-Ca gel than for LMP-Ca and PGA-Ca gels, respectively (Fig. 5-6a, b). These lowest G' and G'' values might be due to the random distribution of COO^- groups along the ALMP chains in comparison with LMP and PGA. Whereas, the lowest tanδ of ALMP-Ca gel (Fig. 5-6c) indicated that the flexibility of the gel network was higher than others gels. Due to this flexibility, the gel network structure could be more sensitive to water uptake. Therefore, the released calcium from ALMP-Ca microparticles was faster from LMP-Ca and PGA-Ca microparticles (Fig. 5-3) and destabilization of gel network structure also increased the rutin release (Fig. 5-4).

5.2.4. Conclusion

Microparticles containing rutin were produced using three type of pectins (PGA, LMP, and ALMP) cross-linked by calcium ions. It was shown that rutin release from ALMP-Ca microparticles was higher than from the two others microparticles (LMP-Ca and PGA-Ca). This

higher rutin release was related to the structure, and the properties of the network formed before drying. Thus, the viscoelastic properties of the ALMP-Ca gel showed the lowest storage modulus (G'), loss modulus (G") and tanδ indicating a high flexibility of this gel network in comparison with LMP-Ca and PGA-Ca. This high flexibility of the gel was responsible of the high rutin lost observed for ALMP-Ca beads. In addition, the ALMP-Ca microparticles were more sensitive to water uptake which enhanced calcium and rutin release. We can suppose that the mobility of the polymer chain in this type of microparticle was maintained. It can be noted that both the amount of galacturonate (Gal) and the viscosity of the three pectins were similar. Therefore, the differences in the drug release and the rheological properties observed for ALMP-Ca microparticles and gels in comparison with LMP-Ca and PGA-Ca may be due to the random distribution of Gal rather than the amount of Gal units. Moreover, in the presence of electrostatic interactions between carboxylate and amide groups may also explain the flexibility observed in this type of microparticle.

For LMP-Ca and PGA-Ca microparticles, the water uptake, as well as the calcium and rutin release, were similar and in a lower extent. It could be related to an increase in G' and G'', indicating a strengthened gel with a higher affinity for calcium, especially for PGA.

Principaux résultats et conclusions

Lors du contact entre la solution de polyuronate et la solution de calcium, des billes sont formées instantanément puis elles deviennent des microparticules lorsqu'elles sont séchées et qu'elles perdent une grande partie de leur teneur en eau. Quelque soit le polysaccharide utilisé, le taux d'encapsulation est élevé à cause de la faible solubilité de la rutine dans l'eau (> 75%). La pectine ALMP donne les microparticules les plus petites avec la plus faible teneur en eau mais aussi le plus faible rendement d'encapsulation, lié à une perte de rutine au cours du procédé. Cela peut être expliqué par le fait que le gel formé est plus lâche et qu'il permet la diffusion de la molécule encapsulée. Peu de différences sont notées entre les microparticules obtenues à partir du PGA et de la pectine LMP.

De nouveau, les microparticules de pectine ALMP présentent une meilleure capacité à capter l'eau (elles gonflent donc plus en contact avec une solution aqueuse) et elles relarguent plus facilement le calcium mais aussi la rutine encapsulée. La pectine amidée est connue pour la mise en place de liaisons hydrogènes entre les fonctions amides et carboxylates, changeant ainsi les propriétés du gel formé. La pectine LMP montre une capacité à fixer l'eau bien plus faible mais cependant supérieure à celle du PGA, à cause des groupements méthoxy. Les libérations de calcium et de rutine restent cependant faibles et les microparticules ne gonflent pas dans le milieu intestinal simulé. Ce comportement à la libération très spécifique de la pectine ALMP a déjà été décrit par plusieurs auteurs, notamment lors de l'encapsulation d'arômes.

Afin de mieux comprendre la libération de la rutine à partir de ces trois types de microparticules, les cinétiques ont été modélisées par le modèle de Korsmeyer–Peppas montrant des mécanismes différents pour les microparticules de pectine LMP et PGA par rapport à celles de pectine ALMP. La libération est souvent décrite comme la conséquence de la diffusion de la molécule mais aussi de l'érosion de la matrice de polymère et nous avons essayé de quantifier la part de chaque phénomène. Nous avons ainsi démontré que la libération est essentiellement contrôlée par la diffusion de la rutine au sein de la matrice. Les propriétés de la matrice, et notamment du gel formé, au cours de la fabrication mais aussi au cours de la réhydratation sont donc fondamentales.

Il est ainsi indispensable d'évaluer les propriétés des gels formés par les trois polyuronates avec le calcium. Tout d'abord, nous avons étudié la capacité des

trois polyuronates à fixer le calcium. Le PGA présente une affinité bien plus forte avec des liaisons coopératives. Malgré le DE et DA différents dans le cas de LMP et ALMP, ces derniers présentent une teneur similaire en unité Gal (du fait des différentes concentrations utilisées 1,5 g L^{-1} et 2,0 g L^{-1}). La seule différence entre ces deux polymères est la distribution aléatoire des groupements méthylés et amidés au sein de la chaîne polygalacturonique. Ceci explique le comportement similaire vis-à-vis de la fixation des ions calcium (Fig. 5-5). Il n'y a alors pas que des liaisons électrostatiques qui interviennent dans la formation du gel mais aussi des liaisons hydrogènes et des forces de Van der Waals. Ces liaisons donnent aussi les gels les moins épais comme les billes puis les microparticules les plus petites.

Lors de l'étude du comportement rhéologique, les modules élastiques (G') et visqueux (G'') sont plus faibles pour la pectine ALMP et évoluent selon l'ordre suivant : ALMP-Ca gel < LMP-Ca gel < PGA-Ca gel. Ces faibles valeurs confirment que le réseau formé par le gel de pectine ALMP est plus lâche et plus flexible que pour la pectine LMP ou le PGA. En effet, il ne peut pas y avoir un mécanisme classique de gélification selon le modèle « boite à œuf » car les groupements greffés sur la pectine diminuent les points de jonction. Grâce à cette flexibilité plus importante du réseau des gels ALMP, il est plus sensible à la captation de l'eau. La diffusion du calcium est alors facilitée (plus rapide et plus forte), fragilisant encore la structure et provoquant une libération de rutine bien plus importante que celle obtenue avec des microparticules de pectine LMP ou de PGA.

Nous pouvons donc conclure que les propriétés des microparticules à base de trois polyuronates différents (PGA, LMP et ALMP) pour encapsuler la rutine sont dépendantes de la structure des gels formés au cours de la fabrication et notamment de la force du réseau mis en place au sein de la matrice. Ainsi la taille, la teneur en eau, la capacité à fixer l'eau, la libération de calcium et de rutine sont autant de paramètres qui vont varier en fonction de la flexibilité du gel. Les microparticules à base de pectine ALMP sont de plus petite taille avec une plus faible teneur en eau mais la matrice formée est plus sensible à la captation d'eau, favorisant la diffusion du calcium puis de la rutine. La structure de la matrice est ainsi liée à la structure des gels. En effet la pectine ALMP donne les gels les plus flexibles avec les plus faibles modules viscoélastiques et elle a aussi la plus faible affinité pour le calcium, tout ceci peut être expliqué par sa structure car elle comprend des fonctions méthylées et amidées qui perturbent de façon aléatoire la chaîne polygalacturonate et donc l'établissement de moins des liaisons avec le calcium. Pour les microparticules de pectine

LMP et de PGA, les propriétés du gel sont plus fortes induisant ainsi une meilleure résistance à la captation de l'eau, une plus faible diffusion du calcium et donc une plus faible libération de la rutine encapsulée.

Ce travail met ainsi bien en avant l'importance de bien connaître les propriétés et les mécanismes de gélification des polyuronates utilisés afin de maîtriser les propriétés de protection et de relargage d'une molécule active encapsulée dans ces matrices.

CONCLUSIONS & PERSPECTIVES

Conclusions

Les pectines sont des polyosides anioniques, constituées d'association d'acides galacturoniques plus ou moins estérifiés et/ou amidés. En présence de cations divalents, ces pectines ont tendance à former des gels. Les propriétés physicochimiques de ces gels dépendent fortement de la nature de la pectine utilisée mais aussi de la nature et de la concentration en cations divalents. Le séchage de ces gels conduit à obtenir soit des films soit des microparticules selon le mode de gélification ionique (Fig. 1-1). Ces formes peuvent contenir des molécules d'intérêt. Grâce aux enzymes présentes dans le côlon qui sont spécifiques de la pectine, ces formes peuvent alors induire une libération au niveau colonique conduisant ainsi à une libération ciblée. Ceci rend l'utilisation de la pectine comme agent d'encapsulation très prometteuse.

Ainsi, nous avons préparé des microparticules contenant de la rutine (un antioxydant) en utilisant une pectine faiblement méthylée (LMP), une pectine méthylée et amidée (ALMP) et l'acide polygalacturonique (PGA). La gélification a été réalisée en utilisant des ions calcium selon le protocole décrit (Fig. 1-1a). Nous avons ensuite étudié le profil de libération de la rutine en fonction de ces trois polymères dont les propriétés (masse moléculaire, présence des groupements fonctionnels (ester et amide) et de leur distribution aléatoire sur la chaîne de la pectine) changent. Les résultats ont montré que la libération de la rutine à partir des microparticules ALMP-Ca est plus élevée que les deux autres microparticules (LMP-Ca et PGA-Ca). Pour ces microparticules (ALMP-Ca), nous avons observé une capacité à absorber l'eau et une libération des ions calcium très élevées. De plus, le module élastique (G') et visqueux (G'') de ces formes (ALMP-Ca) avant séchage (état gel) sont faibles par rapport aux gels LMP-Ca et PGA-Ca. Nous avons donc supposé que la structure du réseau formé pour ALMP-Ca est plus flexible : la mobilité des chaînes est plus importante. L'étude de la fixation des ions calcium par ces trois polyosides a montré que les pectines LMP et ALMP ont un comportement similaire et que le PGA fixe une quantité plus importante d'ions calcium. Il est à noter que les concentrations en LMP, ALMP et PGA ont été choisies afin d'obtenir à la fois une concentration équivalente en acide galacturonique (GalA) (5,4 mM, 5,97 mM et 6,02 mM pour PGA, LMP et ALMP, respectivement) et une viscosité similaire. Nous pouvons en conclure que la distribution aléatoire des groupements ester et/ou amide gêne la formation des dimères. Dans le cas de la pectine ALMP, il est fort probable que les liaisons hydrogènes entre les fonctions amines et les fonctions carboxylates soient responsables de la flexibilité du réseau

formé. Ces observations nous ont permis de proposer un schéma qui illustre la structure de ces trois gels pour ALMP-Ca, LMP-Ca et PGA-Ca (Fig. 6-1). Dans le cas de la pectine ALMP, le réseau serait formé essentiellement par un nombre important de réticulations ponctuelles (Gal-Ca-Gal) stabilisées par des liaisons électrostatiques. Pour la pectine LMP, le réseau serait dû aussi à la formation de réticulations ponctuelles mais aussi à la formation de quelques dimères. Enfin, dans le cas du PGA, le réseau serait formé par des dimères et multimères. Cette structure dense dans le cas du PGA-Ca serait responsable du faible gonflement et du faible taux de libération de la rutine.

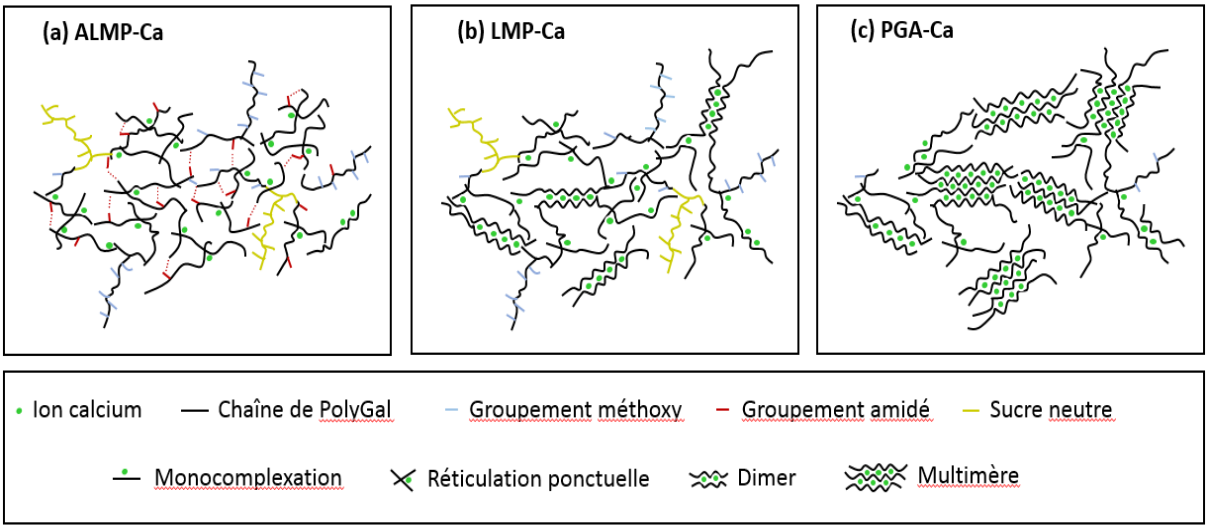

Fig. 6-1. Illustration de la structure des trois gels : ALMP-Ca (a), LMP-Ca (b), PGA-Ca (c)

Nous nous sommes ensuite focalisés sur les gels formés par l'acide polygalacturonique (PGA) en association avec 4 différents divalents cations (Ca^{2+}, Zn^{2+}, Ba^{2+} et Mg^{2+}). Deux aspects ont été abordés : la structure des gels obtenus avant séchage et la cinétique de gélification. Ainsi, nous avons remarqué que des gels peuvent être obtenus pour les trois cations divalents (Ca^{2+}, Zn^{2+}, Ba^{2+}) même à des faibles concentrations en cation divalent à condition que le temps de gélification soit suffisamment élevé ($t \geq 17h$). Pour le Mg^{2+}, les gels n'ont pas pu être obtenus en accord avec la littérature (Donati *et al.*, 2009; Selvarengan *et al.*, 2010). Nous avons établi un diagramme d'état (épaisseur du gel en fonction du temps de gélification (t_{gel}) et de la concentration initiale en cation divalent). La concentration en PGA a été fixée à 10 g L^{-1}. Ce diagramme a montré la présence de trois zones quelle que soit la nature du cations divalents (Ca^{2+}, Zn^{2+}, Ba^{2+}) (Fig. 4-3) : I) une zone où la gélification ne peut pas se produire, II) une zone où la gélification dépend fortement de la concentration initiale du cation et III) une zone où la formation du gel est achevée. Le suivi des propriétés viscoélastiques des gels en fonction du temps de gélification (t_{gel}) a montré que la rigidité augmente puis se stabilise à un

t_{gel} = 150 min. Cette tendance a été observée pour les trois gels formés en présence des trois cations divalents (Ca^{2+}, Zn^{2+}, Ba^{2+}). Lors de cette augmentation de la rigidité, nous avons remarqué que la densité des gels restait constante. En effet, l'augmentation de l'épaisseur du gel est compensée par l'augmentation du nombre de chaînes réticulées du polymère. Nous avons ainsi supposé que la diffusion des cations provoque la formation de plusieurs réticulations ponctuelles. Toutefois, il est difficile de proposer un mécanisme de gélification robuste étant donné les fortes concentrations en PGA (c = 10 g L^{-1}) et en cations divalents (250 mM et 750 mM). L'étude de la cinétique de diffusion des cations divalent a été réalisée en suivant la migration du front de gel dans une cellule placée à l'intérieur d'un Turbiscan. Nous avons observé que le coefficient de diffusion du front de gel (D_{gel}) augmente avec l'augmentation de la concentration de cations (50 mM, 250 mM et 750 mM) et dépend de la nature du cation. Quelle que soit la concentration initiale en cation divalent, ce coefficient de diffusion augmente dans l'ordre : $Zn^{2+} < Ca^{2+} < Ba^{2+}$. Il semblera que la diffusion des ions zinc est plus faible que celle des ions calcium et baryum.

Afin de comprendre l'impact de ces cations divalents sur les mécanismes d'association et sur la structure mise en place, nous nous sommes placés dans des conditions très diluées (c < c*) et des concentrations plus faibles en cations divalents (24 mM dans Partie 1 - Chapitre 3 et 13,5 mM dans Partie 2 - Chapitre 3). L'étude de la viscosité, de la turbidité et de la diffusion des neutrons aux petits angles a montré que le réseau du mélange Ca-LMP est plus homogène et plus visqueux que celui du mélange Zn-LMP (Fig. 7, Partie 1, Chapitre 3). Pour les ions magnésium, nous avons montré que la turbidité et la viscosité restent constantes et proches de celles du polygalacturonate (polyGal) seul, indiquant que ce cation ne forme pas de gel macroscopique. Dans le cas des ions baryum, nous avons observé une augmentation à la fois de la turbidité et de la viscosité avec l'ajout des ions Ba^{2+}. De plus, nous avons remarqué que 75% des ions ajoutés sont piégés dans le réseau du polyGal. L'étude de l'énergie d'association par ITC a montré que pour les trois cations (Ca^{2+}, Zn^{2+} et Ba^{2+}), deux processus ont été observés. Nous avons ainsi attribué le premier processus (endothermique) à la formation de monocomplexes (cation - Gal) et de zones de réticulations et le second processus (exothermique) et pourrait être dû à une réorganisation des chaînes (formation des dimères) (Fig. 3-2). Nous avons également identifié un ratio molaire (R^* = [Cation]/[Gal]) qui correspondrait au passage du premier au second processus. Ce ratio critique noté R^* dépendrait de la nature du cation : il est faible pour l'association Ca-polyGal (R^* = 0,01) et élevé pour les associations Ba-polyGal et Zn-polyGal (R^* = 0,3).

Des études de simulations moléculaires dynamiques ont été par la suite réalisées sur les différents systèmes (Fig. 3-1) afin de comprendre l'origine de ces processus et la différence de structure. Il s'avère que les interactions entre les molécules d'eau de la première sphère de coordination et le cation augmentent selon l'ordre suivant : $Mg^{2+} > Zn^{2+} > Ca^{2+} > Ba^{2+}$. A partir de ce résultat, il est évident que les ions magnésium maintiennent leur sphère d'hydratation, ce qui expliquerait la difficulté de former des gels pour ce cation. L'étude des associations cation - Gal, a montré que le Zn^{2+} se fixe préférentiellement à un seul oxygène du groupement carboxylate (mode monodentate) ; alors que le calcium et le baryum se fixent sur les deux oxygènes du groupement carboxylate (mode bidentate). Ceci pourrait expliquer l'ordre de coefficient de diffusion du front de gel observée ($Zn^{2+} < Ca^{2+} < Ba^{2+}$). Au cours de notre étude, nous avons également discuté le modèle « boîte à œuf » proposé par Grant *et al.* (Grant *et al.*, 1973). En effet, selon nos simulations numériques, il semblerait que l'association de 4 cations Zn^{2+} avec 2 chaînes composées de 8 unités Gal (octamère) est similaire à une structure de type « boîte à œuf » (*egg-box model*). Ce modèle n'est pas applicable à la structure obtenue par l'association des cations Ca^{2+} et Ba^{2+} avec les 2 octamères. Pour les ions magnésium, nous avons observé que Mg^{2+} ne perd pas ses 6 molécules d'eau de la sphère d'hydratation. L'association se fait donc par un partage d'une molécule d'eau de la sphère avec les carboxylates du polyGal (Figure 6, Partie 2, Chapitre 3).

Nous nous sommes également intéressés au comportement en solution des chaînes de la pectine (LMP) et de l'acide polygalacturonique (PGA) en fonction de la concentration en cation monovalent (NaCl). Ainsi, nous avons suivi l'évolution de la viscosité intrinsèque et la taille des chaînes à 4 concentrations en NaCl (0 mM - 1 mM - 10 mM - 100 mM). Nous avons remarqué que la viscosité intrinsèque et le rayon hydrodynamique diminuent lorsque la concentration en NaCl augmente. La structure passe d'un état étendu à un état plus compact. Nous avons noté que les chaînes de pectines étaient plus sensibles aux changements de la force ionique que les chaînes du PGA. De plus, l'analyse des courbes de viscosité a montré que les chaînes de pectines étaient plus rigides que celles du PGA. Nous avons également montré que l'affinité vis-à-vis des ions calcium diminue lorsque la concentration en NaCl augmente. Cette diminution a été clairement observée dans le cas des interactions entre les ions calcium et le PGA. Dans le cas des interactions Ca-LMP, la constante d'affinité est plus faible et reste constante quelle que soit la concentration en NaCl. Ceci pourrait être dû à la forte rigidité des chaînes mais aussi aux faibles nombres d'unités galacturonate (Gal) dans la pectine (30% des unités Gal sont estérifiées).

En conclusion, nous avons montré que les propriétés des matrices d'encapsulation dépendent de la nature du polymère et du cation divalent utilisés. Ainsi, la libération de substances actives encapsulée est liée à la structure et aux propriétés du réseau formé avant séchage (gel). Pour expliquer les changements de structure observés à l'échelle macroscopique, nous avons étudié les association cation-polyoside en régime dilué. Ce qui nous a permis de proposer un mécanisme de gélification.

Perspectives de cette étude

Afin de vérifier la robustesse de notre mécanisme d'association, il serait intéressant d'étudier les interactions entre le PGA et d'autres cations divalents ; en particulier les cations appartenant à la famille des métaux de transition (tels que le Fe^{2+} par exemple).

Dans notre démonstration, nous avons supposé que la structure du gel obtenu est maintenue après l'étape du séchage. Il serait intéressant de vérifier cette hypothèse et d'étudier différentes méthodes de séchage pour pouvoir moduler la structure et donc le profil de libération de la molécule active.

Par ailleurs, l'application de ces matrices pour des applications en emballages (matériaux bio-sourcés, biodégradables) et l'encapsulation des différents types de substances actives serait également intéressante.

REFERENCES

Abodinar A., Smith A. M. and Morris G. A. A novel method to estimate the stiffness of carbohydrate polyelectrolyte polymers based on the ionic strength dependence of zeta potential. *Carbohydrate Polymers*, **2014**. 112: p. 6-9.

Agulhon P., Robitzer M., David L. and Quignard F. Structural Regime Identification in Ionotropic Alginate Gels: Influence of the Cation Nature and Alginate Structure. *Biomacromolecules*, **2012**. 13(1): p. 215–220.

Agulhon P., Robitzer M., Habas J. P. and Quignard F. Influence of both cation and alginate nature on the rheological behavior of transition metal alginate gels. *Carbohydrate Polymers*, **2014**. 112: p. 525–531.

Ahrabi S. F., Madsen G., Dyrstad K., Sande S. A. and Graffner C. Development of pectin matrix tablets for colonic delivery of model drug ropivacaine. *European Journal of Pharmaceutical Sciences*, **2000**. 10(1): p. 43–52.

Alonso-Mougán M., Meijide F., Jover A., Rodríguez-Núuez E. and Vázquez-Tato J. Rheological behavior of an amide pectin. *Journal of Food Engineering*, **2002**. 55(2): p. 123–129.

Assifaoui A., Chambin O. and Cayot P. Drug release from calcium and zinc pectinate beads: Impact of dissolution medium composition. *Carbohydrate Polymers*, **2011**. 85(2): p. 388–393.

Assifaoui A., Lerbret A., Huynh T. D. U., Neiers F., Chambin O., Loupiac C. and Cousin F. Structural behaviour differences in low methoxy pectin solutions in the presence of divalent cations (Ca2+ and Zn2+): a process driven by the binding mechanism of the cation with the galacturonate unit. *Soft Matter*, **2015**. 11(3): p. 551-560.

Assifaoui A., Loupiac C., Chambin O. and Cayot P. Structure of calcium and zinc pectinate films investigated by FTIR spectroscopy. *Carbohydrate Research*, **2010**. 345(7): p. 929-933.

Axelos M. A. V. Ion complexation of biopolymers: Macromolecular structure and viscoelastic properties of gels. *Makromolekulare Chemie. Macromolecular Symposia*, **1990**. 39(1): p. 323–328.

Axelos M. A. V., Lefebvre J. and Thibault J. F. Conformation of a low methoxyl citrus pectin in aqueous solution. *Food Hydrocolloids*, **1987**. 1(5-6): p. 569-570.

Axelos M. A. V. and Thibault J. F. The Chemistry of Low Methoxyl Pectin Gelation, in The Chemistry and Technology of Pectin, Ed: Reginald H. Walter. *Academic Press*: San Diego, California, **1991**. p. 109-118.

Axelos M. A. V., Thibault J. F. and Lefebvre J. Structure of citrus pectins and viscometric study of their solution properties. *International Journal of Biological Macromolecules*, **1989**. 11(3): p. 186-191.

Axelos M.A.V. and Thibault J.-F. Influence of the substituents of the carboxyl groups and of the rhamnose content on the solution properties and flexibility of pectins. *International Journal of Biological Macromolecules*, **1991**. 13(2): p. 77–82.

Baños F. G. D., Díez Peña A. I., Hernánez Cifre J. G., López Martínez M. C., Ortega A. and García de la Torre J. Influence of ionic strength on the flexibility of alginate studied by size exclusion chromatography. *Carbohydrate Polymers*, **2014**. 102: p. 223–230.

BeMiller J. N. Chapter 1: An Introduction to Pectins: Structure and Properties, in Chemistry and Function of Pectins, Ed: Fishman M. L., andJen J. J. *American Chemical Society, Washington, DC*, **1986**. p. 2–12.

Bordbar A. K., Saboury A. A. and Moosavi-Movahedi A. A. The shapes of Scatchard plots for systems with two sets of binding sites. *Biochemical Education*, **1996**. 24(3): p. 172–175.

Borgogna M., Skjåk-Bræk G., Paoletti S. and Donati I. On the Initial Binding of Alginate by Calcium Ions. The Tilted Egg-Box Hypothesis. *J. Phys. Chem. B*, **2013**. 117(24): p. 7277–7282.

Braccini I. and Pérez S. Molecular Basis of Ca^{2+} -Induced Gelation in Alginates and Pectins: The Egg-Box Model Revisited. *Biomacromolecules* **2001**. 2(4): p. 1089-1096.

Brejnholt S. M. Pectin, in Food stabilisers, thickeners and gelling agents (1st ed.), Ed: I. Alan. *Wiley-Blackwell*, **2010**. p. 237–256.

Bru P., Brunel L., Buron H., Cayré I., Ducarre X., Fraux A., Mengual O., et al. Particle Size and Rapid Stability Analyses of Concentrated Dispersions: Use of Multiple Light Scattering Technique, in Particle Sizing and Characterization, Ed: T. Provder, andJ. Texter. *American Chemical Society (ACS)*: Washington, D.C., **2004**. 881: p. 45-60.

Brunchi C. E., Morariu S. and Bercea M. Intrinsic viscosity and conformational parameters of xanthan in aqueous solutions: Salt addition effect. *Colloids and Surfaces B: Biointerfaces*, **2014**. 122: p. 512–519.

Bulone D., Martorana V., Xiao C. and San Biagio P. L. Role of Sucrose in Pectin Gelation: Static and Dynamic Light Scattering Experiments. *Macromolecules*, **2002**. 35(21): p. 8147–8151.

Burapapadh K., Takeuchi H. and Sriamornsak P. Novel pectin-based nanoparticles prepared from nanoemulsion templates for improving *in vitro* dissolution and *in vivo* absorption of poorly water-soluble drug. *European Journal of Pharmaceutics and Biopharmaceutics*, **2012**. 82(2): p. 250–261.

Caffall K. H. and Mohnen D. The structure, function, and biosynthesis of plant cell wall pectic polysaccharides. *Carbohydrate Research*, **2009**. 344(14): p. 1879–1900.

Calabrò M. L., Tommasini S., Donato P., Stancanelli R., Raneri D., Catania S., Costa C., et al. The rutin/β-cyclodextrin interactions in fully aqueous solution: spectroscopic studies and biological assays. *Journal of Pharmaceutical and Biomedical Analysis*, **2005**. 36(5): p. 1019–1027.

Capel F., Nicolai T., Durand D., Boulenguer P. and Langendorff V. Influence of Chain Length and Polymer Concentration on the Gelation of (Amidated) Low-Methoxyl Pectin Induced by Calcium. *Biomacromolecules*, **2005**. 6(6): p. 2954–2960.

Capel F., Nicolai T., Durand D., Boulenguer P. and Langendorff V. Calcium and acid induced gelation of (amidated) low methoxyl pectin. *Food Hydrocolloids*, **2006**. 20(6): p. 901-907.

Carbinatto F. M., de Castro A. D., Evangelista R. C. and Cury B. S. F. Insights into the swelling process and drug release mechanisms from cross-linked pectin/high amylose starch matrices *Asian Journal of Pharmaceutical Sciences*, **2014**. 9(1): p. 27–34.

Cardoso S. M., Coimbra M. A. and da Silva J. A. L. Temperature dependence of the formation and melting of pectin–Ca^{2+} networks: a rheological study. *Food Hydrocolloids*, **2003**. 17(6): p. 801-807.

Carrington S., Odell J., Fisher L., Mitchell J. and Hartley L. Polyelectrolyte behaviour of dilute xanthan solutions: Salt effects on extensional rheology. *Polymer*, **1996**. 37(13): p. 2871–2875.

Catoire L., Derouet C., Redon A. M., Goldberg R. and Penhoat C. H. An NMR study of the dynamic single-stranded conformation of sodium pectate. *Carbohydrate Research*, **1997**. 300(1): p. 19–29.

Cescutti P. and Rizzo R. Divalent cation interactions with oligogalacturonides. *J. Agric. Food Chem.* , **2001**. 49(7): p. 3262-3267.

Chamberlain E. K. and Rao M. A. Effect of concentration on rheological properties of acid-hydrolyzed amylopectin solutions. *Food Hydrocolloids*, **2000**. 14(2): p. 163–171.

Chambin O., Dupuis G., Champion D., Voilley A. and Pourcelot Y. Colon-specific drug delivery: Influence of solution reticulation properties upon pectin beads performance. *International Journal of Pharmaceutics*, **2006**. 321(1-2): p. 86-93.

Chanliaud E., Saulnier L. and Thibault J. F. Heteroxylans from maize bran in aqueous solution. Part II: Studies of polyelectrolyte behaviour. *Carbohydrate Polymers*, **1997**. 32(3-4): p. 315–320.

Chen J., Liang R. H., Liu W., Luo S. J., Liu C. M., Wu S. S. and Wang Z. J. Extraction of pectin from Premna microphylla turcz leaves and its physicochemical properties. *Carbohydrate Polymers*, **2014**. 102: p. 376–384.

Chotiko A. and Sathivel S. Development of a combined low-methoxyl-pectin and rice-bran-extract delivery system to improve the viability of *Lactobacillus plantarum* under acid and bile conditions. *LWT - Food Science and Technology*, **2016**. 66: p. 420–427.

Cros S., Garnier C., Axelos M. A. V., lmberty A. and Perez S. Solution Conformations of Pectin Polysaccharides: Determination of Chain Characteristics by Small Angle Neutron Scattering, Viscometry, and Molecular Modeling *Biopolymers*, **1999**. 39(3): p. 339-352.

Das S., Ng K. Y. and Ho P. C. Formulation and Optimization of Zinc-Pectinate Beads for the Controlled Delivery of Resveratrol. *AAPS PharmSciTech*, **2010**. 11(2): p. 729-742.

De S. and Robinson D. Polymer relationships during preparation of chitosan–alginate and poly-l-lysine–alginate nanospheres. *Journal of Controlled Release*, **2003**. 89(1): p. 101–112.

Debongnie P., Mestdagh M. and Rinaudo M. An E.P.R. and potentiometric study of the complexation of copper ions by galacturonic acid and galacturonans. *Carbohydrate Research*, **1987**. 170(2): p. 137–149.

Dhalleine C., Assifaoui A., Moulari B., Pellequer Y., Cayot P., Lamprecht A. and Chambin O. Zinc-pectinate beads as an in vivo self-assembling system for pulsatile drug delivery. *International Journal of Pharmaceutics*, **2011**. 414(1-2): p. 28-34.

Donati I., Asaro F. and Paoletti S. Experimental Evidence of Counterion Affinity in Alginates: The Case of Nongelling Ion Mg2+. *J. Phys. Chem. B*, **2009**. 113(39): p. 12877–12886.

Draget K. I., Steinsvåg K., Onsøyen E. and Smidsrød O. Na- and K-alginate; effect on Ca^{2+}-gelation. *Carbohydrate Polymers*, **1998**. 35(1-2): p. 1-6.

Dronnet V. M., Renard C. M. G. C., Axelos M. A. V. and Thibault J. F. Characterisation and selectivity of divalent metal ions binding by citrus and sugar-beet pectins. *Carbohydrate Polymers*, **1996**. 30(4): p. 253–263.

Durand A. Aqueous solutions of amphiphilic polysaccharides: Concentration and temperature effect on viscosity. *European Polymer Journal*, **2007**. 43(5): p. 1744–1753.

Durand D. and Bertrand C. Calcium-induced gelation of low methoxy pectin solutions — thermodynamic and rheological considerations. *International Journal of Biological Macromolecules*, **1990**. 12(1): p. 14-18.

Einstein A. Investigations on the Theory of Bromnian Movement. *Dover: New York*, **1926**. p. 1-18.

El-Nawawi S. A. and Heikal Y. A. Factors affecting the production of low-ester pectin gels. *Carbohydrate Polymers*, **1995**. 26(3): p. 189–193.

Fang Y., Al-Assaf S., Phillips G. O., Nishinari K., Funami K. and Williams P. A. Binding behavior of calcium to polyuronates: Comparison of pectin with alginate. *Carbohydrate Polymers*, **2008**. 72(2): p. 334-341.

Fang Y., Al-Assaf S., Phillips G. O., Nishinari K., Funami K., Williams P. A. and Li L. Multiple Steps and Critical Behaviors of the Binding of Calcium to Alginate. *J Phys Chem B.*, **2007**. 111(10): p. 2456-2462.

Fang Y., Al-Assaf S., Phillips G. O., Nishinari K., Funami T., Williams P. A. and Li L. Multiple Steps and Critical Behaviors of the Binding of Calcium to Alginate. *J Phys Chem B.*, **2007**. 111(10): p. 2456-2462.

Fishman M. L., Chau H. K., Kolpak F. and Brady J. Solvent Effects on the Molecular Properties of Pectins. *J. Agric. Food Chem.*, **2001**. 49(9): p. 4494–4501.

Fishman M. L., Gillespie D. T., Sondey S. M. and Barford R. A. Characterization of pectins by size exclusion chromatography in conjunction with viscosity detection. *J. Agric. Food Chem.*, **1989**. 37(3): p. 584–591.

Fishman M. L., Gillespie D. T., Sondney S. M. and El-Atawy Y. S. Intrinsic viscosity and molecular weight of pectin components. *Carbohydrate Research*, **1991**. 215(1): p. 91-104.

Fraeye I., Colle I., Vandevenne E., Duvetter T., Van Buggenhout S., Moldenaers P., Van Loey A., et al. Influence of pectin structure on texture of pectin–calcium gels. *Innovative Food Science & Emerging Technologies*, **2010**. 11(2): p. 401-409.

Fraeye I., Doungla E., Duvetter T., Moldenaers P., Van Loey A. and Hendrickx M. Influence of intrinsic and extrinsic factors on rheology of pectin–calcium gels. *Food Hydrocolloids*, **2009**. 23(8): p. 2069-2077.

Garnier C., Axelos M. A. V. and Thibault J. F. Phase diagrams of pectin-calcium systems: Influence of pH, ionic strength, and temperature on the gelation of pectins with different degrees of methylation. *Carbohydrate Research*, **1993**. 240: p. 219–232.

Garnier C., Axelos M. A. V. and Thibault J. F. Phase diagrams of pectin-calcium systems: Influence of pH, ionic strength, and temperature on the gelation of pectins with different degrees of methylation. *Carbohydrate Research*, **1993**. 240(35): p. 219–232.

Garnier C., Axelos M. A. V. and Thibault J. F. Selectivity and cooperativity in the binding of calcium ions by pectins. *Carbohydrate Research*, **1994**. 256(1): p. 71–81.

Ghimici L., Nichifor M. and Wolf B. Ionic Polymers Based on Dextran: Hydrodynamic Properties in Aqueous Solution and Solvent Mixtures. *J. Phys. Chem. B, 2009, 113 (23), pp 8020–8025*, **2009**. 113(23): p. 8020–8025.

Gilsenan P. M., Richardson R. K. and Morris E. R. Thermally reversible acid-induced gelation of low-methoxy pectin. *Carbohydrate Polymers*, **2000**. 41(4): p. 339–349.

Girod F. S., Ternet H., Freche M., Lacout J. L. and Rodriguez F. Controlled release properties and final macroporosity of a pectin microspheres–calcium phosphate composite bone cement. *Acta Biomaterialia*, **2010**. 6(6): p. 2294–2300.

Graham H. D. Isolation of gellan gum from foods by use of monovalent cations. *Journal of Food Science*, **1991**. 56(5): p. 1342–1346.

Grant G. T., Morris E. R., Rees D. A., Smith P. J. C. and Thom D. Biological interactions between polysaccharides and divalent cations: the egg-box model. *Febs Letters*, **1973**. 32(1): p. 195–198.

Gross M. O., Rao V. N. M. and Smit C. J. B. Rheological characterization of low methoxyl pectin gel by normal creep and relaxation. *Journal of Texture Studies*, **1980**. 11(3): p. 271–290.

Harding S. E., Vårum K. M., Stokke B. T. and Smidsrød O. Molecular weight determination of polysaccharides. Advances in carbohydrate analysis, Ed: White C. A. Greenwich: *JAI Press Ltd*, **1991**. p.63–144.

Hazel J. R. and Sidell B. D. A method for the determination of diffusion coefficients for small molecules in aqueous solution. *Analytical Biochemistry*, **1986**. 166(2): p. 335-341.

Higiro J., Herald T. J., Alavi S. and Bean S. Rheological study of xanthan and locust bean gum interaction in dilute solution: Effect of salt. *Food Research International*, **2007**. 40(4): p. 435-447.

Hoogendam C. W., de Keizer A., Cohen Stuart M. A., Bijsterbosch B. H., Smit J. A. M., van Dijk J. A. P. P., van der Horst P. M., et al. Persistence Length of Carboxymethyl Cellulose As Evaluated from Size Exclusion Chromatography and Potentiometric Titrations. *Macromolecules*, **1998**. 31(18): p. 6297–6309.

Hourdet D. and Muller G. Solution properties of pectin polysaccharides II. Conformation and molecular size of high galacturonic acid content isolated pectin chains. *Carbohydrate Polymers*, **1991**. 16(2): p. 113-135.

Hua X., Wang K., Yang R., Kang J. and Zhang J. Rheological properties of natural low-methoxyl pectin extracted from sunflower head. *Food Hydrocolloids*, **2015**. 44: p. 122–128.

Huynh T. D. U., Lerbret A., Neiers F., Chambin O. and Assifaoui A. Binding of divalent cations to polygalacturonate: a mechanism driven by the hydration water. *J. Phys. Chem. B*, **2016**. 120(5): p. 1021–1032.

Hwang J. and Kokini J. L. Contribution of the side branches to rheological properties of pectins. *Carbohydrate Polymers*, **1992**. 19(1): p. 41–50.

Hwang J., Pyun Y. R. and Kokini J. L. Sidechains of pectins: some thoughts on their role in plant cell walls and foods. *Food Hydrocolloids*, **1993**. 7(1): p. 39-53.

Iijima M., Hatakeyama T., Nakamura K. and Hatakeyama H. Effect of annealing on calcium pectin gel formation by thermomechanical analysis. *Journal of Thermal Analysis and Calorimetry*, **2002**. 70: p. 815-824.

Invitrogen C. Chapter 7: Theory of Binding Data Analysis, in Technical Resource Guide - Fourth edition: Fluorescence Polarization, Ed: *CHBE 310 at Rice*, **2006**. p. (7)-1-18.

Jantrawut P., Assifaoui A. and Chambin O. Influence of low methoxyl pectin gel textures and *in vitro* release of rutin from calcium pectinate beads. *Carbohydr Polym.*, **2013**. 97(2): p. 335-342.

Jonassen H., Kjøniksen A. L. and Hiorth M. Effects of ionic strength on the size and compactness of chitosan nanoparticles. *Colloid and Polymer Science*, **2012**. 290(10): p. 919-929.

Jonassen H., Kjøniksen A. L. and Hiorth M. Stability of Chitosan Nanoparticles Cross-Linked with Tripolyphosphate. *Biomacromolecules*, **2012**. 13(11): p. 3747–3756.

Jonassen H., Treves A., Kjøniksen A. L., Smistad G. and Hiorth M. Preparation of Ionically Cross-Linked Pectin Nanoparticles in the Presence of Chlorides of Divalent and Monovalent Cations. *Biomacromolecules*, **2013**. 14(10): p. 3523–3531.

Jug M., Kosalec I., Maestrelli F. and Mura P. Development of low methoxy amidated pectin-based mucoadhesive patches for buccal delivery of triclosan: Effect of cyclodextrin complexation. *Carbohydrate Polymers*, **2012**. 90(4): p. 1794–1803.

Jung J., Arnold R. D. and Wicker L. Pectin and charge modified pectin hydrogel beads as a colon-targeted drug delivery carrier. *Colloids and Surfaces B: Biointerfaces*, **2013**. 104: p. 116–121.

Karakasyan C., Legros M., Lack S., Brunel F., Maingault P., Ducouret G. and Hourdet D. Cold Gelation of Alginates Induced by Monovalent Cations. *Biomacromolecules*, **2010**. 11(11): p. 2966–2975.

Kastner H., Einhorn-Stoll U. and Senge B. Structure formation in sugar containing pectin gels – Influence of Ca^{2+} on the gelation of low-methoxylated pectin at acidic pH. *Food Hydrocolloids*, **2012**. 27(1): p. 42-49.

Kim H. S. A kinetic study on calcium alginate bead formation. *Korean Journal of Chemical Engineering*, **1990**. 7(1): p. 1-6.

Kim M. J., Ju H. K., Kim Y., Yoo S. H. and Kim Y. S. Effects of amidation and/or methylesterification of pectin on aroma release at different calcium concentration. *Food Hydrocolloids*, **2016**. 52: p. 343–349.

Kim W. J., Rao V. N. M. and Smit C. J. B. Effect of chemical composition on compressive mechanical properties of low ester pectin gels. *Journal of Food Science*, **1978**. 43(2): p. 572–575.

Kim Y., Kim Y. S., Yoo S. H. and Kim K. O. Molecular structural differences between low methoxy pectins induced by pectin methyl esterase II: Effects on texture, release and perception of aroma in gels of similar modulus of elasticity. *Food Chemistry*, **2014**. 145: p. 950–955.

Kim Y., Yoo Y. H., Kim K. O., Park J. B. and Yoo S. H. Textural properties of gelling system of low-methoxy pectins produced by demethoxylating reaction of pectin methyl esterase. *Journal of Food Science*, **2008**. 73(5): p. C367–C372.

Kjøniksen A. L., Hiorth M. and Nyström B. Temperature-induced association and gelation of aqueous solutions of pectin. A dynamic light scattering study. *European Polymer Journal*, **2004**. 40(11): p. 2427-2435.

Koda S., Nomura H. and Nagasawa M. Raman spectroscopic studies on the interaction between divalent counterion and polyion. *Biophysical Chemistry*, **1983**. 18(4): p. 361–367.

Kohn R. Ion binding on polyuronates - alginate and pectin. *Pure and Applied Chemistry*, **1975**. 42(3): p. 371-397.

Kontogiorgos V., Margelou I., Georgiadis N. and Ritzoulis C. Rheological characterization of okra pectins. *Food Hydrocolloids*, **2012**. 29(2): p. 356–362.

Lai L. S. and Chiang H. F. Rheology of decolorized hsian-tsao leaf gum in the dilute domain. *Food Hydrocolloids*, **2002**. 16(5): p. 427–440.

Lapasin R. and Pricl S. Rheology of polysaccharide systems, in Rheology of industrial polysaccharides: Theory and applications, Ed: R. Lapasin, andS. Pricl. *Glasgow: Blackie Academic and Professional*, **1995**. p. 250–494.

Li X., Al-Assaf S., Fang Y. and Phillips G. O. Characterisation of commercial LM-pectin in aqueous solution. *Carbohydrate Polymers*, **2013**. 92(2): p. 1133-1142.

Liang R. H., Chen J., Liu W., Liu C. M., Yu W., Yuan M. and Zhou X. Q. Extraction, characterization and spontaneous gel-forming property of pectin from creeping fig (*Ficus pumila Linn*.) seeds. *Carbohydrate Polymers*, **2012**. 87(1): p. 76–83.

Liao H., Ai W., Zhang K., Nakauma M., Funami T., Fang Y., Nishinari K., et al. Mechanisms of oligoguluronate modulating the calcium-induced gelation of alginate. *Polymer*, **2015**. 74: p. 166–175.

Lima A. M. F., Soldi V. and Borsali R. Dynamic light scattering and viscosimetry of aqueous solutions of pectin, sodium alginate and their mixtures: effects of added salt, concentration, counterions, temperature and chelating agent. *J. Braz. Chem. Soc.*, **2009**. 20(9): p.

Lin H., Aizawa K., Inakuma T., Yamauchi R. and Kato K. Physical properties of water-soluble pectins in hot- and cold-break tomato pastes. *Food Chemistry*, **2005**. 93(3): p. 403–408.

Liners F. and Van Cutsem P. Immunocytochemical localization of homopolygalacturonic acid on plant cell walls. *Micron and Microscopica Acta*, **1991**. 22(3): p. 265-266.

Lips A., Clark A. H., Cutler N. and Durand D. Measurement of cooperativity of binding of calcium to neutral sodium pectate. *Food Hydrocolloids*, **1991**. 5(1-2): p. 87–99.

Liu L., Fishman M. L., Kost J. and Hicks K. B. Pectin-based systems for colon-specific drug delivery via oral route. *Biomaterials*, **2003**. 24(19): p. 3333–3343.

Löfgren C., Guillotin S., Evenbratt H., Schols H. and Hermansson A. M. Effects of Calcium, pH, and Blockiness on Kinetic Rheological Behavior and Microstructure of HM Pectin Gels. *Biomacromolecules*, **2005**. 6(2): p. 646–652.

Löfgren C., Guillotin S. and Hermansson A. M. Microstructure and Kinetic Rheological Behavior of Amidated and Nonamidated LM Pectin Gels. *Biomacromolecules*, **2006**. 7(1): p. 114–121.

Löfgren C. and Hermansson A. M. Synergistic rheological behaviour of mixed HM/LM pectin gels. *Food Hydrocolloids*, **2007**. 21(3): p. 480–486.

Löfgren C., Walkenström P. and Hermansson A. M. Microstructure and Rheological Behavior of Pure and Mixed Pectin Gels. *Biomacromolecules*, **2002**. 3(6): p. 1144-1153.

Lootens D., Capel F., Durand D., Nicolai T., Boulenguer P. and Langendorff V. Influence of pH, Ca concentration, temperature and amidation on the gelation of low methoxyl pectin. *Food Hydrocolloids*, **2003**. 17(3): p. 237–244.

Luo Y., Pan K. and Zhong Q. Casein/pectin nanocomplexes as potential oral delivery vehicles. *International Journal of Pharmaceutics*, **2015**. 486(1-2): p. 59–68.

Luzio G. A. and Cameron R. G. Demethylation of a model homogalacturonan with the salt-independent pectin methylesterase from citrus: Part II. Structure–function analysis. *Carbohydrate Polymers*, **2008**. 71(2): p. 300–309.

Malovíková A., Rinaudo M. and Milas M. Comparative interactions of magnesium and calcium counterions with polygalacturonic acid. *Biopolymers*, **1994**. 34(8): p. 1059–1064.

Mancini M., Moresi M. and Sappino F. Rheological behaviour of aqueous dispersions of algal sodium alginates. *Journal of Food Engineering*, **1996**. 28(3-4): p. 283–295.

Manning G. S. Limiting laws and counterion condensation in polyelectrolyte solutions IV. The approach to the limit and the extraordinary stability of the charge fraction. *Biophysical Chemistry*, **1977**. 7(2): p. 95-102.

Manunza B., Deiana S., Pintore M. and Gessa C. Molecular dynamics study of polygalacturonic acid chains in aqueous solution. *Carbohydrate Research*, **1997**. 300(1): p. 85–88.

Masuelli M. A. Viscometric study of pectin. Effect of temperature on the hydrodynamic properties. *International Journal of Biological Macromolecules*, **2011**. 48(2): p. 286-291.

Matia-Merino L., Lau K. and Dickinson E. Effects of low-methoxyl amidated pectin and ionic calcium on rheology and microstructure of acid-induced sodium caseinate gels. *Food Hydrocolloids*, **2004**. 18(2): p. 271–281.

Matthew J. A., Howson S. J., Keenan M. H.J. and Belton P. S. Improvement of the gelation properties of sugarbeet pectin following treatment with an enzyme preparation derived from Aspergillus niger — Comparison with a chemical modification. *Carbohydrate Polymers*, **1990**. 12(3): p. 295-306.

May C. D. Industrial pectins: Sources, production and applications. *Carbohydrate Polymers*, **1990**. 12(1): p. 79-99.

McConaughy S. D., Stroud P. A., Boudreaux B., Hester R. D. and McCormick C. L. Structural Characterization and Solution Properties of a Galacturonate Polysaccharide Derived from *Aloe vera* Capable of in Situ Gelation. *Biomacromolecules*, **2008**. 9(2): p. 472–480.

Mohnen D. Pectin structure and biosynthesis. *Current Opinion in Plant Biology*, **2008**. 11(3): p. 266-277.

Morariu S., Brunchi C. E. and Bercea M. The Behavior of Chitosan in Solvents with Different Ionic Strengths. *Ind. Eng. Chem. Res.*, **2012**. 51(39): p. 12959–12966.

Morris G. A., de al Torre J. G., A. O., Castile J., A. S. and Harding S. E. Molecular flexibility of citrus pectins by combined sedimentation and viscosity analysis. *Food Hydrocolloids*, **2008**. 22(8): p. 1435-1442.

Morris G. A., Foster T. J. and Harding S. E. The effect of the degree of esterification on the hydrodynamic properties of citrus pectin. *Food Hydrocolloids*, **2000**. 14(3): p. 227–235.

Morris G. A., García de la Torre J., Ortega A., Castile J., Smith A. and Harding S. E. Molecular flexibility of citrus pectins by combined sedimentation and viscosity analysis. *Food Hydrocolloids*, **2008**. 22(8): p. 1435–1442.

Morris G. A., Ralet M. C., Bonnin E., Thibault J. F. and Harding S. E. Physical characterisation of the rhamnogalacturonan and homogalacturonan fractions of sugar beet (Beta vulgaris) pectin. *Carbohydrate Polymers*, **2010**. 82(4): p. 1161–1167.

Mualikrishna G. and Tharanathan R. N. Characterization of pectic polysaccharides from pulse husks. *Food Chemistry*, **1994**. 50(1): p. 87-89.

Muller F., Manet S., Jean B., Chambat G., Boué F., Heux L. and Cousin F. SANS Measurements of Semiflexible Xyloglucan Polysaccharide Chains in Water Reveal Their Self-Avoiding Statistics. *Biomacromolecules*, **2011**. 12(9): p. 3330-3336.

Munjeri O., Collett J. H. and Fell J. T. Hydrogel beads based on amidated pectins for colon-specific drug delivery: the role of chitosan in modifying drug release. *Journal of Controlled Release*, **1997**. 46(3): p. 273–278.

Narayanan J., Deotare V. W., Bandyopadhyay R. and Sood A. K. Gelation of Aqueous Pectin Solutions: A Dynamic Light Scattering Study. *Journal of Colloid and Interface Science*, **2002**. 245(2): p. 267-273.

Nayak A. K., Pal D. and Santra K. Development of calcium pectinate-tamarind seed polysaccharide mucoadhesive beads containing metformin HCl. *Carbohydrate Polymers*, **2014**. 101: p. 220–230.

Ngouémazong D. E., Jolie R. P., Cardinaels R., Fraeye I., Van Loey A., Moldenaers P. and Hendrickx M. Stiffness of Ca^{2+}-pectin gels: combined effects of degree and pattern of methylesterification for various Ca^{2+} concentrations. *Carbohydrate Research*, **2012**. 348: p. 69-76.

Ngouémazong D. E., Kabuye G., Fraeye I., Cardinaels R., Van Loey A., Moldenaers P. and Hendrickx M. Effect of debranching on the rheological properties of Ca^{2+}–pectin gels. *Food Hydrocolloids*, **2012**. 26(1): p. 44-53.

Ngouémazong D. E., Tengweh F. F., Fraeye I., Duvetter T., Cardinaels R., Van Loey A., Moldenaers P., et al. Effect of de-methylesterification on network development and nature of Ca^{2+} -pectin gels: Towards understanding structure-function relations of pectin. *Food Hydrocolloids*, **2012**. 26(1): p. 89–98.

Nguyen A. T. B., Winckler P., Loison P., Wache Y. and Chambin O. Physico-chemical state influences *in vitro* release profile of curcumin from pectin beads. *Colloids and Surfaces B: Biointerfaces*, **2014**. 121(1): p. 290–298.

Noto R., Martorana V., Bulone D. and San Biagio P. L. Role of Charges and Solvent on the Conformational Properties of Poly(galacturonic acid) Chains: A Molecular Dynamics Study. *Biomacromolecules*, **2005**. 6(5): p. 2555-2562.

O'Donoghue E. M. and Somerfield S. D. Biochemical and rheological properties of gelling pectic isolates from buttercup squash fruit. *Food Hydrocolloids*, **2008**. 22(7): p. 1326–1336.

Oosterveld A., Beldman G., Searle-van Leeuwen M. J. F. and Voragen A. G. J. Effect of enzymatic deacetylation on gelation of sugar beet pectin in the presence of calcium. *Carbohydrate Polymers*, **2000**. 43(3): p. 249–256.

Owens H. S., Swenson H. A. and Schultz T. H. Chapter 3: Factors Influencing Gelation with Pectin, in Natural plant hydrocolloids, Ed: *Advances in Chemistry,*, **1954**. 11: p. 10–15.

Pals D. T. F. and Hermans J. J. Sodium salts of pectin and of carboxy methyl cellulose in aqueous sodium chloride. I. Viscosities. *Recueil des Travaux Chimiques des Pays-Bas*, **1952**. 71(5): p. 433–457.

Peppas N. A. and Sahlin J. J. A simple equation for the description of solute release. III. Coupling of diffusion and relaxation. *International Journal of Pharmaceutics*, **1989**. 57(2): p. 169-172.

Ping Z. H., Nguyen Q. T., Chen S. M., Zhou J. Q. and Ding Y. D. States of water in different hydrophilic polymers – DSC and FTIR studies. *Polymer*, **2001**. 42(20): p. 8461–8467.

Plazinski W. Molecular basis of calcium binding by polyguluronate chains. Revising the egg-box model. *J Comput Chem.*, **2011**. 32(14): p. 2988-2995.

Potter K., Balcom B. J., Carpenter T. A. and Hall L. D. The gelation of sodium alginate with calcium ions studied by magnetic resonance imaging (MRI). *Carbohydrate Research*, **1994**. 257(1): p. 117-126.

Powell D. A., Morris E. R., Gidley M. J. and Rees D. A. Conformations and interactions of pectins: II. Influence of residue sequence on chain association in calcium pectate gels. *Journal of Molecular Biology*, **1982**. 155(4): p. 517–531.

Racape E., Thibault J. F., Reitsma J. C. E. and Pilnik W. Properties of Amidated Pectins. II. Polyelectrolyte Behavior and Calcium Binding of Amidated Pectins and Amidated Pectic Acids. *Biopolymers*, **1989**. 28(8): p. 1435 - 1448.

Rao M. A., Van Buren J. P. and Cooley H. J. Rheological changes during gelation of high-methoxyl pectin/fructose dispersions: effect of temperature and aging. *Journal of Food Science*, **1993**. 58(1): p. 173–176.

Rees D. A. and Wight A. W. Polysaccharide conformation. Part VII. Model building computations for α-1,4 galacturonan and the kinking function of L-rhamnose residues in pectic substances. *J. Chem. Soc. B*, **1971**. p. 1366-1372.

Ridley B. L., O'Neill M. A. and Mohnen D. Pectins structure, biosynthesis, and oligogalacturonide-related signaling. *Phytochemistry*, **2001**. 57(6): p. 929–967.

Ritger P. L. and Peppas N. A. A simple equation for description of solute release II. Fickian and anomalous release from swellable devices. *Journal of Controlled Release*, **1987**. 5(1): p. 37-42.

Rolin C. Pectin. Industrial Gums: Polysaccharides and Their Derivatives, Ed: James N. BeMiller, andRoy L. Whistler. *Elsevier Inc.*, **1993**. p.257–293.

Rosenthal H. E. A graphic method for the determination and presentation of binding parameters in a complex system. *Analytical Biochemistry*, **1967**. 20(3): p. 525–532.

Schefer L., Usov I. and Mezzenga R. Anomalous Stiffening and Ion-Induced Coil–Helix Transition of Carrageenans under Monovalent Salt Conditions. *Biomacromolecules*, **2015**. 16(3): p. 985–991.

Scheller H.V., Jensen J. K., Sørensen S.O., Harholt J. and Geshi N. Biosynthesis of pectin. *Physiol Plant*, **2007**. 129(2): p. 283–295.

Schmelter T., Wientjes R., Vreeker R. and Klaffke W. Enzymatic modifications of pectins and the impact on their rheological properties. *Carbohydrate Polymers*, **2002**. 47(2): p. 99–108.

Schmidt I., Cousin F., Huchon C., Boué F. and Axelos M. A.V. Spatial structure and composition of polysaccharide-protein complexes from Small Angle Neutron Scattering. *Biomacromolecules*, **2009**. 10(6): p. 1346–1357.

Schmidt I., Cousin F., Huchon C., Boué F. and Axelos M. A.V. Spatial Structure and Composition of Polysaccharide−Protein Complexes from Small Angle Neutron Scattering. *Biomacromolecules*, **2009**. 10(6): p. 1346–1357.

Schweins R., Hollmann J. and Huber K. Dilute solution behaviour of sodium polyacrylate chains in aqueous NaCl solutions. *Polymer*, **2003**. 44(23): p. 7131–7141.

Selvarengan P., Kubicki J. D., Guégan J. P. and Châtellier X. Complexation of carboxyl groups in bacterial lipopolysaccharides: Interactions of H^+, Mg^{2+}, Ca^{2+}, Cd^{2+}, and UO_2^{2+} with Kdo and galacturonate molecules via quantum mechanical calculations and NMR spectroscopy. *Chemical Geology*, **2010**. 273(1–2): p. 55–75.

Siepmann J. and Siepmann F. Mathematical modeling of drug delivery. *International Journal of Pharmaceutics*, **2008**. 364(2): p. 328–343.

Silva D. A., Brito A. C. F., de Paula R. C. M., Feitosa J. P. A. and Paula H. C. B. Effect of mono and divalent salts on gelation of native, Na and deacetylated *Sterculia striata* and *Sterculia urens* polysaccharide gels. *Carbohydrate Polymers*, **2003**. 54(2): p. 229–236.

Simon S., Dugast J. Y., Le Cerf D., Picton L. and Muller G. Amphiphilic polysaccharides. Evidence for a competition between intra and intermolecular associations in dilute system. *Polymer*, **2003**. 44(26): p. 7917–7924.

Simpson B. K., Egyankor K. B. and Martin A. M. Extraction, purification and determination of pectin in tropical fruits. *Journal of Food Processing and Preservation*, **1984**. 8(2): p. 63–72.

Skjåk-Bræk G., Grasdalen H. and Smidsrød O. Inhomogeneous polysaccharide ionic gels. *Carbohydrate Polymers*, **1989**. 10(1): p. 31–54.

Smidsrød O. Molecular Basis for some Physical Properties of Alginates in the Gel State *Faraday Discuss. Chem. Soc.*, **1974**. 57: p. 263-274.

Smidsrød O. and Christensen B. E. Molecular structure and physical behaviour of seaweed colloids as compared with microbial polysaccharides, in Seaweed resources in Europe: Uses and potential, Ed: Guiry M. D., andBlunden G. *JohnWiley&SonsLtd.*: NewYork, USA, **1991**. p. 185–217.

Smidsrød O. and Haug A. Estimation of the relative stiffness of the molecular chain in polyelectrolytes from measurements of viscosity at different ionic strengths. *Biopolymers*, **1971**. 10(7): p. 1213–1227.

Soltania S. and Madadlou A. Two-step sequential cross-linking of sugar beet pectin for transforming zein nanoparticle-based Pickering emulsions to emulgels. *Carbohydrate Polymers*, **2016**. 136: p. 738–743.

Sousa A. G., Nielsen H. L., Armagan I., Larsen J. and Sørensen S. O. The impact of rhamnogalacturonan-I side chain monosaccharides on the rheological properties of citrus pectin. *Food Hydrocolloids*, **2015**. 47: p. 130–139.

Sriamornsak P. and Kennedy R. A. Swelling and diffusion studies of calcium polysaccharide gels intended for film coating. *International Journal of Pharmaceutics*, **2008**. 358(1-2): p. 205–213.

Sriamornsak P. and Nunthanid J. Calcium pectinate gel beads for controlled release drug delivery: II. Effect of formulation and processing variables on drug release. *J Microencapsul.*, **1999**. 16(3): p. 303-313.

Stephens A. M., Phillips G. O. and Williams P. A. Food polysaccharides and their applications. 2nd ed., Ed. New York: *N.Y.: CRC Press*, **2006**.

Stoddart R. W., Spires I. P. C. and Tipton K. F. Solution properties of polygalacturonic acid. *Biochem J.*, **1969**. 114(4): p. 863–870.

Ström A., Ribelles P., Lundin L., Norton I., Morris E. R. and Williams M. A. K. Influence of Pectin Fine Structure on the Mechanical Properties of Calcium-Pectin and Acid-Pectin Gels. *Biomacromolecules*, **2007**. 8(9): p. 2668-2674.

Ström A., Schuster E. and Goh S. M. Rheological characterization of acid pectin samples in the absence and presence of monovalent ions. *Carbohydrate Polymers*, **2014**. 113: p. 336–343.

Synytsya A., Čopíková J., Matějka P. and Machovič V. Fourier transform Raman and infrared spectroscopy of pectins. *Carbohydrate Polymers*, **2003**. 54(1): p. 97-106.

Thakur B. R., Singh R. K. and Handa A. K. Chemistry and uses of pectin — A review. *Critical Reviews in Food Science and Nutrition*, **1997**. 37(1): p. 47-73.

Thibault J. F. and Rinaudo M. Interactions of mono- and divalent counterions with alkali- and enzyme-deesterified pectins in salt-free solutions. *Biopolymers*, **1985**. 24(11): p. 2131–2143.

Tho I., Sande S. A. and Kleinebudde P. Disintegrating pellets from a water-insoluble pectin derivative produced by extrusion/spheronisation. *European Journal of Pharmaceutics and Biopharmaceutics*, **2003**. 56(3): p. 371–380.

Tho I., Sande S. A. and Kleinebudde P. Cross-linking of amidated low-methoxylated pectin with calcium during extrusion/spheronisation: Effect on particle size and shape. *Chemical Engineering Science*, **2005**. 60(14): p. 3899–3907.

Thom D., Grant G. T., Morris E. R. and Rees D. A. Characterisation of cation binding and gelation of polyuronates by circular dichroism. *Carbohydrate Research*, **1982**. 100(1): p. 29–42.

Topuz F., Henke A., Richtering W. and Groll J. Magnesium ions and alginate do form hydrogels a rheological study. *Soft Matter*, **2012**. 8(18): p. 4877-4881.

Vega E. D., Vásquez E., Diaz J. R. A. and Masuelli M. A. Influence of the Ionic Strength in the Intrinsic Viscosity of Xanthan Gum. An Experimental Review. *Journal of Polymer and Biopolymer Physics Chemistry*, **2015**. 3(1): p. 12-18.

Ventura I., Jammal J. and Bianco-Peled H. Insights into the nanostructure of low-methoxyl pectin–calcium gels. *Carbohydrate Polymers*, **2013**. 97(2): p. 650-658.

Voragen A. G. J., Pilnik W., Thibault J. F., Axelos M. A. V. and Renard C. M. G. C. Pectins, in Food Polysaccharides and Their Applications, Ed: Stephen A. M. *Marcel Dekker,*: New York, **1995**. 10: p. 287-339.

Walkinshaw M. D. and Arnott S. Conformations and interactions of pectins: I. X-ray diffraction analyses of sodium pectate in neutral and acidified forms. *Journal of Molecular Biology*, **1981**. 153(4): p. 1055-1073.

Wang K., Hua X., Yang R., Kang J. and Zhang W. Hydrodynamic behavior and gelling properties of sunflower head pectin in the presence of sodium salts. *Food Hydrocolloids*, **2014**. 36: p. 238–244.

Weast R. C., Astle M. J. and Beyer W. H. CRC Handbook of chemiStly and physics, 66th Edn. Ed.: *CRC Press, Florida, USA*, **1986**.

Wehr J. B., Menzies N. W. and Blamey F. P. C. Alkali hydroxide-induced gelation of pectin. *Food Hydrocolloids*, **2004**. 18(3): p. 375–378.

Wu Z. L., Takahashi R., Sawada D., Arifuzzaman M., Nakajima T., Kurokawa T., Hu J., et al. *In Situ* Observation of Ca2+ Diffusion-Induced Superstructure Formation of a Rigid Polyanion. *Macromolecules*, **2014**. 47(20): p. 7208–7214.

Xin Y., Bligh M. W., Kinsela A. S., Wang Y. and Waite T. D. Calcium-mediated polysaccharide gel formation and breakage: Impact on membrane foulant hydraulic properties. *Journal of Membrane Science*, **2015**. 475: p. 395–405.

Yang Y., Campanella O. H., Hamaker B. R., Zhang G. and Gu Z. Rheological investigation of alginate chain interactions induced by concentrating calcium cations. *Food Hydrocolloids*, **2013**. 30(1): p. 26–32.

Yapo B. M. Biochemical Characteristics and Gealling Capacity of Pectin from Yellow Passion Fruit Rind as Affected by Acid Extractant Nature. *J. Agric. Food Chem.*, **2009**. 57(4): p. 1572–1578.

Yapo B. M. Pectic substances: From simple pectic polysaccharides to complex pectins—A new hypothetical model. *Carbohydrate Polymers*, **2011**. 86(2): p. 373–385.

Yapo B. M. and Koffi K. L. Utilisation of model pectins reveals the effect of demethylated block size frequency on calcium gel formation. *Carbohydrate Polymers*, **2013**. 92(1): p. 1-10.

Yoo S. H., Fishman M. L., Hotchkiss A. T. Jr. and Lee H. G. Viscometric behavior of high-methoxy and low-methoxy pectin solutions. *Food Hydrocolloids*, **2006**. 20(1): p. 62-67.

Yoo S. H., Lee B. H., Savary B. J., Lee S., Lee H. G. and Hotchkiss A. T. Characteristics of enzymatically-deesterified pectin gels produced in the presence of monovalent ionic salts. *Food Hydrocolloids*, **2009**. 23(7): p. 1926–1929.

Zaidel D. N. A., Chronakis I. S. and Meyer A. S. Enzyme catalyzed oxidative gelation of sugar beet pectin: Kinetics and rheology. *Food Hydrocolloids*, **2012**. 28(1): p. 130–140.

Zhang H., Dubin P. L., Kaplan J., Moorefield C. N. and Newkome G. R. Dissociation of Carboxyl-Terminated Cascade Polymers: Comparison with Theory. *J. Phys. Chem. B*, **1997**. 101(18): p. 3494–3497.

Zhao W., Guo X., Pang X., Gao L., Liao X. and Wu J. Preparation and characterization of low methoxyl pectin by high hydrostatic pressure-assisted enzymatic treatment compared with enzymatic method under atmospheric pressure. *Food Hydrocolloids*, **2015**. 50: p. 44–53.

ANNEXES

Annex 1: Summary of the results of ITC

Polymer (nature and amount)		M^{2+} (nature, amount) and molar ratio (R)	Experimental conditions	K x 10^{-4} (M^{-1})	ΔH (kJ mol^{-1})	Reference
Alginate	1.4 mM of Guluronate	Ca (9 mM) 0 < R < 0.5	NaCl (0mM), neutral pH, T=25°C	K_1= 133 K_2= 1.0	ΔH_1= 3.9 ΔH_2= - 6.3	1
			NaCl (10mM), neutral pH, T=25°C	K_1= 77.1 K_2= 1.3	ΔH_1= 1.5 ΔH_2= - 16.1	
			NaCl (25mM), neutral pH, T=25°C	K_1= 50.1 K_2= 1.0	ΔH_1= 1.3 ΔH_2= - 7.9	
			NaCl (50mM), neutral pH, T=25°C	K_1= 40.1 K_2= 0.3	ΔH_1= 0.1 ΔH_2= - 111.6	
		Ca (18 mM)	NaCl (100 mM), neutral pH, T=25°C	K_1= 30.9 K_2= 0.5	ΔH_1= 0.0 ΔH_2= - 6.5	
Two types of alginates (M/G=0.56 and 1.17)	1.0 mM and 2.0 mM of Guluronate[a]	Ca (7.5mM) 0 < R < 1.25	Acetate buffer (20 mM), pH=5, T=25°C	K_2= 1.1	ΔH_2= -11.6	2
				K_2= 1.1	ΔH_2= -15.0	
Mannuronan	3.5 mM of monomers	Mg 0 < R < 0.5	$NaClO_4$(50 mM)	K_1= 1.7 x 10^{-4}	ΔH_1= 3.1	3
Guluronan				K_1= 0.04	ΔH_1= 0.2	
Polyalternating				K_1= 7.3 x 10^{-4}	ΔH_1= -0.1	
Pectin	1.9 mM of Gal [b]	Ca (55mM) 0 < R < 4.7	Phosphate buffer (5 mM) pH=7, T=37°C	1) exothermic (0-4mM of Ca) (ΔH_1>0) 2) strong endothermic reaction (ΔH_2<0)		4
Poly (sodium acrylates)	0.8 mM of monomer	Ca (200 mM) 0 < R < 0.6	Water, pH=7, T=25°C	K_1= 15.4	ΔH_1= 17	5

(a) the concentrations of alginates are 0.26 g L^{-1} and 0.52 g L^{-1} were converted to molar concentration assuming that the molar weight of guluronate is 176 g/mol; (b) the weight percentage of pectin is 0.9%w/w was converted to molar concentration taking into consideration the % of DE (62%) and the % of galacturonic acid (89%), and the molar weight of guluronate is 176 g/mol

1. De S. and Robinson D. *Journal of Controlled Release*, **2003**. 89(1): p. 101–112.
2. Fang Y., Al-Assaf S., Phillips G. O., Nishinari K., Funami K., Williams P. A. and Li L. *J Phys Chem B.*, **2007**. 111(10): p. 2456-2462.
3. Donati I., Asaro F. and Paoletti S. *J. Phys. Chem. B*, **2009**. 113(39): p. 12877–12886.
4. Espinal-Ruiz M., Parada-Alfonso F., Restrepo-Sánchez L. P., Narváez-Cuenca C. E. and McClements D. J. *J Agric Food Chem.*, **2014**. 62(52): p. 12620-12630.
5. Sinn C. G., Dimova R. and Antonietti M. *Macromolecules*, **2004**. 37(9): p. 3444–3450.

Annex 2: FTIR bands of pectin with assignments

Pectin vibration (cm^{-1})	Assignment	Reference
1750 1650 1100 - 1200	COO-R (esterified carboxyl groups) COO^- (free carboxyl groups) Ether (R-O-R) and C-C bond	(Monsoor, 2001) (Pectin-Sigma-96H0580 & 30F0108)
1749 1630	C=O (COOH, $COOCH_3$) COO^-	(Chatjigakis, 1998) (Pectin-Sigma-DE = 31%, 68% & 93%)
1740 1650 1607	C=O str $-NH_2$ COO^- str, as (stretching, antisymmetric)	(Bociek, 1975) (Pectin-DE = 68.4% & 81%, LMP 320, LMP 400…)
1752 1686 1500 – 1200 1200 ± 50 1100 ± 50	C=O str (ester groups) C=O str (Amide I) C-O-H bendings, -CH2, -CH bendings v(C-O) as (ester) v(C-O) as (ether)	(Engelsen, 1996) (Pectin-98 Amidated-DE=20-55%, DA=4-24%)
1200 - 900 1016 1004 1200 – 950 1200 – 950	C-O and ring vibrations Sodium pectate Magnesium pectate Calcium pectate Zinc pectate	(Wellner, 1998) (Potassium pectinate – DE = 23.8, 59.1 & 93.4%)
1762 – 1740 1770 - 1760 1633, 1607 1419, 1405 1645 1403 1720 1250 1200 – 1000	C=O stretching of COOH v(C=O) (OOC-CH3) COO^- asymmetric COO^- symmetric δ (H2O) ν, $\delta(C\text{-}OH)_{COOH}$ $\nu(C=O)_{Acetyls}$ v(COC) of acetyl C-O, C-C	(Synytsya, 2003) (Polygalacturonic aicd, K-Pec, Commercial citrus & Sugar beer pectin)
1148 1105 1080 1052 1024	v(C-O-C) ring (C-O, C-C) v(C-O) + δ(OCH) ring (C-O, C-C) ring (C-O, C-C)	(Sivchik, 1978) (D-glucose - Monosaccharides)
1600 1735 1670	COO^- (carboxylic acid) $COOCH_3$ (methyl ester groups) $CO\text{-}NH_2$ (primary amide groups)	(Assifaoui, 2010) (Ca-LMP & Zn-LMP)

Annex 3: Raw data of Turbiscan

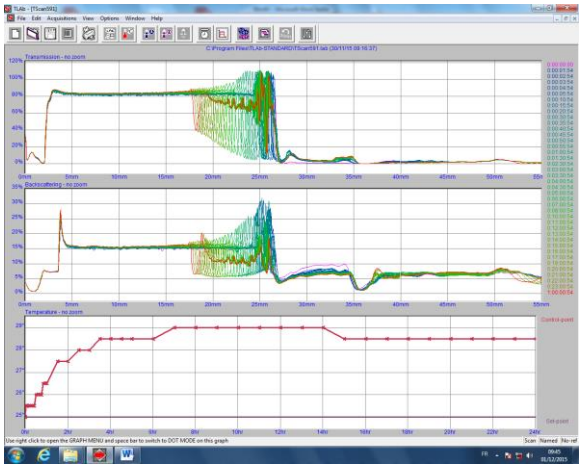

Ca^{2+} - 50mM – 24 h

Zn^{2+} - 50mM – 24 h

Ba^{2+} - 50mM – 24 h

Mg^{2+} - 50mM – 24 h

The raw data of Turbiscan for different divalent cations at cation concentration of 50 mM were presented in Annex 3. The turbidity measurement by Turbiscan was started after adding cation solutions ($CaCl_2$, $ZnCl_2$, $BaCl_2$, and $MgCl_2$) in the small tube. The light transmission from the mixtures was then measured periodically along the height from the bottom up to the top, whereas the diffusion of front gels was moving downward.

Turbiscan data were reported as a change in transmitted light versus time measured in the middle of the test tube (see raw data). The time of scan was installed: every 1 min for 4 min; 5 min for 50 min; 30 min for 3h 30 min; and 1h for 24h.

It was not easy to determine a value of the light transmission for each measured time due to these graphs were not flat and less smooth. Thus, to determine the value of transmission for a certain time, we chose a point from which began to appear the first plateau.

Annex 4: Images obtained after the Turbiscan experiments

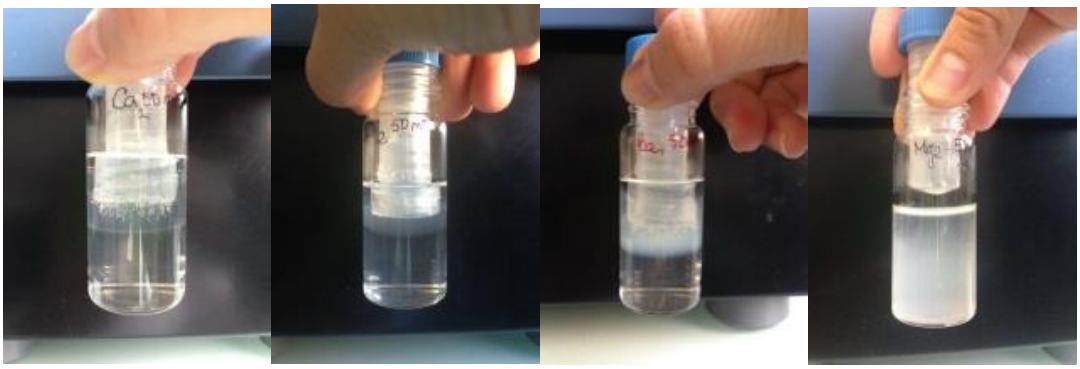

A. PolyGal – $Ca^{2+}/Zn^{2+}/Ba^{2+}/Mg^{2+}$ (50 mM)

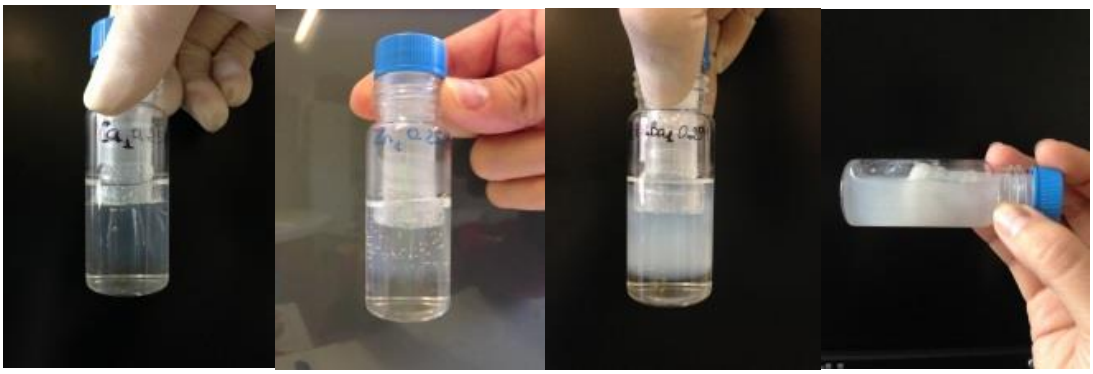

B. PolyGal – $Ca^{2+}/Zn^{2+}/Ba^{2+}/Mg^{2+}$ (250 mM)

C. PolyGal – $Ca^{2+}/Zn^{2+}/Ba^{2+}/Mg^{2+}$ (750 mM)

The mixtures of polyGal-divalent cations were obtained after the Turbiscan experiments (24h): A. PolyGal–$Ca^{2+}/Zn^{2+}/Ba^{2+}/Mg^{2+}$ (50 mM); B. PolyGal- $Ca^{2+}/Zn^{2+}/Ba^{2+}/Mg^{2+}$ (250 mM); C. PolyGal–$Ca^{2+}/Zn^{2+}/Ba^{2+}/Mg^{2+}$ (750 mM), respectively. In the Turbiscan tube, the precipitations of polyGal-Mg were observed around the membrane at Mg^{2+} concentrations of 250 and 750 mM. Whereas, the gels were formed by other cations (Ca^{2+}, Zn^{2+}, and Ba^{2+}) at the cation concentrations used (50, 250 and 750 mM).

Résumé

Dans ce travail de thèse, nous avons étudié les interactions entre un polyoside anionique (pectine) et des cations monovalent (Na^+) et divalents (Ca^{2+}, Zn^{2+}, Ba^{2+}, Mg^{2+}) en régime dilué ($c < c^*$) et concentré ($c \approx c^*$). Ainsi, une pectine faiblement méthylée (LMP) a été étudiée en comparaison avec l'acide polygalacturonique (PGA). L'affinité de ces polyosides pour fixer les ions calcium diminue quand la concentration en NaCl augmente. Elle est plus élevée dans le cas du Ca-polyGal en comparaison avec Ca-LMP ; ceci peut être expliqué par la faible rigidité des chaînes observée pour le polyGal. Les interactions entre les quatre cations divalents (Ca^{2+}, Zn^{2+}, Ba^{2+}, Mg^{2+}) et les deux biopolymères (PolyGal et LMP) en régime dilué ont été étudiées afin d'obtenir des informations sur la structure du réseau, le mode d'association et l'énergie d'association. Nous avons donc proposé un mécanisme d'association qui est composé de deux étapes : i) formation de monocomplexes et de réticulations ponctuelles et ii) formation de dimères. Le passage de l'étape (i) à l'étape (ii) est caractérisé par un ratio molaire critique ($R^*=[M^{2+}]/[Gal]$) qui dépend du nombre et de la stabilité des réticulations ponctuelles entre le polymère et le cation. Pour le Mg-polyGal, l'association est due à une condensation des ions magnésium autour des chaînes du polyGal. Les résultats de simulations ont montré que l'association de 4 cations Zn^{2+} avec 2 chaînes composées de 8 unités Gal est similaire à une structure de type « boîte à œuf ». Ce modèle n'est pas applicable à la structure obtenue par l'association des cations Ca^{2+} et Ba^{2+}. Les associations entre les polyGals et les cations divalents à une concentration en polymère proche de la concentration de recouvrement (c^*) permettent d'obtenir des gels uniquement pour les trois cations (Ca^{2+}, Zn^{2+}, Ba^{2+}). Les propriétés viscoélastiques de ces gels ainsi que la cinétique de gélification ont été étudiés. Dans le cas des gels, la première étape du mécanisme d'association proposé (formation de monocomplexes et de réticulations ponctuelles) s'accompagne d'une augmentation de l'épaisseur du gel ; alors que la deuxième étape (formation de dimères) conduit à une densification du gel. Nous avons remarqué que le coefficient de diffusion du front de gel suit l'ordre suivant : $Ba^{2+} > Ca^{2+} > Zn^{2+} > Mg^{2+}$; ceci peut être relié à l'affinité entre les molécules d'eau de la sphère de coordination et le cation. En effet, l'affinité du cation pour l'eau augmente selon l'ordre inverse : $Ba^{2+} < Ca^{2+} < Zn^{2+} < Mg^{2+}$. Enfin, nous avons utilisé ces trois polyosides (PGA, LMP et ALMP - pectine faiblement méthylée amidée) en association à des ions calcium pour fabriquer des microparticules contenant la rutine afin de cibler sa libération au niveau intestinal. Nous avons ainsi relié la cinétique de libération de la rutine à la structure du réseau mis en place lors de l'étape de gélification. Les microparticules à base de pectine

ALMP présentent une capacité à fixer l'eau et un taux de libération de la rutine plus élevés que les microparticules à base de LMP et PGA. Le gel Ca-ALMP est plus flexible et présente des modules viscoélastiques plus faibles que les gels Ca-PGA et Ca-LMP. Nous avons attribué ceci à la distribution aléatoire des groupements ester et/ou amide dans ALMP qui gênerait la formation des dimères : les liaisons hydrogènes entre les fonctions amines et les fonctions carboxylates seraient donc responsables de la flexibilité du réseau formé.

Mots-clés : **Pectines ; cations divalents ; NaCl ; gel ; mécanisme d'association ; structure ; encapsulation.**

Abstract

In this thesis, we studied the interactions between an anionic polysaccharide (pectin) and monovalent cation (Na^+) and divalent cations (Ca^{2+}, Zn^{2+}, Ba^{2+}, Mg^{2+}) in dilute regime ($c < c^*$) and concentrate regime ($c \approx c^*$). Thus, a low methoxy pectin (LMP) was studied in comparison with a polygalacturonic acid (PGA). The affinity to bind calcium ions for these polysaccharides decreases as the NaCl concentration increases. This binding affinity was higher for Ca-polyGal than for Ca-LMP due to the low rigidity of chains observed in the polyGal. The interactions between four divalent cations (Ca^{2+}, Zn^{2+}, Ba^{2+}, Mg^{2+}) and the two biopolymers (polyGal and LMP) in the dilute regime were studied in order to obtain information about the network structure, the mode of association and the binding energy. Therefore, we propose a mechanism of the binding which consists of two steps: i) formation of monocomplexations and point-like cross-links ii) formation of dimers. The threshold molar ratio ($R^* = [M^{2+}]/[Gal]$), between these two steps depends on the number and the stability of the point-like cross-links between polyGal chains and the cation. Mg^{2+} interacts so strongly with water that is remains weakly bound to polyGal (polycondensation) by sharing water molecules from its first coordination shell with the carboxylate groups of polyGal. Molecular dynamic simulations of galacturonate chains in explicit water showed that the « egg-box » model is more adapted for zinc cations than for calcium and barium. When the concentration of the polyGal is close to the overlap concentration (c^*), the addition of divalent cations allows to obtain gels for only three cations (Ca^{2+}, Zn^{2+}, Ba^{2+}). The viscoelastic properties of these gels and the gelation kinetics were studied. In the case of gel formation, the first step (formation of monocomplexations and point-like cross-links) is accompanied by an increase in the gel thickness; while the second step (formation of dimers) leads to a densification of the gel. We found that the diffusion coefficient of the gel front increased according the following order:

$Ba^{2+} > Ca^{2+} > Zn^{2+} > Mg^{2+}$; this may be related to the affinity between the water molecules from the coordination sphere and the cation. Indeed, the affinity of the cation for water molecules increases in the reverse order: $Ba^{2+} < Ca^{2+} < Zn^{2+} < Mg^{2+}$. Finally, we have used the three polysaccharides (PGA, LMP and ALMP - amidated low methoxyl pectin) in association with calcium ions to produce microparticles containing rutin to target drug release in the intestine. We have linked the rutin release kinetics to the network structure established in the gelation step. ALMP microparticles had higher ability to uptake water and thus higher drug release rate than two others microparticles (Ca-LMP and Ca-PGA). The Ca-ALMP gel was more flexible and had the lower viscoelastic modulus than Ca-PGA and Ca-LMP gels. We attributed this to the random distribution of ester and/or amide groups in ALMP, which hinders the formation of dimers: the hydrogen bonds between the amine groups and carboxylate groups are responsible for the flexibility of the network formed.

<u>Keywords</u>: Pectins; divalent cations; NaCl; gel; binding mechanism; structure; encapsulation.